

c.1

HYBRID MULTIDENTATE LIGANDS:  
AMIDO PHOSPHINE COMPLEXES OF THE GROUP VIII METALS

by

PATRICIA ANNE MACNEIL

B.Sc. (Honours), St. Mary's University, 1977

M.Sc., University of Toronto, 1979

A THESIS SUBMITTED IN PARTIAL FULFILMENT OF  
THE REQUIREMENTS FOR THE DEGREE OF  
DOCTOR OF PHILOSOPHY

in

THE DEPARTMENT OF CHEMISTRY

We accept this thesis as conforming  
to the required standard

THE UNIVERSITY OF BRITISH COLUMBIA

April, 1983

© Patricia Anne MacNeil, 1983

In presenting this thesis in partial fulfilment of the requirements for an advanced degree at the University of British Columbia, I agree that the Library shall make it freely available for reference and study. I further agree that permission for extensive copying of this thesis for scholarly purposes may be granted by the head of my department or by his or her representatives. It is understood that copying or publication of this thesis for financial gain shall not be allowed without my written permission.

Department of Chemistry

The University of British Columbia  
1956 Main Mall  
Vancouver, Canada  
V6T 1Y3

Date April 21, 1983

## Abstract

The hybrid ligands  $\text{HN}(\text{SiMe}_2\text{CH}_2\text{PPh}_2)_2$  and  $\text{HN}(\text{C}_6\text{H}_5\text{CH}_2)(\text{SiMe}_2\text{CH}_2\text{PPh}_2)$  react readily with n-butyllithium to yield the corresponding lithium salts. Metathesis of Group VIII transition metal halides with  $\text{LiN}(\text{SiMe}_2\text{CH}_2\text{PPh}_2)_2$  produces a variety of amido phosphine complexes. For the nickel triad, these derivatives have the formula  $[\text{MClN}(\text{SiMe}_2\text{CH}_2\text{PPh}_2)_2]$  ( $\text{M} = \text{Ni}, \text{Pd}, \text{Pt}$ ); a variety of rhodium and iridium complexes  $[\text{M}(\text{L})\text{N}(\text{SiMe}_2\text{CH}_2\text{PPh}_2)_2]$  ( $\text{M} = \text{Rh}, \text{Ir}$ ;  $\text{L} = \text{CO}, \eta^2\text{-C}_8\text{H}_{14}, \text{C}_2\text{H}_4, \text{PMe}_3, \text{PPh}_3$ ) and  $[\text{M}(\text{COD})\text{N}(\text{C}_6\text{H}_5\text{CH}_2)(\text{SiMe}_2\text{CH}_2\text{PPh}_2)]$  ( $\text{M} = \text{Rh}, \text{Ir}$ ;  $\text{COD} = 1,5\text{-cyclooctadiene}$ ) have also been prepared and characterized. Single crystal x-ray structural analysis of  $[\text{NiClN}(\text{SiMe}_2\text{CH}_2\text{PPh}_2)_2]$  indicates that it adopts a distorted square planar stereochemistry, whereas the palladium analogue  $[\text{PdClN}(\text{SiMe}_2\text{CH}_2\text{PPh}_2)_2]$  is almost perfectly square planar. Based primarily on spectral data, all of these Group VIII amido phosphines are assigned square planar geometries with mutually trans phosphines, with the tridentate ligand coordinated to the metal through the amide nitrogen and both phosphine centres.

The amino phosphine dichlorides,  $[\text{MCl}_2\text{NH}(\text{SiMe}_2\text{CH}_2\text{PPh}_2)_2]$  ( $\text{M} = \text{Ni}, \text{Pd}, \text{Pt}$ ) are prepared from the free ligand. The nickel derivative,  $[\text{NiCl}_2\text{NH}(\text{SiMe}_2\text{CH}_2\text{PPh}_2)_2]$ , has been shown by crystallographic analysis to have a very distorted tetrahedral geometry; no interaction between the NH moiety and the nickel centre is observed. Reaction of these amino phosphines with triethyl amine cleanly produces the corresponding amido phosphines.

$[\text{NiClN}(\text{SiMe}_2\text{CH}_2\text{PPh}_2)_2]$  reacts at low temperatures with Grignards or alkyl lithium reagents to yield a series of hydrocarbyl complexes

$[\text{Ni}(\text{R})\text{N}(\text{SiMe}_2\text{CH}_2\text{PPh}_2)_2]$  ( $\text{R} = \text{Me}, \text{allyl}, \text{vinyl}, \text{phenyl}$ ). These alkyl (aryl) complexes react readily at room temperature under one atmosphere of carbon monoxide to give  $\text{Ni}(\text{O})$  species,  $[\text{Ni}(\text{CO})_2\text{N}(\text{COR})(\text{SiMe}_2\text{CH}_2\text{PPh}_2)_2]$ , in which the ligand chelates in a bidentate fashion (through the phosphines) owing to migration of the acyl group to the amide nitrogen. For the methyl and phenyl derivatives, the intermediate  $\text{Ni}(\text{II})$  acyl complexes have also been isolated. As shown by crystal structural analysis, insertion of  $\text{CO}$  into the nickel vinyl bond results in an  $\eta^2$ -acryloyl  $\text{Ni}(\text{O})$  species in which the hybrid ligand has undergone further rearrangement to an imidate structure.

Some of the rhodium and iridium amidophosphines,  $[\text{M}(\text{L})\text{N}(\text{SiMe}_2\text{CH}_2\text{PPh}_2)_2]$  ( $\text{M} = \text{Rh}, \text{L} = \eta^2\text{-C}_8\text{H}_{14}, \text{PPh}_3$ ;  $\text{M} = \text{Ir}, \text{L} = \eta^2\text{-C}_8\text{H}_{14}, \text{C}_2\text{H}_4$ ) and  $[\text{M}(\text{COD})\text{N}(\text{C}_6\text{H}_5\text{CH}_2)(\text{SiMe}_2\text{CH}_2\text{PPh}_2)]$  ( $\text{M} = \text{Rh}, \text{Ir}$ ) are catalyst precursors for the homogeneous hydrogenation of simple olefins under mild conditions (1 atm.  $\text{H}_2$ ,  $22^\circ\text{C}$ ). For the rhodium amido phosphines, olefin isomerization is a competing process with hydrogenation, whereas with  $[\text{Ir}(\eta^2\text{-C}_8\text{H}_{14})\text{N}(\text{SiMe}_2\text{CH}_2\text{PPh}_2)_2]$  only straightforward reduction is observed.

A number of iridium(III) amido phosphine hydrides has been prepared. The five-coordinate, 16-electron complex  $[\text{Ir}(\text{H})_2\text{N}(\text{SiMe}_2\text{CH}_2\text{PPh}_2)_2]$ , formed from  $[\text{Ir}(\eta^2\text{-C}_8\text{H}_{14})\text{N}(\text{SiMe}_2\text{CH}_2\text{PPh}_2)_2]$  under dihydrogen, reacts readily with neutral ligands to stereoselectively produce mer cis- $[\text{Ir}(\text{H})_2(\text{L})\text{N}(\text{SiMe}_2\text{CH}_2\text{PPh}_2)_2]$  ( $\text{L} = \text{CO}, \text{PMe}_3$ ). Oxidative addition of dihydrogen to  $[\text{Ir}(\text{L})\text{N}(\text{SiMe}_2\text{CH}_2\text{PPh}_2)_2]$  ( $\text{L} = \text{PMe}_3, \text{PPh}_3$ ) produces hydride derivatives in which the tridentate ligand is coordinated facially. X-ray analysis of fac cis- $[\text{Ir}(\text{H})_2(\text{PMe}_3)\text{N}(\text{SiMe}_2\text{CH}_2\text{PPh}_2)_2]$  has provided conclusive evidence for this

facial stereochemistry. The amine trihydrides fac and mer- $[\text{Ir}(\text{H})_3\text{NH}(\text{Si}-\text{Me}_2\text{CH}_2\text{PPh}_2)_2]$  have been characterized; their formation formally corresponds to a ligand-assisted heterolytic cleavage of dihydrogen.

Table of Contents

	Page
Abstract	ii
Table of Contents	v
List of Figures	viii
List of Tables	xi
Glossary of Abbreviations	xiii
Acknowledgement	xv
Introduction	1
<u>Chapter I</u>	3
Transition Metal Dialkyl Amides and Bis(Trimethyl silyl)	3
Amides: Synthesis, Structure and Bonding	
Hybrid Amido Phosphine Ligands	15
Amido Phosphine Complexes of the Nickel Triad	20
Amido Phosphines of Rhodium and Iridium	35
<u>Chapter II</u>	41
Migratory Insertion of Carbon Monoxide into Metal-Carbon	41
Bonds	
Migratory Insertion of Carbon Monoxide into Nickel(II)-	45
Carbon Bonds	
Ancillary Ligand Rearrangements Promoted by the Migratory	47
Insertion of Carbon Monoxide into Nickel(II)-Carbon Bonds	
Migratory Insertion of Carbon Monoxide into Palladium(II)-	69
Carbon Bonds	

	Page
<u>Chapter III</u>	72
Homogeneous Catalytic Hydrogenation of Olefins	72
Employing Rhodium and Iridium Complexes:	
General Principles	
Dihydride Catalysts	76
Monohydride Catalysts	80
Homogeneous Catalytic Hydrogenation using Rhodium and	82
Iridium Amido Phosphines	
<u>Chapter IV</u>	94
Oxidative Addition of Dihydrogen to Square-Planar Iridium(I)	94
Complexes	
Stereoselective Formation of Iridium(III) Amides and	102
Ligand-Assisted Heterolytic Splitting of Dihydrogen	
Stereoselective Ligand Additions to $[\text{Ir}(\text{H})_2\text{N}(\text{SiMe}_2\text{CH}_2\text{PPh}_2)_2]$	112
Oxidative Addition of Dihydrogen to $[\text{IrLN}(\text{SiMe}_2\text{CH}_2\text{PPh}_2)_2]$	116
(L = CO, $\text{PMe}_3$ , $\text{PPh}_3$ )	
Spectral Trends in the Stereochemical Assignment of	123
Iridium(III) Amido Phosphine Hydrides	
Hydrido Intermediates Involved in Catalytic Hydrogenations	126
using Rhodium and Iridium Amido Phosphines	
<u>Chapter V</u>	
Experimental: General Information	128
Preparation of the Hybrid Ligands	130

	Page
Amido Phosphine Complexes of the Nickel Triad	133
Conversion of Ni(II), Pd(II), and Pt(II) dichloro amino diphosphines to the corresponding chloro amido diphosphines	136
Alkyl Derivatives of the Ni(II) and P(II) Amido Phosphines	136
Carbonylation Reactions	139
Amido Phosphine Complexes of Rhodium and Iridium	142
Hydrogenation Procedure	147
Iridium(III) Amido Phosphine and Amine Trihydrides	147
References	155
<u>Appendix:</u> Crystallographic Data	163

List of Figures

		page
<u>Fig. 1.1</u>	Transition metal complexes incorporating bis(trimethyl silyl) amide ligands; shaded areas represent metals for which these derivatives have been characterized.	5
<u>Fig. 1.2</u>	$\pi$ -Bonding in a transition metal dialkyl amide complex.	9
<u>Fig. 1.3</u>	Structure of $[\text{Cr}(\text{NPr}_2)_3]$ (reproduced with permission).	12
<u>Fig. 1.4</u>	Structure of $[\text{Mn}\{\text{N}(\text{SiMe}_3)_2\}_2\text{THF}]$ (reproduced with permission).	14
<u>Fig. 1.5</u>	Structure of $[\text{Mn}\{\text{N}(\text{SiMe}_3)_2\}_2]_2$ (reproduced with permission).	14
<u>Fig. 1.6</u>	Structure of $[\text{NiN}(\text{SiMe}_3)_2(\text{PPh}_3)_2]$ (reproduced with permission).	14
<u>Fig. 1.7</u>	Structure of $\{\text{LiN}(\text{SiMe}_3)_2\}_3$ (reproduced with permission).	18
<u>Fig. 1.8</u>	$^1\text{HNMR}$ (100 MHz) spectrum of $[\text{NiClN}(\text{SiMe}_2\text{CH}_2\text{PPh}_2)_2]$ in $\text{C}_7\text{D}_8$ .	22
<u>Fig. 1.9</u>	X-ray crystal structure of $[\text{NiClN}(\text{SiMe}_2\text{CH}_2\text{PPh}_2)_2]$ .	23
<u>Fig. 1.10</u>	Proposed conformational flipping of ligand backbone of $[\text{NiClN}(\text{SiMe}_2\text{CH}_2\text{PPh}_2)_2]$ in solution.	25
<u>Fig. 1.11</u>	X-ray crystal structure of $[\text{PdClN}(\text{SiMe}_2\text{CH}_2\text{PPh}_2)_2]$ .	27
<u>Fig. 1.12</u>	$^1\text{HNMR}$ (80 MHz) spectrum of $[\text{PtClN}(\text{SiMe}_2\text{CH}_2\text{PPh}_2)_2]$ in $\text{C}_6\text{D}_6$ .	30
<u>Fig. 1.13</u>	X-ray crystal structure of $[\text{NiCl}_2\text{NH}(\text{SiMe}_2\text{CH}_2\text{PPh}_2)_2]$ .	32
<u>Fig. 1.14</u>	a) Structure of $[\text{PdCl}_2(\text{tBu})_2\text{P}(\text{CH}_2)_5\text{P}(\text{tBu})_2]_2$ . b) Possible dimeric structure of $^2[\text{PdCl}_2\text{NH}(\text{SiMe}_2\text{CH}_2\text{PPh}_2)_2]$ .	34
<u>Fig. 1.15</u>	$^1\text{HNMR}$ (100 MHz) spectrum of $[\text{Rh}(\text{C}_2\text{H}_4)\text{N}(\text{SiMe}_2\text{CH}_2\text{PPh}_2)_2]$ in $\text{C}_6\text{D}_6$ .	37
<u>Fig. 1.16</u>	$^1\text{HNMR}$ (400 MHz) spectrum of $[\text{Rh}(\text{COD})\text{N}(\text{C}_6\text{H}_5\text{CH}_2)(\text{SiMe}_2\text{CH}_2\text{PPh}_2)]$ in $\text{C}_6\text{D}_6$ .	40

		Page
<u>Fig. 2.1</u>	$^1\text{H}$ NMR (80 MHz) spectrum of $[\text{Ni}(\text{CH}_3)\text{N}(\text{SiMe}_2\text{CH}_2\text{PPh}_2)_2]$ in $\text{C}_7\text{D}_8$ .	49
<u>Fig. 2.2</u>	$^1\text{H}$ NMR (80 MHz) spectrum of $[\text{Ni}(\text{CH}=\text{CH}_2)\text{N}(\text{SiMe}_2\text{CH}_2\text{PPh}_2)_2]$ in $\text{C}_6\text{D}_6$	49
<u>Fig. 2.3</u>	$^1\text{H}$ NMR (80 MHz) spectrum of $[\text{Ni}(\text{CO})_2\text{N}(\text{COCH}_3)(\text{SiMe}_2\text{CH}_2\text{-PPh}_2)_2]$ in $\text{C}_7\text{D}_8$ .	51
<u>Fig. 2.4</u>	IR(KBr disc) spectrum of $[\text{Ni}(\text{CO})_2\text{N}(\text{COCH}_3)(\text{SiMe}_2\text{CH}_2\text{-PPh}_2)_2]$ .	51
<u>Fig. 2.5</u>	$^1\text{H}$ NMR (80 MHz) spectrum of $[\text{Ni}(\text{COC}_6\text{H}_5)\text{N}(\text{SiMe}_2\text{CH}_2\text{-PPh}_2)_2]$ in $\text{C}_6\text{D}_6$ .	55
<u>Fig. 2.6</u>	a) $^1\text{H}$ NMR (80 MHz) spectrum of $[\text{Ni}(\text{COCH}_3)\text{N}(\text{SiMe}_2\text{CH}_2\text{-PPh}_2)_2]$ in $\text{C}_7\text{D}_8$ at 298°K.	57
	b) $^1\text{H}$ NMR (80 MHz) spectrum of $[\text{Ni}(\text{COCH}_3)\text{N}(\text{SiMe}_2\text{CH}_2\text{-PPh}_2)_2]$ in $\text{C}_7\text{D}_8$ at 243°K.	57
<u>Fig. 2.7</u>	$^1\text{H}$ NMR (400 MHz) spectrum of $[\text{Ni}(\text{CO})\text{N}(\text{COC}_2\text{H}_3)(\text{SiMe}_2\text{CH}_2\text{-PPh}_2)_2]$ in $\text{C}_6\text{D}_6$ .	59
<u>Fig. 2.8</u>	a) Vinyl proton region (400 MHz $^1\text{H}$ NMR) of $[\text{Ni}(\text{CO})\text{N}(\text{COC}_2\text{H}_3)(\text{SiMe}_2\text{CH}_2\text{-PPh}_2)_2]$	59
	b) Spectral simulation of vinyl proton ABCXY pattern: $J_{1,3} = 11.72$ , $J_{2,3} = 7.57$ , $J_{1,p1} = 6.59$ , $J_{1,p2} = 1.46$ , $J_{3,p1} = 13.92$ , $J_{3,p2} = 3.17$ , $J_{2,p2} = 4.15$ .	59
<u>Fig. 2.9</u>	X-ray crystal structure of $[\text{Ni}(\text{CO})\text{N}(\text{COC}_2\text{H}_3)(\text{SiMe}_2\text{CH}_2\text{-PPh}_2)_2]$ . (alternate chelate ring conformation is indicated by unshaded thermal ellipsoids).	61
<u>Fig. 2.10</u>	$\pi$ -system of the $\text{Ni}(0) \eta^2$ -acryloyl complex ( imidate tautomer ).	66
<u>Fig. 3.1</u>	Orbital representation of dihydrogen activation by a transition metal complex.	73
<u>Fig. 3.2</u>	Hydrogenation profile for reaction of 1-hexene with $[\text{Rh}(\text{PPh}_3)\text{N}(\text{SiMe}_2\text{CH}_2\text{PPh}_2)_2]$ (1 atm. $\text{H}_2$ , 22°C).	85
<u>Fig. 3.3</u>	Hydrogenation profile for reaction of 1-hexene with $[\text{Ir}(\text{COD})\text{N}(\text{C}_6\text{H}_5\text{CH}_2)(\text{SiMe}_2\text{CH}_2\text{PPh}_2)_2]$ (1 atm. $\text{H}_2$ , 22°C).	86
<u>Fig. 3.4</u>	Hydrogenation profile for reaction of 1-hexene with $[\text{Ir}(\text{COE})\text{N}(\text{SiMe}_2\text{CH}_2\text{PPh}_2)_2]$ (1 atm. $\text{H}_2$ , 22°C).	88

<u>Fig. 4.1</u>	General mechanism for oxidative additions involving Vaska-type complexes, $[\text{Ir}(\text{CO})\text{Cl}(\text{PR}_3)_2]$ .	98
<u>Fig. 4.2</u>	Proposed mechanism for the oxidative addition of dihydrogen to $[\text{Ir}(\text{CO})(\sigma\text{-carb})(\text{PPh}_3)_2]$ .	100
<u>Fig. 4.3</u>	$^1\text{H}$ NMR (80 MHz) spectrum of $[\text{Ir}(\text{H})_2\text{N}(\text{SiMe}_2\text{CH}_2\text{PPh}_2)_2]$ in $\text{C}_6\text{D}_6$ .	103
<u>Fig. 4.4</u>	$^1\text{H}$ NMR (270 MHz) spectrum <i>mer</i> - $[\text{Ir}(\text{H})_3\text{NH}(\text{SiMe}_2\text{CH}_2\text{PPh}_2)_2]$ in $\text{C}_6\text{D}_6$ .	105
<u>Fig. 4.5</u>	a) $^1\text{H}$ NMR (400 MHz) spectrum of <i>fac</i> - $[\text{Ir}(\text{H})_3\text{NH}(\text{SiMe}_2\text{CH}_2\text{PPh}_2)_2]$ in $\text{C}_6\text{D}_6$ . b) Hydride region (400 MHz $^1\text{H}$ NMR) of <i>fac</i> - $[\text{Ir}(\text{H})_3\text{NH}(\text{SiMe}_2\text{CH}_2\text{PPh}_2)_2]$ . c) Spectral simulation of hydride AA'MXX' pattern: $^2J_{\text{A},\text{A}'} = 2.2$ , $^2J_{\text{A},\text{M}} = ^2J_{\text{A}',\text{M}} = 5.5$ , $^2J_{\text{A},\text{X}} = ^2J_{\text{A}',\text{X}} = -19.0$ , $^2J_{\text{M},\text{X}} = ^2J_{\text{M},\text{X}'} = 14.0$ , $^2J_{\text{A},\text{X}'} = ^2J_{\text{A}',\text{X}} = 130.0$ , $^2J_{\text{X},\text{X}'} = 1.0$ .	107 107 107
<u>Fig. 4.6</u>	$^1\text{H}$ NMR (400 MHz) spectrum of <i>mer cis</i> - $[\text{Ir}(\text{H})_2(\text{PMe}_3)\text{N}(\text{SiMe}_2\text{CH}_2\text{PPh}_2)_2]$ in $\text{C}_6\text{D}_6$ .	114
<u>Fig. 4.7</u>	a) Hydride region (400 MHz $^1\text{H}$ NMR) of <i>fac</i> - $[\text{Ir}(\text{H})_2(\text{PMe}_3)\text{N}(\text{SiMe}_2\text{CH}_2\text{PPh}_2)_2]$ . b) Spectral simulation of hydride AA'XX'Y pattern: $^2J_{\text{A},\text{X}} = ^2J_{\text{A}',\text{X}} = -21.0$ , $^2J_{\text{A},\text{Y}} = ^2J_{\text{A}',\text{Y}} = 21.0$ , $^2J_{\text{A},\text{X}'} = ^2J_{\text{A}',\text{X}'} = 147.0$ , $^2J_{\text{A},\text{A}'} = 4.0$ , $^2J_{\text{X},\text{Y}} = 9.0$ , $^2J_{\text{X},\text{X}'} = 4.0$ .	118 118
<u>Fig. 4.8</u>	X-ray crystal structure of <i>fac</i> - $[\text{Ir}(\text{H})_2(\text{PMe}_3)\text{N}(\text{SiMe}_2\text{CH}_2\text{PPh}_2)_2]$	119
<u>Fig. 4.9</u>	Proposed mechanism for the oxidative addition of dihydrogen to $[\text{Ir}(\text{L})\text{N}(\text{SiMe}_2\text{CH}_2\text{PPh}_2)_2]$ .	122

List of Tables

		page
<u>Table I</u>	Crystallographic data for the Group VIII metal bis (trimethyl silyl) amides and amido phosphines	29
<u>Table II</u>	$^1\text{H}$ NMR data for: $(\text{Ph}_2\text{PCH}_2\text{SiMe}_2)_2\text{NH}$ $\text{LiN}(\text{SiMe}_2\text{CH}_2\text{PPh}_2)_2$ $[\text{MClN}(\text{SiMe}_2\text{CH}_2\text{PPh}_2)_2]$ (M = Ni, Pd, Pt) $[\text{Ni}(\text{R})\text{N}(\text{SiMe}_2\text{CH}_2\text{PPh}_2)_2]$ (R = CH <sub>3</sub> , C <sub>2</sub> H <sub>3</sub> , C <sub>3</sub> H <sub>5</sub> , C <sub>6</sub> H <sub>5</sub> ) $[\text{Pd}(\text{R})\text{N}(\text{SiMe}_2\text{CH}_2\text{PPh}_2)_2]$ (R = CH <sub>3</sub> , C <sub>3</sub> H <sub>5</sub> ) $[\text{Ni}(\text{CN})\text{N}(\text{SiMe}_2\text{CH}_2\text{PPh}_2)_2]$	151
<u>Table III</u>	$^1\text{H}$ NMR data for: $[\text{Ni}(\text{CO})_2\text{N}(\text{COR})(\text{SiMe}_2\text{CH}_2\text{PPh}_2)_2]$ (R = CH <sub>3</sub> , C <sub>2</sub> H <sub>3</sub> , C <sub>3</sub> H <sub>5</sub> , C <sub>6</sub> H <sub>5</sub> ) $[\text{Ni}(\text{COR})\text{N}(\text{SiMe}_2\text{CH}_2\text{PPh}_2)_2]$ (R = CH <sub>3</sub> , C <sub>6</sub> H <sub>5</sub> ) $[\text{Ni}(\text{CO})\text{N}(\text{COC}_2\text{H}_3)(\text{SiMe}_2\text{CH}_2\text{PPh}_2)_2]$ $[\text{Pd}(\text{COCH}_3)\text{N}(\text{SiMe}_2\text{CH}_2\text{PPh}_2)_2]$	152
<u>Table IV</u>	$^1\text{H}$ NMR data for: $[\text{Ir}(\text{L})\text{N}(\text{SiMe}_2\text{CH}_2\text{PPh}_2)_2]$ (L = CO, C <sub>2</sub> H <sub>4</sub> , C <sub>8</sub> H <sub>14</sub> , PMe <sub>3</sub> , PPh <sub>3</sub> ) $[\text{Rh}(\text{L})\text{N}(\text{SiMe}_2\text{CH}_2\text{PPh}_2)_2]$ (L = CO, C <sub>2</sub> H <sub>4</sub> , C <sub>8</sub> H <sub>14</sub> , PMe <sub>3</sub> , PPh <sub>3</sub> ) $[\text{M}(\text{C}_8\text{H}_{12})\text{N}(\text{SiMe}_2\text{CH}_2\text{PPh}_2)_2]$ (M = Rh, Ir)	153

<u>Table V</u>	<sup>1</sup> HNMR data for: [Ir(H) <sub>2</sub> N(SiMe <sub>2</sub> CH <sub>2</sub> PPh <sub>2</sub> ) <sub>2</sub> ] <u>mer</u> and <u>fac</u> -[Ir(H) <sub>3</sub> NH(SiMe <sub>2</sub> CH <sub>2</sub> PPh <sub>2</sub> ) <sub>2</sub> ] <u>mer cis</u> -[Ir(L)(H) <sub>2</sub> N(SiMe <sub>2</sub> CH <sub>2</sub> PPh <sub>2</sub> ) <sub>2</sub> ] (L = CO, PMe <sub>3</sub> ) <u>mer trans</u> -[Ir(H) <sub>2</sub> (CO)N(SiMe <sub>2</sub> CH <sub>2</sub> PPh <sub>2</sub> ) <sub>2</sub> ] <u>fac cis</u> -[Ir(H) <sub>2</sub> (PMe <sub>3</sub> )N(SiMe <sub>2</sub> CH <sub>2</sub> PPh <sub>2</sub> ) <sub>2</sub> ]	
<u>Table VI</u>	Bond lengths for [NiClN(SiMe <sub>2</sub> CH <sub>2</sub> PPh <sub>2</sub> ) <sub>2</sub> ]	164
<u>Table VII</u>	Bond lengths for [PdClN(SiMe <sub>2</sub> CH <sub>2</sub> PPh <sub>2</sub> ) <sub>2</sub> ]·C <sub>7</sub> H <sub>8</sub>	165
<u>Table VIII</u>	Bond lengths for [NiCl <sub>2</sub> NH(SiMe <sub>2</sub> CH <sub>2</sub> PPh <sub>2</sub> ) <sub>2</sub> ]	166
<u>Table IX</u>	Bond lengths for [Ni(CO)N(COC <sub>2</sub> H <sub>3</sub> )(SiMe <sub>2</sub> CH <sub>2</sub> PPh <sub>2</sub> ) <sub>2</sub> ]	167
<u>Table X</u>	Bond lengths for <u>fac</u> -[Ir(H) <sub>2</sub> (PMe <sub>3</sub> )N(SiMe <sub>2</sub> CH <sub>2</sub> PPh <sub>2</sub> ) <sub>2</sub> ]	168
<u>Table XI</u>	Bond angles for [NiClN(SiMe <sub>2</sub> CH <sub>2</sub> PPh <sub>2</sub> ) <sub>2</sub> ]	169
<u>Table XII</u>	Bond angles for [PdClN(SiMe <sub>2</sub> CH <sub>2</sub> PPh <sub>2</sub> ) <sub>2</sub> ]·C <sub>7</sub> H <sub>8</sub>	170
<u>Table XIII</u>	Bond angles for [NiCl <sub>2</sub> NH(SiMe <sub>2</sub> CH <sub>2</sub> PPh <sub>2</sub> ) <sub>2</sub> ]	171
<u>Table XIV</u>	Bond angles for [Ni(CO)N(COC <sub>2</sub> H <sub>3</sub> )(SiMe <sub>2</sub> CH <sub>2</sub> PPh <sub>2</sub> ) <sub>2</sub> ]	172
<u>Table XV</u>	Bond angles for <u>fac</u> -[Ir(H) <sub>2</sub> (PMe <sub>3</sub> )N(SiMe <sub>2</sub> CH <sub>2</sub> PPh <sub>2</sub> ) <sub>2</sub> ]	173

### Glossary of Abbreviations

Å	angstrom unit, $10^{-8}$ cm
br	broad
n-Bu	n-butyl
$\text{cm}^{-1}$	wave number
COA	cyclooctane, $\text{C}_8\text{H}_{16}$
COE	cyclooctene, $\text{C}_8\text{H}_{14}$
COD	cyclooctadiene, $\text{C}_8\text{H}_{12}$
$\text{Cp}^*$	pentamethyl cyclopentadienyl, $(\text{CH}_3)_5\text{C}_5$
d	doublet
dec	decomposition
diphos	1,2-bis(diphenylphosphino)ethane, dppe
DME	dimethoxyethane
dmpe	1,2-bis(dimethylphosphino)ethane
$d^n$	formal d-electron configuration
dt	doublet of triplets
Et	ethyl, $\text{C}_2\text{H}_5$
fac	facial
gem	geminal
{H}	proton decoupled (NMR)
HOMO	highest occupied molecular orbital
Hz	hertz, $\text{sec}^{-1}$
IR	infra-red
J	coupling constant

$J_{\text{app}}$	apparent coupling constant (virtual coupling)
L	a neutral unidentate ligand
LUMO	lowest unoccupied molecular orbital
m	moderate intensity (IR) multiplet (NMR)
M	the central metal atom in a complex
Me	methyl, $\text{CH}_3$
mer	meridional
ml	millilitre
NMR	nuclear magnetic resonance
ol	olefin
Ph	phenyl, $\text{C}_6\text{H}_5$
ppm	chemical shift in parts per million
py	pyridine
quart	quartet
quint	quintet
R	an alkyl group
t	triplet
THF	tetrahydrofuran
$\nu$	stretching frequency (in $\text{cm}^{-1}$ )
X	an anionic ligand (usually halide)
s	strong intensity (IR) singlet (NMR)
w	weak intensity

### Acknowledgement

I would like to express my appreciation to my research supervisor, Dr. Michael Fryzuk, for his encouragement, enthusiasm, patience, and instruction which have provided a productive and enjoyable atmosphere in which to work.

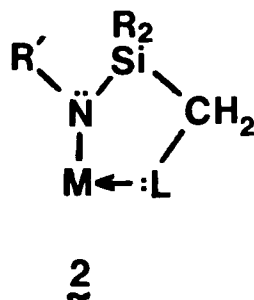
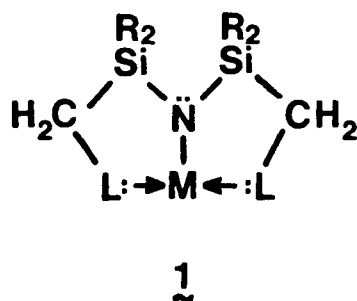
A special thanks to Dr. Axel Westerhaus for his interesting ideas and discussions, and especially, for his refreshing perspective on chemistry.

## Introduction

Since even subtle variations in ligand design can be manifested in drastic steric and electronic changes in their transition metal complexes, a great deal of research has been devoted to the synthesis of new ligands. As a result, many different ligands possessing a wide range of donor atoms (C, O, H, P, N, S etc.) are known.

A rather useful, if somewhat inaccurate, means of ligand classification, involves designation (on the basis of the donor atom(s)) as either "hard" or "soft". According to the hard-soft acid-base theory (HSAB)<sup>1</sup>, hard bases prefer to bind to hard acids and soft bases to soft acids. Generally, transition metals follow this rule as evidenced by the fact that soft tertiary phosphines form relatively few derivatives of the hard, early transition metals<sup>2,3,4,5</sup> (Ti, Zr, Hf, V, Nb, Ta). In contrast, phosphine complexes of the later transition metals are legion<sup>6,7,8</sup>. However, the hard amido ligand is quite common for the early metals, whereas few stable Group VIII amides are known<sup>9</sup>.

An alternative ligand system is the hybrid ligand. The term "hybrid" has been previously used by Sacconi<sup>10</sup> and others<sup>11,12</sup> to describe mixed donor ligands containing both phosphine and amine centres. However, in this account "hybrid" is used in a slightly different context, referring to the fact that the target ligands possess both hard and soft donor atoms arranged in a chelating fashion. Two such possible metal chelates are illustrated below in structures 1 and 2. The tridentate hybrid ligand 1 can be formally classified as a uninegative six-electron donor and, as such, can be likened to the ubiquitous cyclopentadienyl group,  $\eta^5\text{-C}_5\text{H}_5^-$ .



Similarly, the bidentate  $\lambda$  resembles the allyl ligand,  $\eta^3\text{-C}_3\text{H}_5^-$ , in that both are uninegative four-electron donors. In these examples, the amido function acts as the hard donor while L represents a variety of soft donors, such as tertiary phosphines, arsines, olefins, thioethers, and isocyanides.

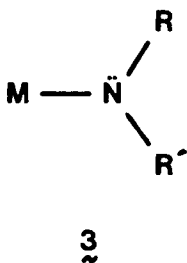
The impetus to the design of these hybrid ligands lies in their dual character of donor types. It would be expected that such ligands would be acceptable for a wide range of transition metals. Use of the chelate effect<sup>13</sup> should ensure multidenticity, especially where mismatching of hard/soft pairs is concerned. In addition, new reactivity should be observed in their transition metal derivatives, as compared to the analogous complexes of the monodentate donors. These proposals have indeed proven to be correct. Although this account is concerned only with hybrid amido phosphine complexes of the Group VIII metals, the coordination chemistry and reactivity of zirconium and hafnium amido phosphines have also been investigated<sup>14,15</sup>.

## Chapter I

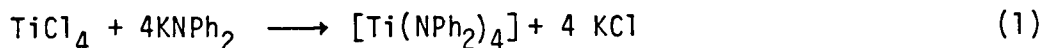
### Transition Metal Dialkyl Amides and Bis(Trimethylsilyl) Amides

#### Synthesis

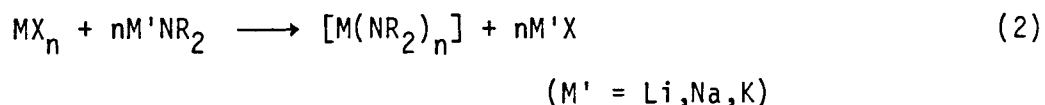
Although isoelectronic with the ubiquitous alkyl group, the amide donor ( $-\text{NR}_2$ ) has achieved far less prominence as a transition metal ligand. It would appear that this is in part due to the significance of transition metal alkyls as reactive intermediates in many important catalytic processes<sup>16</sup> (for example, Fischer-Tropsch reactions, hydroformylation, Monsanto's acetic acid synthesis). However, stable amide complexes have been obtained for most of the elements. The majority are molecular compounds containing the basic structural unit shown below in 3.



The first transition metal amide,  $[\text{Ti}(\text{NPh}_2)_4]$ , was prepared by Dermer and Fernelius<sup>17</sup> in 1935 via the metathesis reaction outlined in equation 1.

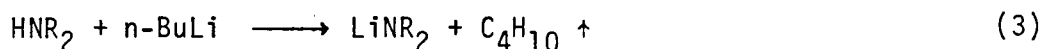


In fact, most transition metal amides are prepared by such a metathetical exchange between an alkali amide and a metal halide (equation 2). This



route has been employed to synthesize amide complexes for practically the entire transition series.

The extensive use of this preparative method lies in the facile formation of the required alkali amides; in particular lithio dialkyl amides and bis(trimethylsilyl) amides are readily prepared from the corresponding amine and n-butyllithium (equation 3). Most of the alkyl and aryl lithium salts are stable, colorless solids which have low solubility



in organic solvents; in contrast, the bis(trimethylsilyl) analogues are very soluble in a variety of organic solvents. It should be noted that one of the most extensively used methods for the formation of transition metal alkyls also involves a metathetical exchange between the corresponding lithium alkyl or Grignard reagent and a metal halide.

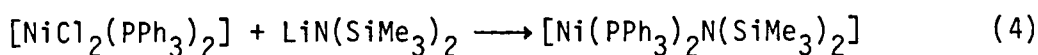
Metathesis, as in equation 2, was employed by Burger and Wannagat<sup>18</sup> in 1965 to synthesize the first transition metal bis(trimethylsilyl)amide

derivatives, having the formula  $[M\{N(SiMe_3)_2\}_3]$  ( $M = Cr, Fe$ ) and  $[M\{N(SiMe_3)_2\}_2]$  ( $M = Mn, Co, Ni$ ). Since then, bis(trimethylsilyl)amides of most of the transition metals have been obtained (Fig. 1.1)

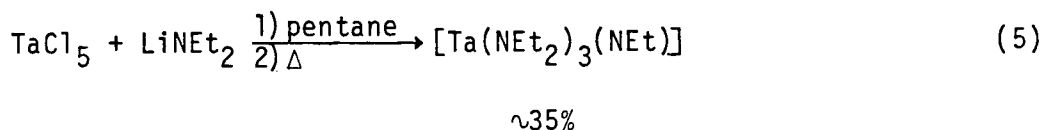
22 Ti	23 V	24 Cr	25 Mn	26 Fe	27 Co	28 Ni	29 Cu
40 Zr	41 Nb	42 Mo	43 Tc	44 Ru	45 Rh	46 Pd	47 Ag
72 Hf	73 Ta	74 W	75 Re	76 Os	77 Ir	78 Pt	79 Au

Fig. 1.1 Transition metal complexes incorporating bis(trimethyl silyl) amide ligands; shaded areas represent metals for which these derivatives have been characterized

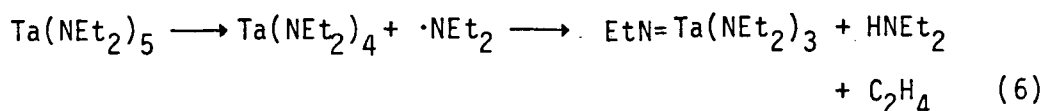
In some cases, metathetic synthesis of transition metal amides produces surprising results, such as a valency change of the metal or the formation of metal imides. An example of the former was reported by Bradley<sup>19</sup> in 1972; upon reaction of  $\text{LiN}(\text{SiMe}_3)_2$  with a Ni(II) halide, an unexpected Ni(I) species was isolated and crystallographically characterized (equation 4). Another interesting result is the formation of a tantalum



imide<sup>20</sup> upon reaction of  $\text{LiNEt}_2$  with  $\text{TaCl}_5$  (equation 5). Although the

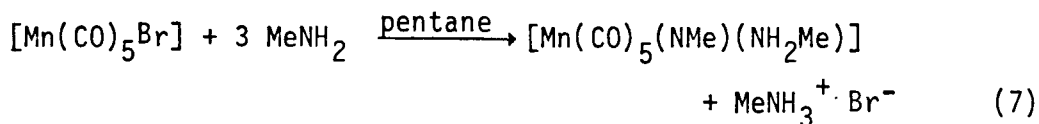


mechanism of this decomposition has not been fully elucidated, it is believed to occur via release of a diethyl amino radical from the expected pentakis compound, which then attacks the unstable quadrivalent  $\text{Ta}(\text{NEt})_4$  to produce the imide, diethylamine, and ethylene (equation 6).

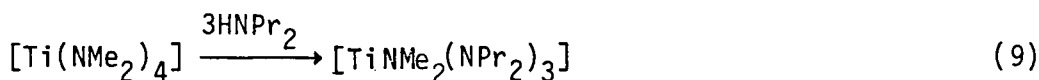
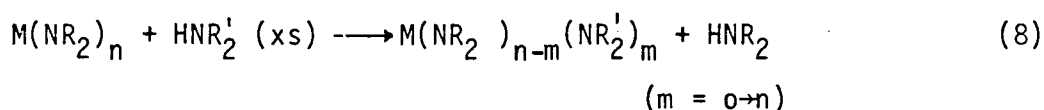


An alternative preparative route to transition metal amides involves reaction of a metal halide with an amine, with concomitant formation of amine hydrohalide. This method has been mainly applied to the early

transition metals in higher oxidation states. An example<sup>21</sup> is the formation of the manganese complex  $[\text{Mn}(\text{CO})_5(\text{NHMe})(\text{NH}_2\text{Me})]$  (equation 7).



Another possible, although seldom used, route to amido complexes is a type of "transamination" reaction, in which the more volatile amine is usually displaced (equation 8). However, the degree of displacement is largely controlled by steric factors. The synthesis of  $[\text{TiNMe}_2(\text{NPr})_3]$  serves to illustrate the utility of this method (equation 9)<sup>22</sup>.



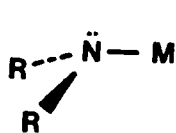
### Structure and Bonding

One useful classification of transition metal dialkylamides and bis(trimethylsilyl) amides involves designation as either homoleptic or heteroleptic. The former category include those derivatives containing only one type of ligand (eg.  $[\text{Cr}(\text{NPr}_2)_3]$ ) while the latter are complexes having amide as well as other donor ligands (eg.  $[\text{Co}\{\text{N}(\text{SiMe}_3)_2\}_2\text{PPh}_3]$ ). For the early transition metals, there are numerous examples of homoleptic species;

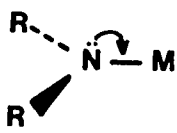
however, heterolepic complexes are far less common, a rather surprising fact in view of the wide variety of ancillary ligands possible. It is interesting to note that the exact opposite trend is observed for transition metal alkyls.

For both categories of amide complex, there are comparatively few examples of stable derivatives towards the right hand side of the transition series. This trend may be explained in part by noting that a potentially unfavorable bonding situation arises upon interaction of the "hard" amido function with a "soft" transition metal, such as  $\text{Pd}^{2+}$  or  $\text{Rh}^{1+}$ . On the basis of the hard-soft acid-base theory<sup>1</sup>, it is not surprising that amide complexes of the later transition metals would be destabilized, at least in comparison to those involving the early, "hard" transition metals (for example,  $\text{Zr}^{\text{IV}}$ ,  $\text{Nb}^{\text{V}}$ ). However, incorporation of silyl groups at nitrogen makes the amido ligand more polarizable. In fact, the bis(trimethylsilyl) amido ligand forms stable complexes with a number of transition metals in low oxidation states.

Other rationalizations for the paucity of amides of the later transition metals have centred on the bonding properties of the amide ligand. Three bonding modes can be envisioned for a  $\sigma$ -bonded alkylamido ligand. One possibility is approximately  $\text{sp}^3$  hybridization of the nitrogen, resulting in



4



5



6

a pyramidal geometry (4). Alternatively,  $d\pi-p\pi$  bonding of the nitrogen lone pair with metal d-orbitals of correct symmetry results in a trigonal-planar geometry at nitrogen (5). There are also amide derivatives in which the bridging structure (6) is involved, although this type of bonding may be prevented by using bulky R groups at nitrogen.

Since the amide moiety acts as both a two electron  $\sigma$ -donor as well as a two electron  $\pi$ -donor (Fig. 1.2), it would seem reasonable that the electron deficient early transition metals, which possess vacant d-orbitals, should form stronger metal-amide bonds than the electron rich metals towards the right of the periodic table.

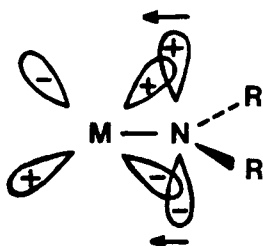
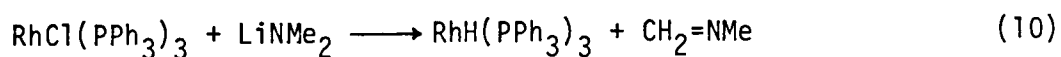


Fig. 1.2  $\pi$ -Bonding in a transition metal dialkyl amide complex

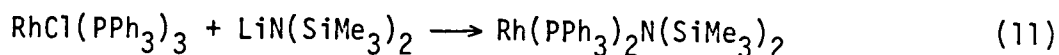
The importance of  $\pi$ -bonding is supported by the observation that bis(trimethylsilyl)amido derivatives of the later transition metals are significantly more stable than their dialkylamido analogues. Substantial evidence indicates that, for Si-N compounds, there is significant delocalization of the nitrogen lone pair into empty silicon d-orbitals, resulting in contraction of the Si-N bond length from the expected value of  $\sim 1.82 \text{ \AA}$ , for a Si-N  $\sigma$ -bond, to the observed values of  $1.65 - 1.75 \text{ \AA}$ . In addition, the structural data for  $\text{HN}(\text{SiH}_3)_2$ ,  $\text{HN}(\text{SiMe}_3)_2$ , and  $\text{F}_2\text{BN}(\text{SiH}_3)_2$ <sup>23</sup> indicate that all contain

nitrogen in a planar, rather than pyramidal environment; planarity of the  $\text{NSi}_2$  fragment would be necessary in order to maximize  $\pi$ -backbonding. As a consequence, it would be expected that the decreased  $\pi$ -donor ability of bis(trimethylsilyl)amides, as compared to dialkylamides, should tend to be more favorable for coordination with electron rich metals.

In addition to thermodynamic considerations, the inherent instability of amides of the late transition metals can be seen to be a result of available pathways for decomposition (ie. kinetic instability). It has long been known that, for alkyl groups possessing  $\beta$ -hydrogens,  $\beta$ -elimination of transition metal alkyls is a dominant, and often troublesome, mode of decomposition. The corresponding reaction with transition metal amides, resulting in formation of metal hydride and imine, had previously been considered as an insignificant process, since the amides of the early metals are all thermally stable at room temperature. In fact, purification is usually carried out by distillation or sublimation at high temperatures. However, dialkylamides of rhodium do indeed decompose via  $\beta$ -elimination of the metal amide bond (equation 10)<sup>24</sup>; as a result, rhodium dialkylamides have yet to be isolated. This decomposition route can be blocked through



the incorporation of an amido group having no  $\beta$ -hydrogens; thus, Lappert<sup>25</sup> isolated the first rhodium amide by coordination with the bis(trimethylsilyl) amido ligand (equation 11).



Even so, at room temperature, this complex loses hexamethyldisilazane, probably via an ortho metallation/reductive elimination sequence.

In addition to the amide's ability to form both  $\sigma$  and  $\pi$  bonds, the steric requirements of the substituents at nitrogen greatly influence the structures of transition metal amides. Homoleptic and heteroleptic derivatives having coordination numbers ranging from two to six have been prepared, the stoichiometry depending largely on the steric bulk of the ligand. Monomeric, four-coordinate complexes,  $[\text{M}(\text{NR}_2)_4]$  ( $\text{M} = \text{Ti}, \text{V}, \text{Mo}$ ), can even be obtained with the least sterically demanding dimethylamido ligand<sup>26</sup>. However, the analogous complexes of  $\text{Zr}^{\text{IV}}$  and  $\text{Hf}^{\text{IV}}$  are believed to be polymeric, both in solution and in the solid state, although the metal's exact coordination number is not known. The unstable dimethylamide derivatives of  $\text{Ti}(\text{III})$ ,  $\text{V}(\text{III})$ , and  $\text{Cr}(\text{III})$  are believed to be dimeric<sup>27,28,29</sup>, at least in solution. Higher coordination numbers have been observed, especially for the second and third row metals. X-ray diffraction analysis of  $\text{Nb}(\text{NMe}_2)_5$  has shown it to have a square pyramidal geometry<sup>30</sup> whereas  $\text{Ta}(\text{NEt}_2)_5$  is trigonal bipyramidal, undoubtedly a manifestation of the more bulky ethyl (vs. methyl) groups. A regular octahedral  $\text{WN}_6$  core is observed for the complex  $[\text{W}(\text{NMe}_2)_6]$ <sup>31</sup>.

The structure of the  $\text{Cr}(\text{III})$  complex<sup>32</sup>, given in Fig.13, is representative of a monomeric homoleptic dialkylamide. Note the planarity in all three amide units, as well as the fact that the Cr-N bond lengths

( $\sim 1.87 \text{ \AA}$ ) are significantly shorter than predicted ( $\sim 1.97 \text{ \AA}$ ).

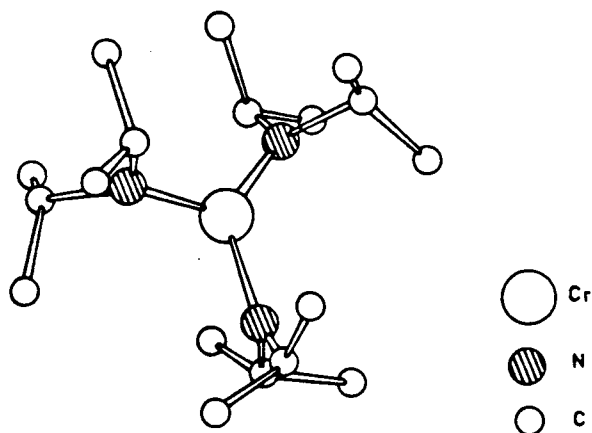


Fig. 1.3     Structure of  $[\text{Cr}(\text{NPr}_2)_3]$  (reproduced with permission)

As expected on the basis of both thermodynamic and kinetic considerations, bis(trimethylsilyl)amides of the later transition metals are considerably more robust than their dialkylamido analogues. Although not exactly ubiquitous, representative complexes include those of Mn(II), Fe(III), Ru(II), Co(I), Co(II), Ni(I), Ni(II), Rh(I), Ir(I), Cu(I), Ag(I), and Au(I). In all cases, these derivatives are prepared via reaction of an appropriate metal halide precursor with the lithium amide. In contrast, attempts at preparing simple dialkylamides of these metals have largely been unsuccessful. However, if the amido function is substituted with electron-withdrawing groups, such as in  $^-\text{NCl}_2$  or  $^-\text{N}(\text{CN})_2$ , isolable species of Mn(II), Fe(II), Co(II), Ni(II), Pt(IV), and

Cu(II) are obtained. Once again, this would appear to be a result of the reduced  $\sigma$ -basicity and/or  $\pi$ -donor ability of the amide nitrogen.

The Cr(III) complex shown in Fig. 1.3 also illustrates how a bulky amido ligand can be used to stabilize low coordination numbers. Especially remarkable in this regard is the bis(trimethylsilyl)amido ligand,  $^-\text{N}(\text{SiMe}_3)_2$ . Although typical coordination numbers for the lanthanides are eight through ten, monomeric three-coordinate complexes having the formula  $[\text{Ln}\{\text{N}(\text{SiMe}_3)_2\}_3]$  ( $\text{Ln} = \text{La}, \text{Ce}, \text{Pr}, \text{Nd}, \text{Sm}, \text{Eu}, \text{Gd}, \text{Ho}, \text{Yb}$  and  $\text{Lu}$ )<sup>33</sup> have been characterized. X-ray analysis has shown that the erbium and ytterbium derivatives have pyramidal  $\text{LnN}_3$  units, as compared to the trigonal-planar arrangement observed in three-coordinate transition metal amides.

In fact, the most common coordination number for the transition metal bis(trimethylsilyl)amides is the rather unusual three coordination. The pink Mn(II) complex,  $[\text{Mn}\{\text{N}(\text{SiMe}_3)_2\}_2\text{THF}]$ <sup>34</sup> (Fig. 1.4) is one such example; although quite thermally stable, the THF may be removed by heating at 120°C in vacuo, yielding a dimeric species,  $[\{\text{MnN}(\text{SiMe}_3)_2\}_2]$ <sup>35</sup> (Fig. 1.5). X-ray crystallographic analysis of the Fe(III) species,  $[\text{Fe}\{\text{N}(\text{SiMe}_3)_2\}_3]$ , has shown it to have a trigonal-planar structure<sup>36</sup>. Bradley and Hursthouse have also elaborated the structures of the related three-coordinate complexes,  $[\text{Co}\{\text{N}(\text{SiMe}_3)_2\}_2\text{PPh}_3]$ <sup>19</sup>,  $[\text{CoN}(\text{SiMe}_3)_2(\text{PPh}_3)_2]$ <sup>37</sup>, and  $[\text{NiN}(\text{SiMe}_3)_2(\text{PPh}_3)_2]$ <sup>19</sup> (Fig. 1.6). It is reasonable to assume that the Cu(I) complex,  $[\text{CuN}(\text{SiMe}_3)_2(\text{PPh}_3)_2]$ , has a very similar geometry to its Ni(I) and Co(I) analogues.

Two coordinate bis(trimethylsilyl)amides are also known. Burger and

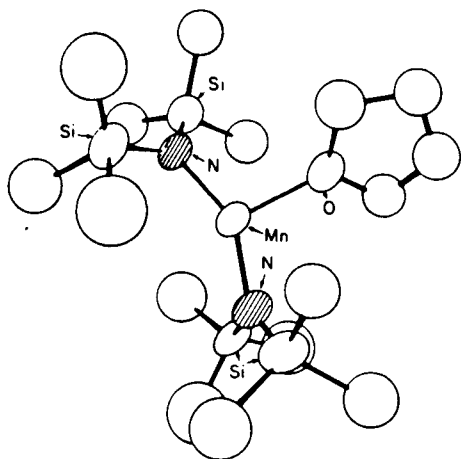


Fig. 1.4

Structure of  $[\text{Mn}\{\text{N}(\text{SiMe}_3)_2\}_2\cdot\text{THF}]$   
(reproduced with permission)

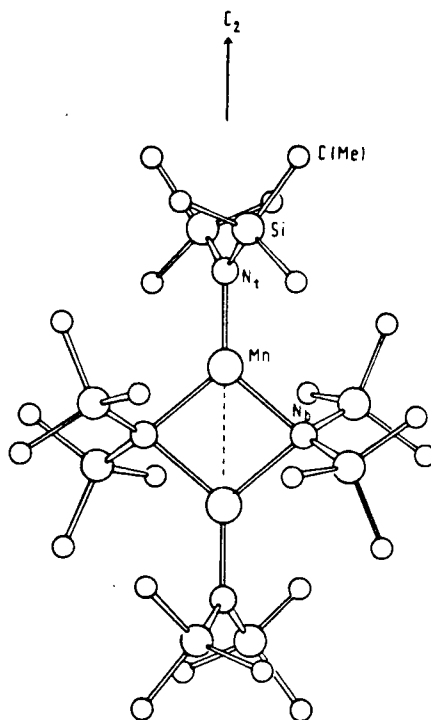


Fig. 1.5

Structure of  $[\text{Mn}\{\text{N}(\text{SiMe}_3)_2\}_2]_2$   
(reproduced with permission)

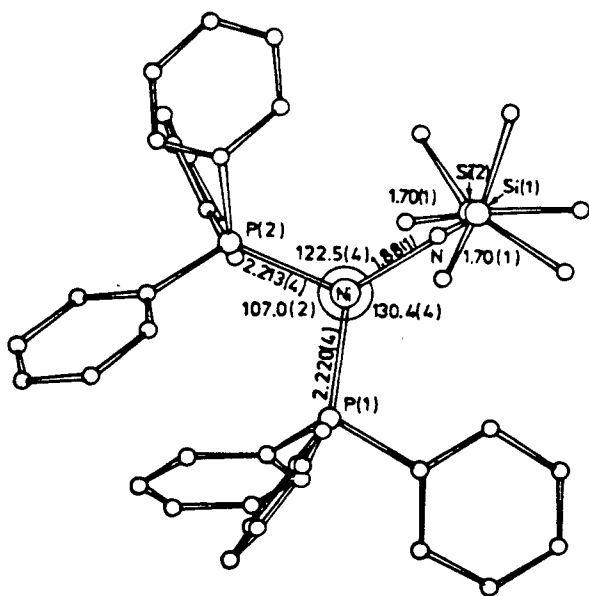


Fig. 1.6

Structure of  $[\text{NiN}(\text{SiMe}_3)_2(\text{PPh}_3)_2]$  (reproduced with permission)

Wannagat<sup>38</sup> have postulated a linear structure for the Ni(II)silyl amide,  $[\text{Ni}\{\text{N}(\text{SiMe}_3)_2\}_2]$ . Its isolation as a red oil has precluded definitive structural characterization. On the basis of IR, NMR and UV spectral information,  $[\text{Co}\{\text{N}(\text{SiMe}_3)_2\}_2]$ , is also linear<sup>39</sup>. Likewise, the two-coordinate Au(I) derivatives,  $[\text{AuN}(\text{SiMe}_3)_2\text{L}]$  ( $\text{L} = \text{PMe}_3, \text{PPh}_3, \text{AsPh}_3$ ) are expected to be linear<sup>40</sup>.

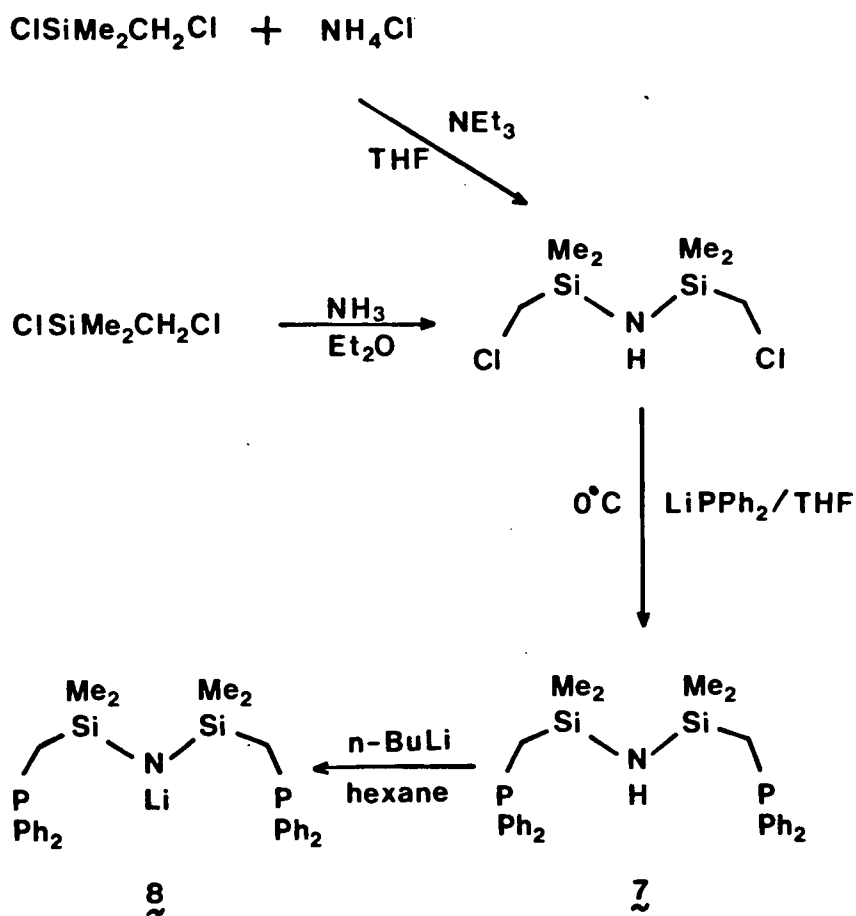
In summary, extensive x-ray crystallographic data for a wide variety of transition metal dialkylamides, indicates a planar, or nearly planar  $\text{NR}_2$  unit; this has been attributed to the contribution of  $d\pi\text{-}p\pi$  bonding at the metal. For the related bis(trimethylsilyl)amido complexes, the  $\text{Si}_2\text{N}$  moiety is invariably planar, probably as a consequence of similar  $\pi$ -backbonding,  $\text{Si}\text{---}\text{N}$ , involving the silicon centres. In addition to modifying the electronic properties of the amide nitrogen, the incorporation of sterically bulky silyl groups, having a necessarily planar arrangement, drastically affects the molecular geometry of its transition metal derivatives. As a result, not only does the use of bis(trimethylsilyl)amides allow for the stabilization of the later transition metal M-N bond, but also gives rise to complexes of unusually low coordination number.

#### Hybrid Amido Phosphine Ligands

Stabilization of Group VIII transition metal amide M-N bonds can be achieved through the incorporation of the amide function as part of a hybrid ligand. We have synthesized several such ligands; the preparation of the tridentate ligand  $\text{HN}(\text{SiMe}_2\text{CH}_2\text{PPh}_2)_2$ , **7**, is outlined in Scheme 1.1. The synthesis is particularly attractive in that it requires inexpensive,

readily available starting materials; the yields are very good (~80% overall), and, even though care must be taken to exclude oxygen and traces of water, the procedure is quite straightforward. Typically the ligand is produced on a 50 g scale via this route.

**Scheme 1.1**



The reaction proceeds by the dropwise addition of 1,3-bis (chloromethyl)tetramethyldisilazane to a cold THF solution of  $\text{LiPPh}_2$ . After work-

up, the product is recrystallized from minimum hexanes at  $-30^{\circ}\text{C}$  to give colorless crystals. This compound, as well as those which will be referred to later, has been fully characterized by usual spectroscopic means, i.e.  $^1\text{H}$ ,  $^{13}\text{C}$  and  $^{31}\text{P}$ NMR as well as IR and elemental analysis. In particular, the silyl methyl groups of **7** appear as a doublet ( $^4J_{\text{H,P}} = 1.0 \text{ Hz}$ ) due to long range coupling with phosphorous; this feature has been observed by Schore and others in related systems<sup>41,42</sup>.

The ligand is readily deprotonated with *n*-butyllithium in hexane to give its crystalline lithium salt, **8**. Molecular weight analysis of **8** by the Signer method<sup>43</sup> has indicated that it is trimeric in benzene solution. Although its structure has not been elucidated by X-ray crystallography, it would seem reasonable that, in the solid state, it should resemble that observed for the closely related  $\text{LiN}(\text{SiMe}_3)_2$  (Fig.1.7)<sup>44</sup>. However, lithio bis(trimethylsilyl)amide is dimeric in benzene; a comparison between these lithium salts is therefore somewhat tenuous. Spectroscopic analysis ( $^1\text{H}$  and  $^{31}\text{P}\{^1\text{H}\}$ NMR) of **8** has not been particularly enlightening, except as a means of assigning purity, since the  $^1\text{H}$ NMR and  $^{31}\text{P}\{^1\text{H}\}$  signals are rather broad.

Bidentate hybrid ligands have also been prepared; Scheme1.2 outlines the synthesis of  $\text{HN}(\text{PhCH}_2)(\text{SiMe}_2\text{CH}_2\text{PPh}_2)$ , **9**. High yields of this derivative may be obtained by reaction of  $\text{LiPPh}_2$  with  $\text{C}_6\text{H}_5\text{CH}_2\text{NH}(\text{SiMe}_2\text{CH}_2\text{Cl})$  in THF. Once again, the colorless crystalline lithium salt, **10**, is readily formed upon treatment of **9** with *n*-BuLi in hexane. However, this derivative differs from the tridentate **8** in that it is very thermally sensitive. Although stable at  $-30^{\circ}\text{C}$  for up to six months, storage at room temperature results in

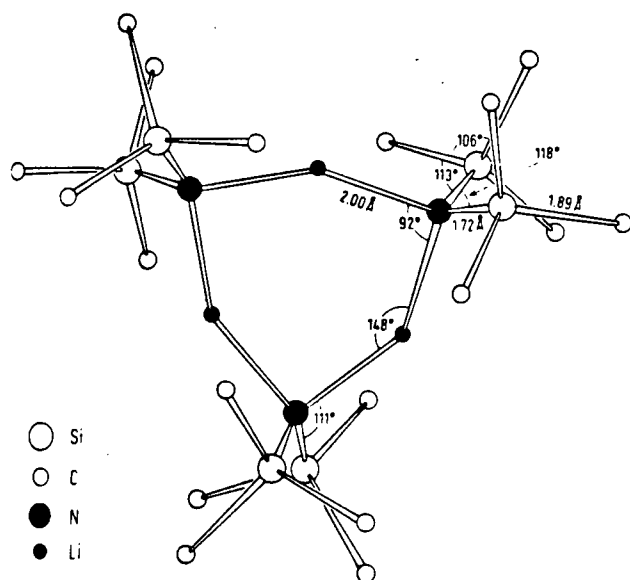
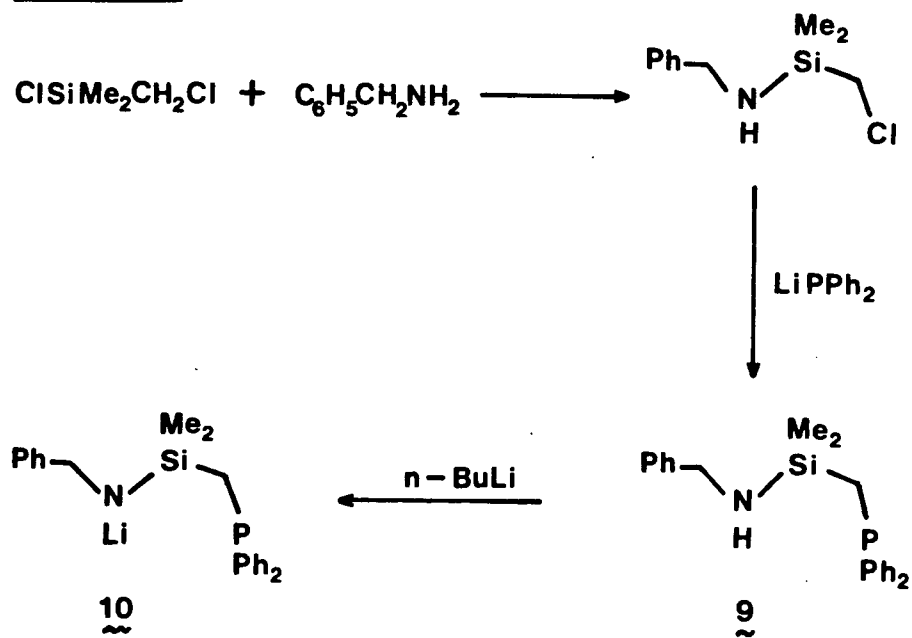


Fig. 1.7 Structure of  $\{\text{LiN}(\text{SiMe}_3)_2\}_3$  (reproduced with permission)

**Scheme 1.2**

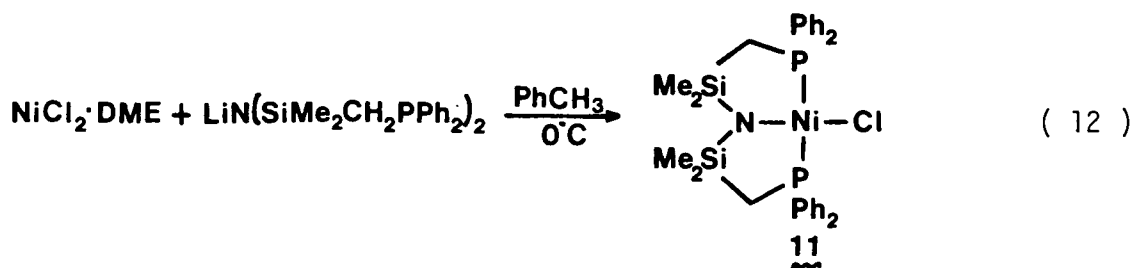


decomposition to a mauve colored oil. Signer analysis in benzene gives a molecular weight midway between a dimer and trimer. The  $^1\text{H}$ NMR spectrum also implicates two different forms of this lithium salt since there are two broad  $\text{SiCH}_3$  signals, two  $\text{CH}_2\text{P}$  resonances and two broad  $\text{PhCH}_2$  absorptions; upon heating to  $80^\circ\text{C}$ , only one species is observed.

### Amidophosphine Complexes of the Nickel Triad

As expected on the basis of previous work by Bradley, Lappert, and others, these lithium amidophosphines are convenient starting materials for metathetical reactions with a variety of transition metal halides. The ligand, in these complexes of the Group VIII metals, acts as a uninegative six-electron donor, coordinating in a tridentate manner through the amide nitrogen and both phosphorous centres.

The nickel amide 11 is most conveniently prepared from  $\text{NiCl}_2 \cdot \text{DME}$ , since this starting material can be easily obtained completely anhydrous and is also slightly soluble in organic solvents (equation 12). The



analogous reaction using anhydrous  $\text{NiCl}_2$  or  $\text{NiBr}_2$  proceeds in much lower yield, probably owing to their very low solubilities. Alternatively, 11 may be prepared from  $\text{NiCl}_2(\text{PR}_3)_2$  ( $\text{R} = \text{Me}$  or  $\text{Ph}$ ); however, in the case of  $\text{NiCl}_2(\text{PPh}_3)_2$ , difficulties were encountered in recrystallizing the product away from the involatile phosphine by-product ( $\text{PPh}_3$ ). The analytically pure, diamagnetic nickel amide is obtained, after recrystallization from toluene/hexane, as large diamond-shaped, deep-brown crystals. This complex is moderately air-sensitive and very hygroscopic; it is soluble in a wide range of organic solvents, including benzene, toluene and acetone and is moderately soluble in cyclohexane.

As previously mentioned, the analogous reaction of  $\text{NiCl}_2(\text{PR}_3)_2$  ( $\text{R} = \text{Et}$  or  $\text{Ph}$ ) with  $\text{LiN}(\text{SiMe}_3)_2$  results in reduction of the starting  $\text{Ni(II)}$  complex to form a three-coordinate  $\text{Ni(I)}$  species,  $\text{NiN}(\text{SiMe}_3)_2(\text{PR}_3)_2$ . This unexpected result has been rationalized as being due to combined steric and electronic factors. Presumably, the  $\pi$ -acceptor ability of the phosphines may help to stabilize the low oxidation state at  $\text{Ni}$ . In addition, the large steric bulk of these ligands may prevent formation of the expected square-planar  $\text{Ni(II)}$  complex,  $\text{Ni}\{\text{N}(\text{SiMe}_3)_2\}_2(\text{PR}_3)_2$ . However, it is evident from this result that electron transfer plays a significant role in the formation of metal-amide bonds. The fact that we observe no such reduction may be explained by assuming that initial coordination of the tridentate ligand's phosphine centres may serve to cage any radicals formed prior to metathesis and thus prevent a net reduction of the metal centre.

A linear, tridentate ligand may coordinate to a transition metal in either a meridional, planar stereochemistry or a facial, pyramidal stereochemistry depending upon both the stereoelectronic constraints of the metal as well as the flexibility of the ligand backbone. Spectroscopically, the most definitive means for establishing the mode of ligation in these complexes is from  $^1\text{H}$ NMR data. The spectrum of  $\text{Ni}\{\text{N}(\text{SiMe}_3)_2\}_2(\text{PR}_3)_2$  (Fig.1.8) will serve to illustrate. A virtual triplet<sup>45</sup> for the  $\text{CH}_2\text{P}$  protons centred at 1.2 - 1.7 ppm is indicative of a trans orientation of the chelating phosphines;  $J_{\text{app}}$  is usually 5 - 6 Hz. Shaw has demonstrated that virtual coupling arises in such  $\text{A}_2\text{A}'_2\text{XX}'$  spin systems when  $J_{\text{XX}'}$  is very large.

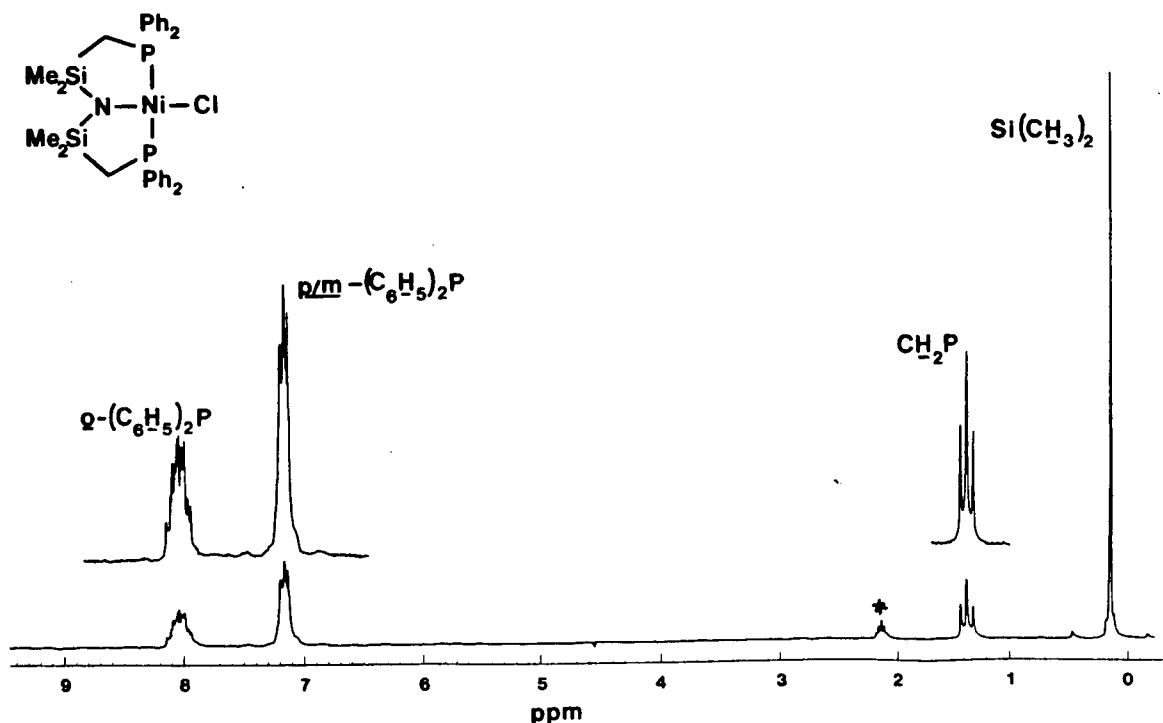


Fig. 1.8  $^1\text{H}$ NMR(100MHz)spectrum of  $[\text{NiClN}(\text{SiMe}_2\text{CH}_2\text{PPh}_2)_2]$  in  $\text{C}_7\text{D}_8$   
(asterisk indicates residual solvent protons).

For these amidophosphine complexes, the trans phosphines are strongly coupled; as a result, an apparent  $\text{A}_4\text{X}_2$  pattern is observed for the  $\text{CH}_2\text{P}$  protons. Another useful spectral correlation has been pointed out by Moore and Robinson<sup>46</sup> who noted that a chemical shift difference of  $0.6 \rightarrow 1.0$  ppm between the ortho and para/meta protons of the phosphine phenyl groups, when the spectrum is recorded in deuterated aromatic solvents, is also indicative of mutually trans diphosphines.

That this trans disposition persists in the solid state has been demonstrated by X-ray crystallographic analysis of 11. As can be seen from Fig. 1.9, this complex adopts a distorted square planar geometry; instead of the expected 90° value for the two Cl-Ni-P bond angles, the

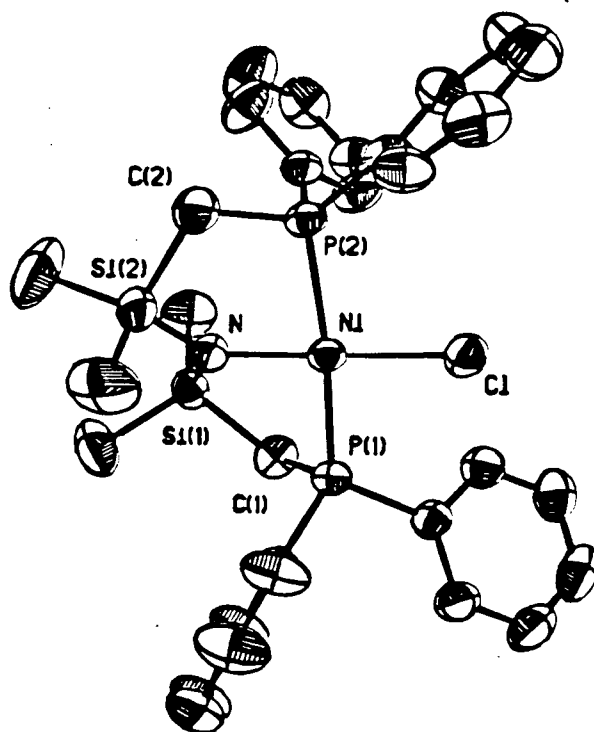


Fig. 1.9 X-ray crystal structure of [NiClN(SiMe<sub>2</sub>CH<sub>2</sub>PPh<sub>2</sub>)<sub>2</sub>]

observed values are  $93.74(2)^\circ$  and  $95.40(2)^\circ$ . Especially significant is the puckering of the chelate ring backbone: the planar  $\text{ClNiNSi}_2$  unit is tilted by approximately  $40^\circ$  with respect to the coordination plane of the nickel complex. As a result, one silicon atom is disposed  $0.89 \text{ \AA}$  above, and the other  $1.25 \text{ \AA}$  below, the coordination plane; in addition, the methyl groups on Si(1) are staggered with respect to the methyls of Si(2) in order to minimize unfavorable steric interactions.

Since, in the solid state, this nickel complex has near  $C_2$  symmetry, the silyl methyls should be diastereotopic in solution. Similarly, the methylene protons should be diastereotopic. However, this would only be the case if the chelate ring were rigid in solution. In actuality, only one  $\text{SiCH}_3$  signal is observed in the  $^1\text{H}$ NMR at ambient temperature. Two possible explanations for this observation are accidental degeneracy or a very rapid conformational flipping of the chelate ring. Variable temperature  $^1\text{H}$ NMR down to  $-78^\circ\text{C}$  resulted in broadened peaks as well as a decrease (by  $50 \pm 5\%$ ) in peak intensity, as measured by integration versus residual solvent protons ( $d^6$ -acetone or  $d^8$ -toluene). Surprisingly, at  $-80^\circ\text{C}$ , the originally orange-brown solution, sealed in an NMR tube under nitrogen, turns bright green with no visible precipitate. Originally we believed that this color change and the decrease in peak intensity was due to the paramagnetic tetrahedral isomer of the nickel amide which was being stabilized at low temperature. Exchange of the axial and equatorial sites in the puckered rings could therefore be occurring via a square planar/tetrahedral equilibrium (well known for  $\text{Ni(II)}$  phosphines)<sup>47</sup>. However, low temperature visible and near IR spectroscopy failed to support this

hypothesis; no absorptions attributable to tetrahedral  $d^8$  complexes could be observed. In addition, the Evans' method did not indicate any paramagnetic species in solution at low temperature.<sup>48</sup>

Additional evidence that a tetrahedral isomer was not involved in this axial/equatorial exchange was given by the results of the following experiment. It is well known that strong field ligands tend to stabilize low spin transition metal complexes. Therefore, it would be expected that the cyano derivative,  $[\text{Ni}(\text{CN})\text{N}(\text{SiMe}_2\text{CH}_2\text{PPh}_2)_2]$ , readily prepared from 11 and  $\text{Me}_3\text{SiCN}$ , should exist exclusively as the square planar, diamagnetic isomer. Exchange via a tetrahedral isomer could therefore be ruled out. However, the  $^1\text{H}$ NMR of this complex, even down to  $-80^\circ\text{C}$ , is identical to that of its chloro analogue 11. Therefore, the required conformational flipping of the ligand backbone is very likely occurring by a simple rotation of the planar  $\text{NSi}_2$  fragment through the square plane of the complex (Fig.1.10).

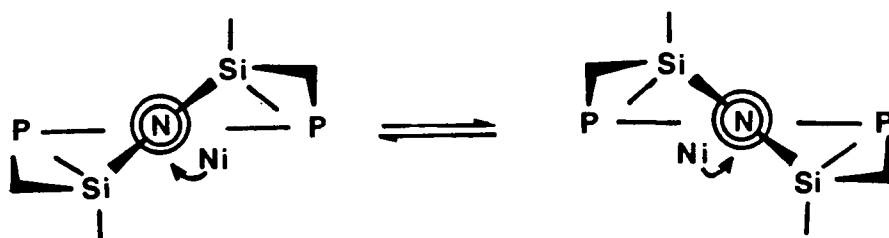
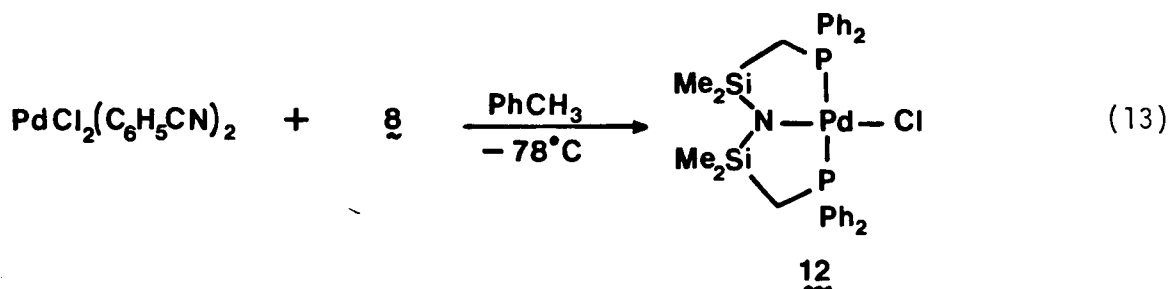


Fig. 1.10 Proposed conformational flipping of ligand backbone of  $[\text{NiClN}(\text{SiMe}_2\text{CH}_2\text{PPh}_2)_2]$  in solution

The corresponding reaction of  $\text{LiN}(\text{SiMe}_2\text{CH}_2\text{PPh}_2)_2$  with  $\text{PdCl}_2(\text{PhCN})_2$  proceeds smoothly at  $-78^\circ\text{C}$  to give the palladium amide 12 in good yield (equation 13). Like its nickel analogue, moisture and oxygen must be



rigorously excluded during the preparation; once formed, the solid is stable at room temperature under nitrogen for extended periods of time. Recrystallization from toluene/hexane produces large orange blocks of this derivative as a toluene solvate. To our knowledge, this is the first example of a stable palladium amide; presumably, previous attempts to form Pd-N bonds resulted only in reduction to Pd(I) or palladium metal. In fact, if this reaction is carried out at temperatures above  $0^\circ\text{C}$ , rapid darkening of the solution is observed and the yield of 12 is very low. Thus, it would appear that reduction poses a problem at ambient temperature. Once again, these observations point to the participation of electron transfer in the formation of metal amide bonds and the importance of coordination of the phosphine arms of the tridentate ligand prior to metathesis.

The spectral features of this complex are very similar to those of its nickel analogue. Diagnostic of a trans disposition of the chelating phosphines is a virtual triplet in the  $^1\text{H}$ NMR; the silyl methyls appear as

a sharp singlet. However, its solid state structure is quite different from that of  $\mathbf{11}$  (Fig. 1.11). Note the almost perfect square planar geometry

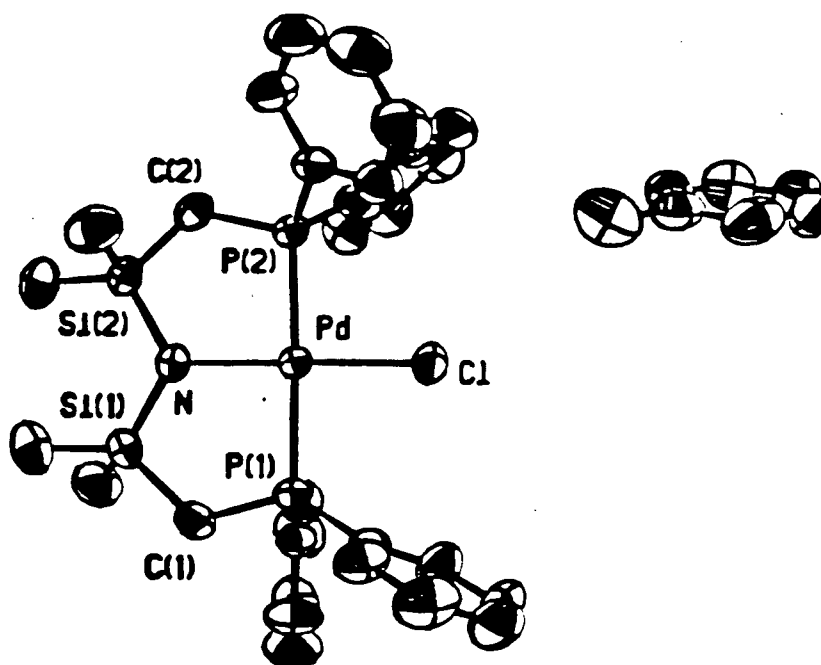


Fig. 1.11 X-ray crystal structure of  $[\text{PdClN}(\text{SiMe}_2\text{CH}_2\text{PPh}_2)_2]$

at palladium, as demonstrated by the Cl-Pd-N and P-Pd-P bond angles of almost  $180^\circ$ . Instead of the puckering observed in the nickel complex, the  $\text{NSi}_2$  unit of  $\mathbf{12}$  is virtually coplanar with the coordination plane of the

complex. This variation in structure is undoubtedly a consequence of the longer Pd-P(2.3078(5), 2.3112(5) Å) and Pd-N(2.063(2) Å) as compared to Ni-P(2.2086(6), 2.1975(5) Å) and Ni-N(1.924(2) Å) bonds. As a result, the SiMe<sub>2</sub> groups are eclipsed with respect to one another and the complex has near C<sub>2v</sub> symmetry. Thus, the solution and solid state structures for 12 are the same.

Although only six amides of the Group VIII metals have been subjected to crystallographic structural analysis, it is interesting to note a number of trends (Table I). Not surprisingly, little contraction in the M-N bond lengths is observed over the theoretical values, indicating a decreased  $\pi$ -donor ability of the amide nitrogen. This is probably a direct consequence of delocalization of the nitrogen lone pair into Si d-orbitals, which is manifested in short N-Si bonds (theoretical value = 1.88 Å), planar NSi<sub>2</sub> units, and expanded Si-N-Si bond angles (as compared to the 120° value expected for sp<sup>2</sup> hybridized nitrogen).

Although there are two reports<sup>49,50</sup> of simple platinum(II) amides, [PtCl(NHPh)(PEt<sub>3</sub>)<sub>2</sub>] and [Pt(NPh<sub>2</sub>)(PEt<sub>3</sub>)<sub>2</sub>Cl], no such complex incorporating a bis(trimethylsilyl)amide has been prepared. However, we have isolated such a stable platinum complex which completes the series [MCln(SiMe<sub>2</sub>-CH<sub>2</sub>PPh<sub>2</sub>)<sub>2</sub>] for the entire nickel triad. Although this derivative is readily prepared in good yield as fine yellow crystals from reaction of the lithium amide 8 with Zeise's salt, [K{PtCl<sub>3</sub>(C<sub>2</sub>H<sub>4</sub>)}], (equation 14); little, if any, product was obtained with a variety of other platinum precursors (such as PtCl<sub>2</sub>(COD), trans-PtCl<sub>2</sub>(PR<sub>3</sub>)<sub>2</sub>, R = Ph or Et, PtCl<sub>2</sub>(PhCN)<sub>2</sub>, trans-Pt(H)Cl(PEt<sub>3</sub>)<sub>2</sub>).

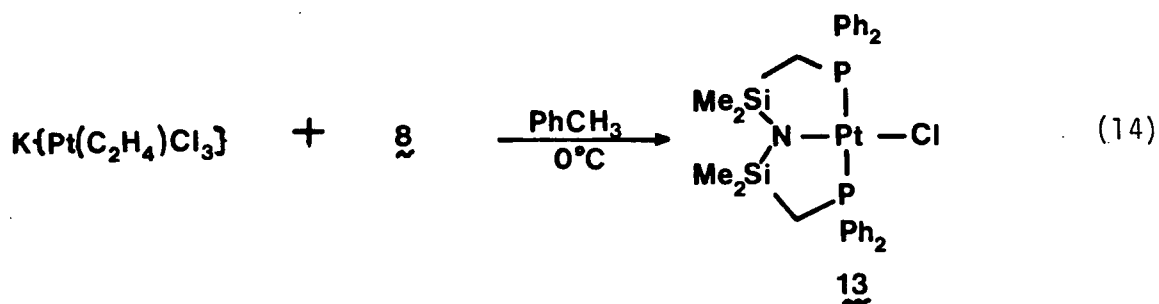
Table I Crystallographic data for the Group VIII metal bis (trimethyl silyl) amides and amido phosphines

<u>Complex</u>	<u>M-N</u>	<u>M-N (theor.)</u>	<u>N-Si</u>	<u>&lt;SiNSi</u>
$\text{Co}\{\text{N}(\text{SiMe}_3)_2\}_2\text{PPh}_3$	1.934	1.96	1.70 (av)	125.5
$\text{CoN}(\text{SiMe}_3)_2(\text{PPh}_3)_2$	1.924	1.96	1.69 (av)	128.0
$\text{Ni}\{\text{N}(\text{SiMe}_3)_2\}(\text{PPh}_3)_2$	1.870	1.86 †	1.71	126.4
$\text{Fe}\{\text{N}(\text{SiMe}_3)_2\}_3$	1.918	1.95	1.73	121.24
$\text{NiClN}(\text{SiMe}_2\text{CH}_2\text{PPh}_2)_2$	1.929	1.86	1.72	128.13
$\text{PdClN}(\text{SiMe}_2\text{CH}_2\text{PPh}_2)_2$	2.063	2.10 †	1.72	122.27

Bond lengths, in Å; bond angles in degrees.

† for sq. planar Ni (tet. = 1.91)

† Bragg-Slater (all other theoretical values are from covalent radii).



X-ray crystallographic analysis of this complex was obviated by the marked resemblance of its  $^1\text{H}$ NMR spectral characteristics to those of the corresponding nickel and palladium amidophosphines. The by now familiar virtual triplet for the  $\text{CH}_2\text{P}$  protons is further split into a 1:4:1 triplet by coupling with Pt-195 (Fig. 1.12) ( $^{195}\text{Pt}$ , 33.5% natural abundance;  $^3J_{\text{H,Pt}} = 31.0 \text{ Hz}$ ). It is therefore reasonable to assume that its structure is very similar to that of the palladium amide.

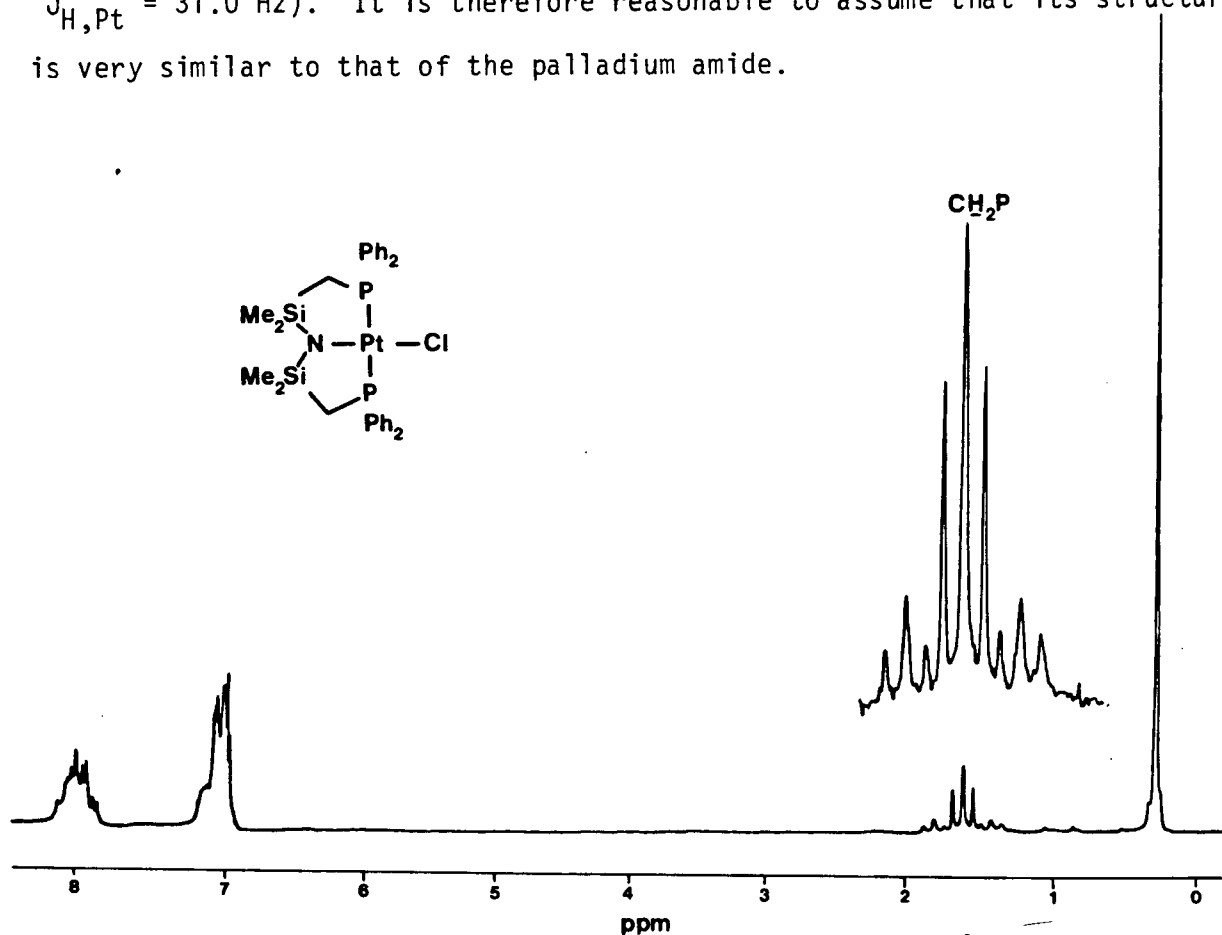
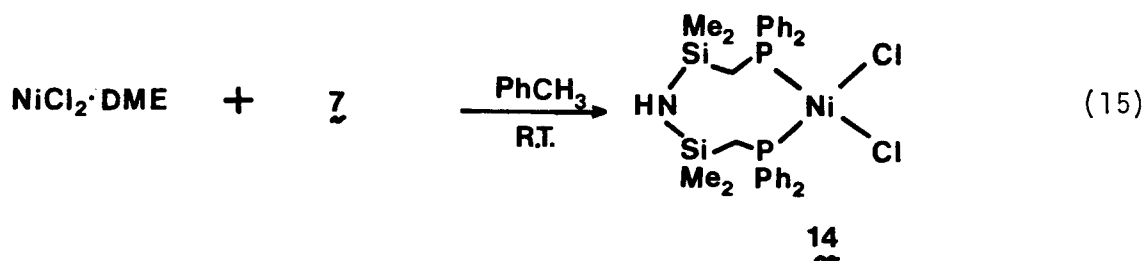


Fig. 1.12  $^1\text{H}$ NMR(80MHz) spectrum of  $[\text{PtClN}(\text{SiMe}_2\text{CH}_2\text{PPh}_2)_2]$  in  $\text{C}_6\text{D}_6$

The amidophosphines  $\underline{11}$ ,  $\underline{12}$ ,  $\underline{13}$  may be more readily prepared, and in higher yield, from the corresponding aminophosphine dichlorides,  $[\text{MCl}_2\text{NH}(\text{SiMe}_2\text{CH}_2\text{PPh}_2)_2]$ . Not surprisingly, the free ligand  $\underline{7}$ , being a potential neutral four-electron bidentate, readily coordinates to the metals of the nickel triad. The nickel complex  $\underline{14}$  is prepared at room temperature simply by stirring a toluene solution of  $\text{NiCl}_2 \cdot \text{DME}$  and  $\text{HN}(\text{SiMe}_2\text{CH}_2\text{PPh}_2)_2$  for 30 minutes (equation 15). Upon removal of solvent from the resultant deep-red solution, a green solid is formed which,



after recrystallization from  $\text{CH}_2\text{Cl}_2$ /hexane forms blue-black blocks. Such drastic color changes are well known for  $\text{Ni}(\text{II})$  complexes which undergo square planar/tetrahedral equilibria; the  $^1\text{H}$ NMR, which has many broad resonances between 0 and 20 ppm, also indicates the presence of paramagnetic and diamagnetic species<sup>51</sup>.

The solid state structure of  $\underline{14}$  displays a distorted tetrahedral geometry at nickel (Fig. 1.13). Note that this molecule possesses no elements of symmetry. The  $\text{Ni}-\text{Cl}$  (2.2216(8) and 2.2058(8) Å) and  $\text{Ni}-\text{P}$  (2.3180(7) and 2.3469(7) Å) bond lengths are typical of tetrahedral  $\text{Ni}(\text{II})$  complexes. Of most significance, there appears to be no interaction, either inter- or intramolecular, between the N-H moiety and the Ni centre.

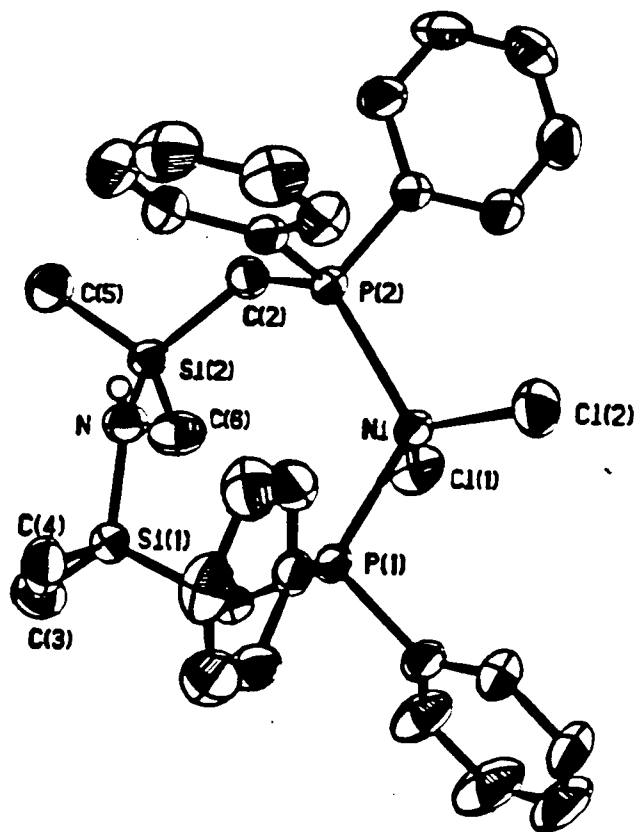
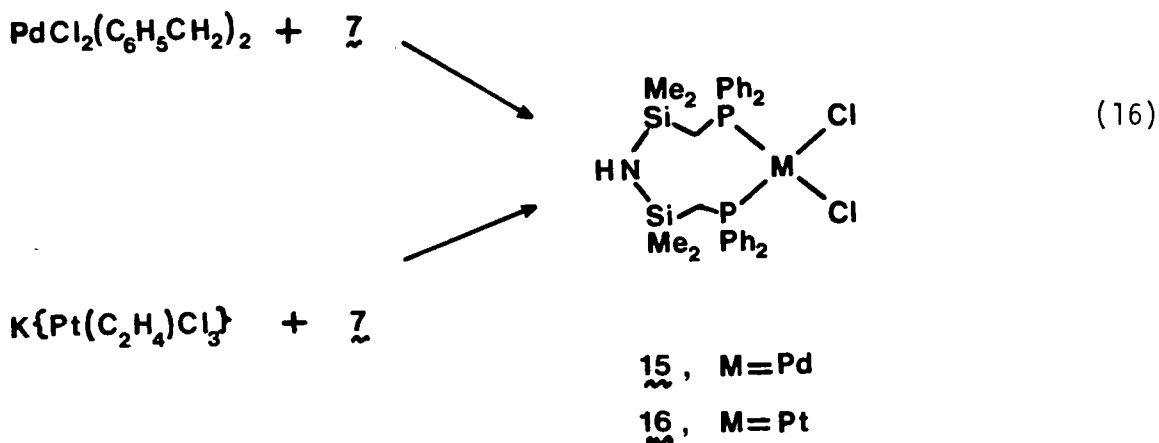


Fig. 1.13 X-ray crystal structure of  $[\text{NiCl}_2\text{NH}(\text{SiMe}_2\text{CH}_2\text{PPh}_2)_2]$

This is not too surprising in view of the fact that  $\nu_{\text{NH}}$  of this complex is identical to that of the free ligand ( $3365 \text{ cm}^{-1}$ ). Apparently, delocalization of the nitrogen lone pair into empty Si d-orbitals renders it unavailable for coordination. This is in sharp contrast to the closely related molecule  $[\text{NiBr}_2\text{NH}(\text{CH}_2\text{CH}_2\text{PPh}_2)_2]$  which has a 5-coordinate, square-pyramidal structure<sup>52</sup> with Ni-N bond length of  $2.01(3) \text{ \AA}$ .

The corresponding reaction of the free ligand with  $\text{PdCl}_2(\text{PhCN})_2$  produces 15 as large yellow plates; the analogous procedure using Zeise's salt gives the platinum aminophosphine as large colorless blocks (equation 16). It is assumed that, on the basis of their  $^1\text{H}$ NMR spectra, these derivatives are square planar with mutually cis phosphines; the characteristically broadened  $\text{CH}_2\text{P}$  resonances indicate weakly coupled cis phosphines.



However, the extremely low solubility might be indicative of a dimeric or polymeric form reminiscent of Pd and Pt complexes prepared and characterized by Shaw<sup>53</sup> (Fig. 1.14). This may also help to explain the decrease in  $\nu_{\text{NH}}$  ( $3305\text{ cm}^{-1}$  for 15;  $3280\text{ cm}^{-1}$  for 16) in these complexes as compared to the free ligand. Possibly, this is a result of hydrogen bonding between the N-H groups and the chlorides.

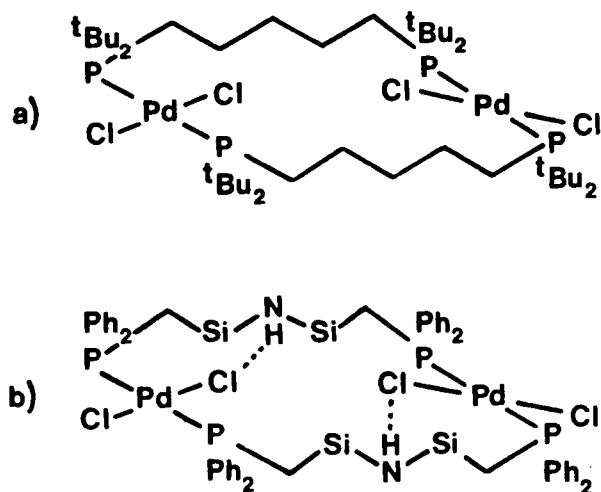
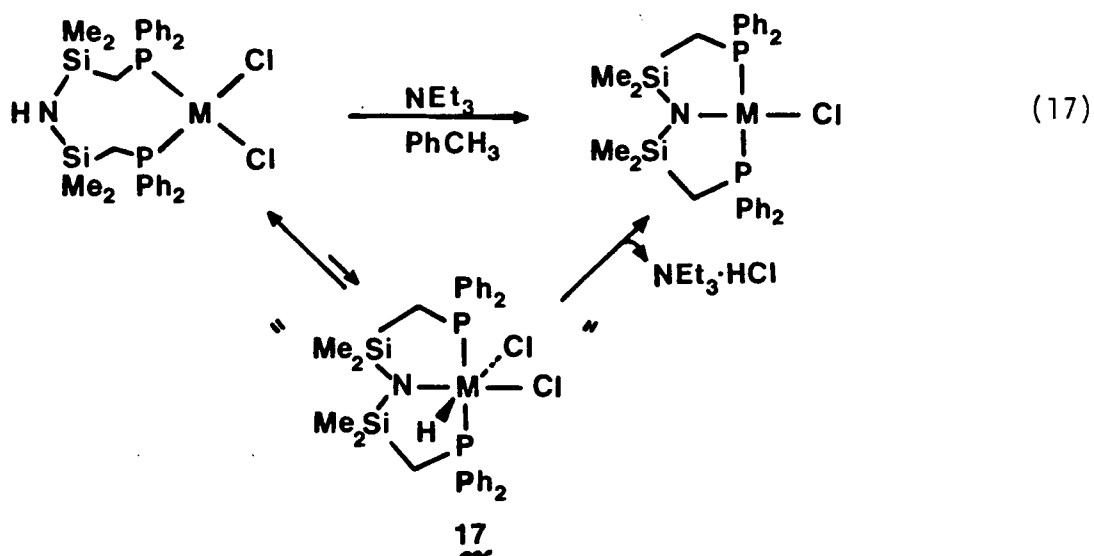


Fig. 1.14 a) Structure of  $[\text{PdCl}_2\{\text{R}_2\text{P}(\text{CH}_2)_5\text{PR}_2\}]_2$  ( $\text{R} = {}^t\text{Bu}$ )  
 b) Possible dimeric structure of  $[\text{PdCl}_2\text{NH}(\text{SiMe}_2\text{CH}_2\text{PPh}_2)_2]$

As indicated earlier, these complexes can be used to prepare the corresponding amidophosphines. Reaction of 14 with triethylamine at room temperature proceeds within minutes to give high yields of 11 (equation 17). However, this reaction is much slower for the Pd and Pt derivatives, requiring 24 h to go to completion. Reaction of 15 and 16

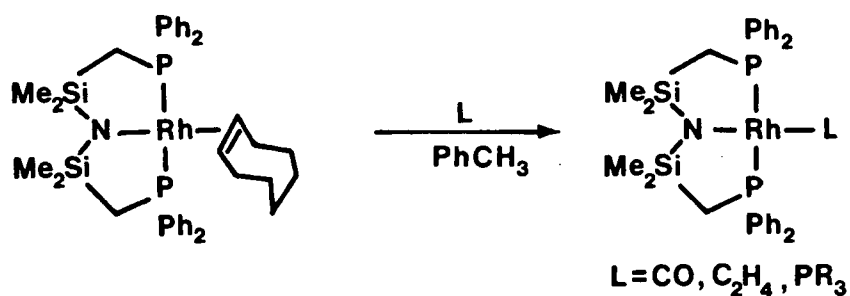
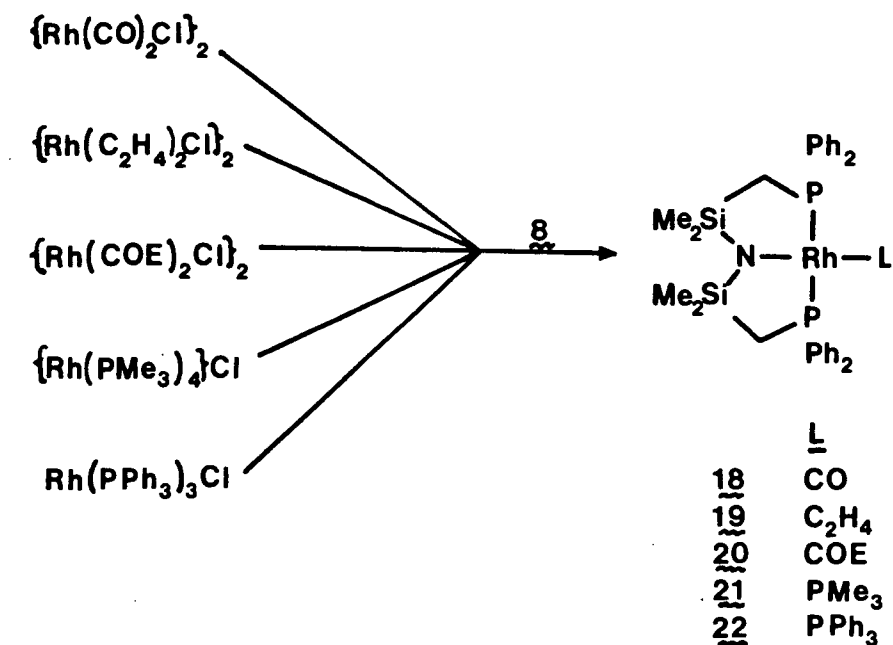


with other bases, such as pyridine, was unsuccessful, resulting only in starting materials. The action of pyridine on **14** gave only  $\text{NiCl}_2(\text{py})_4$ , whereas the poorly coordinating 2,4,6-trimethyl-pyridine gave no reaction at all. It is particularly significant that the reaction of  $\text{NiCl}_2(\text{PR}_3)_2$  and  $\text{HN}(\text{SiMe}_3)_2$  with  $\text{NEt}_3$  results in no amide formation; only starting materials were recovered. Thus, it would seem that a plausible mechanism for the amide conversion involves initial coordination of the phosphines followed by activation of the distal N-H (similar to the well-known cyclometallations involving ligand C-H activation<sup>54,55,56</sup>). Although oxidative addition of the N-H group to form an intermediate of the type **17** is quite probable, no evidence has as yet been obtained to support such a process.

#### Amidophosphines of Rhodium and Iridium

It would appear that reaction of  $\text{LiN}(\text{SiMe}_2\text{CH}_2\text{PPh}_2)_2$  with a Group VIII metal halide is a general route to stable amidophosphines, as evidenced by the isolation of a variety of Rh(I) derivatives by this method (see Scheme 1.3). As for the complexes of the nickel triad, all of these species are monomeric, analytically pure, highly crystalline solids which are very air and moisture sensitive. The carbonyl, phosphine, and ethylene derivatives may alternatively be prepared in high yield by reaction of **20** with the desired neutral ligand (equation 18).

**Scheme 1.3**



(18)

In all of these complexes, the hybrid ligand is coordinated in a tridentate manner, binding to the rhodium centre through both phosphines and the N atom, resulting in square planar, 16-electron species. The

exclusive trans disposition of the chelating phosphines was once again established primarily from  $^1\text{H}$ NMR data, in particular the  $\text{CH}_2\text{P}$  virtual triplet at  $\sim 1.8$  ppm ( $J_{\text{app}} \sim 5$  Hz). A typical spectrum is shown in (Fig. 1.15). The  $^{31}\text{P}\{^1\text{H}\}$ NMR spectra are very straightforward  $\text{A}_2\text{X}$  patterns

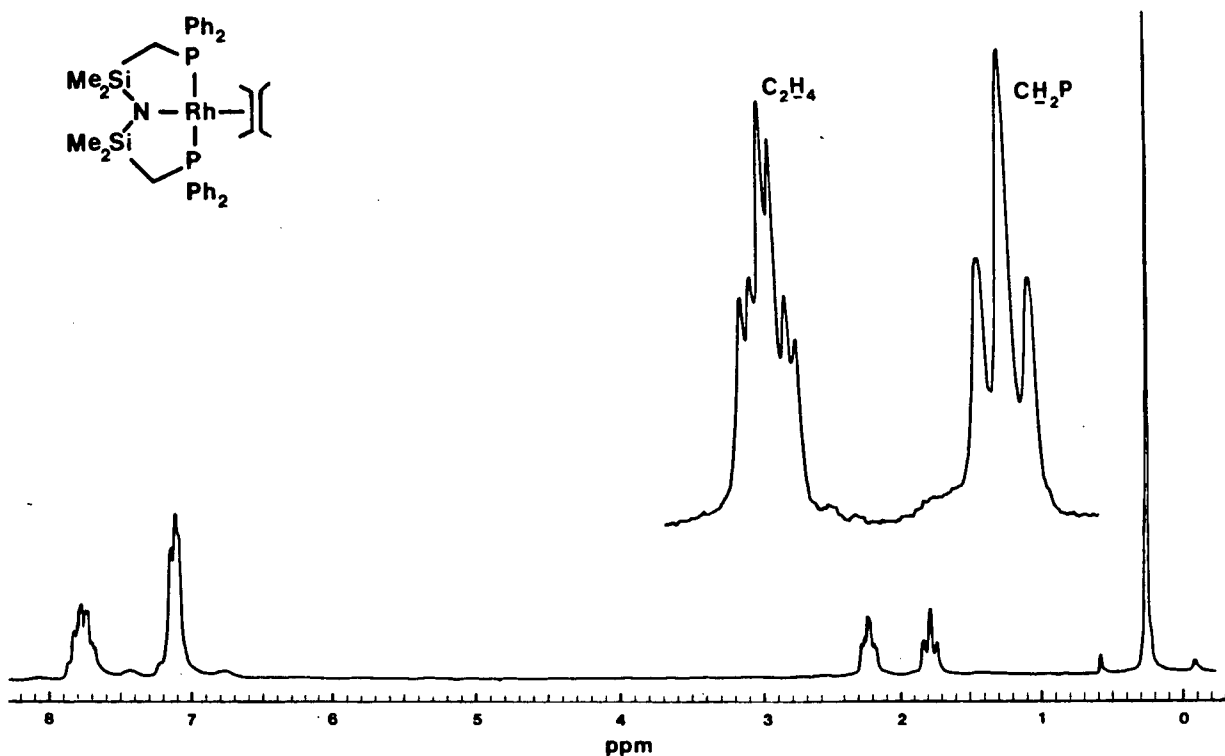


Fig. 1.15  $^1\text{H}$ NMR(100MHz) spectrum of  $[\text{Rh}(\text{C}_2\text{H}_4)\text{N}(\text{SiMe}_2\text{CH}_2\text{PPh}_2)_2]$  in  $\text{C}_6\text{D}_6$

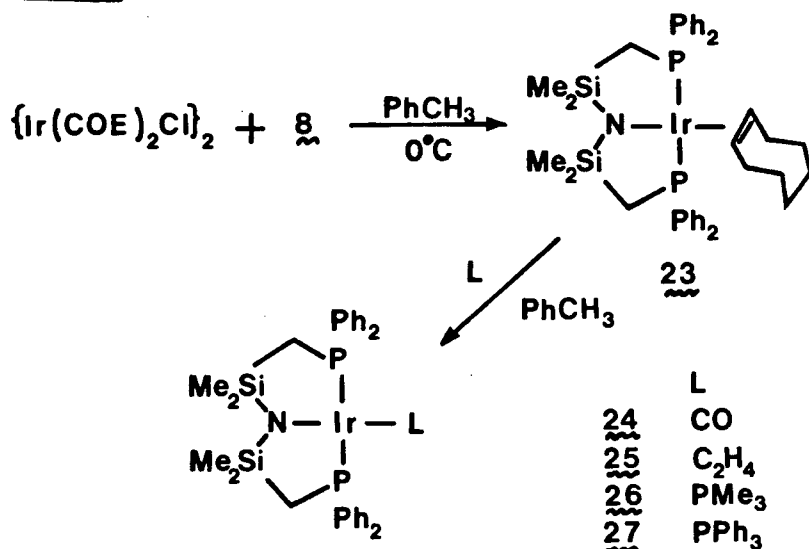
for the cyclooctene, carbonyl, and ethylene derivatives and  $\text{A}_2\text{BX}$  patterns for the  $\text{PMe}_3$  and  $\text{PPh}_3$  complexes. The  $^{31}\text{P}$ - $^{103}\text{Rh}$  coupling constants for

the ligand's  $\text{PPh}_2$  groups are typically in the range of 130 - 140 Hz (normal values for Rh(I) species), while  $^1\text{J}_{\text{Rh,P}}$  for the ancillary  $\text{PMe}_3$  or  $\text{PPh}_3$  in **21** and **22** is somewhat higher (150 - 160 Hz), a reflection of the weak trans influence of the amide group<sup>57</sup>.

It is rather remarkable that, prior to our efforts in this area, only one rhodium amide complex,  $[\text{RhN}(\text{SiMe}_3)_2(\text{PPh}_3)_2]^{25}$ , had been characterized. However, although this complex is stable under inert atmospheres in the solid state, decomposition, with concomitant elimination of  $\text{HN}(\text{SiMe}_3)_2$ , occurs in benzene solution at 25°C ( $t_{1/2} = 12$  h). In contrast, deuterobenzene solutions of our rhodium amidophosphines, sealed in NMR tubes under nitrogen, show no decomposition, even after several months at 25°C. This is possibly a consequence of steric constraints imposed by the two five-membered chelate rings; ortho-metallation (and subsequent reductive elimination of the amide) of the phenyl substituents would be expected to be unfavorable on steric grounds.

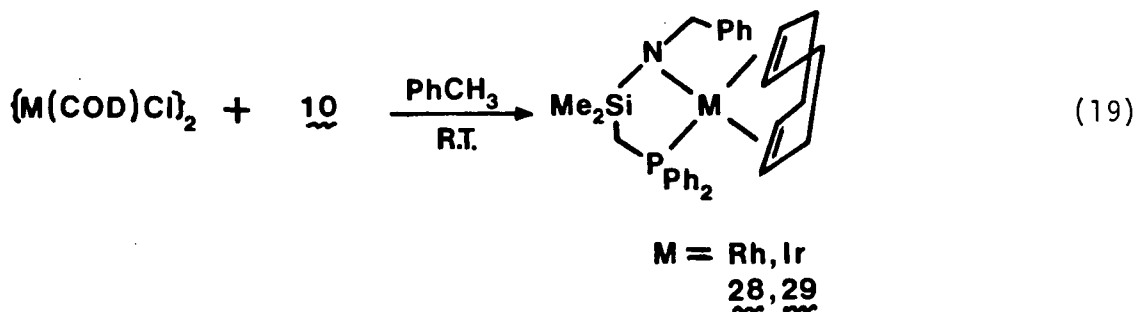
The analogous iridium derivatives **23**  $\rightarrow$  **27** may be prepared in a similar manner or, more simply, via reaction of the iridium cyclooctene amide **23** with the required neutral ligand in toluene at room temperature (Scheme 1.4) (except for  $\text{L} = \text{PPh}_3$  which requires refluxing in toluene for 24 h). In contrast to the previous preparations of the rhodium analogues, the solvent used in the synthesis of the iridium amides is crucial; when diethyl ether is employed inseparable mixtures of products are formed whereas the use of toluene results in high yields of the pure complexes. The  $^1\text{HNMR}$  spectra of these derivatives indicate that all are square-planar

**Scheme 14**



complexes with trans phosphines. It should be noted that only one other iridium amide,  $[\text{Ir}(\text{COD})\text{N}(\text{SiMe}_3)_2(\text{PEt}_3)]$ , has been prepared to date<sup>58</sup>.

Rhodium and iridium amidophosphines have also been synthesized incorporating bidentate hybrid ligands. The preparation of the cyclooctadiene derivatives  $[\text{M}(\text{COD})\text{N}(\text{PhCH}_2)(\text{SiMe}_2\text{CH}_2\text{PPh}_2)]$  is very straightforward (equation 19); carried out at room temperature, the products are obtained in virtually quantitative yields as analytically pure crystals. Although exceptionally air and moisture sensitive, these complexes, either as solids or in solution undergo no decomposition (via



$\beta$ -elimination) under inert atmospheres. Molecular weight measurements (Signer) indicate that these species are monomeric in solution (benzene). The  $^1\text{H}$ NMR (see Fig. 1.16) are quite straightforward, the most informative resonances being the sharp  $\text{SiCH}_3$  singlet at 0.04 ppm and the doublet ( $^2J_{\text{H,P}} = 13.0 \text{ Hz}$ ) for the  $\text{CH}_2\text{P}$  protons. Surprisingly, the COD ligand is not readily displaced, so, as yet, a series of these complexes has not been prepared. Addition of either  $\text{PMe}_3$  or dmpe to a toluene solution of either 28 or 29 results only in the isolation of starting materials. Carbon monoxide does displace the diene ligand but the stoichiometry of the resultant rhodium complex, isolated as deep red crystals, has not been elucidated.

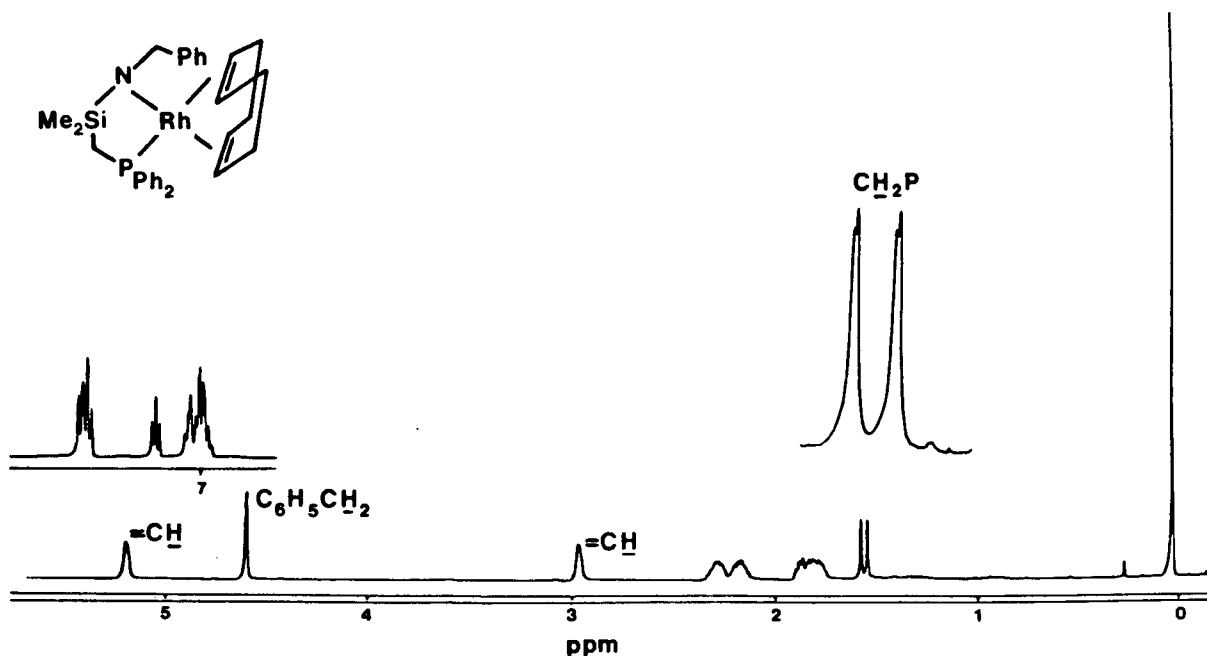


Fig. 1.16  $^1\text{H}$ NMR(400MHz) spectrum of  $[\text{Rh}(\text{COD})\text{N}(\text{C}_6\text{H}_5\text{CH}_2)(\text{SiMe}_2\text{CH}_2\text{PPh}_2)]$  in  $\text{C}_6\text{D}_6$

## Chapter II

### Migratory Insertion of Carbon Monoxide into Metal-Carbon Bonds

Due to its involvement in important catalytic<sup>59</sup> (hydroformylation, "Reppe" reactions, Monsanto's acetic acid process) and stoichiometric reactions<sup>60</sup> (carbonylation of organic halides using Collman's reagent or  $\text{Ni}(\text{CO})_4$ ), the migratory insertion of carbon monoxide into transition metal alkyl bonds has been the object of intensive research<sup>61,62</sup>. The ability of metal alkyls to form acyl derivatives upon exposure to CO was first reported by Coffield, Kozikowski, and Closson<sup>63</sup> in 1957 (equation 20). Since then, examples of this reaction have been observed for most transition metals. Although detailed kinetic studies have not been carried out for most of these cases, analogy is usually made to the prototypical  $\text{MeMn}(\text{CO})_5$  complex for which the reaction mechanism has been well elaborated.



The basic feature of a migratory insertion reaction is that an unsaturated group (Y) becomes inserted between two atoms originally bound together (M-X) as in equation 21. The unsaturated molecule may be CO, an olefin, diene, acetylene, aldehyde, nitrile,  $\text{SO}_2$ , or  $\text{O}_2$ , while the ligand X may be H, alkyl, aryl, vinyl,  $\text{OR}^-$ ,  $\text{NR}_2^-$ ,  $\text{NR}_3$ ,  $\text{OH}^-$ ,  $\text{H}_2\text{O}$ , halide or another metal.

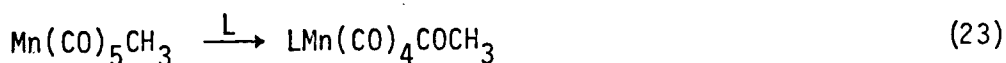


It is important to note the distinction between an oxidative addition and an insertion reaction since a reaction of the type shown in equation 22 is sometimes regarded as an insertion of M into an H-H bond. However,



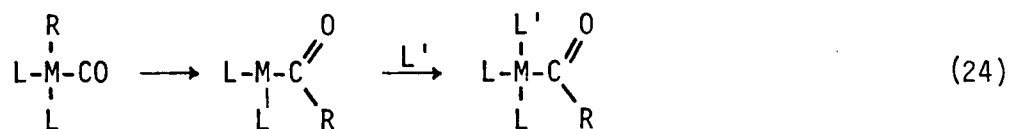
a migratory insertion reaction results in no net change in the metal's formal oxidation state whereas an oxidative addition (equation 22) involves a net two electron oxidation of the metal centre. Migratory insertions may be either intramolecular or intermolecular; the former class of reactions requires simultaneous coordination of the unsaturated group and the ligand X at the metal, while the latter proceed by external nucleophilic attack of Y on M-X. In some cases, especially with CO, reaction may be reversible; the reverse reaction of equation 21 is termed an "extrusion", "deinsertion", or a "decarbonylation" and may be promoted thermally, photo-lytically, or chemically (eg. using  $Rh(PPh_3)_3Cl$ ).

In the case of alkyl  $\rightarrow$  acyl migratory insertions, reaction occurs intramolecularly, usually in the presence of an external Lewis base ligand, which fills the coordination site left vacant after insertion has taken place; usually phosphines, carbon monoxide, or amines serve this purpose (equation 23).



The most common cases of CO insertion involve transition metal carbonyl alkyl complexes in which the inserting CO is already coordinated, although there are a significant number of examples of acyl formation using metal alkyls having no carbonyl ligands. In the latter case, it is believed that the incoming CO coordinates prior to insertion. Thus a vacant site cis to the alkyl group must be generated in order for reaction to occur. Similarly, if the starting material is a carbonyl alkyl complex, a carbonyl ligand must be cis to the alkyl group.

The term "migratory insertion" is best applied to these reactions since it has been established (mainly through labelling studies) that, rather than a direct insertion of CO into the M-C bond, this process is better considered as a 1,2-migration of an alkyl group to a cis coordinated carbonyl ligand<sup>64,65,66</sup>. Although this has only been firmly established for a few cases of CO migratory insertion (Notably the  $\text{MeMn(CO)}_5$  system), Halpern<sup>67</sup> has suggested that R group migration probably occurs in most, if not all, cases of alkyl  $\longrightarrow$  acyl transformations. A general two-step mechanism, involving a coordinatively unsaturated acyl intermediate, is outlined in equation 24.



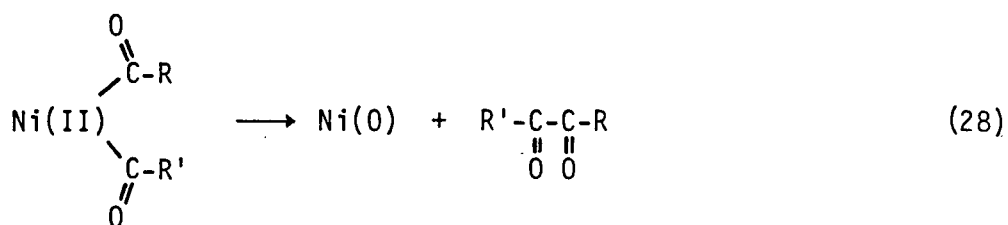
The reactivity of CO with transition metal alkyls is often completely independent of the nature of the solvent; such is the case with  $[\text{EtPt(CO)}-(\text{AsPh}_3)\text{Cl}]$ <sup>68</sup>. However, for  $[\text{CH}_3\text{Mn(CO)}_5]$ <sup>66</sup>,  $[\text{CpFe(CO)}_2\text{CH}_3]$ <sup>69</sup>, and  $[\text{CpMo(CO)}_3\text{-CH}_3]$ <sup>70</sup>, it has been shown that more highly coordinating and/or polar

solvents markedly increase the rate of CO insertion (the solvent-assisted pathway). This effect has been ascribed to a possible solvent-promoted breaking of the M-R bond, although little solid evidence has been provided as yet for a solvated acyl intermediate. When the solvent is highly coordinating, competition occurs between reaction of L' (see equation 24) with the acyl intermediate and its reversion to the alkyl. However, in non-polar solvents, reaction proceeds by direct attack of L on the acyl intermediate. Such an intermediate may be either a coordinatively unsaturated monohapto acyl or a coordinatively saturated dihapto acyl. The latter possibility would seem quite feasible in view of the preponderance of transition metal alkyl derivatives for which the acyl moiety is coordinated in an  $\eta^2$ -fashion.

Based on studies using transition metal complexes with chiral R groups, it was found that CO migratory insertions are very stereospecific and usually proceed with retention of configuration at carbon<sup>71,72</sup>. However, very little extensive investigation has been made on the effect of the R group on the rate of these reactions. Generally, it has been noted that electron-releasing groups tend to promote insertions whereas electron-withdrawing groups significantly decrease rates. Reaction of CO with  $\text{RMn}(\text{CO})_5$  follows the sequence  $\text{R}=\text{n-Pr} > \text{Et} > \text{Me} > \text{CH}_2\text{Ph}$  and  $\text{CF}_3$ <sup>73</sup>. Similarly the analogous reaction of  $\text{CpMo}(\text{CO})_3\text{R}$  with  $\text{PPh}_3$  shows a decrease in the rate with  $\text{R}=\text{Et} > \text{Me} > \text{CH}_2\text{Ph} > \text{CH}_2\text{CH}=\text{CH}_2$ <sup>74</sup>. Thus it would appear that the reactivity reflects the strength of the M-R bond.

In light of these observations, it should not be surprising that





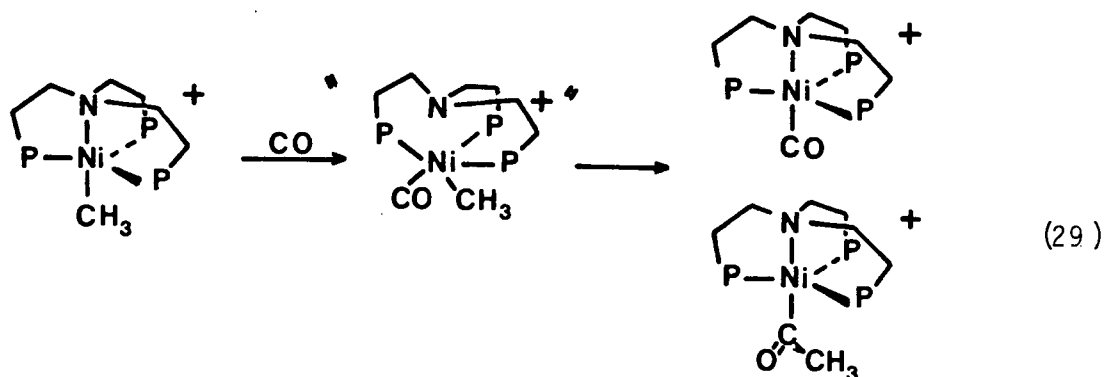
The first example<sup>81</sup> of a Ni(II) acyl species was reported in 1970. Reaction of  $[\text{CpNi}(\sigma, \pi\text{-cyclooctene})]$  with high pressures of CO resulted in an acyl derivative,  $[\text{CpNi}(\text{COC}_8\text{H}_{13})]$ ; however, attempts to isolate this complex were unsuccessful and characterization was based solely on mass spectrometric data.

However, Klein<sup>82,83</sup> has isolated stable acetyl nickel complexes of the type  $[\text{Ni}(\text{COCH}_3)\text{X}(\text{PMe}_3)_2]$  ( $\text{X}=\text{Cl}, \text{Br}$ ). Single crystal x-ray structural analysis has established the trans square planar structure of these nickel acyl derivatives. Although moderately stable, these acetyl complexes slowly lose CO under inert atmospheres with concomitant regeneration of the starting nickel alkyl.

Similarly, reaction of  $[\text{Ni}(\text{R})\text{ClL}_2]$  ( $\text{R} = \text{CH}_2\text{CMe}_2\text{Ph}$  or  $\text{CH}_2\text{SiMe}_3$ ;  $\text{L} = \text{PMe}_3$  or  $\text{PMe}_2\text{Ph}$ ) under one atmosphere CO at room temperature yielded the corresponding acyl complexes  $[\text{Ni}(\text{COR})\text{ClL}_2]$ <sup>84</sup>. X-ray crystal structure analysis of  $[\text{Ni}(\text{COCH}_2\text{SiMe}_3)\text{Cl}(\text{PMe}_3)_2]$  indicates a distorted square planar geometry with trans disposed phosphines. Surprisingly, these reactions are irreversible, even with prolonged heating.

Sacconi<sup>85</sup> has reported the isolation of five-coordinate cationic nickel acyl complexes of formula  $[\text{Ni}(\text{COR})\text{L}]\text{BPh}_4$  ( $\text{R} = \text{CH}_3, \text{C}_2\text{H}_5, \text{CH}_2\text{Ph}$ ;  $\text{L} = \text{tris}(2\text{-diphenylarsinoethyl})\text{amine}:(\text{nas}_3), \text{tris}(2\text{-diphenylphosphinoethyl})\text{amine}:(\text{nP}_3)$ ) from the alkyl complexes  $[\text{Ni}(\text{R})\text{L}]\text{BPh}_4$ . For the methyl derivative,

an intermediate has been identified; crystallographic analysis has shown this intermediate to be a "solid solution" of the cationic acyl and a cationic carbonyl (equation 29).



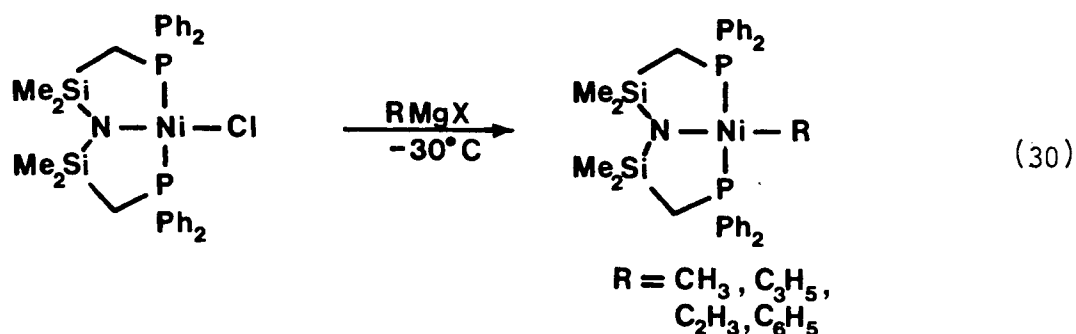
The proposed reaction scheme involves an undetected intermediate in which the nitrogen is no longer bound, in order to provide a coordination site for the incoming CO. These acyl complexes are stable both in solution and in the solid state under an atmosphere of CO; however, under nitrogen or argon, gradual loss of CO reforms the starting alkyl derivative.

Fahey<sup>86</sup> has isolated a nickel benzoyl complex from the reaction of  $[\text{Ni}(\text{C}_6\text{H}_5)\text{Cl}(\text{PET}_3)_2]$  with CO (1-2 atmospheres) at 25°C in hexane. The product,  $[\text{Ni}(\text{COC}_6\text{H}_5)\text{Cl}(\text{PET}_3)_2]$  was produced as orange crystals. A number of other nickel acyl complexes has also been characterized; however, these species were prepared via oxidative addition of an alkyl, vinyl, or aryl halide to  $[\text{Ni}(\text{PET}_3)_2(1,5\text{-COD})]$  rather than CO insertion.

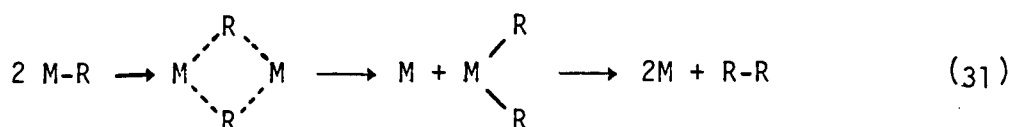
#### Ancillary Ligand Rearrangements Promoted by the Migratory Insertion of Carbon Monoxide into Nickel(II)-Carbon Bonds

As anticipated, reaction of  $[\text{NiClN}(\text{SiMe}_2\text{CH}_2\text{PPh}_2)_2]$  with Grignard

or alkyl lithium reagents produces the corresponding alkyl (or aryl) complexes in high yields (equation 30). The only restriction to this preparation is that the R group cannot have  $\beta$ -hydrogens; thus, the ethyl derivative,  $\text{Ni}(\text{Et})\text{N}(\text{SiMe}_2\text{CH}_2\text{PPh}_2)_2$ , could not be isolated, presumably owing to rapid decomposition via a  $\beta$ -elimination mechanism. Typically, synthesis of these hydrocarbyl (ie. alkyl, aryl, vinyl) derivatives is



carried out at high dilution ( $\sim 10^{-3}\text{M}$  in toluene, THF, or  $\text{Et}_2\text{O}$ ) and low temperature ( $\sim -30^\circ\text{C}$ ) in order to prevent reductive coupling reactions<sup>87</sup>, an often troublesome decomposition route for metal alkyls (equation 31)



These nickel hydrocarbyls are isolated as highly crystalline, analytically pure solids which are very air and moisture sensitive; however, under inert atmospheres they are stable for several months. Recrystallization is typically carried out from neat hexane at  $-30^\circ\text{C}$ , owing to the high solubility of these derivatives in organic solvents.

Structural characterization has been largely based on  $^1\text{H}$ NMR data; the spectra of  $[\text{Ni}(\text{CH}_3)\text{N}(\text{SiMe}_2\text{CH}_2\text{PPh}_2)_2]$  (Fig. 2.1) and  $[\text{Ni}(\text{CH}=\text{CH}_2)\text{N}(\text{SiMe}_2\text{CH}_2\text{PPh}_2)_2]$  (Fig. 2.2) serve as illustrative examples. The virtual

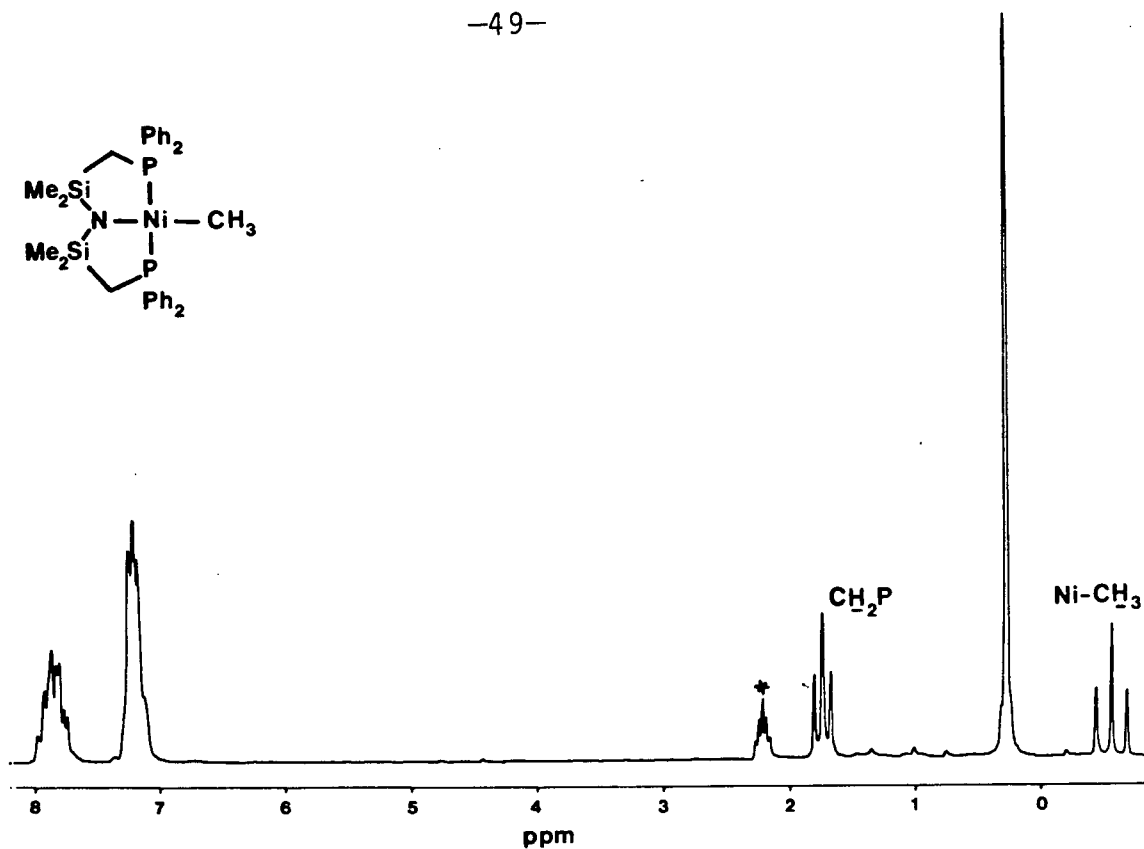


Fig. 2.1  $^1\text{H}$ NMR(80 MHz) spectrum of  $[\text{Ni}(\text{CH}_3)\text{N}(\text{SiMe}_2\text{CH}_2\text{PPh}_2)_2]$  in  $\text{C}_7\text{D}_8$

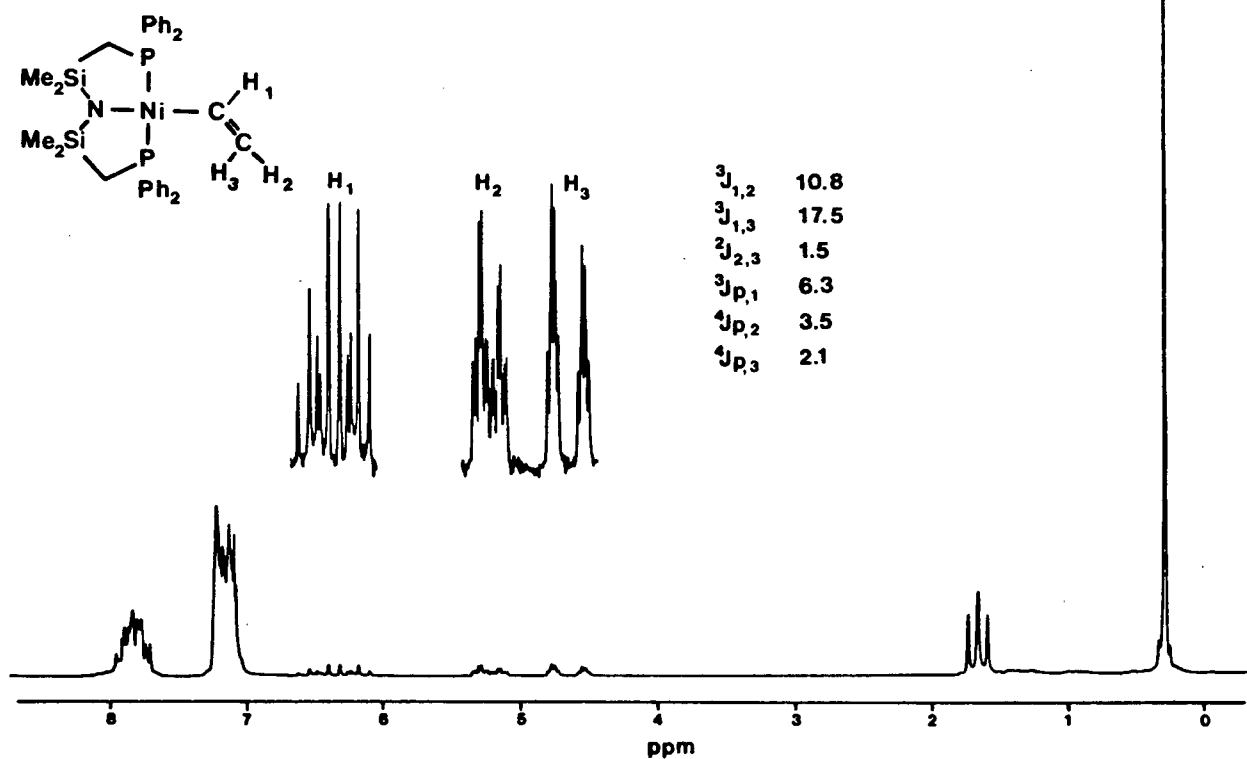


Fig. 2.2  $^1\text{H}$ NMR(80 MHz) spectrum of  $[\text{Ni}(\text{CH}=\text{CH}_2)\text{N}(\text{SiMe}_2\text{CH}_2\text{PPh}_2)_2]$  in  $\text{C}_6\text{D}_6$

triplet for the  $\text{CH}_2\text{P}$  protons is once again diagnostic of a trans orientation of the chelating phosphines; such a conformation is quite predictable in light of the fact that all known  $[\text{NiX(R)}(\text{PR}_3)_2]$  species have square planar geometries with mutually trans phosphines<sup>88,89</sup>. In addition, the methyl group of  $[\text{Ni}(\text{CH}_3)\text{N}(\text{SiMe}_2\text{CH}_2\text{PPh}_2)_2]$  appears as a sharp triplet upfield of TMS owing to cis coupling with the tridentate ligand's two phosphine centres ( $J_{\text{H,P}} = 10.0$  Hz). Although the vinyl derivative displays a complicated  $\text{ABCX}_2$  pattern for the vinyl protons, phosphorus decoupling significantly simplified the spectrum so that analysis of the proton-proton coupling constants was possible.

When R is the allyl group,  $\text{C}_3\text{H}_5$ , the  $^1\text{H}$ NMR is a classic  $\text{AX}_4$  pattern for the allyl protons (phosphorus coupling merely broadens these signals slightly). Since the syn and anti protons are equivalent, it is apparent that exchange is occurring, presumably via rapid (at least on the NMR time scale)  $\eta^3 \rightarrow \eta^1$  interconversions. Upon cooling to  $-80^\circ\text{C}$ , no changes were observed in the allyl proton resonances.

"Whenever an alkyl-metal complex is produced, one is almost obliged to treat it with CO to see if it will undergo migratory insertion"<sup>90</sup>. The reactivity of the nickel hydrocarbyl amido phosphines towards CO was therefore investigated. Indeed, all of these nickel species react readily under one atmosphere of carbon monoxide at room temperature to give nickel(0) derivatives in which the chelating mode of the ligand has been altered.

With  $[\text{Ni}(\text{CH}_3)\text{N}(\text{SiMe}_2\text{CH}_2\text{PPh}_2)_2]$ , carbonylation occurs very rapidly

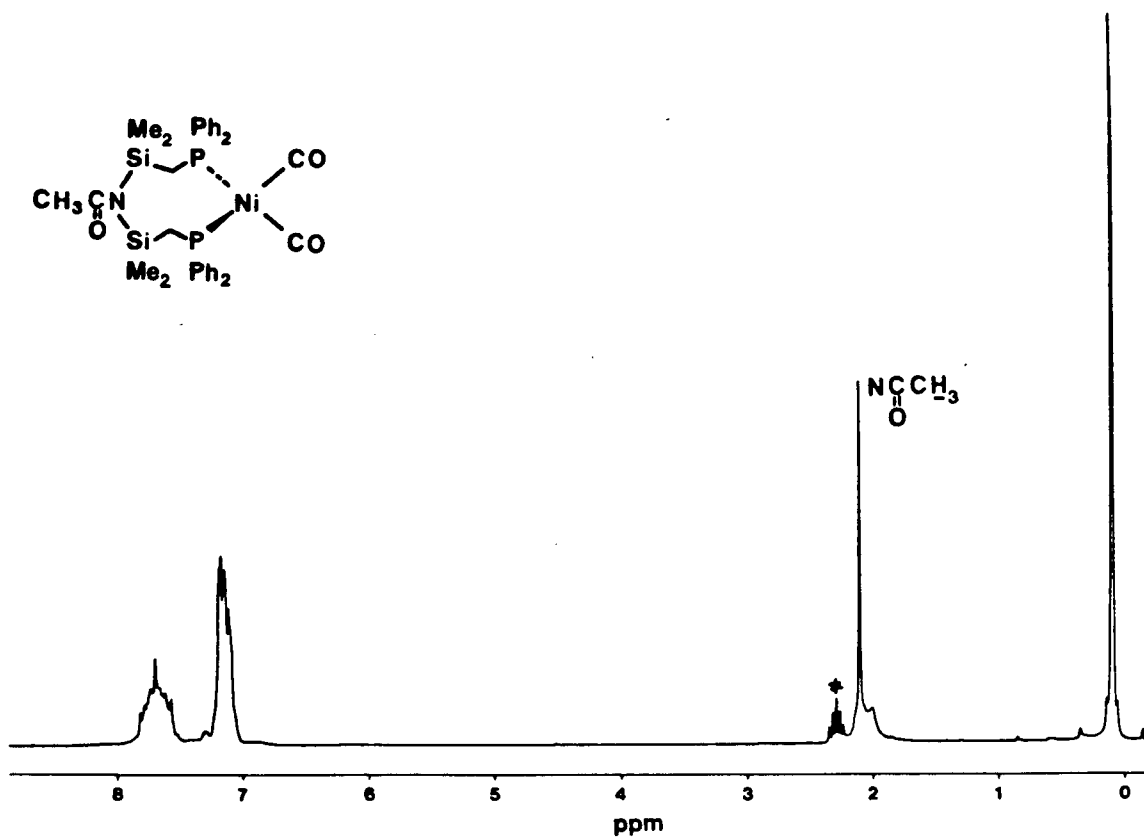


Fig. 2.3  $^1\text{H}$ NMR(80 MHz) spectrum of  $[\text{Ni}(\text{CO})_2\text{N}(\text{COCH}_3)(\text{SiMe}_2\text{CH}_2\text{PPh}_2)_2]$  in  $\text{C}_7\text{D}_8$

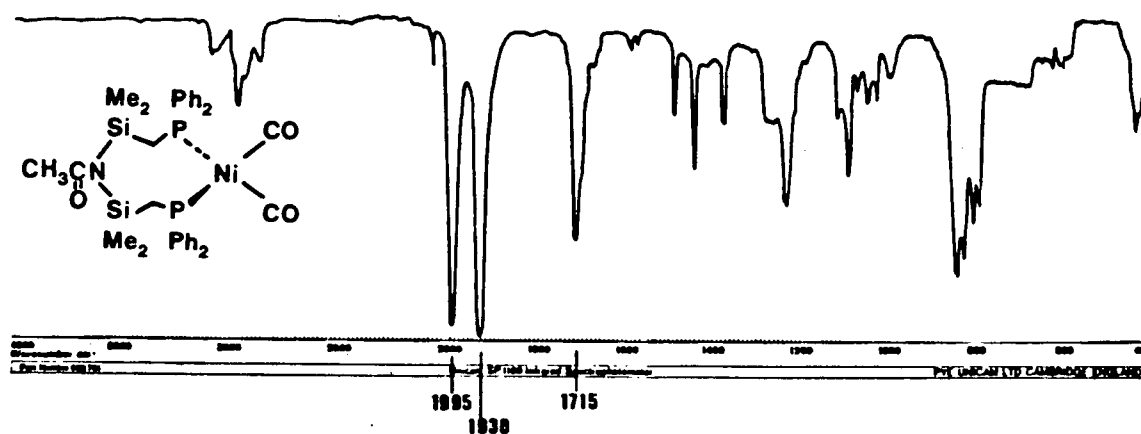
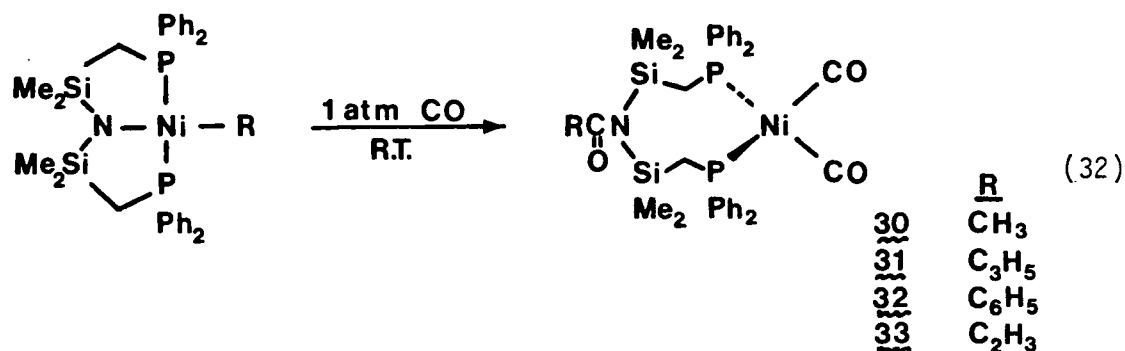


Fig. 2.4 IR(KBr disc) spectrum of  $[\text{Ni}(\text{CO})_2\text{N}(\text{COCH}_3)(\text{SiMe}_2\text{CH}_2\text{PPh}_2)_2]$

to produce the Ni(0) species in virtually quantitative yield (by NMR) (equation 32); the initially gold-orange solution fades within seconds of exposure to CO and after five minutes is completely colorless.

Colorless crystals of 30 are obtained from hexane; the chemical and molecular weight (Signer) analysis are consistent with the monomeric complex  $[\text{Ni}(\text{CO})_2\text{N}(\text{COMe})(\text{SiMe}_2\text{CH}_2\text{PPh}_2)_2]$ . The  $^1\text{H}$ NMR (Fig. 2.3) displays a broad

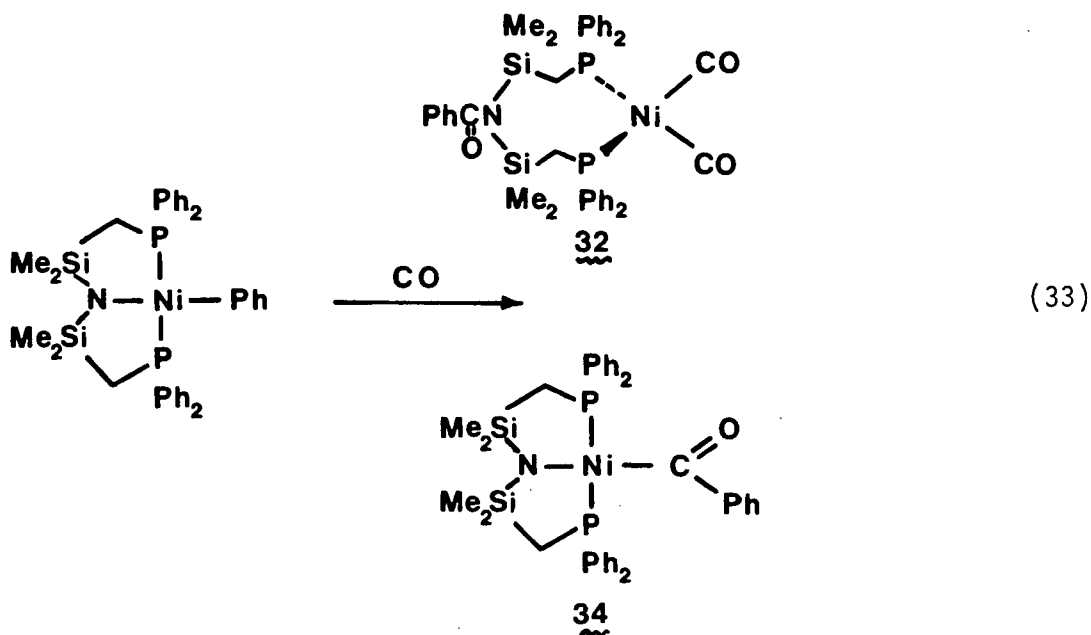


signal for the  $\text{CH}_2\text{P}$ , indicative of weak coupling to two cis phosphines. When the reaction is carried out under  $^{13}\text{CO}$ , the sharp singlet due to the acetyl protons ( $^{13}\text{COCH}_3$ ) is split into a doublet due to  $^{13}\text{C}$  coupling ( $J_{\text{H},^{13}\text{C}} = 6.35 \text{ Hz}$ ). The most significant structural information comes from the infra-red spectra of 30 (Fig. 2.4). In addition to the N-acetyl band at  $1715 \text{ cm}^{-1}$ , two very strong terminal carbonyl stretches at  $1995$  and  $1930 \text{ cm}^{-1}$ , indicative of two cis carbonyls, are also observed. These bands shift appropriately (to  $1680$ ,  $1955$  and  $1890 \text{ cm}^{-1}$ , respectively) upon incorporation of  $^{13}\text{CO}$ . The absorption at  $1715 \text{ cm}^{-1}$  is quite typical<sup>91</sup> of organic amides,  $-\text{NCOR}$ , which usually have  $\nu_{\text{COR}}$  values of  $1625$ - $1725 \text{ cm}^{-1}$ ; however, this is a rather high frequency stretch for nickel acyl  $\text{Ni-COR}$  groupings which absorb in the  $1600$ - $1650 \text{ cm}^{-1}$  range<sup>82-86</sup>.

The  $^{13}\text{C}\{^1\text{H}\}$ NMR of  $^{13}\text{C}$  enriched 30 is also consistent with the proposed structural formulation in that the terminal carbonyls appear as a triplet at 200.2 ppm due to cis phosphorus coupling ( $^2J_{31\text{P},13\text{C}} = 2.4 \text{ Hz}$ ) while the amide carbonyl ( $\text{Si}_2\text{NCOCH}_3$ ) is a singlet at 161.9 ppm. These chemical shifts are quite typical for transition metal carbonyl ( $\text{M-CO}$ )<sup>92</sup> and amide carbonyl functionalities<sup>93</sup>.

An identical reaction obtains for the nickel allyl derivative,  $[\text{Ni}(\text{C}_3\text{H}_5)\text{N}(\text{SiMe}_2\text{CH}_2\text{PPh}_2)_2]$ ; this reaction is also complete in five minutes and the product is obtained as colorless crystals in ~80% recrystallized yield. Once again, the IR consists of two very strong terminal carbonyl stretches at 1995 and 1935  $\text{cm}^{-1}$ , as well as a strong N-acyl band at 1715  $\text{cm}^{-1}$ . No other product is observed. The spectral and analytical data for 31 indicate that, like 30 it is a Ni(0) derivative in which the hybrid ligand is coordinated in a bidentate fashion through the phosphine donors.

However, the nickel hydrocarbyls having the  $\text{sp}^2$ -carbon ligands, vinyl and phenyl, show somewhat different migratory insertion behavior: not only is the reaction much slower but several products have been identified. After stirring a toluene solution of  $[\text{Ni}(\text{C}_6\text{H}_5)\text{N}(\text{SiMe}_2\text{CH}_2\text{PPh}_2)_2]$  under one atmosphere of CO for seven hours, a mixture of two products was obtained in an approximate 1:1 ratio (by NMR) (equation 33). Identification of the benzoyl nickel complex 34 and the Ni(0) derivative 32 was made possible by recrystallization of the crude product from neat hexane followed by Pasteur type separation of the orange prisms of 34 from the colorless crystals of 32. If this reaction is monitored by  $^1\text{H}$ NMR, it



is observed that the nickel benzoyl complex is formed rapidly and quantitatively at room temperature (<30 minutes); the subsequent formation of the Ni(0) complex is much slower, requiring several days. Pure 34 can thus be easily obtained by exposing a solution of [Ni(C<sub>6</sub>H<sub>5</sub>)-N(SiMe<sub>2</sub>CH<sub>2</sub>PPh<sub>2</sub>)<sub>2</sub>] to CO for only twenty minutes followed by recrystallization from toluene/hexane; 32 is produced exclusively if the solution is stirred under CO for three days. As expected, a C<sub>6</sub>D<sub>6</sub> solution of 34, sealed in an NMR tube under CO, slowly reacts to quantitatively form the Ni(0) complex 32. Interestingly, the <sup>1</sup>HNMR spectrum of 34 is rather complex (Fig. 2.5), consisting of two sharp SiMe<sub>3</sub> peaks (of equal intensity), an

AB quartet of virtual triplets for the  $\text{CH}_2\text{P}$  protons and a complicated set of phenyl resonances. Upon heating to  $80^\circ\text{C}$ , the two silyl methyl

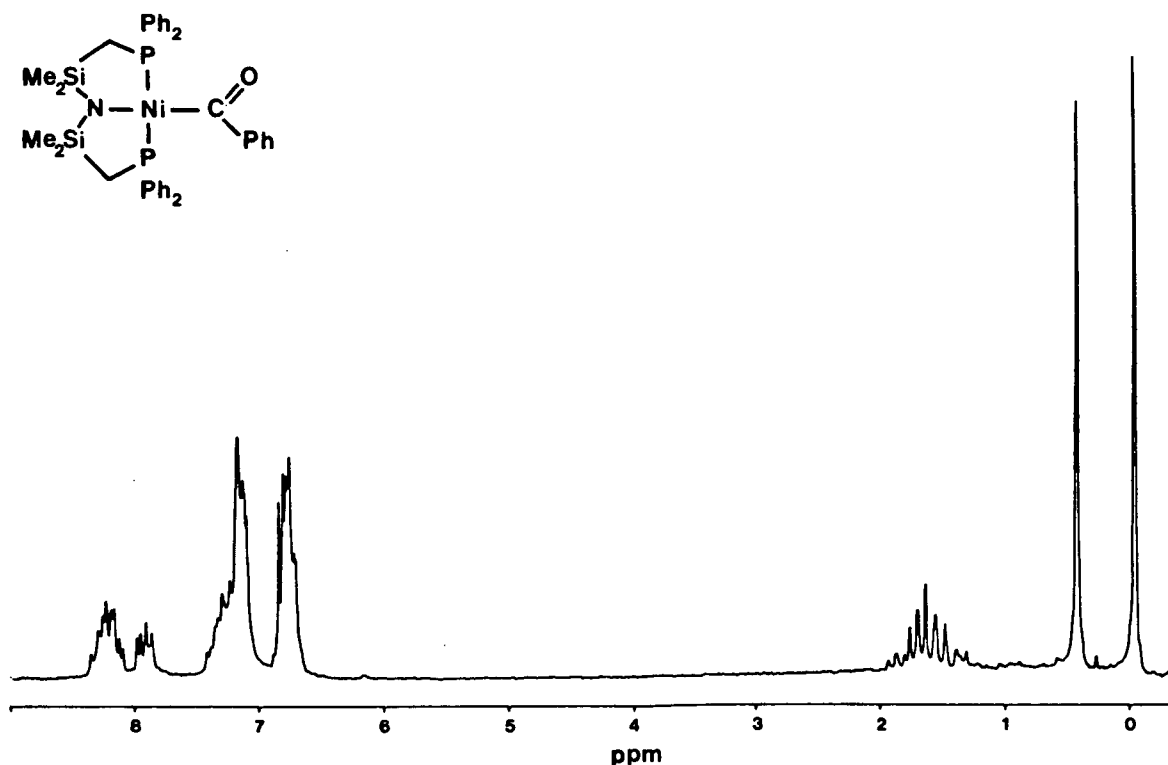
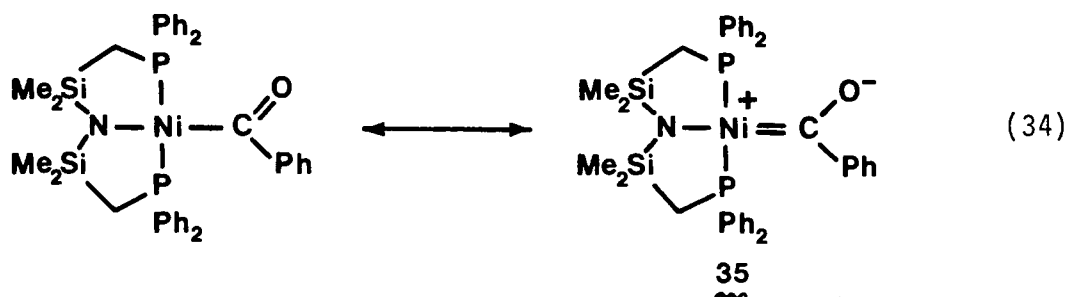


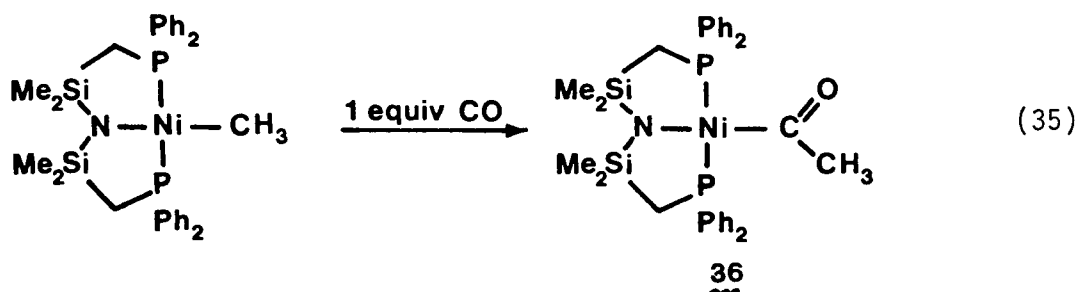
Fig. 2.5  $^1\text{H}$ NMR(80 MHz) spectrum of  $[\text{Ni}(\text{COC}_6\text{H}_5)\text{N}(\text{SiMe}_2\text{CH}_2\text{PPh}_2)_2]$  in  $\text{C}_6\text{D}_6$

peaks collapse to a broad singlet. The spectral data are consistent with restricted rotation of the  $\text{NiCOPh}$  group about the  $\text{Ni-C}$  bond, which is probably a result of steric interactions of the nickel benzoyl fragment with the tridentate ligand's phenyl substituents. Alternatively, this

could be explained as a consequence of multiple Ni-C bonding as shown in 35 (equation 34).



The corresponding nickel acetyl complex 36 can also be prepared by the stoichiometric addition of one equivalent of CO to a toluene solution of [Ni(CH<sub>3</sub>)N(SiMe<sub>2</sub>CH<sub>2</sub>PPh<sub>2</sub>)<sub>2</sub>] (equation 35). The <sup>1</sup>HNMR of this complex



consists of a broad singlet for the SiMe<sub>3</sub> protons at room temperature which becomes a sharp doublet upon cooling to -30°C (Fig. 2.6). Once again, this is consistent with restricted rotation about the Ni-COCH<sub>3</sub> bond. Both the benzoyl and acetyl derivatives 34 and 36 are stable, crystalline solids but do evolve CO upon heating, to regenerate the starting hydrocarbyl complex.

For the nickel-vinyl starting material, reaction with CO is complete in three hours, as indicated by the formation of a colorless solution of 33.

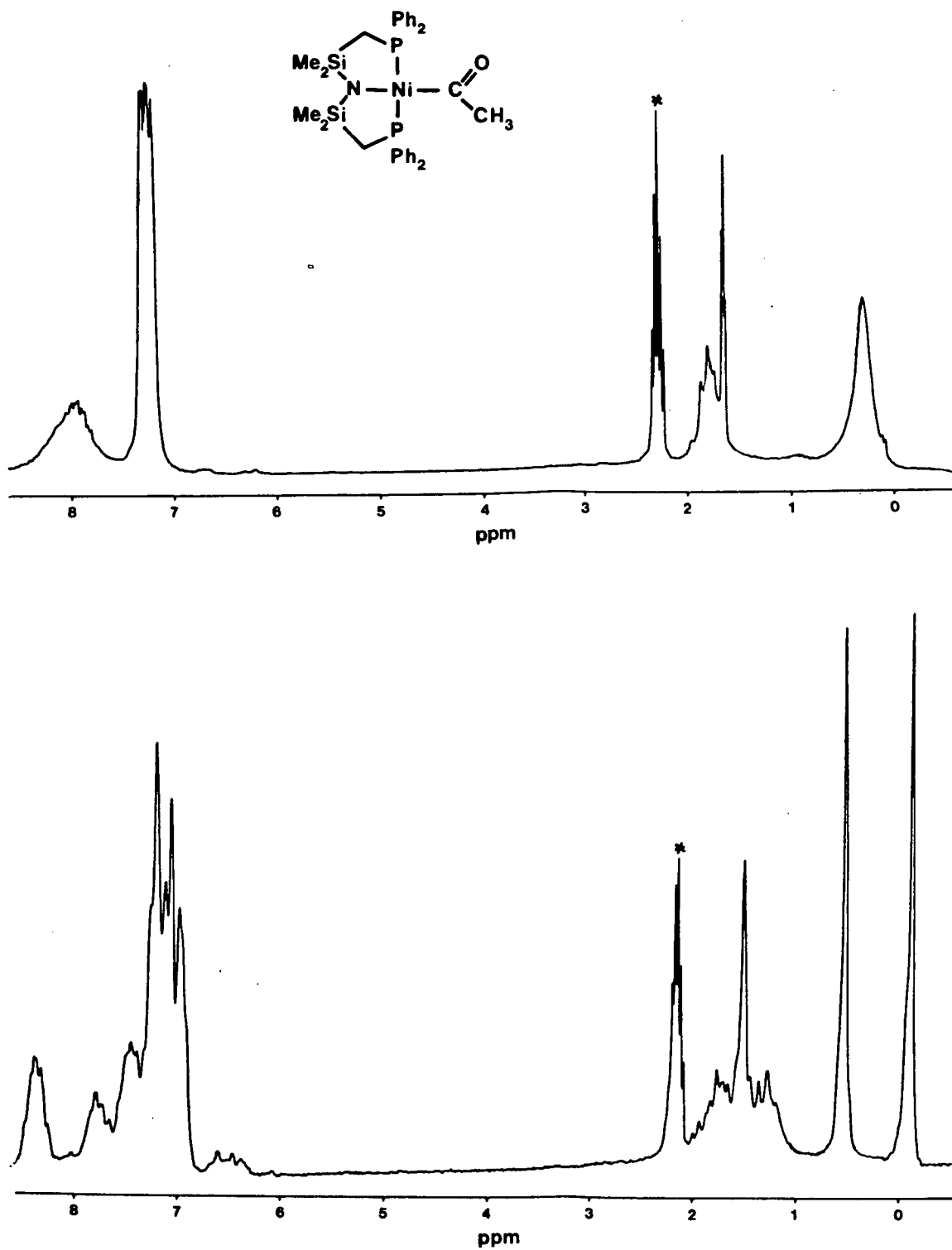
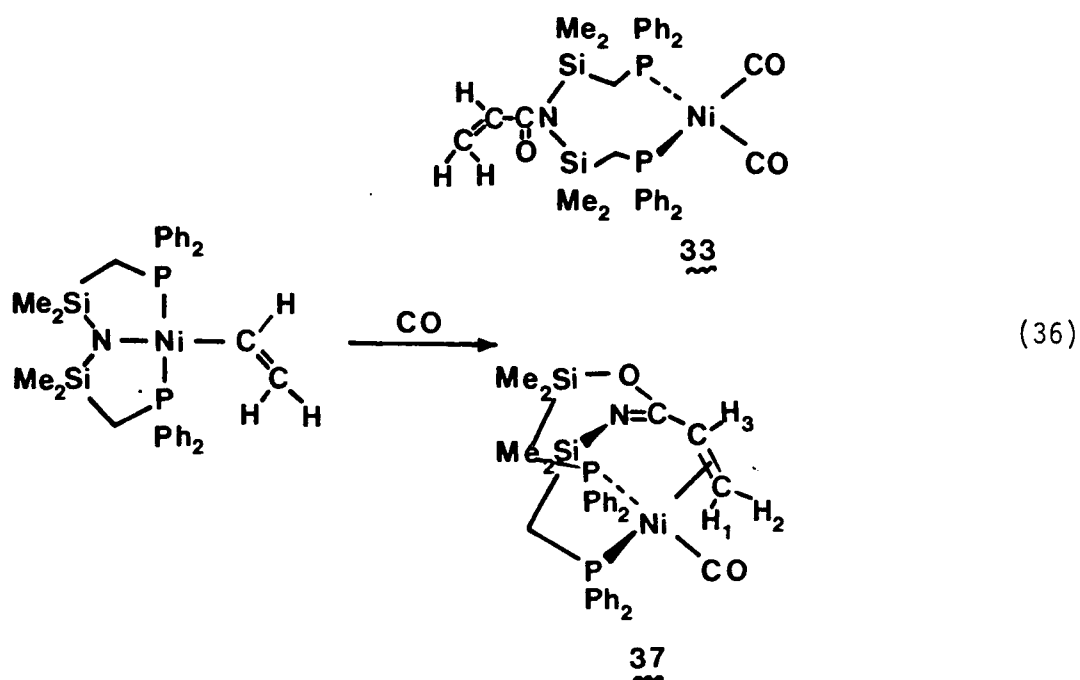


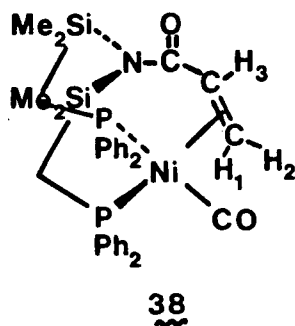
**Fig. 2.6** a)  $^1\text{H}$ NMR(80MHz) spectrum of  $[\text{Ni}(\text{COCH}_3)\text{N}(\text{SiMe}_2\text{CH}_2\text{PPh}_2)_2]$  in  $\text{C}_7\text{D}_8$  at  $298^\circ\text{K}$ .  
 b)  $^1\text{H}$ NMR(80MHz) spectrum of  $[\text{Ni}(\text{COCH}_3)\text{N}(\text{SiMe}_2\text{CH}_2\text{PPh}_2)_2]$  in  $\text{C}_7\text{D}_8$  at  $243^\circ\text{K}$ .



However, the <sup>1</sup>HNMR of the pale yellow oily residue, left after solvent removal, indicates that, in addition to the expected N-acryloyl species 33 (which is the major product in ~90% yield, by NMR), another Ni(0) product is formed (equation 36). Although initially a minor component of the product mixture, this species may be selectively separated as fine yellow crystals by repeated recrystallizations from hexane. In fact, attempts to obtain pure 33 have been unsuccessful, since it slowly loses a CO ligand in solution or under vacuum to produce 37. Thus the yield of 37 can be increased to ≥90% (by NMR) by slow removal of CO under high vacuum over a two day period, as indicated by the gradual deepening of the solution to a clear yellow-orange color. The reversible nature of

this reaction is demonstrated by the fact that yellow  $C_6D_6$  solutions of analytically pure 37, sealed in NMR tubes under one atmosphere of  $CO$ , fade to colorless within minutes; 33 is the only observed species.

Originally,  $\zeta$  was formulated, on the basis of extensive spectral data, as an  $\eta^2$ -acryloyl complex wherein the rearranged ligand binds in a tridentate fashion through the  $\pi$ -system of the vinyl group as well as the two phosphine centres. Since the coordinated olefin of this complex,



as depicted in structure 38, has enantiotopic faces, the  $\text{SiMe}_3$  groups are diastereotopic and should therefore give rise to four resonances in the  $^1\text{H}$ NMR. This is indeed the case, as shown by the 400 MHz spectrum illustrated in Fig. 2.7. In addition, the  $\text{CH}_2\text{P}$  protons are also diastereotopic and display four sets of doublets of doublets. The olefinic protons are shifted upfield, as compared to the starting nickel-vinyl complex, and are split by two inequivalent phosphorous nuclei; although complicated, simulation of this ABCXY pattern (Fig. 2.8) allows full assignment of proton-proton and proton-phosphorus coupling constants. The infra-red data are also consistent with this formulation owing to the single very strong terminal carbonyl absorption at  $1950\text{ cm}^{-1}$  as well as a strong band at  $1625\text{ cm}^{-1}$ , ascribed to  $\nu_{\text{COC}_2\text{H}_3}$  of the  $\eta^2$ -acryloyl

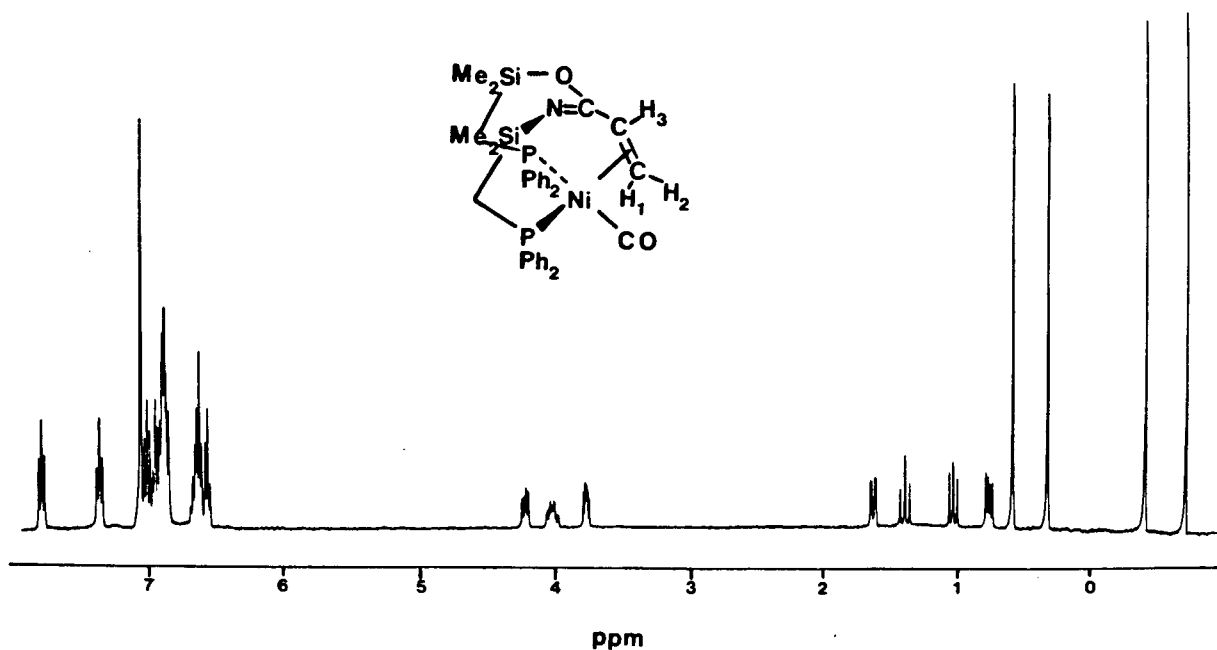


Fig. 2.7  $^1\text{H}$ NMR(400MHz) spectrum of  $[\text{Ni}(\text{CO})\text{N}(\text{COC}_2\text{H}_3)(\text{SiMe}_2\text{CH}_2\text{PPh}_2)_2]$  in  $\text{C}_6\text{D}_6$

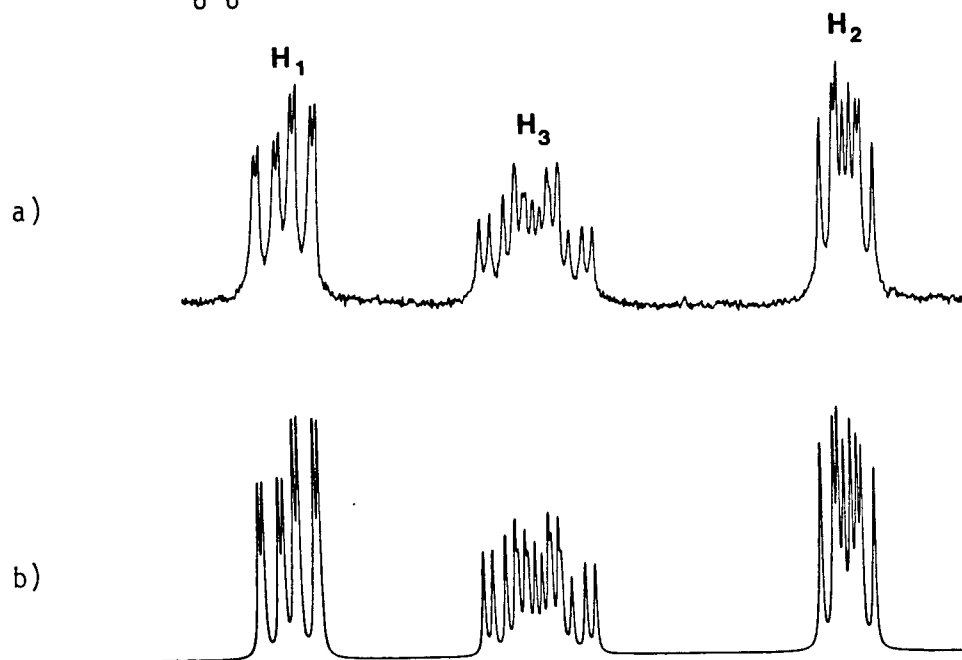


Fig. 2.8 a) Vinyl proton region (400 MHz  $^1\text{H}$ NMR) of  $[\text{Ni}(\text{CO})\text{N}(\text{COC}_2\text{H}_3)(\text{SiMe}_2\text{CH}_2\text{PPh}_2)_2]$   
 b) Spectral simulation of vinyl proton ABCXY pattern:  
 $J_{1,3} = 11.72$ ,  $J_{2,3} = 7.57$ ,  $J_{1,p1} = 6.59$ ,  $J_{2,p1} = 5.62$ ,  
 $J_{1,p2} = 1.46$ ,  $J_{3,p1} = 13.92$ ,  $J_{3,p2} = 3.17$ ,  $J_{2,p2} = 4.15$ .

group. Further evidence is provided by the  $^{31}\text{P}\{^1\text{H}\}$ NMR spectrum which consists of an AX doublet of doublets ( $\delta\text{A} = 16.38$  ppm;  $\delta\text{X} = -1.38$ ;  $J_{\text{AX}} = 57.9$  Hz) due to the inequivalent phosphine centres.

However, the x-ray crystal structure of 37 is slightly different than predicted (Fig. 2.9). Although the coordination about the nickel centre is correct as postulated for 38, with one terminal carbonyl, a

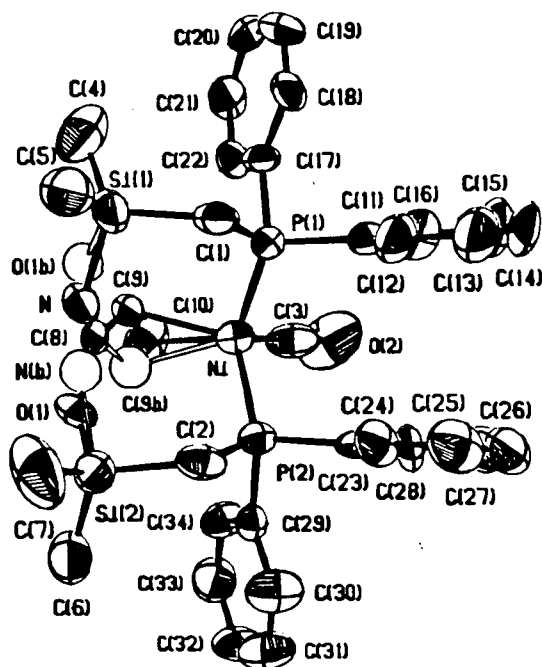


Fig. 2.9 X-ray crystal structure of  $[\text{Ni}(\text{CO})\text{N}(\text{COC}_2\text{H}_3)(\text{SiMe}_2\text{CH}_2\text{PPh}_2)_2]$  (alternate chelate ring conformation is indicated by unshaded thermal ellipsoids).

coordinated olefin, and two phosphines, the hybrid ligand backbone has undergone a further rearrangement. A "silatropic shift" of one of the silicon centres to the carbonyl oxygen of the N-acryloyl fragment results in the observed "imide" structure. Nonetheless, all of the aforementioned spectral data are consistent with the solid state structure of Fig. 2.9.

Several questions are now raised by the crystallographic structural characterization of 37. Does this solid state structure persist in solution or is it merely a result of crystal packing effects? In the absence of X-ray crystallographic data for 30, 31, and 32, is this type of amide  $\rightarrow$  imide isomerization also occurring with the other Ni(0) complexes? If not, why does only the acryloyl fragment rearrange?

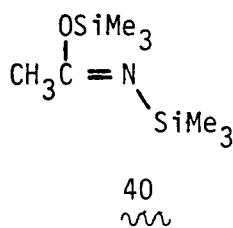
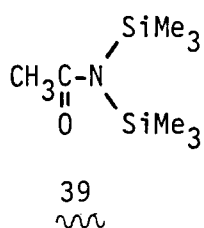
All spectral information acquired to date suggests that the solid state structure of 37 is identical to its structure in solution. The infra-red spectra in solution ( $\text{CH}_2\text{Cl}_2$ , toluene, or hexane) have identical values of  $\nu_{\text{COC}_2\text{H}_3}$  ( $1625\text{ cm}^{-1}$ ) as observed for a KBr disc of 37. Unfortunately, distinction cannot be made, on an IR basis, between the amide and the imide tautomers, since the absorption ranges overlap ( $1625 - 1725\text{ cm}^{-1}$  for the former versus  $1600 - 1675\text{ cm}^{-1}$  for the latter)<sup>91</sup>. Although four silyl methyl resonances would be expected in the  $^1\text{H}$ NMR for both 37 and 38, the large chemical shift range of the  $\text{SiCH}_3$  signals ( $-0.67 \rightarrow +0.67\text{ ppm}$ ) as well as the fact that only two of these peaks display phosphorus coupling ( $J_{\text{H,P}} = 0.98\text{ Hz}$ ) would be more consistent with the imide structure.

The  $^{31}\text{P}\{^1\text{H}\}$ NMR indicates a rather large chemical shift difference, of almost 18 ppm, between the two phosphine doublets. Although the phosphines of  $\text{38}$  are diastereotopic, such a drastic shift difference seems quite unreasonable; an AB quartet might be more appropriate. When the  $^{31}\text{P}\{^1\text{H}\}$ NMR spectrum of  $^{15}\text{N}$ -labelled  $\text{37}$  is recorded, only the resonance at -1.38 ppm displays phosphorus - $^{15}\text{N}$  coupling. Once again, this implies that the imidate  $\text{37}$  is the only form present in solution, since the three-bond  $^{31}\text{P}$ - $^{15}\text{N}$  coupling in the  $^{15}\text{NSiMe}_2\text{CH}_2\text{PPh}_2$  fragment should be greater than the four-bond coupling in the  $^{15}\text{N}=\text{COSiMe}_2\text{CH}_2\text{PPh}_2$  fragment. The unusually high chemical shift value of -1.38 ppm (as compared to all of the previously prepared Group VIII amido phosphines which have  $^{31}\text{P}\{^1\text{H}\}$  signals in the 10  $\rightarrow$  35 ppm range) might be explained in terms of ring strain imposed by the coordination of the olefin. Studies by Garrou<sup>94</sup> have shown that the  $^{31}\text{P}$  shift value of a transition metal complex incorporating a chelating phosphine is significantly dependent upon the size of the metal-chelate ring. It is quite possible that upon coordination of the olefin in  $\text{37}$  the resulting chelate ring is somewhat strained, thereby weakening one of the Ni-P bonds and giving rise to the relatively high field  $^{31}\text{P}$  shift.

Although the  $^{31}\text{P}\{^1\text{H}\}$ NMR,  $^1\text{H}$ NMR, and IR are somewhat inconclusive as to the solution structure of  $\text{37}$  it would seem reasonable to postulate the imidate form. At present, the  $^{29}\text{Si}$ NMR of  $^{15}\text{N}$ -labelled  $\text{37}$  is being investigated in hope of affirming this proposal.

In light of the well-documented lability of trimethyl silyl groups in organic compounds<sup>95,96</sup>, the imidate rearrangement of the nickel  $\eta^2$ -

acryloyl should not be too surprising. This type of behavior has been extensively investigated for the popular silylating agent bis (trimethylsilyl) acetamide<sup>97-100</sup>. The <sup>1</sup>HNMR of this compound at room temperature (CDCl<sub>3</sub>) indicates an approximate 1:1 ratio of the amide (N,N) and imidate (N,O) forms 39 and 40. In contrast, the



mono(trimethylsilyl) amides, such as N-methyl-N-trimethylsilylacetamide, have generally been accepted as having the amide structure. However, both the mono and bis silyl compounds show temperature dependent NMR behavior, which can be rationalized as either the result of hindered rotation about the C-N bond or SiMe<sub>3</sub> group exchange<sup>101</sup>. Other spectral studies<sup>102</sup>, involving <sup>13</sup>C and <sup>29</sup>SiNMR, has also confirmed the presence of both tautomeric forms at room temperature for a variety of compounds R<sup>1</sup>CONR<sup>2</sup>SiMe<sub>2</sub>R<sup>3</sup> (R<sup>1</sup> = CH<sub>3</sub>, C<sub>2</sub>H<sub>5</sub>O; R<sup>2</sup> = H, CH<sub>3</sub>, C<sub>6</sub>H<sub>5</sub>, Si(CH<sub>3</sub>)<sub>3</sub>, p-CH<sub>3</sub>C<sub>6</sub>H<sub>4</sub>, p-ClC<sub>6</sub>H<sub>4</sub>, p-CH<sub>3</sub>OC<sub>6</sub>H<sub>4</sub>; R<sup>3</sup> = CH<sub>3</sub>, C<sub>6</sub>H<sub>5</sub>, p-CH<sub>3</sub>C<sub>6</sub>H<sub>4</sub>, p-CH<sub>3</sub>OC<sub>6</sub>H<sub>4</sub>). Generally, there is a <sup>29</sup>Si shift difference of ~9 ppm for an NSi (δ = ~10 ppm) versus an OSi grouping (δ ~19 ppm); a shift difference of ~15 ppm is observed between the amide and the imidate forms in the <sup>13</sup>CNMR. By determining the relative concentrations of the tautomers over a wide temperature range, it was concluded that the amide form is favored by electron donating groups at N and by decreasing temperature.

In contrast, the Ni(0) species  $\underline{30}$ ,  $\underline{31}$ ,  $\underline{32}$  and  $\underline{33}$  show no evidence of tautomerism. The  $^1\text{H}$ NMR of  $\underline{30}$  has only one singlet for the  $\text{SiMe}_2$  protons even down to  $-80^\circ\text{C}$  and up to  $120^\circ\text{C}$ . The broad signal for the  $\text{CH}_2\text{P}$  protons does sharpen to a doublet at high temperatures, but this is probably a consequence of conformational changes in the eight-membered chelate ring. The  $^{31}\text{P}\{^1\text{H}\}$ NMR of  $\underline{30}$  is a singlet (an identical situation obtains for  $\underline{31}$ ,  $\underline{32}$ , and  $\underline{33}$ ) whereas the imidate form of  $\underline{30}$  should give two peaks (a mixture of amide and imidates would, of course, complicate the spectra further). Similarly, the  $^{13}\text{C}\{^1\text{H}\}$ NMR of the Ni(0) complexes indicates the presence of only one tautomer in solution at room temperature, although the chemical shift values are not sufficiently disparate to unequivocally distinguish between the two possible structures ( $^{13}\text{C}$  values for the COR unit of  $\underline{30} \rightarrow \underline{33}$  lie in the range 162 - 158 ppm, whereas the chemical shift for  $\underline{37}$  is 166 ppm).

Molecular models of  $\underline{37}$  and  $\underline{38}$  indicate that the formation of either structure seems equally favorable on steric grounds. However, delocalization of electron density from the nickel-olefinic bond into the  $\text{C}=\text{N}$   $\pi$ -system may be the driving force for the silatropic rearrangement observed for the  $\eta^2$ -acryloyl nickel complex (Fig. 2.10); such an extended  $\pi$ -system is not available in the amide form, or, of course, in those N-acyls having R groups other than vinyl.

Although the ligand rearrangement observed in the formation of the complexes  $[\text{Ni}(\text{CO})_2\text{N}(\text{COR})(\text{SiMe}_2\text{CH}_2\text{PPh}_2)_2]$  ( $\text{R} = \text{Me, allyl, vinyl, phenyl}$ ) may at first seem rather unusual, variable temperature  $^1\text{H}$  and  $^{31}\text{P}$  NMR as

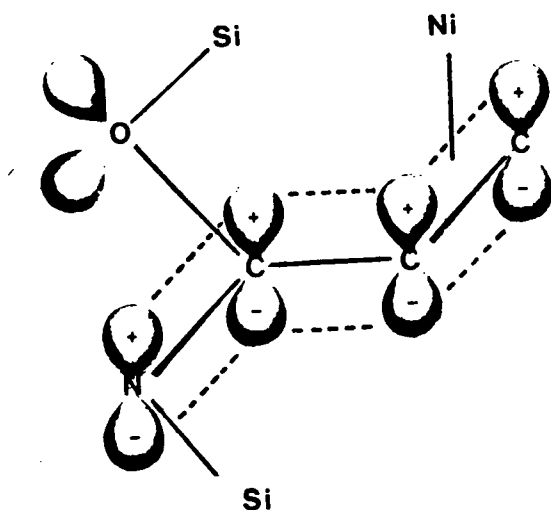
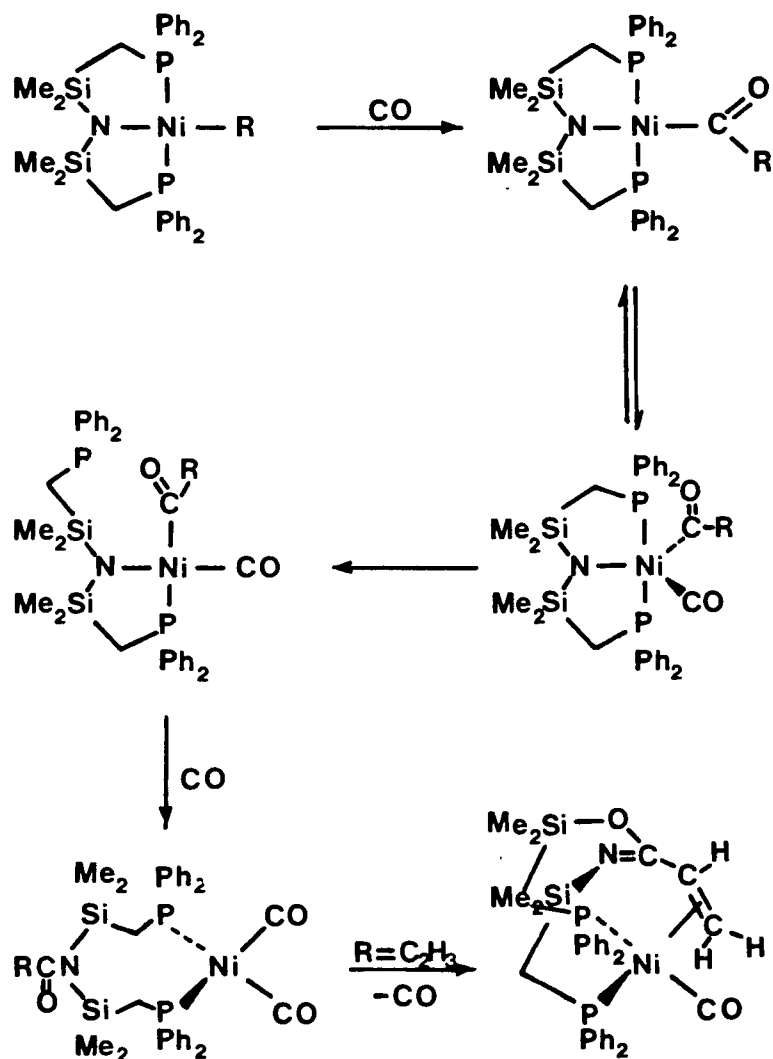


Fig. 2.10  $\pi$ -system of the nickel  $\eta^2$ -acryloyl complex (imidate form)

well as labelling experiments have suggested a possible mechanism. At low temperature, the acetyl complex<sup>36</sup> forms immediately upon exposure of a  $C_7D_8$  solution of  $[Ni(CH_3)N(SiMe_2CH_2PPh_2)_2]$  to CO. Upon warming to  $-40^\circ C$ , the  $Ni(0)$  species is gradually formed, the reaction going to completion in approximately two hours. The  $^{31}P\{^1H\}$ NMR at  $-40^\circ C$  contains only two singlets throughout the course of the reaction, one at 26.7 ppm (due to the starting material) and the other at 15.5 ppm (due to the acetyl complex<sup>36</sup> and the  $Ni(0)$  derivative<sup>30</sup>, which have degenerate chemical shifts). No other species was detected. A possible mechanism could therefore involve initial insertion of CO into the nickel-carbon bond, resulting in a nickel-acyl (or aroyl) species which then undergoes

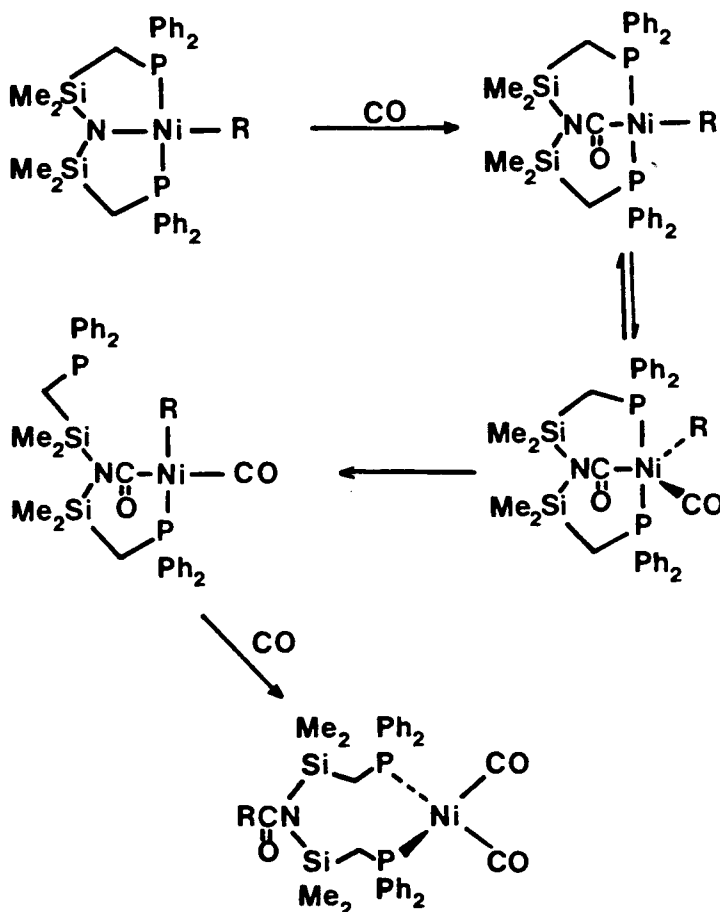
reductive elimination of the acyl group to the amide nitrogen. A plausible mechanism is outlined in Scheme 2.1.

**Scheme 2.1**



An alternative mechanism proceeding through an initial insertion of carbon monoxide into the Ni-N bond to form an intermediate Ni(II) carbamoyl could conceivably produce the same results (Scheme 2.2).

**Scheme 2.2**



However, the isolation of the acetyl complex <sup>36</sup> and the benzoyl derivative <sup>34</sup> would seem to decrease the significance of this pathway. In addition, Marks<sup>103</sup> has shown that for the alkyl dialkylamide complex [Th(Cp\*)<sub>2</sub>(NMe<sub>2</sub>)-

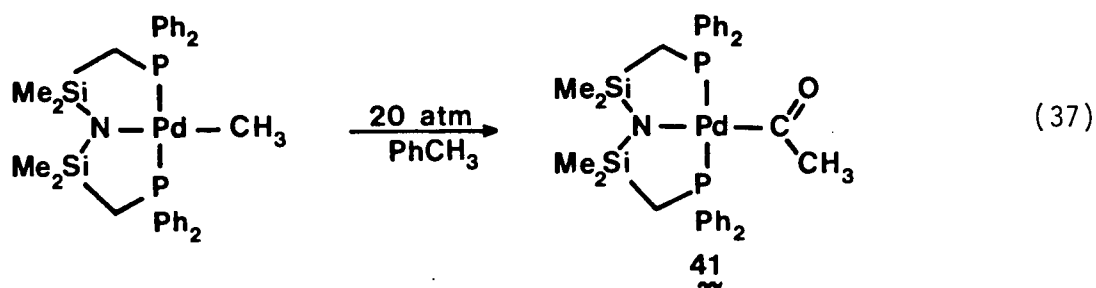
$\text{CH}_3$ ], CO insertion into the Th-C bond was observed, even though the dialkylamide  $[\text{Th}(\text{Cp}^*)_2(\text{NMe}_2)_2]$  readily forms the carbamoyl complex  $[\text{Th}(\text{Cp}^*)_2(\text{CONMe}_2)_2]$ . Thus, it would seem that the migratory aptitude of an alkyl group is greater than for an amide,  $\text{NR}_2$ , ligand. Finally, the fact that the rhodium and iridium amido phosphines  $[\text{MLN}(\text{SiMe}_2\text{CH}_2\text{PPh}_2)_2]$  ( $\text{M} = \text{Rh}, \text{Ir}$ ;  $\text{L} = \text{COE}, \text{PPh}_3$ ) react in a straightforward manner under CO to give the corresponding carbonyl  $[\text{M}(\text{CO})\text{N}(\text{SiMe}_2\text{CH}_2\text{PPh}_2)_2]$  as the sole product, also implies that CO insertion into the M-N bond is not a facile process with these Group VIII amido phosphines.

#### Migratory Insertion of Carbon Monoxide into Palladium(II)-Carbon Bonds

The alkyl derivatives  $[\text{Pd}(\text{CH}_3)\text{N}(\text{SiMe}_2\text{CH}_2\text{PPh}_2)_2]$  and  $[\text{Pd}(\text{C}_3\text{H}_5)\text{N}(\text{SiMe}_2\text{CH}_2\text{PPh}_2)_2]$  are readily prepared via metathesis of  $[\text{PdClN}(\text{SiMe}_2\text{CH}_2\text{PPh}_2)_2]$  with Grignard reagents, in a similar manner as outlined for their nickel analogues. In contrast to the nickel allyl complex,  $[\text{Pd}(\text{C}_3\text{H}_5)\text{N}(\text{SiMe}_2\text{CH}_2\text{PPh}_2)_2]$  demonstrates only the  $\eta^1$  mode of bonding at ambient temperatures (by  $^1\text{H}$ NMR). Upon increasing the temperature, the allyl resonances broaden; above  $50^\circ\text{C}$ , an  $\text{AX}_4$  pattern ( $^{31}\text{P}$  decoupled) is observed, indicating rapid  $\eta^3 \rightarrow \eta^1$  interconversions of the syn and anti allyl protons. Once again, these palladium alkyls are crystalline, air and moisture sensitive solids which are very soluble in a wide variety of organic solvents.

In view of the fact that square planar palladium(II) complexes of the type trans- $[\text{Pd}(\text{PR}_3)_2(\text{CH}_3)\text{X}]$  ( $\text{X} = \text{Cl}, \text{Br}$ ;  $\text{PR}_3 = \text{PEt}_3, \text{PPh}_3, \text{PPh}_2\text{Me}$ ) react readily with CO (1-3 atmospheres) at room temperature to give the

corresponding palladium acetyl derivatives<sup>104-106</sup>, it is rather surprising that the palladium alkyl amido phosphines are completely unreactive to CO under these conditions. However, under 20 atmospheres CO, the palladium acyl 41 is the only observed product, which is obtained from hexane as analytically pure red crystals (equation 37). No further reaction with CO took place. The more robust nature of the palladium alkyls, as compared to their nickel analogues, parallels previous CO



migratory insertion reactivity patterns and is undoubtedly a consequence of increased Pd-C bond strength.

The reactivity of the corresponding platinum derivatives could not be surveyed since  $[\text{PtClN}(\text{SiMe}_2\text{CH}_2\text{PPh}_2)_2]$  does not undergo metathesis with Grignard or alkyl lithium reagents. A variety of reaction conditions was investigated as well as a number of different alkylating agents but only intractable mixtures or starting material were isolated. An alternate route using  $\text{AgBF}_4$  or  $\text{AgClO}_4$  in  $\text{CH}_2\text{Cl}_2$  or  $\text{CH}_3\text{CN}$  in an attempt to abstract the chloride resulted only in the formation of a silver mirror but no  $\text{AgCl}$ . A possible explanation for this anomalous behavior is that the Pt-Cl bond has been strengthened due to the weak trans influence of the amide nitrogen<sup>107</sup>.

This is supported by the Pt-Cl stretching frequency at  $317\text{ cm}^{-1}$ , indicating a very strong Pt-Cl bond. Similar behavior has been observed in other platinum complexes containing a trans X-Pt-NR<sub>2</sub> grouping<sup>108</sup>.

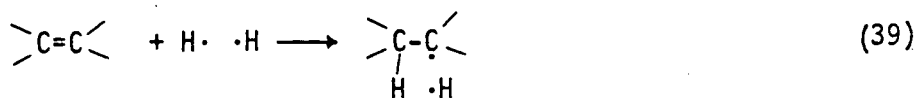
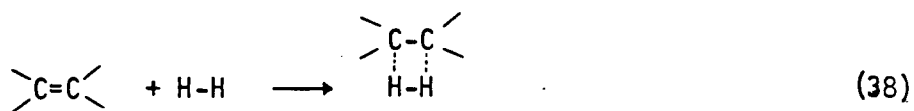
### Chapter III

#### Homogeneous Catalytic Hydrogenation of Olefins Employing Rhodium and Iridium Phosphine Complexes.

##### General Principles

Since the discovery of Wilkinson's catalyst,  $\text{RhCl}(\text{PPh}_3)_3$ , in 1965<sup>109,110</sup> rhodium phosphine complexes have been employed extensively in catalytic homogeneous hydrogenations of substrates containing olefinic or acetylenic bonds. In fact, these reactions have been more thoroughly studied than any other class of organometallic transformation. Obviously, this is in part due to their synthetic (and possible industrial) utility. However, interest has also been spurred by the complexity of these reactions, which pose intricate mechanistic challenges, as well as the immense variation possible in the catalyst design.

The general mechanistic picture for all homogeneous catalytic hydrogenations can be broken down into three distinct stages: dihydrogen activation, substrate activation, and hydrogen transfer. The role of the transition metal catalyst in the reaction of dihydrogen with an unsaturated organic molecule is mainly to circumvent the orbital symmetry restrictions (Woodward-Hoffman) presented by the concerted reaction of two diatomic, or pseudodiatom, molecules such as  $\text{O}_2$ ,  $\text{H}_2$ ,  $\text{N}_2$ ,  $\text{C}_2\text{H}_4$  (equation 38)<sup>111</sup>. A stepwise process would theoretically be possible (equation 39), but since this involves high energy hydrogen atoms, reaction does not occur by this route either. However, if the hydrogen is first bonded to one or two other atoms, such as a transition metal, addition of dihydrogen to an unsaturated



carbon-carbon bond is both thermodynamically and symmetry allowed. Since the d-orbitals of these transition metals are of correct symmetry to interact directly with  $\text{H}_2$  (Fig.3.1), two metal-hydride bonds may be formed; the process is thus a homolytic splitting of dihydrogen. Hydrogen transfer from this hydride complex to the olefin is now possible. Such a homolytic

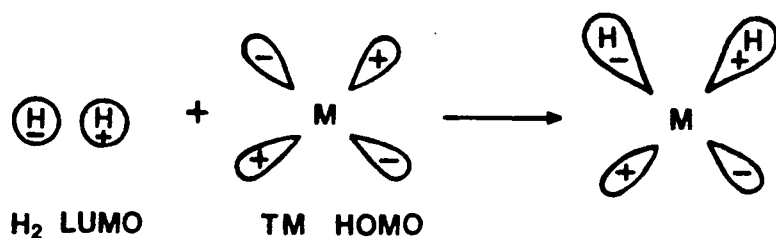
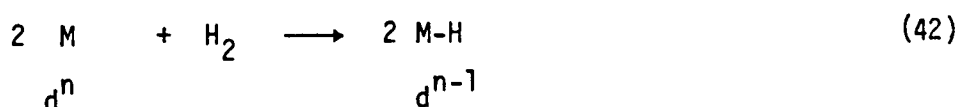
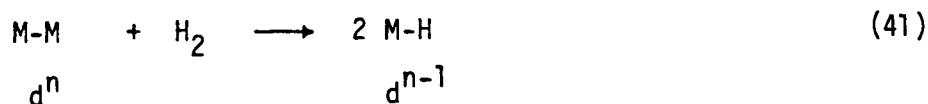
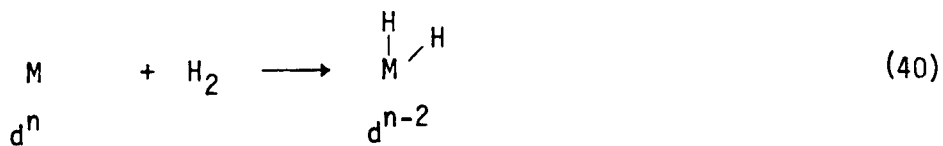


Fig. 3.1 Orbital representation of dihydrogen activation by a transition metal complex

cleavage of  $\text{H}_2$  requires a formal two electron oxidation of the transition metal, or one electron oxidation of two metal centres (equations 40-42).



This explains in part why rhodium and iridium complexes, which readily undergo two electron transformations between the +1 and +3 oxidation states, are so effective and widely used in these catalytic reactions.

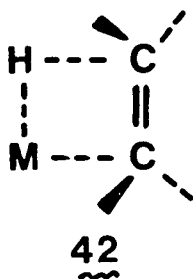
Another means of activating dihydrogen, which obviates a formal oxidation of the metal, involves heterolytic splitting<sup>112</sup> (equation 43). Often, this reaction is promoted by addition of base, or by hydrogenolysis of an ancillary alkyl ligand. Although this process can also be envisioned as an oxidative addition of dihydrogen, followed by reductive elimination



of HX (X = halide, alkyl or aryl), heterolytic cleavage usually occurs only with metals in higher oxidation states<sup>112</sup>.

Both homolytic and heterolytic activation of H<sub>2</sub> require at least one free coordination site. This may be achieved by use of an initially coordinatively unsaturated complex or through ligand dissociation from a coordinatively saturated species. Substrate activation also requires an open coordination site since this is usually accomplished by binding of the unsaturate to the metal centre to form a transition metal  $\pi$ -olefin complex. Although the simultaneous coordination of hydrogen and substrate by the metal atom is often necessary (except in the case of free radical mechanisms), the satisfaction of this criterion does not guarantee hydrogenation. A number of quite stable hydrido olefin or diene complexes is

known, an example being cis, trans- $[\text{IrH}_2(\text{COD})(\text{PMePh}_2)_2]^+{}^{113}$ ; their reluctance to undergo migratory insertion of the olefin into the M-H bond has been ascribed to lack of the required coplanar arrangement of the metal, hydride, and olefin  $\pi$ -bond (42).



It has been demonstrated that, in all cases (except free radical), hydrogen transfer proceeds in a stepwise manner to generate an intermediate  $\sigma$ -alkyl metal complex<sup>114-117</sup>. As a result, some of these systems also isomerize olefins and/or catalyze exchange of  $\text{D}_2$  and olefinic protons. Depending upon the metal complex, the final reductive elimination of saturated alkane may occur via an intramolecular or intermolecular mechanism (vide infra).

In broad terms, two major catalytic pathways are available for a transition-metal catalyzed reduction of an unsaturate<sup>118</sup>. The "hydride route" involves oxidative addition of  $\text{H}_2$  to the metal centre, to form a metal-hydride, followed by substrate coordination. Alternatively, the "unsaturate route", which proceeds by the binding of substrate prior to dihydrogen activation, may be operative, although it would appear that oxidative addition of  $\text{H}_2$  to a metal-olefin complex should ordinarily be less facile (due to the  $\pi$ -acidity of the olefin). Unfortunately, kinetic measurements alone cannot differentiate between these two paths. Assign-

ment of the "hydride" route is usually based on the isolation, or spectral characterization, of metal hydride species. However, if no hydrides are observed, but there is evidence for metal-olefin derivatives formed during the reaction, the "unsaturate route" is often invoked. Metal formation in the absence of substrate also infers this pathway.

Classification of catalyst precursors generally involves designation as either a monohydride or a dihydride system, depending upon the nature of the proposed active hydride species generated at some point in the catalytic cycle. In these cases, identification of the metal hydrides is not necessarily direct, that is, they are not always isolable or even detectable spectroscopically; often their participation in the catalytic cycle is inferred by mechanistic studies, isotopic labelling experiments, or by analogy to related systems for which hydrido species have been unequivocally identified.

It should be noted that the term "catalyst precursor" refers to the synthesized transition metal complex (which is not necessarily a pre-formed metal hydride); this is distinct from the actual catalyst which may be present in only very low concentrations and thus undetectable under the particular reaction conditions. In fact, mechanistic studies by Halpern have indicated that isolable or spectroscopically dominant species formed during the hydrogenation cycle are usually not involved in the kinetically significant catalytic pathway<sup>119,120</sup>.

### Dihydride Catalysts

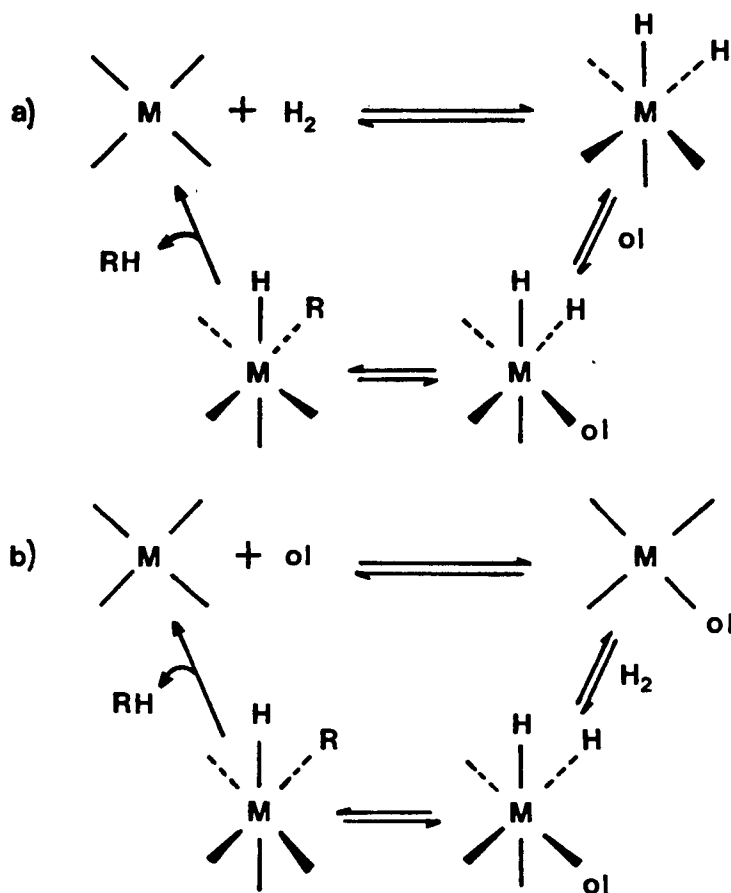
The complexity of homogeneous catalytic hydrogenation reactions has often precluded definitive mechanistic analysis or has led to conflicting

postulates of reaction pathways, depending upon interpretation of kinetic and spectral data. Even for the most extensively studied system, Wilkinson's catalyst, there is still some controversy. However, a number of key steps has been well documented and are generally accepted as applicable to most dihydride catalysts.

There are two major classes of rhodium phosphine dihydride catalyst precursors: neutral complexes of the type  $[\text{RhL}_3\text{X}]$  ( $\text{X}$  = halide,  $\text{L}$  = tertiary phosphine or arsine) such as Wilkinson's catalyst, or cationic rhodium phosphines of the general form  $[\text{RhL}_2(\text{diene})]^+$ , which have been extensively investigated by Shrock and Osborne, Brown and Halpern<sup>121-123</sup>. In the former case, the necessary free coordination site(s) are generated through dissociation of phosphine at some point in the catalytic cycle, whereas for the latter case hydrogenation of the diene ligand results in an unsaturated (often solvated) reactive intermediate. The preponderance of phosphine ligands in these catalysts is due in part to their necessary lability as well as their stabilizing influence on the dihydride intermediate.

The general mechanism is shown in Scheme 3.1. For these complexes, dihydrogen activation occurs via homolytic splitting; such an oxidative addition produces exclusively the cis dihydride<sup>124,125</sup>. Often this step is reversible. Olefin coordination then occurs to form a dihydrido  $\pi$ -olefin complex. Alternatively, olefin coordination can precede oxidative addition of  $\text{H}_2$ , as is the case for strongly binding olefins or where the catalyst has chelating diphosphine ligands. Since the chelating phosphines must be mutually cis, oxidative addition of  $\text{H}_2$  (also cis) would give an intermediate having hydrides trans to the phosphine centres. To overcome this unfavorable situation, reduction occurs instead by the "unsaturate route".

The oxidative addition of  $H_2$  to the metal-olefin derivative is thought to be rate-determining for this pathway.



Scheme 3.1 General mechanism for hydrogenation of olefinic substrates using transition metal dihydride catalysts:

a) hydride route      b) unsaturated route

Regardless of the sequence of the first two steps, an intermediate dihydrido olefin metal complex is generated; the next step in the catalytic cycle involves a migratory insertion of the olefin into a cis metal hydrogen bond. For systems operating by the "hydride" route, it is believed that this step is rate-determining. The resulting cis-hydrido  $\sigma$ -alkyl then

rapidly, and irreversibly, reductively eliminates to give the saturated alkane product. Since this step is so fast, cis hydrido alkyl species are rarely observed.

These dihydride catalysts are highly stereospecific, resulting in overall cis addition of dihydrogen. The stereochemistry of reduction by  $\text{Rh}(\text{PPh}_3)_3\text{Cl}$  was elegantly demonstrated by Wilkinson, who showed that catalytic deuteration of maleic and fumaric acids in benzene/ethanol gave meso-2,3-dideuterosuccinic acid and d,l-2,3-dideuterosuccinic acid, respectively<sup>126</sup>. Originally, these results were interpreted as being due to a simultaneous transfer of both deuterium atoms. However, it is now clear that this transfer is indeed stepwise but that the high rate of the product-forming reductive-elimination-step, as compared to the migratory insertion reaction, usually precludes olefin isomerization or  $\text{H}_2/\text{D}_2$  exchange.

Many of these catalysts are very selective<sup>127</sup>, showing a decrease in reactivity with increasing substitution at the olefinic bond. This would appear to be a result of steric interference by bulky phosphine groups, thereby impeding the coordination of internal, versus terminal, olefins and/or by slowing the migratory insertion step. For the highly unsaturated complex  $[\text{Rh}(\text{diphos})]^+$ , steric inhibition would be expected to be insignificant; in fact, this complex efficiently hydrogenates substituted olefins and even aromatic rings, such as benzene, toluene and xylenes.

Generally, it is observed that most second-row metal complexes are more reactive towards hydrogenation than their third-row congeners. This is undoubtedly a result of the increased stability of higher oxidation

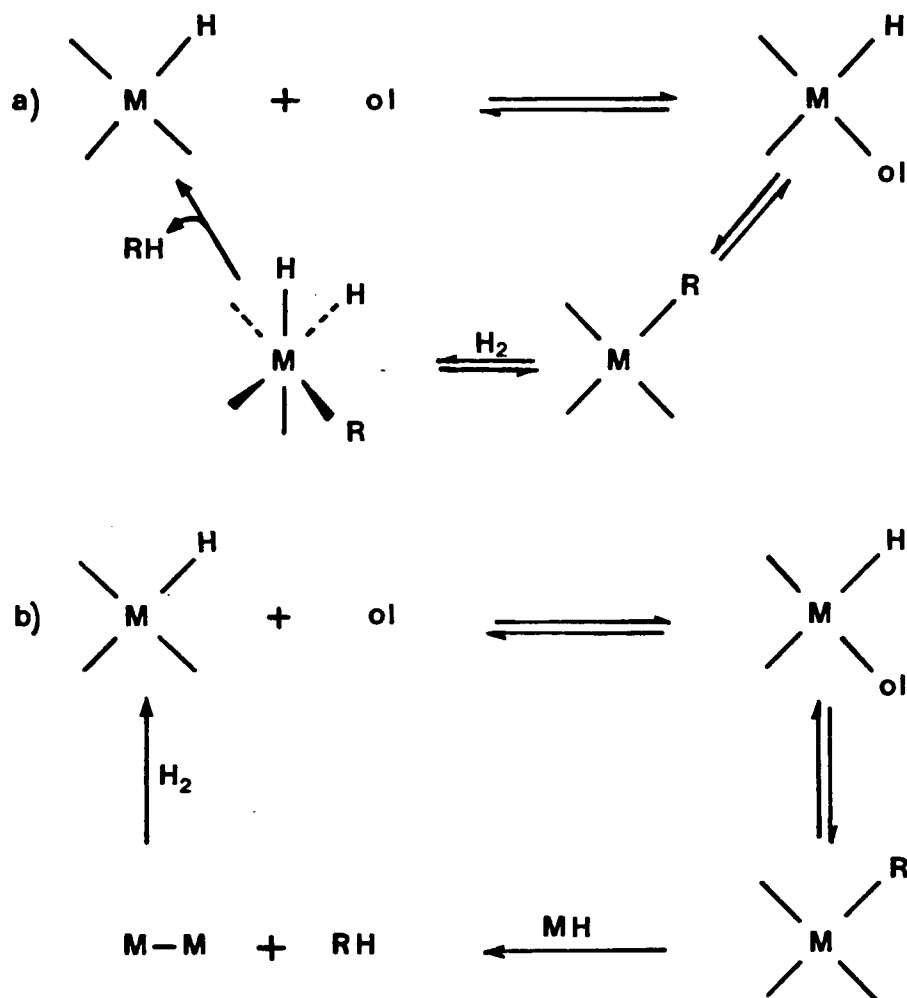
states of the third row metals due, in part, to the increased strength of their metal-hydride bonds. However, Crabtree has reported a number of catalysts of the type  $[\text{Ir}(\text{COD})\text{L}_2]^+$  which are more effective in the reduction of olefins and dienes than their rhodium analogues<sup>128</sup>. Comparison of reaction pathways for these iridium catalysts to typical rhodium dihydride systems is rather tenuous at this point.

### Monohydride Catalysts

Two possible mechanistic pathways for monohydride systems are outlined in Scheme 3.2. Owing to the paucity of kinetic data, it is difficult to assign either pathway with any certainty. The major cloudy area concerns the product-forming reductive elimination; this presumably may occur via either an intramolecular mechanism or a binuclear reductive elimination with a second mole of M-H. Once again, overall cis addition of dihydrogen to the olefinic bond is observed.

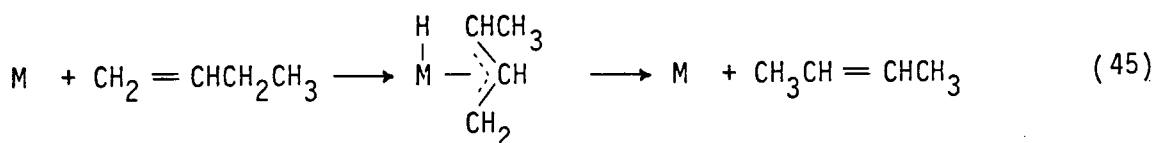
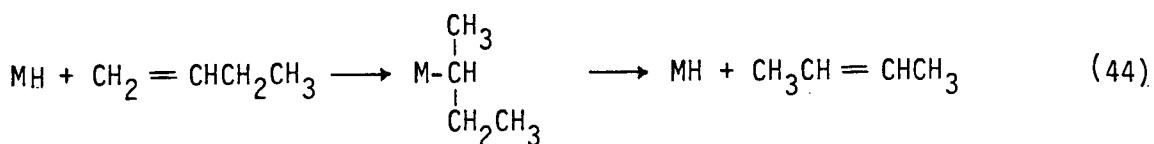
An interesting, although often troublesome, feature of these catalysts, such as  $[\text{RhH}(\text{CO})(\text{PPh}_3)_3]$  and  $[\text{IrH}(\text{CO})_2(\text{PPh}_3)_2]$ , is their tendency to promote olefin isomerization and isotopic exchange between  $\text{D}_2$  and olefinic protons<sup>129</sup>. This can occur via  $\beta$ -elimination<sup>130</sup> of the coordinated alkyl intermediate (equation 44) if the reductive elimination is slow relative to alkyl formation. Possibly, this is a consequence of the slow oxidative addition of  $\text{H}_2$  to the metal-alkyl intermediate (intramolecular path). Olefin isomerization sometimes occurs via monohydride catalysts in the absence of hydrogen; such a process involves oxidative addition of the

olefin to form a  $\pi$ -allyl hydride derivative<sup>131</sup>, which can then reductively eliminate in two possible ways, one of which leads to isomerized olefin (equation 45). However, few examples of olefin isomerization by this pathway are well documented.



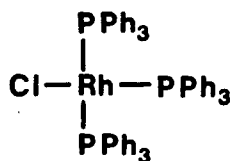
Scheme 3.2 General mechanism for hydrogenation of olefinic substrates using transition metal monohydride catalysts:  
(a) intramolecular pathway (b) intermolecular pathway

Monohydride catalysts show a very pronounced preference towards reduction of terminal versus internal olefins; in fact,  $[\text{HRh}(\text{CO})(\text{PPh}_3)_3]$  is completely ineffectual for the hydrogenation of cyclohexene<sup>132</sup>. Once again, this presumably is a result of steric inhibition by the bulky phosphine ligands.

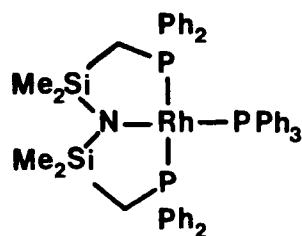


### Homogeneous Catalytic Hydrogenation using Rhodium and Iridium Amido Phosphines

It is not surprising, in view of their structural resemblance to Wilkinson's catalyst<sup>43</sup> that some of the rhodium and iridium amido diphosphines,  $[\text{M}(\text{L})\text{N}(\text{SiMe}_2\text{CH}_2\text{PPh}_2)_2]$  ( $\text{M} = \text{Rh}$ ,  $\text{L} = \text{COE}$ ,  $\text{PPh}_3$ ;  $\text{M} = \text{Ir}$ ,  $\text{L} = \text{COE}$ ,  $\text{C}_2\text{H}_4$ ) are catalyst precursors for the homogeneous hydrogenation of simple olefins under very mild conditions. Like  $[\text{RhCl}(\text{PPh}_3)_3]$ , these species are 16 electron complexes having labile ligand(s) which, upon dissociation, generate the required vacant coordination sites. The comparison between these systems is especially apt for  $[\text{Rh}(\text{PPh}_3)\text{N}(\text{SiMe}_2\text{CH}_2\text{PPh}_2)_2]$ <sup>22</sup>, which basically differs from Wilkinson's catalyst in the replacement of a chloride ( $\text{Cl}^-$ ) by an amide ( $^-\text{NR}_2$ ) ligand (both weak trans influence ligands).



43



22

In order to be an effective homogeneous hydrogenation catalyst, a transition metal complex must: 1) have good thermal stability, 2) have sufficient solubility in a wide range of solvents, 3) be able to be easily separated from its reaction products, and 4) be substrate selective. For the rhodium and iridium amido phosphine complexes, thermal stability poses no problem since these derivatives are stable in benzene at temperatures up to 120°C. These complexes are exceptionally soluble in almost all organic solvents; in fact, most hydrogenation runs were carried out in neat olefin (at 22°C, 1 atmosphere H<sub>2</sub>), employing a substrate to catalyst ratio of approximately 1000:1. Catalyst separation is also straightforward since the volatile reduction products can be vacuum-transferred away from the involatile metal complex prior to analysis. The iridium complexes demonstrate a pronounced preference for terminal versus internal olefins; however, in the case of the rhodium amidophosphines selectivity is, surprisingly, rather poor.

As previously indicated, most rhodium phosphine dihydride catalysts show very little, if any, tendency toward olefin isomerization. Assuming that for the rhodium amido phosphines hydrogenation proceeds, in analogy to Wilkinson's catalyst, through a dihydride intermediate (via either the

"hydride" or "unsaturate" route), only straightforward reduction of olefinic substrates would be expected. However, product analysis by  $^1\text{H}$ NMR and, more accurately, by GLC indicates an unexpectedly high percentage of isomerized olefin. When either  $[\text{Rh}(\eta^2\text{-C}_8\text{H}_{14})\text{N}(\text{SiMe}_2\text{CH}_2\text{PPh}_2)_2]$  or  $[\text{Rh}(\text{PPh}_3)\text{N}(\text{SiMe}_2\text{CH}_2\text{PPh}_2)_2]$  is employed as catalyst precursor, the turnover number<sup>133</sup> for isomerization of 1-hexene to cis/trans-2-hexene ( $\sim 70/\text{h}$ ) is higher than for hydrogenation to hexane ( $\sim 50/\text{h}$ ). Similar behavior obtains for the rhodium and iridium bidentate amido phosphines; with  $[\text{Ir}(\text{COD})\text{N}(\text{C}_6\text{H}_5\text{CH}_2)(\text{SiMe}_2\text{CH}_2\text{PPh}_2)]$ , the turnover number for hydrogenation is approximately 120/h as compared to  $\sim 40/\text{h}$  for isomerization (the rhodium analogue is about four times slower). These results are illustrated by the hydrogenation profile graphs in Fig. 3.2 and 3.3.

Since no isomerization is observed in the absence of  $\text{H}_2$ , this process is clearly not occurring via oxidative addition of the olefin to form an allyl hydride intermediate (which can then reductively eliminate to produce internal olefins). The anomalous reactivity of these rhodium catalysts is further demonstrated by the observation that internal olefins, such as 2-hexene, are hydrogenated as rapidly as terminal ones; this is in contrast to the preference of terminal versus internal olefins exhibited by classical Wilkinson-type hydrogenation systems. With 2-hexene as substrate, isomerization also occurs; an initial 50/50 mixture of cis/trans-2-hexenes is rapidly isomerized to give a 10:90 ratio of cis/trans isomers, which are then hydrogenated at normal rates.

To complicate matters further, the  $[\text{Ir}(\eta^2\text{-C}_8\text{H}_{14})\text{N}(\text{SiMe}_2\text{CH}_2\text{PPh}_2)_2]$  derivative shows no evidence of isomerization but only straightforward

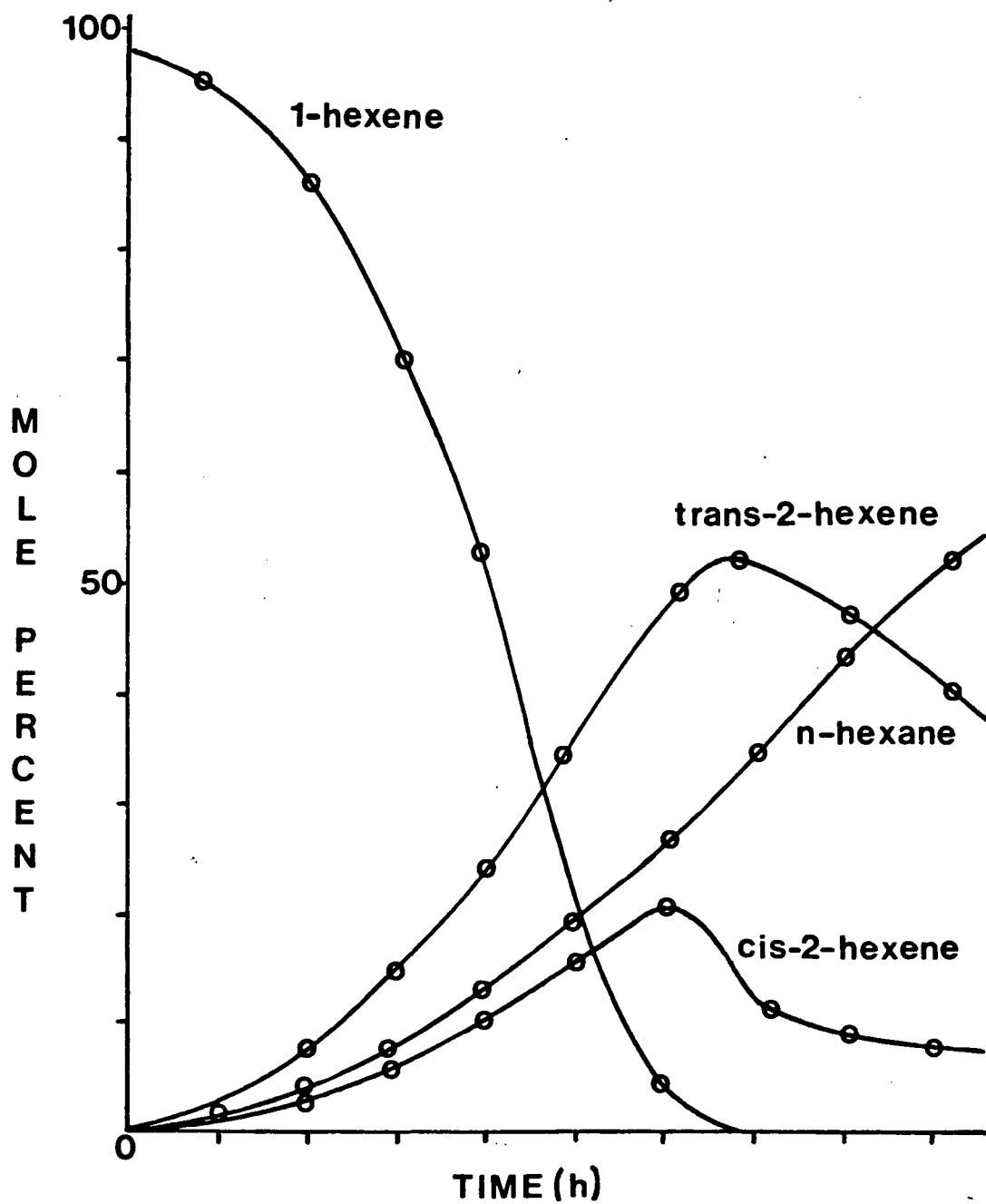


Fig. 3.2 Hydrogenation profile for reaction of 1-hexene with  $[\text{Rh}(\text{PPh}_3)\text{N}(\text{SiMe}_2\text{CH}_2\text{PPh}_2)_2]$  (1 atm.  $\text{H}_2$ , 22°C)

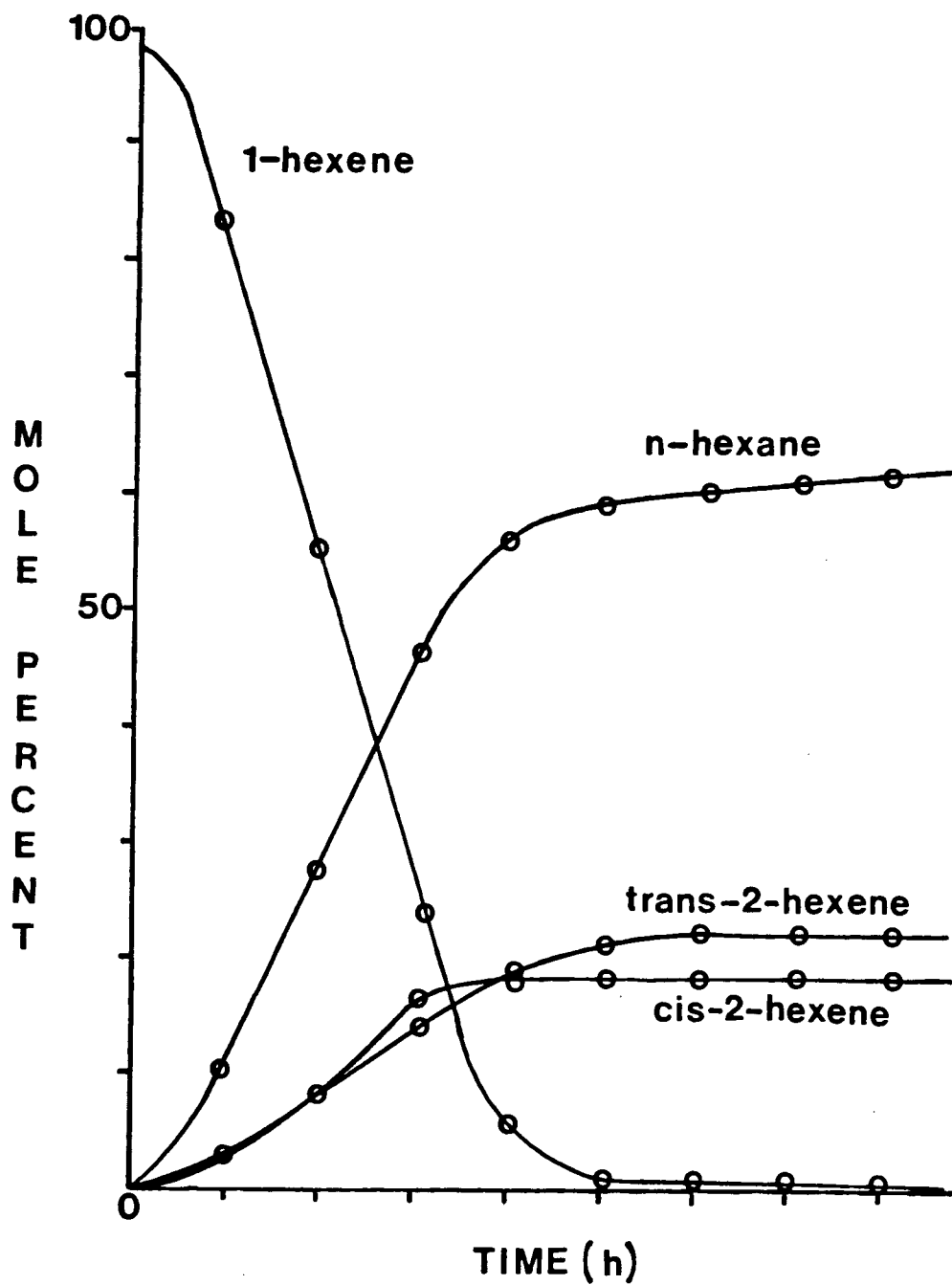
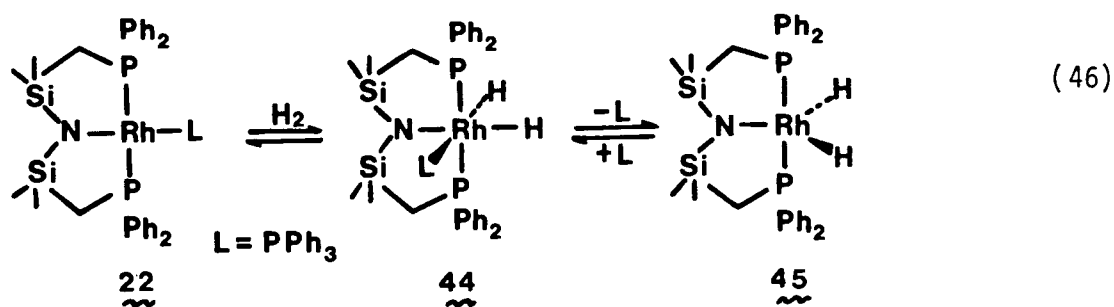


Fig. 3.3 Hydrogenation profile for reaction of 1-hexene with  $[\text{Ir}(\text{COD})\text{N}(\text{C}_6\text{H}_5\text{CH}_2)(\text{SiMe}_2\text{CH}_2\text{PPh}_2)_2]$  (1 atm.  $\text{H}_2$ , 22°C)

reduction of olefins to alkanes under identical hydrogenation conditions (Fig. 3.4); the turnover number, using 1-hexene as substrate, is comparable to that of its rhodium congener ( $\sim 70/h$ ). In contrast to their rhodium analogues, hydrogenation of 2-hexene is extremely slow ( $\sim 2$  turnovers per hour) when using either  $[\text{Ir}(\eta^2\text{-C}_8\text{H}_{14}(\text{N}(\text{SiMe}_2\text{CH}_2\text{PPh}_2)_2)]$  or  $[\text{Ir}(\text{COD})\text{N}(\text{C}_6\text{H}_5\text{CH}_2)(\text{SiMe}_2\text{CH}_2\text{PPh}_2)]$  as catalyst precursor. In fact, after three hours under 1 atmosphere of  $\text{H}_2$  in neat 2-hexene, the iridium cyclooctene complex loses its hydrogenation activity entirely and a catalytically inactive trihydride,  $[\text{Ir}(\text{H})_3\text{NH}(\text{SiMe}_2\text{CH}_2\text{PPh}_2)_2]$ , precipitates out of solution (see next chapter).

Although the mechanistic details of these systems have not been elucidated as yet, analogy to Halpern's conclusions regarding Wilkinson's catalyst would, at least superficially, seem reasonable. Since the "unsaturate" route would be expected to be comparatively inefficient, it would appear that, for the rhodium and iridium tridentate amido phosphines, hydrogenation should operate via the "hydride" route. For the case of the  $[\text{Rh}(\text{PPh}_3)\text{N}(\text{SiMe}_2\text{CH}_2\text{PPh}_2)_2]$ , two possibilities are then presented: oxidative addition of dihydrogen can occur to generate an 18 electron cis-dihydride, which then loses  $\text{PPh}_3$  to produce an unsaturated catalytically active intermediate (equation 46).



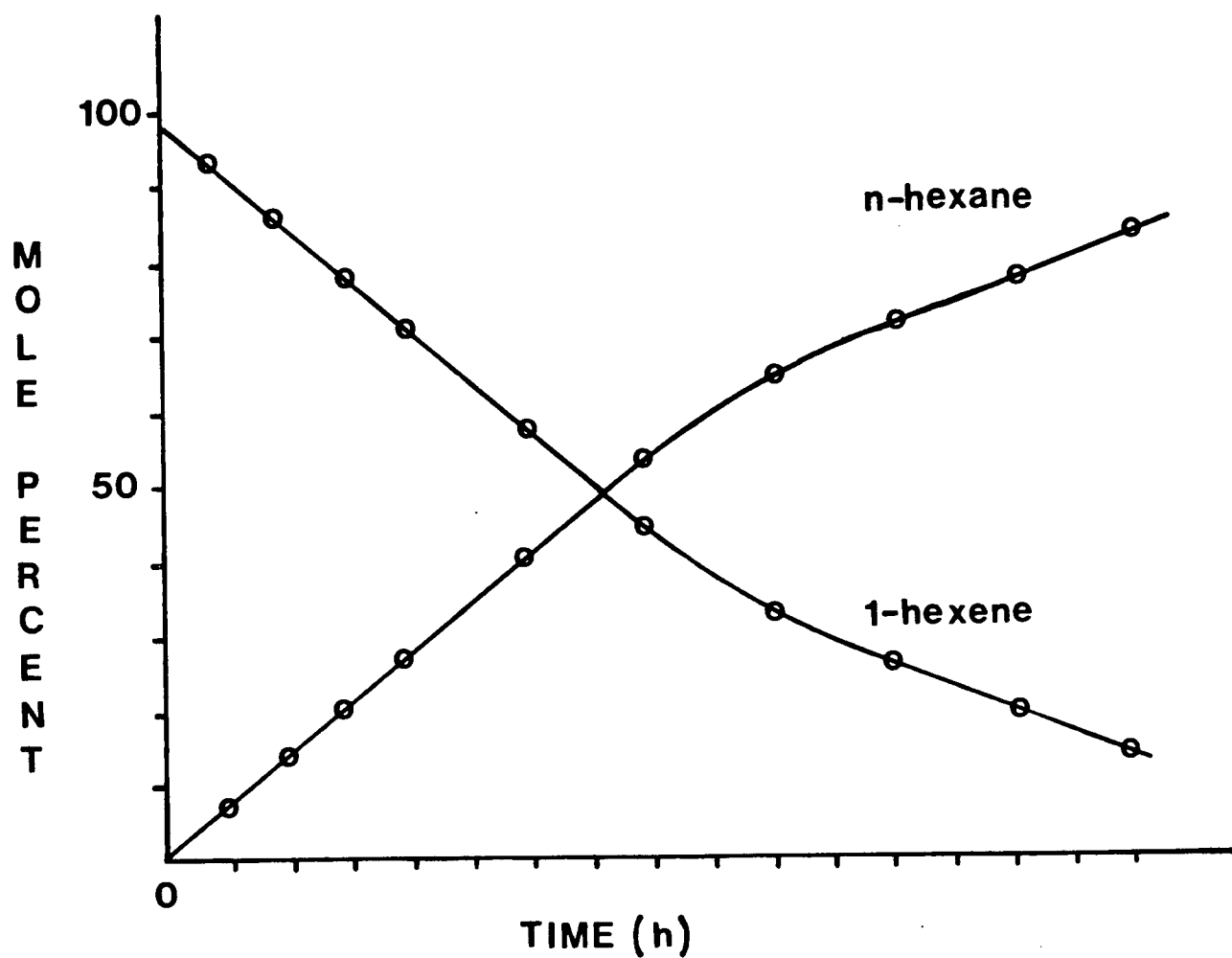
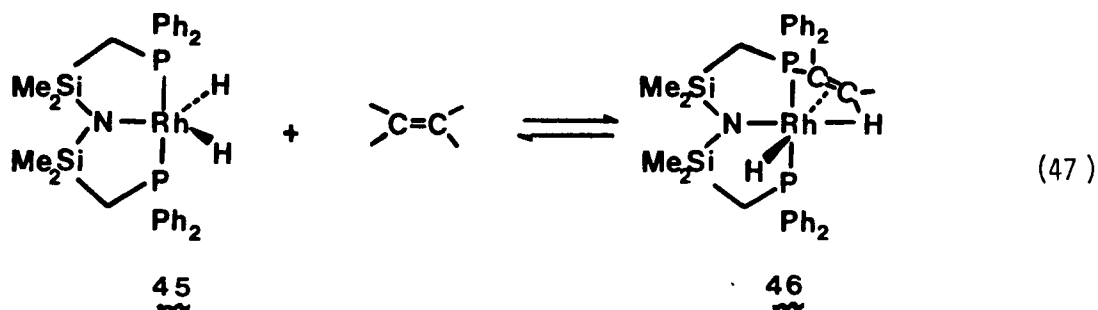
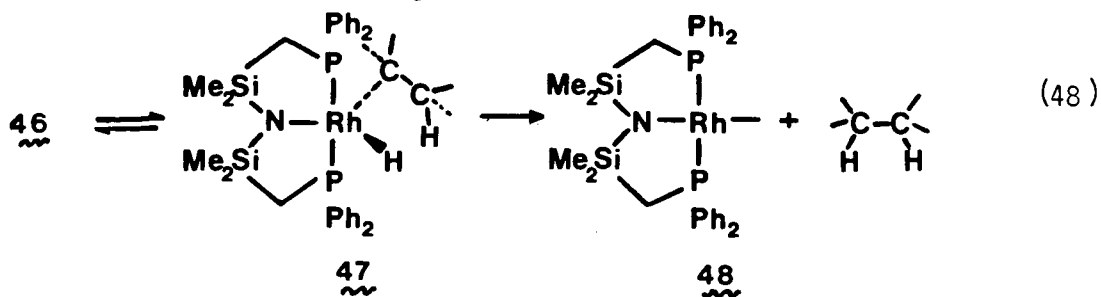


Fig. 3.4 Hydrogenation profile for reaction of 1-hexene with  $[\text{Ir}(\text{COE})\text{N}(\text{SiMe}_2\text{CH}_2\text{PPh}_2)_2]$  (1 atm.  $\text{H}_2$ , 22°C)

Although 44 and 45 have not been identified for the rhodium catalytic systems, their iridium analogues have been isolated and fully characterized (see next chapter). Coordination of the olefin then occurs (equation 47). Migratory insertion would then produce a cis  $\sigma$ -alkyl



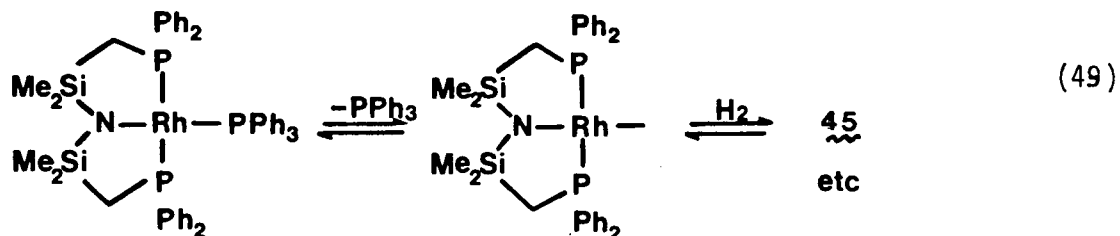
hydride which then rapidly reductively eliminates alkane (equation 48). Oxidative addition of dihydrogen to the highly unsaturated Rh(I) species 48



would re-form 45 and hence start the cycle over again. It is possible that 45, 46, 47 and 48 are solvated, but since no significant effect is observed in either toluene, diethylether, or THF (versus neat olefin), it would appear that such a solvent ligand is very weakly bound and easily displaced.

Alternatively, loss of  $\text{PPh}_3$  prior to oxidative addition of  $\text{H}_2$  could also occur to produce the same results (equation 49). At some point, however, a coordination site must be opened up. The fact that the amido phosphine complexes  $[\text{M}(\text{L})\text{N}(\text{SiMe}_2\text{CH}_2\text{PPh}_2)_2]$  ( $\text{M} = \text{Rh}, \text{Ir}$ ;  $\text{L} = \text{CO}, \text{PMe}_3$ ) do

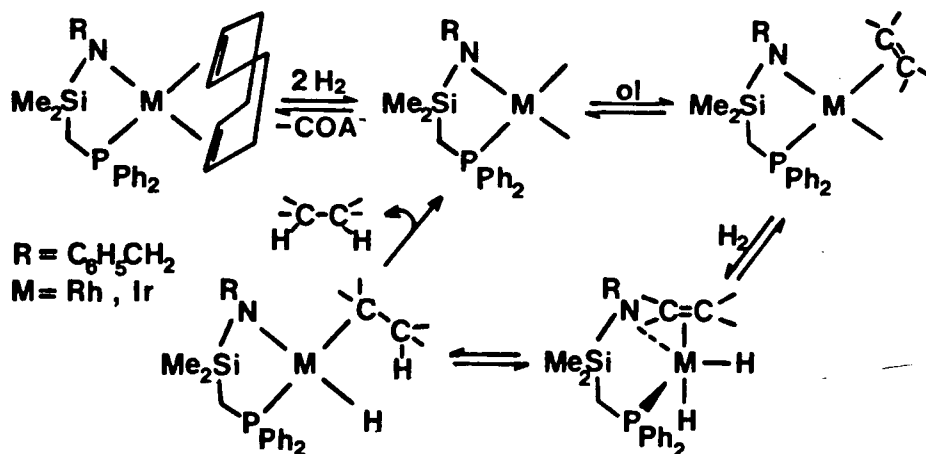
not hydrogenate olefins is probably a result of the reluctance of the carbonyl and  $\text{PMe}_3$  ligands toward dissociation.



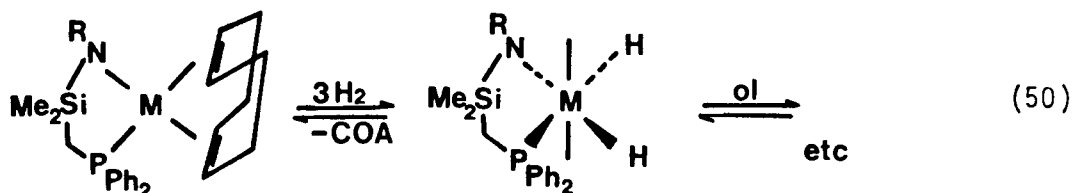
With the  $\eta^2$ -cyclooctene rhodium and iridium catalytic precursors, it would appear that the cyclooctene ligand is displaced rather than hydrogenated, since  $\text{C}_6\text{D}_6$  solutions of these complexes, sealed in NMR tubes under 1 atm  $\text{H}_2$ , show free cyclooctene.

With the bidentate complexes  $[\text{M}(\text{COD})\text{N}(\text{C}_6\text{H}_5\text{CH}_2)(\text{SiMe}_2\text{CH}_2\text{PPh}_2)]$  ( $\text{M} = \text{Rh}, \text{Ir}$ ), it is reasonable to assume that a catalytically active intermediate is generated by uptake of two equivalents of dihydrogen, with concomitant formation of cyclooctane. On the basis of Halpern's work<sup>134</sup> with the isoelectronic  $[\text{Rh}(\text{COD})(\text{diphos})]^+$  system, the following mechanism (Scheme 3.3) seems plausible. Note that the bidentate amido phosphines would be expected to operate by the "unsaturate" route in order to circumvent

**Scheme 3.3**

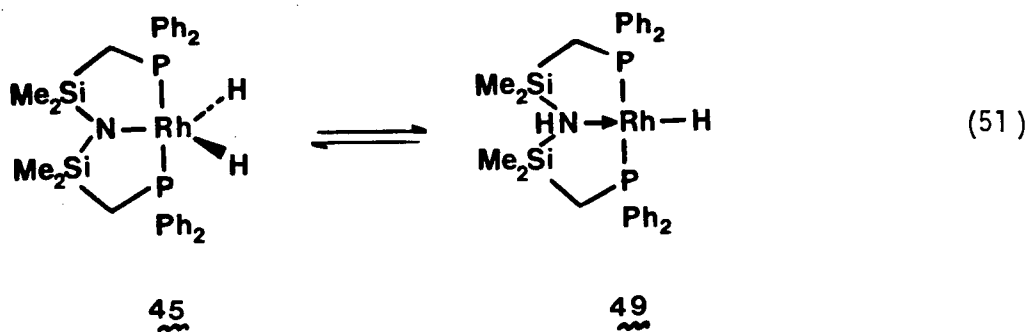


formation of an intermediate having a hydride trans to a phosphine centre (equation 50).



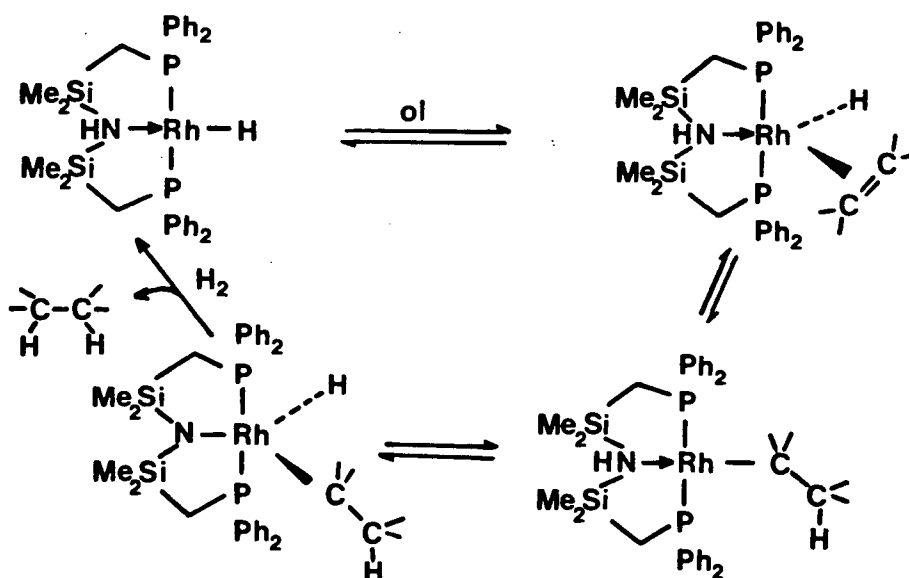
Although these postulated mechanisms (equations 46  $\rightarrow$  49, Scheme 3.3) seem quite acceptable at first glance, a number of questions remain unanswered. Most perplexing is the high isomerization activity of the rhodium amido phosphines. Presumably, for these systems,  $\beta$ -elimination of the coordinated alkyl intermediate 47 to form internal olefins is a competing process with reductive elimination of the saturated alkane. Possibly this is a result of the ligand stereochemistry. As will be discussed in the following chapter, a facial coordination of the tri-dentate ligand has been observed. Therefore, it is conceivable that the rhodium complexes require a fac  $\rightarrow$  mer isomerism during the catalytic cycle so that reversible  $\beta$ -elimination can occur. Such a process may either be unnecessary for the iridium amidodiphosphines or may be fast enough to preclude isomerization.

Another possibility is that the dihydride intermediate 45 undergoes reductive elimination of the metal amide bond to form a monohydride amino phosphine species 49 which then acts as the active catalyst (equation 51).).



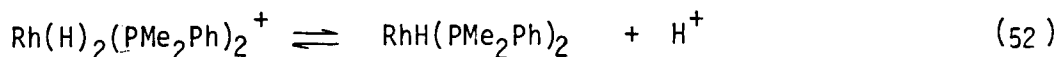
As previously discussed, olefin rearrangement is often a competing process with olefin reduction when employing rhodium monohydride catalysts. The iridium congener to 45  $[\text{Ir}(\text{H})_2\text{N}(\text{SiMe}_2\text{CH}_2\text{PPh}_2)_2]$ , shows no such behavior (even under partial vacuum) but this would seem reasonable in view of the increased stability of the +3 oxidation state for iridium versus rhodium complexes. This could also explain the fact that the iridium cyclooctene complex does not isomerize olefins. Assuming the participation of such an intermediate 49, a possible catalytic cycle is outlined in Scheme 3.4.

**Scheme 3.4**



This cycle would seem to be more facile than for those involving conventional monohydride catalysts since neither a second oxidative addition of  $H_2$  nor a dinuclear reductive elimination (with a second mole of M-H) is necessary. Rather, the product-forming step could be made possible by a prior re-oxidative addition of the N-H group.

Although the process depicted in equation 51, and its importance to the catalytic cycle, might, at first glance, appear to be somewhat speculative, comparison can be made to Shrock and Osborn's well-documented  $[Rh(\text{diene})(PMe_2Ph)_2]^+$  catalyst<sup>135</sup> which, in addition to being effective as an hydrogenation catalyst for simple olefins, also catalyzes olefin isomerization. This activity has been ascribed to an equilibrium in solution between the cationic dihydride species and a neutral monohydride (equation 52 ).

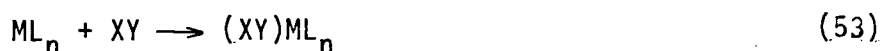


It has been determined that the monohydride is an extremely active isomerization and a good hydrogenation catalyst, whereas the dihydride is a poor hydrogenation catalyst, and possibly inactive toward isomerization. Monohydride formation, as shown in equations 51 and 52, is not really too remarkable but rather, further examples of the well-known heterolytic splitting of  $H_2$ . The striking feature of these systems is that an equilibrium can exist between the monohydride and dihydride intermediate, and thus affect the reactivity during the catalytic cycle.

## Chapter IV

### Oxidative Addition of Dihydrogen to Square-Planar Iridium(I) Complexes

Owing to their significance in a variety of homogeneous catalytic transformations (such as hydrosilation, hydrogenation, hydroformylation, Monsanto's acetic acid synthesis, oxygenation), oxidative addition reactions (equation 53) have been, and continue to be, the focus of intense investigation<sup>136</sup>. The most extensive study has involved the interaction of square-planar  $d^8$  iridium(I) complexes, particularly  $[\text{Ir}(\text{CO})\text{Cl}(\text{PPh}_3)_2]$  (Vaska's complex) and its closely related derivatives with a number of reactant molecules (XY)<sup>124,137</sup>. These reactions are often reversible; the resulting



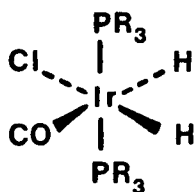
$\text{Ir(III)}$  species vary in stability, depending largely upon the nature of the addendum (XY).

The tendency of a particular transition metal towards oxidative addition of a covalent molecule is influenced by both the nature of the metal complex<sup>137</sup> as well as the reactant<sup>124</sup>. A combination of the electronic and steric properties of the metal complex plays a decisive role in determining the course of these reactions. Generally, third row metals are more reactive than their second row congeners. It has been observed that electron donating ligands promote oxidative additions, whereas  $\pi$ -acid ligand (such as CO or olefin) retard these processes. Thus, increased basicity at the metal centre tends to favour these reactions. The steric bulk of the ligand system is also important; very bulky ligands (such as  $\text{P}(\text{t-Bu})_3$ , can sometimes effectively block oxidative additions. Usually the metal complex must be coordinatively unsaturated or, if saturated,

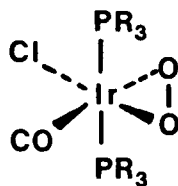
capable of losing a ligand. It has also been demonstrated that the local symmetry at the metal centre is critical since four-coordinate  $d^8$  cobalt(I) and iridium(I) complexes having a non-planar structure do not add dioxygen whereas their square planar analogues are very reactive.

A systematic survey of the oxidative addition behavior of Vaska's complex with a variety of reactants ( $XY = O_2, CH_3I, H_2, I_2, Br_2, Cl_2, HCl$ ) has indicated that the thermodynamic stability of the adduct is directly proportional to the addendum's acidity (that is, the degree of electron transfer from M to XY). Thus, the Ir(III) species formed via reaction of  $[Ir(CO)Cl(PPh_3)_2]$  with  $Cl_2, Br_2$ , or  $I_2$  are more stable than those formed from  $O_2$  or  $H_2$ ; in fact, the former oxidative additions are irreversible whereas the latter are easily reversible.

The structure of the adduct is, not surprisingly, greatly dependent upon the nature of the addendum. In general terms, two categories of reactant molecules can be recognized: those which dissociate (eg.  $H_2$ ) upon addition to a metal complex, or those which remain intact (eg.  $O_2$ ). For the former case, reaction with Vaska's complex generates an octahedral complex <sup>50</sup> in which both atoms (or groups) X and Y are individually bonded to the metal centre. For the latter case, the adduct has a distorted octahedral geometry (<sup>51</sup>), with a Cl-Ir-CO bond angle of approximately  $100^\circ$ .



50

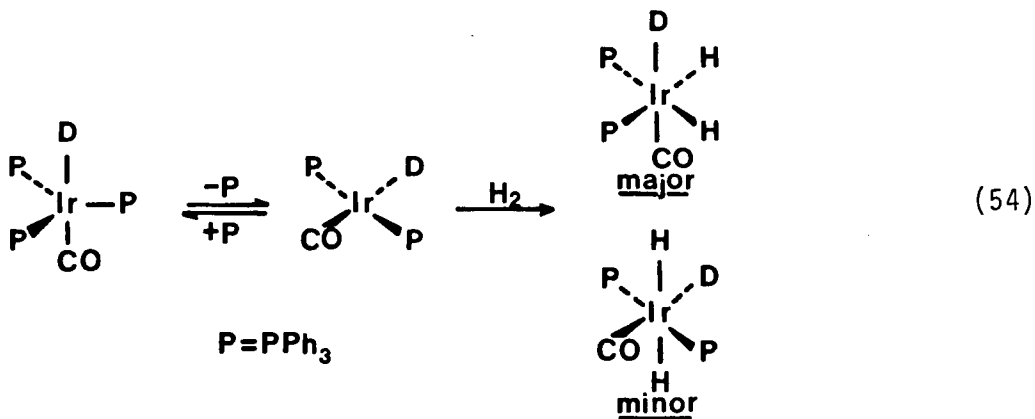


51

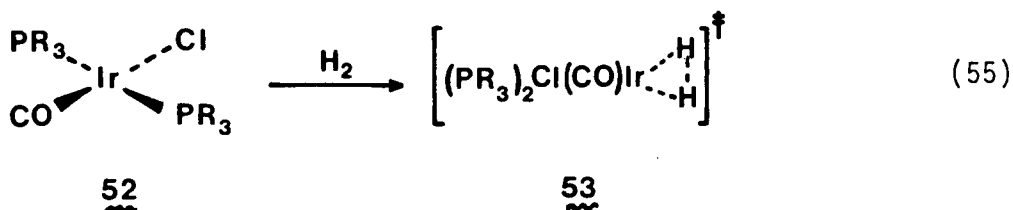
As outlined in Chapter III, activation of dihydrogen by a transition metal complex can occur either via homolytic splitting by one or two metal centres, resulting in a two electron oxidation of the metal centre or two one electron oxidations. Alternatively, heterolytic splitting can take place under appropriate conditions; although the overall reaction cannot be regarded as an oxidative addition, such a process may occur at some stage. For coordinatively unsaturated  $d^8$  metal complexes, homolytic cleavage has been established as the dominant mechanism. Addition of dihydrogen to square-planar iridium derivatives has been shown, both in solution and in the solid state, to be stereospecifically cis. The cis orientation of the two hydrides has been primarily established by spectral methods. In fact, stereochemical assignment by physical methods has been more extensive for iridium hydrides than for any other group of transition metal hydrides, owing to their proliferation, their reasonable stability, and the possibility of several isomeric forms<sup>125</sup>. In particular,  $^1\text{H}$  NMR has provided conclusive information as to the structures of complexes of the form  $[\text{Ir}(\text{H})_2(\text{CO})\text{Cl}(\text{PR}_3)_2]$ . For the case where  $\text{PR}_3 = \text{PPhMe}_2$ , Shaw has observed

two hydride resonances in  $C_6D_6$  at -18.36 ppm (td,  $J_{H,P} = 14.1$  Hz,  $J_{H,H} = 8.4$  Hz) and -7.58 ppm ( $J_{H,P} = 20.2$  Hz)<sup>138</sup>; the high upfield chemical shift is characteristic of hydrides of the later transition metals (0 to -50 ppm, with most in the -20 → -30 range) while the coupling constants are typical of a hydride coupling to a cis phosphine (10 → 40 Hz). The trans orientation of the phosphines is demonstrated by a virtual triplet centred at 1.89 ppm ( $J_{app} = 3.8$  Hz). Infrared data ("thin film" - neat oil) for  $[Ir(H)_2(CO)Cl(PPhMe_2)_2]$  also support the cis assignment of the hydrides since there are two hydride absorptions (2169, 2067  $cm^{-1}$ ) due to the two different  $HIrL$  groupings. It should also be noted that the stereochemistry of dihydrogen addition to  $[Ir(CO)Cl(PR_3)_2]$  is insensitive to the nature of the solvent.

With one possible exception<sup>139</sup>, all oxidative additions of dihydrogen to  $d^8$  metal complexes proceed, or are assumed to proceed (in the absence of detectable hydrides), in such a cis fashion. Harrod's report of a supposedly trans oxidative addition of  $H_2$  to  $[Ir(D)CO(PPh_3)_2]$  (minor isomer) has met with skepticism since isomerization of an initially formed cis adduct would also be consistent with the results (equation 54).



The general observation of cis dihydrides formed in these reactions has led to interpretation in terms of a concerted mechanism<sup>140</sup>, involving a relatively non-polar, three-centre transition state 53 (equation 55).



Another interesting feature of oxidative additions to Vaska-type iridium(I) complexes is that the adduct  $[\text{Ir}(\text{XY})(\text{CO})\text{Cl}(\text{PR}_3)_2]$  almost invariably has the two phosphines in mutually trans positions. A generalized mechanism<sup>124</sup> which has been postulated to explain these results is depicted in Fig.4.1. Approach of the reactant molecule along the Cl-Ir-CO bond axis results in a decrease in the adduct's Cl-Ir-CO bond angle (from its original 180°). Thus, the two phosphine ligands retain their collinear relationship to the metal.

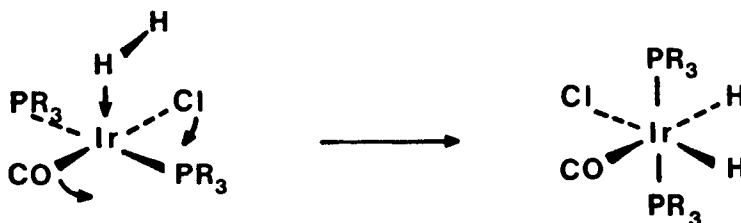
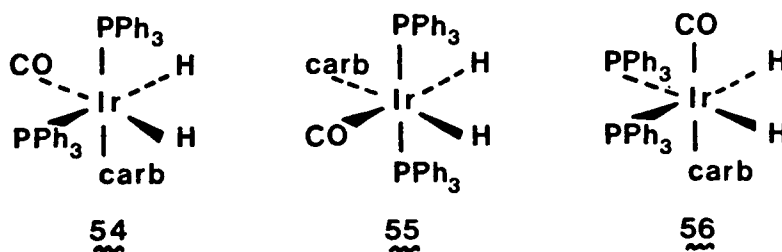


Fig. 4.1 General mechanism for oxidative additions involving Vaska-type complexes,  $[\text{Ir}(\text{CO})\text{Cl}(\text{PR}_3)_2]$

However, recently it has been reported that an alternative stereochemical course for the oxidative addition of dihydrogen can be followed. Although a complete study has not been carried out as yet, it would appear that the nature of the anionic ligand (X) is highly influential in determining the stereochemistry of the adduct. Bresadola<sup>141</sup> has observed that when X is a bulky carborane ( $B_{10}C_2H_{10}R^-$ ), several isomers can be detected depending upon the solvent. If carried out in polar solvents (eg.  $CH_3CN$ ), the unusual dihydride 54 is formed whereas in non-polar solvents (eg.  $CH_2Cl_2$  or  $C_2H_4Cl_2$ ) a mixture of isomers 55 and 56 is formed. Once again, assignment of these structures has been primarily based on  $^1H$ NMR and IR spectral data. On the basis of the mechanism of Fig.4.1, structure 55, having cis dihydrides and trans phosphines would be the expected product.



Isomer 56, although unexpected, can be rationalized to be a result of steric crowding of the bulky carborane ligand, causing a deformation of the iridium complex from an idealized square-planar geometry. The phosphines therefore migrate to positions trans to the incoming dihydrogen molecule, with the carborane and carbonyl ligands remaining collinear with the metal (Fig. 4.2). The formation of the anomalous isomer 54 has yet to be satisfactor-

ily explained, but is presumed to be due to either a thermodynamic solvent effect or the presence of solvated intermediates.

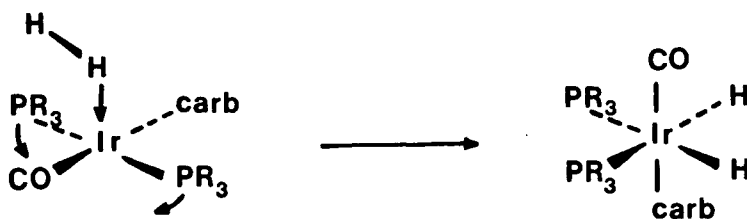
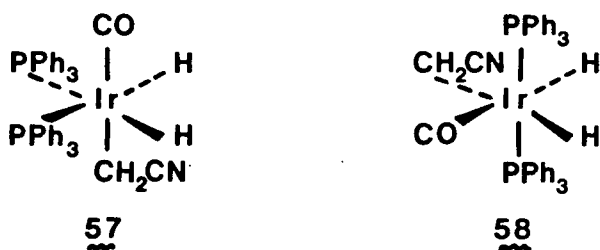


Fig. 4.2 Proposed mechanism for the oxidative addition of dihydrogen to  $[\text{Ir}(\text{CO})(\sigma\text{-carb})(\text{PPh}_3)_2]$

Since this report, another case of a dihydride adduct having cis phosphines has been documented<sup>142</sup>. Reaction of  $\text{H}_2$  with  $[\text{Ir}(\text{CO})(\text{CH}_2\text{CN})(\text{PPh}_3)_2]$  yields initially exclusively isomer 57 which gradually isomerizes in hydrogen-saturated  $\text{CH}_2\text{Cl}_2$  to form a mixture of 57 and 58. Thus, the thermodynamically stable isomer 58 is the expected product on the basis of



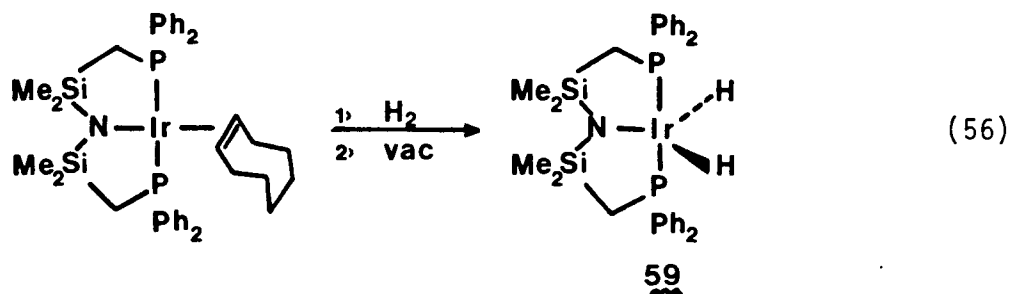
the "normal" (Fig. 4.1) oxidative-addition of  $\text{H}_2$  to Vaska-type complexes. However, the kinetically stable isomer 57 presumably forms via the process outlined in Fig. 4.2. It would appear that this is due to an especially favorable trans conformation of the  $\text{CO-Ir-CH}_2\text{CN}$  unit, owing to the high

$\sigma$ -donor ability of the  $\text{CH}_2\text{CN}$  in combination with the  $\pi$ -acidic character of the carbonyl ligand. The mechanism of interconversion of isomers 57 and 58 has not been elaborated as yet.

### Stereoselective Formation of Iridium(III) Amides and Ligand-Assisted Heterolytic Splitting of Dihydrogen

As previously described (Chapter 3), some of the rhodium and iridium amido phosphine complexes  $[\text{MLN}(\text{SiMe}_2\text{CH}_2\text{PPh}_2)_2]$  ( $\text{M} = \text{Rh}$ ,  $\text{L} = \text{COE}$ ,  $\text{PPh}_3$ ;  $\text{M} = \text{Ir}$ ,  $\text{L} = \text{COE}$ ,  $\text{C}_2\text{H}_4$ ) act as efficient catalyst precursors for the homogeneous hydrogenation of simple olefins. In an effort to delineate the mechanism of these processes and to isolate possible catalytic intermediates, a number of oxidative reactions was carried out and studied. Although the rhodium amido phosphines  $[\text{RhLN}(\text{SiMe}_2\text{CH}_2\text{PPh}_2)_2]$  ( $\text{L} = \text{CO}$ ,  $\text{PMe}_3$ ,  $\text{PPh}_3$ ,  $\text{COE}$ ,  $\text{C}_2\text{H}_4$ ) showed no reaction under four atmospheres of dihydrogen, the analogous iridium derivatives (with the exception of the carbonyl complex) react readily and stereoselectively under one atmosphere of hydrogen to yield a variety of stable iridium(III) hydrides. It is noteworthy that these complexes are the first examples of iridium (III) amides reported to date<sup>143</sup>.

The novel five-coordinate iridium dihydride  $[\text{Ir}(\text{H})_2\text{N}(\text{SiMe}_2\text{CH}_2\text{PPh}_2)_2]$ , **59**, is prepared by stirring a toluene solution of  $[\text{Ir}(\text{C}_8\text{H}_{14})\text{N}(\text{SiMe}_2\text{CH}_2\text{PPh}_2)_2]$  under one atmosphere of dihydrogen for one hour (equation 56). Removal of excess dihydrogen and solvent followed by recrystallization from toluene/hexane gives analytically pure orange crystals. The infrared of **59** (KBr) has one moderate intensity  $\nu_{\text{Ir-H}}$  band at  $2200\text{ cm}^{-1}$ ; the  $^{31}\text{P}\{^1\text{H}\}$  NMR consists of one sharp singlet at 23.9 ppm. The  $^1\text{H}$  NMR spectrum (Fig. 4.3), which is invariant down to  $-80^\circ\text{C}$ , has a single sharp  $\text{Si}(\text{CH}_3)_3$



resonance, a virtual triplet ( $J_{\text{app}} = 5.2 \text{ Hz}$ ) for the  $\text{CH}_2\text{P}$  protons and, of most interest, a sharp triplet at  $-24.9 \text{ ppm}$  (integral value = 2 H). The high upfield chemical shift of this hydride resonance is typical of iridium(III) hydrides and the phosphorus-hydride coupling constant ( $J_{\text{H,P}} = 13.2 \text{ Hz}$ ) lies within the range normally observed for cis H,P couplings<sup>125</sup>. Although no other five-coordinate iridium-dihydrides have

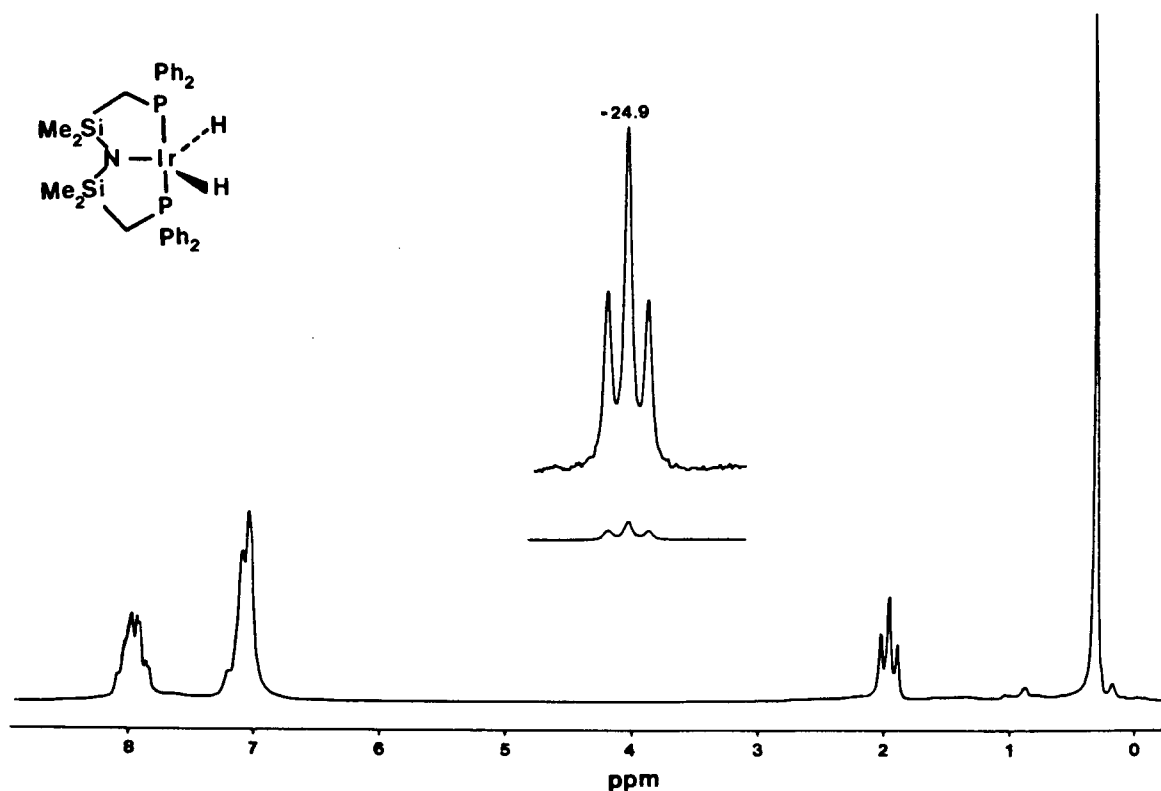
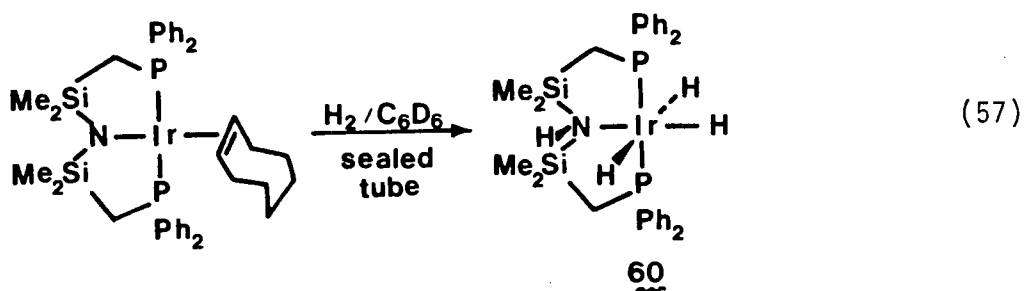


**Fig. 4.3**  $^1\text{H}$ NMR(80MHz) spectrum of  $[\text{Ir}(\text{H})_2\text{N}(\text{SiMe}_2\text{CH}_2\text{PPh}_2)_2]$  in  $\text{C}_6\text{D}_6$

been noted in the literature, the spectral data and chemical analysis support this structural formulation for 59. Since no  $^1\text{H}$ NMR spectral changes are observed upon cooling to  $-80^\circ\text{C}$ , it would appear that this trigonal bipyramidal structure is stereochemically rigid. Further support for this proposal is provided by the completely stereoselective ligand addition reactions of 59 (vide infra).

Surprisingly, if the reaction illustrated in equation (56) is monitored under excess  $\text{H}_2$  (in a sealed NMR tube), formation of the dihydride is not observed. Rather, the product has been assigned, on the basis of spectral data, to have the structure 60, an iridium amine trihydride (equation 57 ). Consistent with this formulation are the



three high-field multiplets at  $-8.97$ ,  $-9.69$ , and  $-24.6$  ppm (Fig. 4.4) in the  $^1\text{H}$ NMR corresponding to the three different Ir-H moieties. The down-field region is also informative as the two Si-CH<sub>3</sub> singlets and the AB quartet of virtual triplets for the CH<sub>2</sub>P protons indicate that the two faces of the iridium complex are inequivalent. Although normally obscured by other signals, the N-H peak can be observed when the starting iridium-

cyclooctene complex is  $^{15}\text{N}$ -labelled; a doublet ( $J_{^{15}\text{N-H}} = 70 \text{ Hz}$ ) at 0.10 ppm has been assigned to the coordinated amine hydrogen.

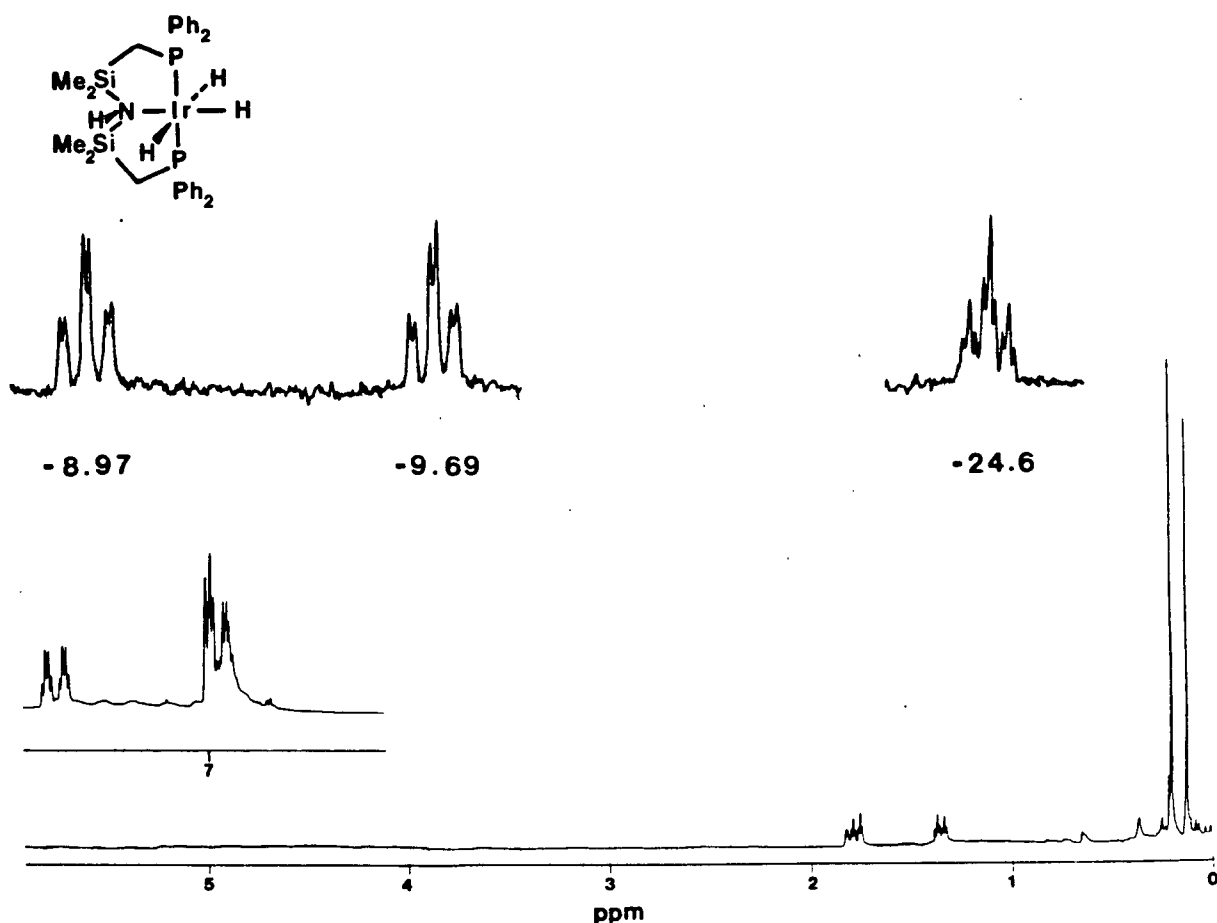


Fig. 4.4  $^1\text{H}$ NMR (270 MHz) spectrum of mer-[Ir(H)<sub>3</sub>NH(SiMe<sub>2</sub>CH<sub>2</sub>PPh<sub>2</sub>)<sub>2</sub>] in C<sub>6</sub>D<sub>6</sub>

In addition, the IR(C<sub>6</sub>D<sub>6</sub> solution under H<sub>2</sub>) has two moderate intensity bands at 2175 cm<sup>-1</sup> and 1705 cm<sup>-1</sup>, attributed to  $\nu_{\text{Ir-H}}$ ; the lower energy absorption is typical of a trans H-M-H grouping<sup>144</sup>. The weak N-H stretch occurs at 3210 cm<sup>-1</sup>. When the reaction is carried out under an atmosphere of deuterium, the IR bands shift appropriately.

The  $^{31}\text{P}\{^1\text{H}\}$ NMR of  $\text{60}$  is a singlet at 11.44 ppm; no signal due to the dihydride  $\text{59}$  (at 23.9 ppm) is observed under excess  $\text{H}_2$ .

Removal of dihydrogen from solutions of  $\text{60}$  quantitatively generates  $\text{59}$ . The reversible nature of this reaction is illustrated by the fact that when  $\text{C}_6\text{D}_6$  solutions of  $\text{59}$  are sealed under  $\sim 1$  atmosphere of  $\text{H}_2$ , the amine trihydride  $\text{60}$  is formed instantaneously. When carried out on a larger scale in Schlenck-type glassware, formation of  $\text{60}$  is indicated by the bright yellow coloration of the solution; removal of excess  $\text{H}_2$  in vacuo immediately produces a deep orange solution, which turns bright yellow again upon exposure to dihydrogen.

It would appear that formation of this unusual species ( $\text{60}$ ) is facilitated by the use of a starting material having a dissociable ligand. When  $[\text{Ir}(\text{COE})\text{N}(\text{SiMe}_2\text{CH}_2\text{PPh}_2)_2]$  is sealed in an NMR tube under hydrogen, free cyclooctene is observed, which is slowly hydrogenated to cyclooctane. A similar reaction obtains for the ethylene derivative,  $[\text{Ir}(\text{C}_2\text{H}_4)\text{N}(\text{SiMe}_2\text{CH}_2\text{PPh}_2)_2]$ ; under one atmosphere of dihydrogen, the mer amine trihydride  $\text{60}$  is rapidly formed and free ethylene is observed in the  $^1\text{H}$ NMR. In the absence of dissociation (ie. for  $[\text{IrLN}(\text{SiMe}_2(\text{CH}_2\text{PPh}_2)_2)_2]$ ,  $\text{L} = \text{PPh}_3, \text{PMe}_3$ ), only straightforward oxidative addition occurs (vide infra).

In an attempt to isolate  $\text{60}$ , a concentrated pentane solution of  $[\text{Ir}(\text{COE})\text{N}(\text{SiMe}_2\text{CH}_2\text{PPh}_2)_2]$  was stirred under one atmosphere of  $\text{H}_2$  (equation 58); after approximately two hours, a fine yellow precipitate formed (in  $\sim 70\%$  yield) which was filtered and washed with cold pentane. The spectral and analytical data are consistent with the facial isomer of  $\text{60}$ .

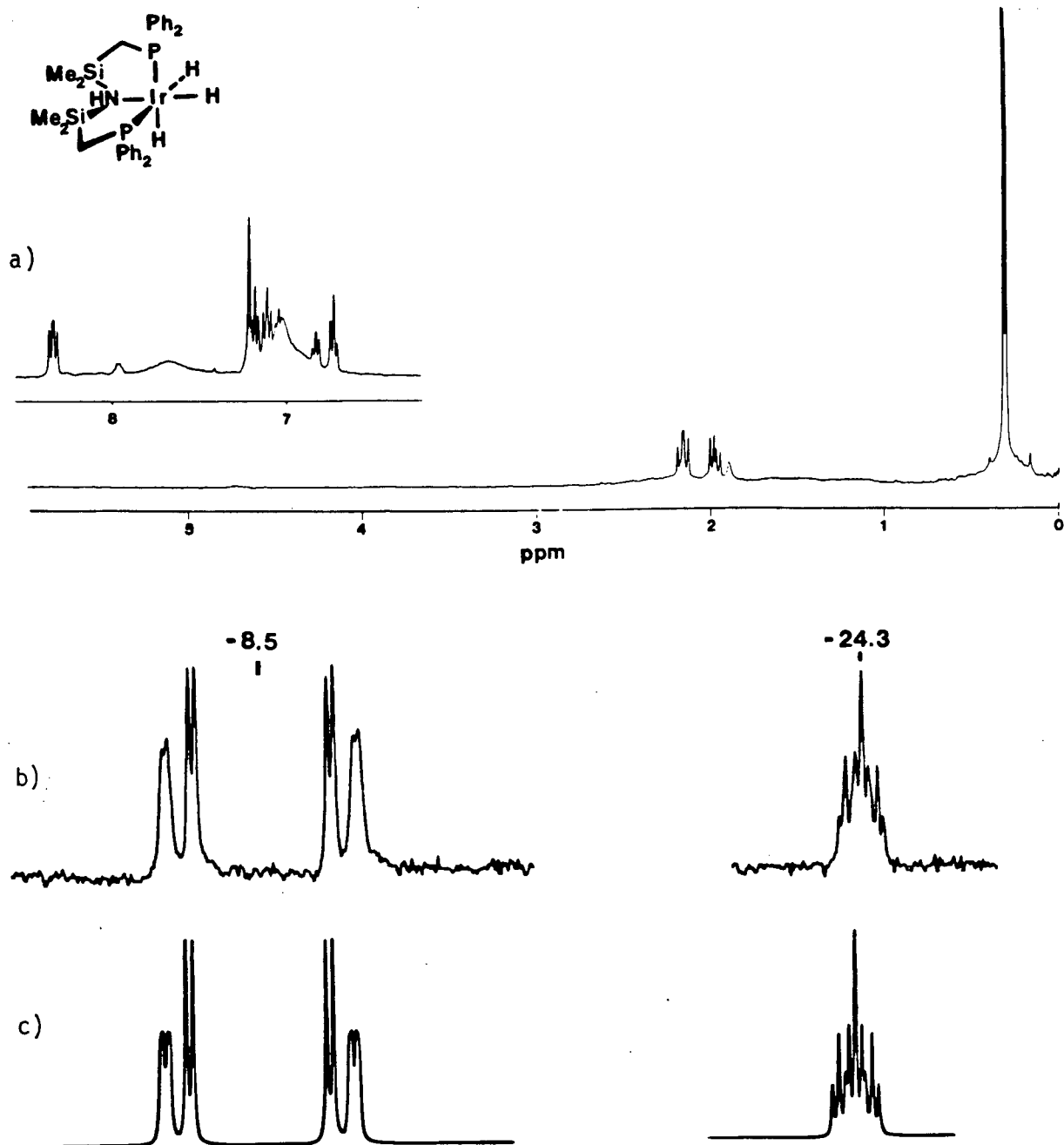
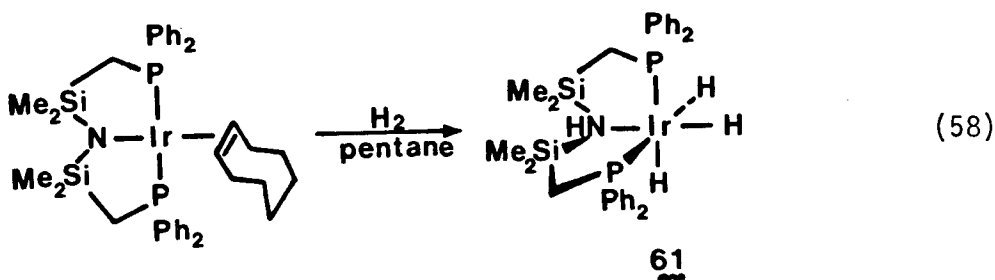


Fig. 4.5 a)  $^1\text{H}$  NMR (400 MHz) of  $\text{fac-}[\text{Ir}(\text{H})_3\text{NH}(\text{SiMe}_2\text{CH}_2\text{PPh}_2)_2]$  in  $\text{C}_6\text{D}_6$ .  
 b) Hydride region (400 MHz  $^1\text{H}$  NMR) of  $\text{fac-}[\text{Ir}(\text{H})_3\text{NH}(\text{SiMe}_2\text{CH}_2\text{PPh}_2)_2]$   
 c) Spectral simulation of hydride  $\text{AA}'\text{MXX}'$  pattern:  
 $^2J_{\text{A,A}'} = 2.2$ ,  $^2J_{\text{A,M}} = ^2J_{\text{A}',\text{M}} = 5.5$ ,  $^2J_{\text{A,X}} = ^2J_{\text{A}',\text{X}'} = -19.0$ ,  
 $^2J_{\text{M,X}} = ^2J_{\text{M,X}'} = 14.0$ ,  $^2J_{\text{A,X}'} = ^2J_{\text{A}',\text{X}} = 130.0$ ,  $J_{\text{X,X}'} = 1.0$

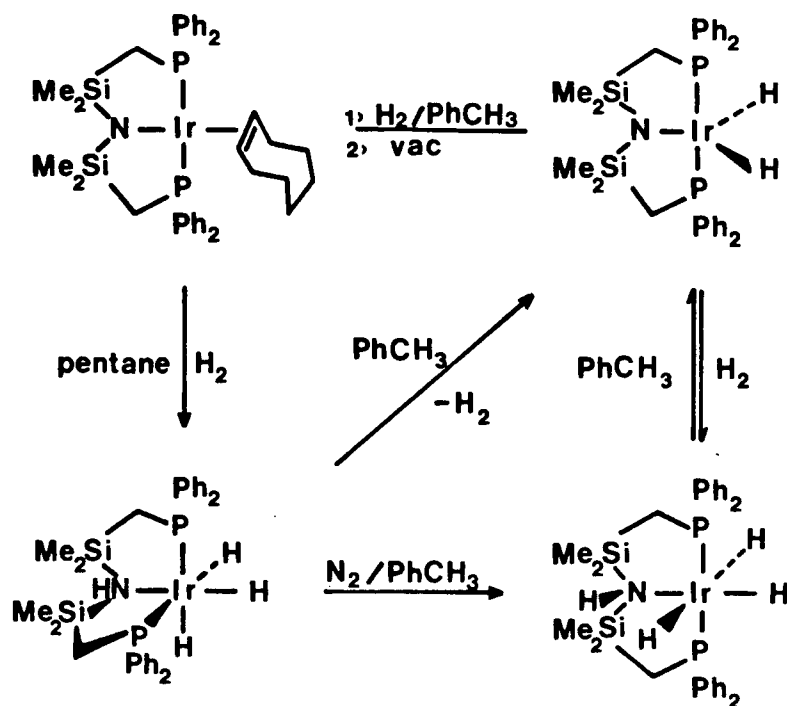


Most significantly, the  $^1\text{H}$ NMR has a complex symmetrical second-order multiplet centred at -8.5 ppm (Fig.4.5a) which is the characteristic pattern<sup>125</sup> for two magnetically inequivalent hydrides trans to two phosphine centres. The resulting AA'MXX' pattern has been simulated (Fig.4.5b) in order to obtain the appropriate coupling constants. The hydride trans to the amine centre appears as a triplet of triplets at -24.3 ppm. In addition, the IR(KBr) has two Ir-H stretching bands at  $2180\text{ cm}^{-1}$  and  $2115\text{ cm}^{-1}$  and a weak N-H stretch at  $3200\text{ cm}^{-1}$ .

In contrast to its meridional isomer, 61 is stable in the solid state even under high vacuum for extended periods of time. However, in solution under  $\text{N}_2$  (in a sealed NMR tube), the fac amine trihydride slowly decomposes to give a mixture of the dihydride 59 and the mer trihydride 60. It would seem conceivable that this process occurs via loss of  $\text{H}_2$  from 61 to give 59 which then adds  $\text{H}_2$  to give the mer-trihydride (Scheme 4.1).

The formation of the fac and mer amine trihydrides can be viewed as an example of an overall heterolytic-splitting of dihydrogen<sup>145</sup>. In this case, the ligand's amide centre facilitates the reaction, acting in a similar manner to the external base normally involved in reactions

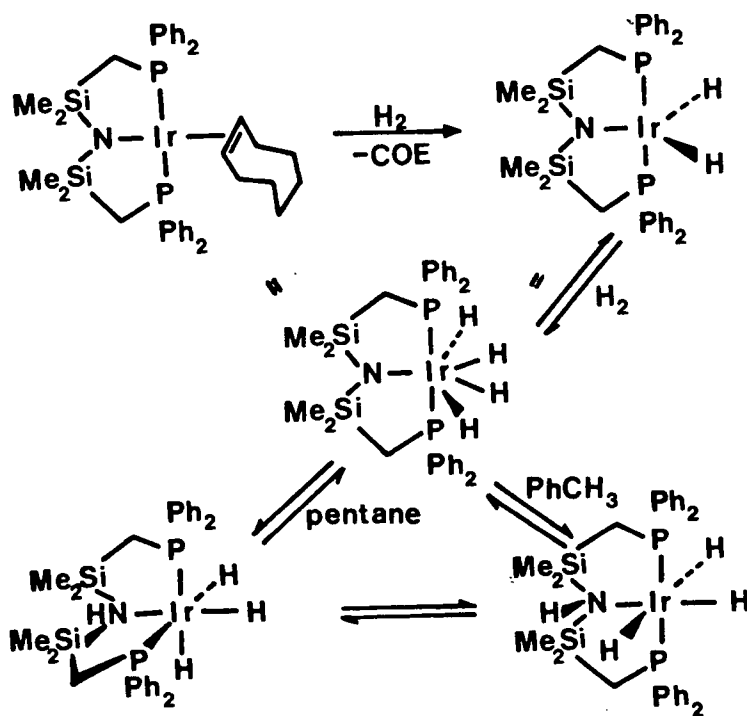
**Scheme 4.1**



of this type. The novel feature of this reaction as compared to most heterolytic splittings of H<sub>2</sub>, is that the protonated anionic group remains coordinated in the iridium product. It is not clear at this point whether formation of  $\text{Ir}^{\text{III}}$  and  $\text{Ir}^{\text{IV}}$  occurs in a concerted process, or in a stepwise manner involving oxidative addition to form an intermediate Ir(V) species which then reductively eliminates (Scheme 4.2). Isolation of the fac isomer from pentane is undoubtedly a result of its expected lower solubility in pentane than the mer isomer (dipole moment measure-

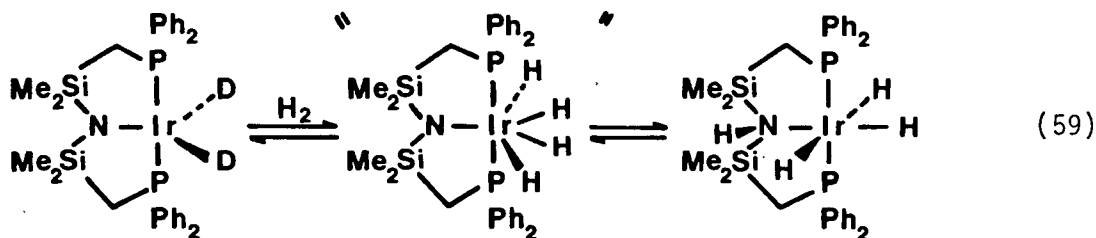
ments for a series of iridium trihydrides indicate a much higher  $\mu_D$  value for the fac versus the mer isomer)<sup>146</sup>; the fac amine trihydride  $61_{VV}$  is therefore 'milked' out of solution. Equilibria involving an Ir(V) intermediate could also account for the observed isomerization of  $61_{VV}$  in toluene; however, no such species has been identified as yet.

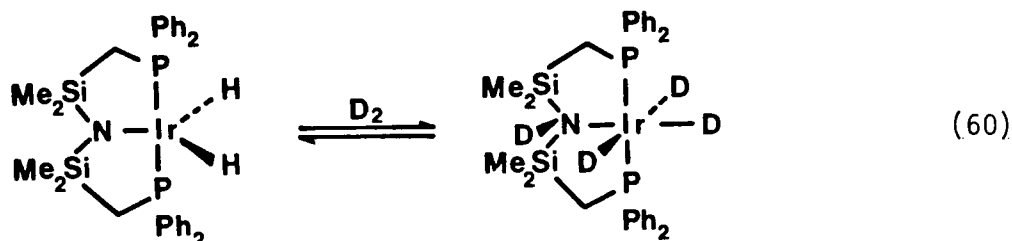
**Scheme 4.2**



In an attempt to gain some insight into the formation of these unusual iridium trihydrides, labelling experiments were carried out.

A  $C_6D_6$  solution of  $[Ir(D)_2N(SiMe_2CH_2PPh_2)_2]$  was sealed under one atmosphere of dihydrogen. Only the mer trihydride 59 was observed; no deuterium-labelled product was detected. Furthermore, a  $C_6D_6$  solution of  $[Ir(H)_2N(SiMe_2CH_2PPh_2)_2]$  sealed under one atmosphere of  $D_2$  yielded only the fully deuterated product  $[Ir(D)_3ND(SiMe_2CH_2PPh_2)_2]$ ; no hydride resonances were observed. It is difficult at this point to explain these results but it is conceivable that an Ir(V) species is once again implicated. A rapid equilibrium between the starting dihydride (or dideuteride) and an intermediate iridium(V) species could result in scrambling (equation 59). In light of the fact that the iridium(V) hydrides  $[IrH_5L_2]$  ( $L = PEt_3, PEt_2Ph, PMe_3$ )<sup>147</sup> and  $[IrH_4\{Bu_2^tPCH_2CHCH_2P^tBu_2\}]$ <sup>148</sup> have magnetically equivalent hydrides (even down to  $-100^\circ C$ ), an iridium (V) intermediate of the type shown in equation 59 would be expected to be highly fluxional and scrambling would therefore be expected to be fast. Alternatively, if reaction is occurring by direct heterolytic cleavage at the iridium amide bond, 59 and 60 must be rapidly interconverting under dihydrogen (equation 60).



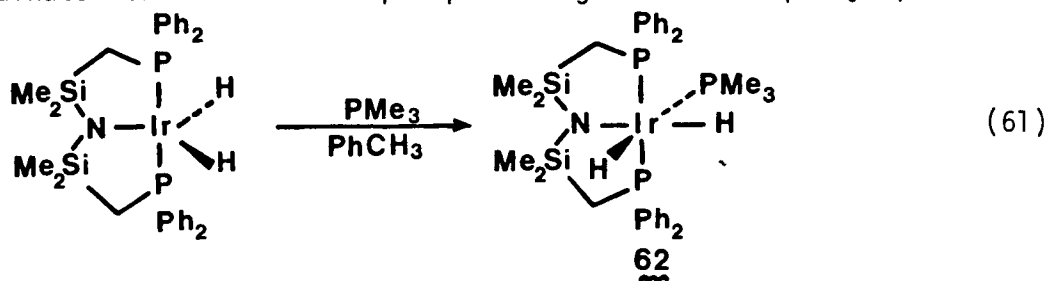


Another unusual aspect of these iridium amine trihydrides is their rapid reactivity with  $\text{CH}_2\text{Cl}_2$ . It is well known that  $\text{CCl}_4$  and even  $\text{CHCl}_3$  often react with transition metal hydrides to form chloride derivatives<sup>149</sup>; however, most are inert to  $\text{CH}_2\text{Cl}_2$ . However, in this solvent, both the mer and fac-trihydrides react (under  $\text{H}_2$ ) to form exclusively another hydride; it is believed that this species is cis- $[\text{IrCl}(\text{H})_2\text{NH}(\text{SiMe}_2\text{CH}_2\text{PPh}_2)_2]$  although it has not been isolated. For the mer trihydride, this transformation is complete in  $\sim 0.5$  hour whereas the analogous reaction with fac-61 takes  $\sim 4$ h.

#### Stereoselective Ligand Additions to $[\text{Ir}(\text{H})_2\text{N}(\text{SiMe}_2\text{CH}_2\text{PPh}_2)_2]$ .

In light of the fact that the iridium dihydride **59** is a coordinatively unsaturated, formally 16-electron iridium(III) derivative, it is not surprising that addition reactions with neutral ligands are facile. When  $\text{PMe}_3$  is added to a toluene solution of **59**, the original orange-colored

solution fades to a pale yellow within minutes. Upon work-up and recrystallization from neat hexane at  $-30^{\circ}\text{C}$ , off-white needles of 62 are obtained (equation 61). The  $^1\text{H}$ NMR (Fig. 4.6) consists of two sharp Si-CH<sub>3</sub> peaks of equal intensity, two sets of doublets of virtual triplets for the CH<sub>2</sub>P, and a complex pattern characteristic of a meridionally coordinated tridentate amidophosphine ligand for the phenyl protons<sup>47</sup>



(in C<sub>6</sub>D<sub>6</sub>). Most informative is the hydride region which is comprised of a doublet of triplets of doublets (dtd) at  $-10.21$  ppm for the hydride trans to the PMe<sub>3</sub> ligand, and a doublet of quartets at  $-19.96$  ppm for the hydride trans to the amide nitrogen. Analysis of these data, in conjunction with IR and  $^{31}\text{P}\{^1\text{H}\}$ NMR spectral information as well as chemical analysis, confirms the structure of 62 to be as depicted, with two mutually cis hydrides and the hybrid ligand coordinated in the usual mer stereochemistry.

A similar reaction obtains for  $[\text{Ir}(\text{H})_2\text{N}(\text{SiMe}_2\text{CH}_2\text{PPh}_2)_2]$  with CO; when a toluene solution of 59 is stirred under one atmosphere of carbon monoxide, the solution becomes virtually colorless within seconds (equation 62). The downfield region of the  $^1\text{H}$ NMR of the product is reminiscent of that of its PMe<sub>3</sub> analogue 62 while the hydride region consists of two doublets of triplets at  $-7.86$  and  $-16.09$  ppm. It is evident from the spectral information that 63 is isostructural with 62,

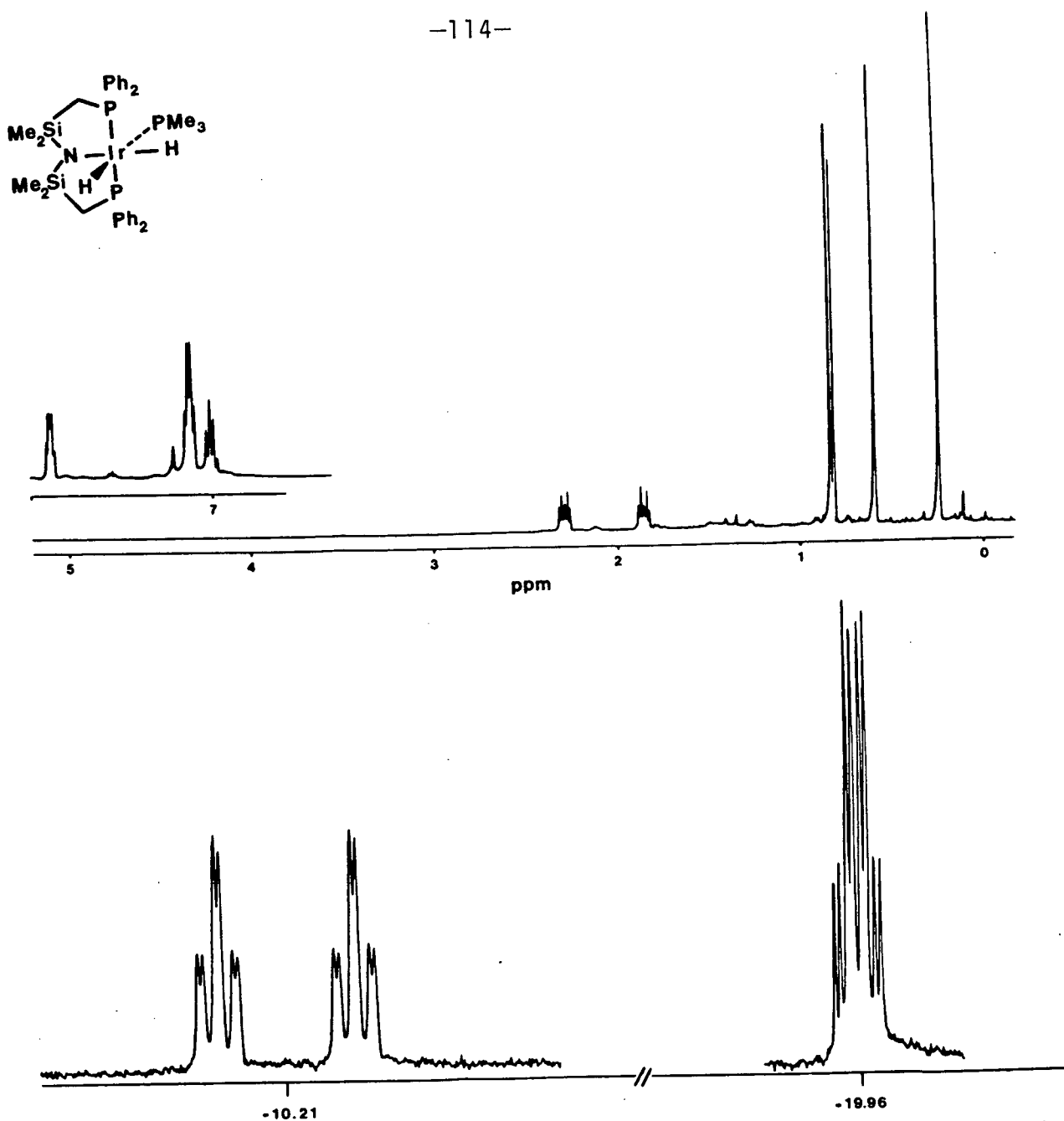
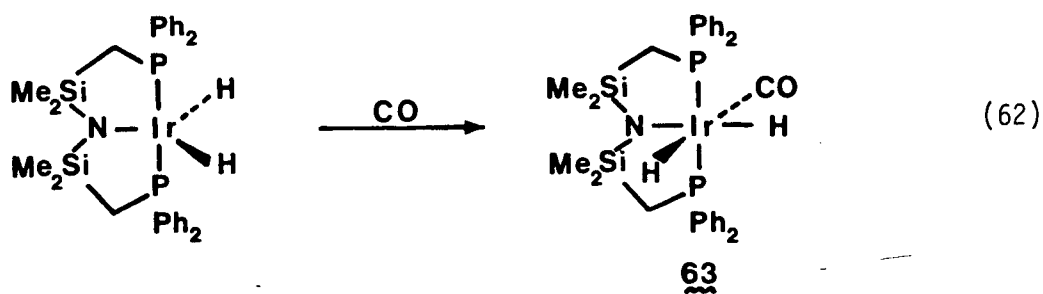


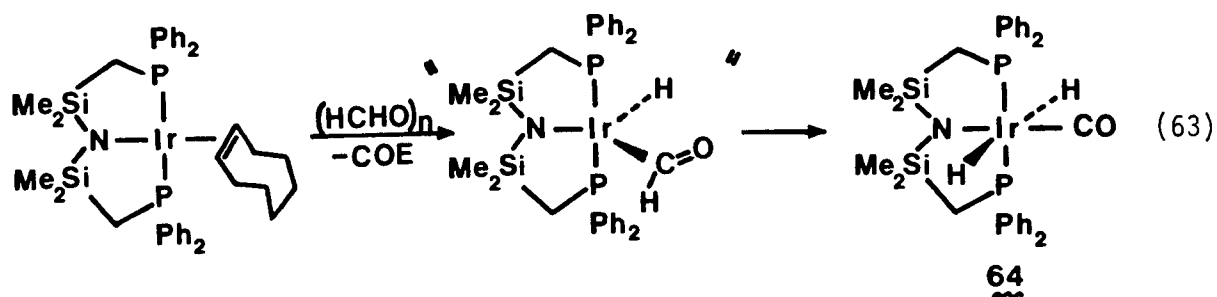
Fig. 4.6  $^1\text{H}$ NMR(400MHz) spectrum of mer cis- $[\text{Ir}(\text{H})_2(\text{PMe}_3)\text{N}(\text{SiMe}_2\text{CH}_2\text{PPh}_2)_2]$  in  $\text{C}_6\text{D}_6$



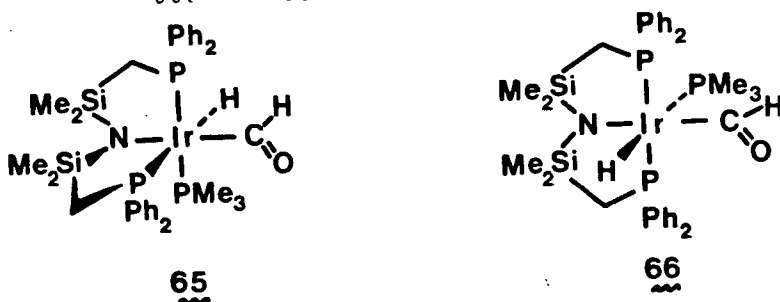
having cis-dihydrides and a meridionally bound amidophosphine ligand.

It should be noted that no other isomer of 62 or 63 is observed under these reaction conditions. In order that the product of mer cis stereochemistry be formed from 59, the ligand L must approach 59 cis to the iridium amide bond; approach of L trans to the iridium amide bond to yield the mer trans isomer is, for some reason, disfavored. It is arguable that such an isomer is formed initially but rearranges to yield the mer cis product. However, this has been shown not to occur by the following observations.

The mer trans-[Ir(H)<sub>2</sub>(CO)N(SiMe<sub>2</sub>CH<sub>2</sub>PPh<sub>2</sub>)<sub>2</sub>] complex 64, although undetected in the previous experiment, can be prepared, albeit by a very different route. Upon vigorously stirring a suspension of [Ir(COE)N(SiMe<sub>2</sub>CH<sub>2</sub>PPh<sub>2</sub>)<sub>2</sub>] and paraformaldehyde in toluene for 24 hours, followed by extraction with hexane, 64 is formed in virtually quantitative yield (NMR). Recrystallization from toluene/hexane gives analytically pure pale yellow crystals. Although the <sup>1</sup>HNMR clearly indicates a trans dihydride derivative (owing to the sharp triplet at -6.00 ppm), unequivocal evidence for this structural assignment is provided by the IR spectrum which has one strong ν<sub>Ir-H</sub> absorption at 1725 cm<sup>-1</sup>. Clearly this product is formed via initial oxidative addition of HCHO to form an hydrido formyl species which then undergoes deinsertion<sup>150</sup> of the formyl carbonyl to give 64 (equation 63). Solutions of 64 do not isomerize to the mer cis isomer 63, even after extended periods of time under one atmosphere CO.



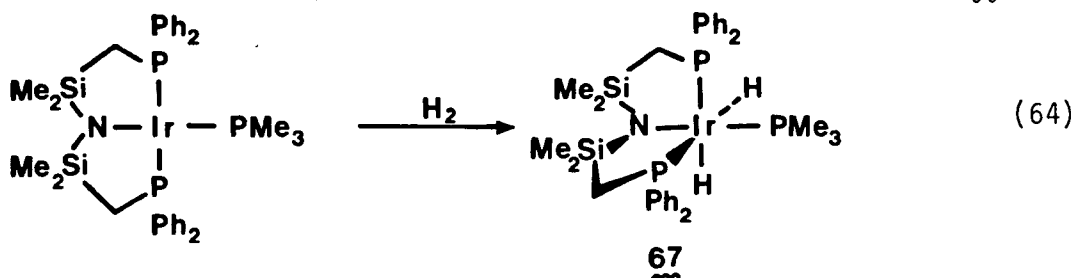
It has been shown that for certain iridium(I) complexes, reaction with paraformaldehyde leads to formation of iridium(III) hydrido formyl species<sup>151</sup>. As anticipated, such derivatives can be isolated from iridium amidophosphines in which ligand dissociation does not occur; such is the case for the reaction of (HCHO)<sub>n</sub> with [Ir(PMe<sub>3</sub>)N(SiMe<sub>2</sub>CH<sub>2</sub>PPh<sub>2</sub>)<sub>2</sub>]. However, this reaction yields an inseparable mixture of two isomers, the ratio of which appears to depend upon reaction time. Although the <sup>1</sup>H NMR (400 MHz) is extremely complicated, it appears that the structures of the products, 65 and 66 are as shown below.



Oxidative Addition of Dihydrogen to [IrLN(SiMe<sub>2</sub>CH<sub>2</sub>PPh<sub>2</sub>)<sub>2</sub>] (L = CO, PMe<sub>3</sub>, PPh<sub>3</sub>).

In light of the exclusive mer stereochemistry of the hybrid ligand in all of its Ni(II), Pd(II), Pt(II), Rh(I), and Ir(I) complexes, the formulation of the fac stereochemistry for 61 and 65 may seem questionable. However, unequivocal evidence has been provided that coordination of the tridentate ligand in a facial manner is indeed possible. Within

minutes of stirring a toluene solution of  $[\text{Ir}(\text{PMe}_3)\text{N}(\text{SiMe}_2\text{CH}_2\text{PPh}_2)_2]$  under one atmosphere of  $\text{H}_2$ , the color rapidly fades until the solution is almost colorless (equation 64). Large, off-white blocks of 67 are



obtained from hexane. Although the downfield of the  $^1\text{H}$ NMR spectrum of 67 is similar to isomeric 62, the hydride region is very different (Fig.4.7) being comprised of a complex, symmetrical multiplet centred at -11.04 ppm. This hydride pattern remains invariant regardless of the spectrometer's operating frequency indicating that it is a single, non first order hydride resonance and that this complex has two chemically equivalent, but magnetically inequivalent, hydrides. Combined with spectral simulation of this AA'XX'Y pattern, analysis of the downfield region of the  $^1\text{H}$ NMR, IR,  $^{31}\text{P}\{^1\text{H}\}$ NMR, and chemical analysis, it was concluded that 67 contained a facially coordinated amidophosphine ligand, with the two hydrides trans to the ligand's phosphine donors.

Confirmation of this fac cis stereochemistry was provided by X-ray crystal structure analysis (Fig.4.8). The  $\text{P}_1\text{-Ir-P}_2$  angle of  $109.58^\circ$  clearly indicates a slightly distorted facial geometry. It is also interesting to note that the  $\text{Si}_2\text{N-Ir}$  unit is non-planar (the metal is  $3.9^\circ$  out of the  $\text{NSi}_2$  coordination plane), a surprising result in view of the exclusive planarity of the  $\text{Si}_2\text{NM}$  fragment in all other transition metal-bis (silyl) amido complexes reported to date. The  $\text{SiNSi}$  angle is

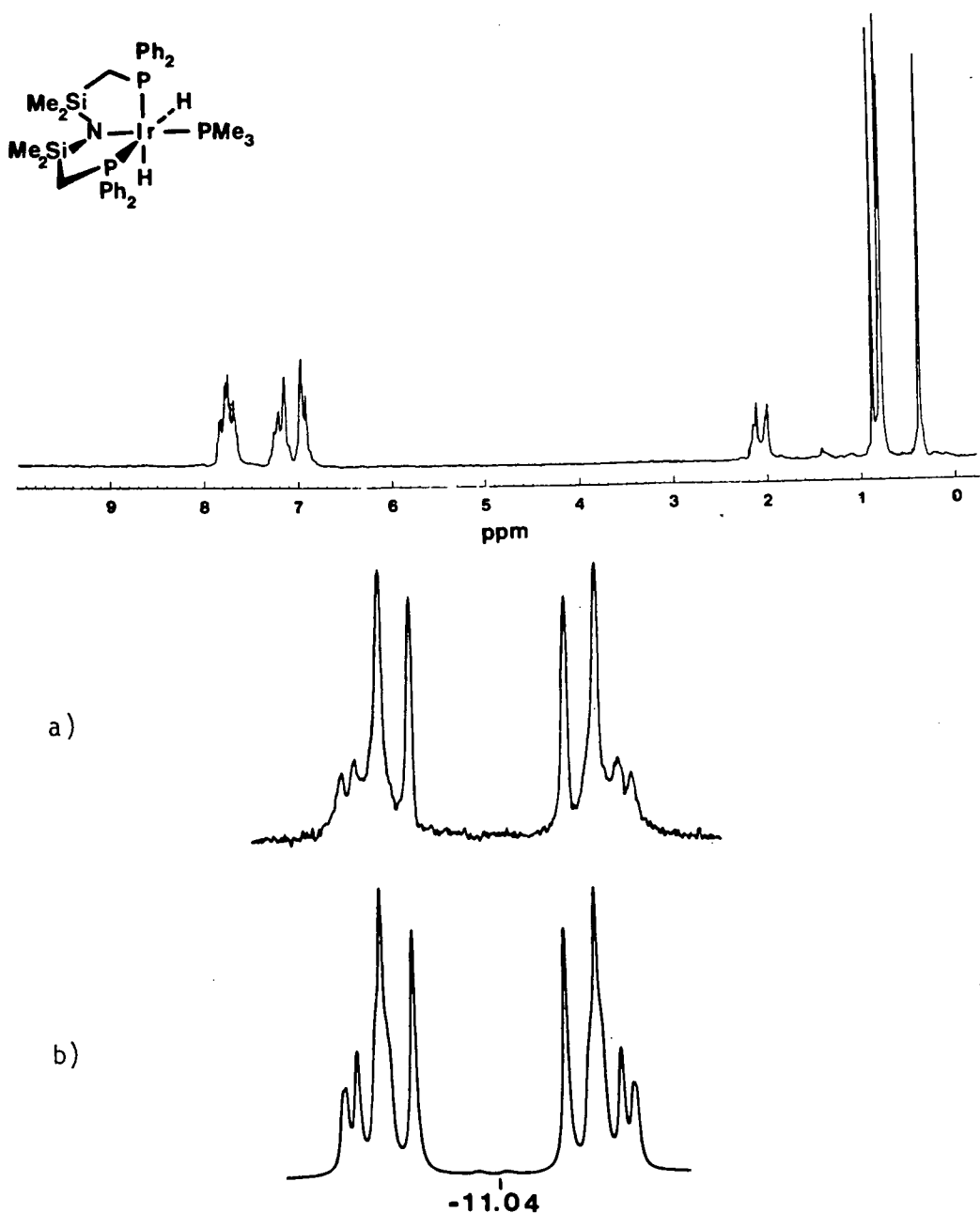


**Fig. 4.7** a)  $^1\text{H}$ NMR (100 MHz) of  $\text{fac-}[\text{Ir}(\text{H})_2(\text{PMe}_3)\text{N}(\text{SiMe}_2\text{CH}_2\text{PPh}_2)_2]$  in  $\text{C}_6\text{D}_6$   
 b) Hydride region (400 MHz  $^1\text{H}$ NMR) of  $\text{fac-}[\text{Ir}(\text{H})_2(\text{PMe}_3)\text{N}(\text{SiMe}_2\text{CH}_2\text{PPh}_2)_2]$   
 c) Spectral simulation of hydride AA'XX'Y pattern:  
 $^2J_{\text{A,X}} = ^2J_{\text{A',X'}} = -21.0$ ,  $^2J_{\text{A,Y}} = ^2J_{\text{A',Y}} = 21.0$ ,  $^2J_{\text{A,X'}} =$   
 $^2J_{\text{A',X}} = 147.0$ ,  $^2J_{\text{A,A'}} = 4.0$ ,  $^2J_{\text{X,Y}} = 9.0$ ,  $^2J_{\text{X,X'}} = 4.0$

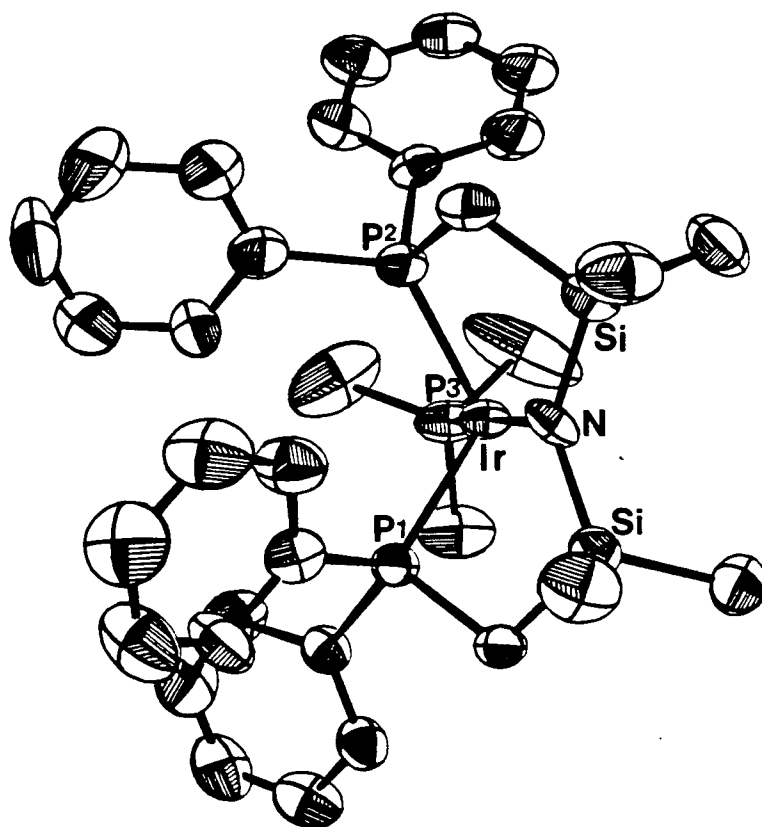
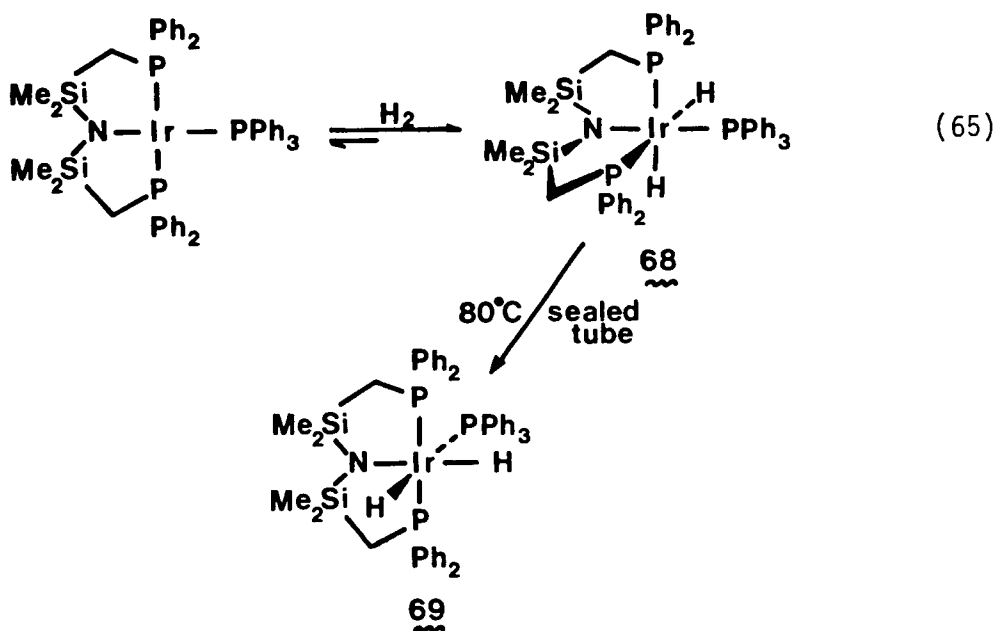


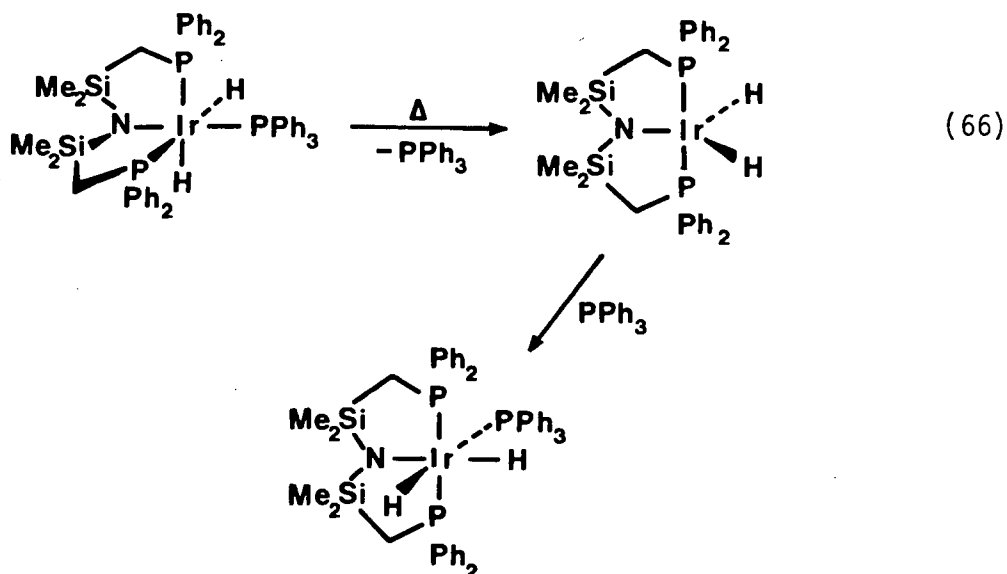
Fig. 4.8 X-ray crystal structure of  $\text{fac-}[\text{Ir}(\text{H})_2(\text{PMe}_3)\text{N}(\text{SiMe}_2\text{CH}_2\text{PPh}_2)_2]$

also much larger ( $131.4^\circ$ ) than expected for  $\text{sp}^2$  hybridized nitrogen. Possibly, these facts are a consequence of steric constraints imposed by the facial orientation of the tridentate ligand.

The product of the oxidative addition of dihydrogen to  $[\text{Ir}(\text{PPh}_3)_2\text{N}(\text{SiMe}_2\text{CH}_2\text{PPh}_2)_2]$  is also a fac dihydride. Once again, reaction occurs rapidly at one atmosphere of  $\text{H}_2$  at room temperature to yield exclusively fac cis- $[\text{Ir}(\text{H})_2(\text{PPh}_3)\text{N}(\text{SiMe}_2\text{CH}_2\text{PPh}_2)_2]$ , <sup>68</sup> (equation 65). However, at



80°C, 68 isomerizes (>90% in 1 hour) in solution to yield mer cis-  
 $[\text{Ir}(\text{H}_2)(\text{PPh}_3)\text{N}(\text{SiMe}_2\text{CH}_2\text{PPh}_2)_2]$  (equation 65). In contrast, 67 shows no  
 such isomerization, when heated at 120°C for 24 hours. Rearrangement of  
68 to 69 is therefore probably occurring by initial loss of  $\text{PPh}_3$  at high



temperature to form 59 which then re-adds  $\text{PPh}_3$  (recall that L approaches 59 cis to the iridium-amide bond) to give the meridional cis dihydride isomer 69 (equation 66). Presumably this route is not open to  $\text{PMe}_3$  analogue 67 due to its reluctance toward  $\text{PMe}_3$  dissociation.

The fac cis complex 68 is also unique from the other iridium dihydrido amido phosphines in that the oxidative addition of dihydrogen is reversible. All of the complexes 59, 62, 63, 64, 67 are exceptionally stable, crystalline materials, both in solution and in the solid state. However, 68 gradually loses dihydrogen under vacuum, or after several hours under  $\text{N}_2$  in solution, to regenerate  $[\text{Ir}(\text{PPh}_3)\text{N}(\text{SiMe}_2\text{CH}_2\text{PPh}_2)_2]$ .

It can be seen from the stereochemistry of the kinetic products of the oxidative addition of  $\text{H}_2$  to the iridium(I) amido phosphines  $[\text{IrLN}(\text{SiMe}_2\text{CH}_2\text{PPh}_2)_2]$  ( $\text{L} = \text{PMe}_3, \text{PPh}_3$ ) that reaction does not occur in a manner analogous to Vaska's complex. In other words, the dihydrogen molecule approaches along the P-Ir-P bond axis, rather than the L-Ir-X axis (for Vaska's complex,  $\text{L} = \text{CO}$  and  $\text{X} = \text{Cl}$ ) (Fig. 4.9). It is an interesting coincidence that the complexes mer cis- $[\text{IrL}(\text{H})_2\text{N}(\text{SiMe}_2\text{CH}_2\text{PPh}_2)_2]$ , prepared via the addition of L ( $= \text{CO}, \text{PMe}_3, \text{PPh}_3$ ) to 59, have the stereochemistry expected on the basis of the "normal" Vaska-type oxidative addition of  $\text{H}_2$  (mechanism as in Fig. 4.1). The disparity in reactivity between the

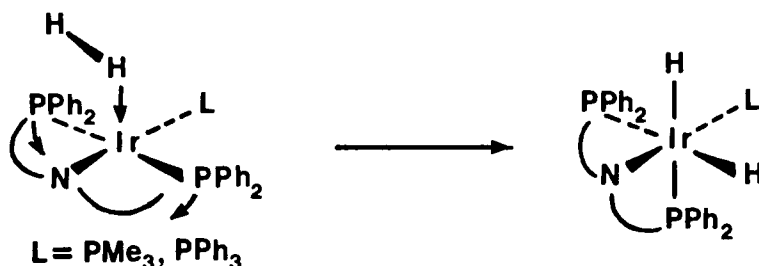


Fig. 4.9 Proposed mechanism for the oxidative addition of dihydrogen to  $[\text{Ir}(\text{L})\text{N}(\text{SiMe}_2\text{CH}_2\text{PPh}_2)_2]$

iridium amidophosphines and  $[\text{Ir}(\text{CO})\text{Cl}(\text{PPh}_3)_3]$  is further emphasized by the fact that  $[\text{Ir}(\text{CO})\text{N}(\text{SiMe}_2\text{CH}_2\text{PPh}_2)_2]$ , which basically differs from Vaska's complex in the substitution of a chloride by an amide centre, does not react with  $\text{H}_2$ , even under four atmosphere pressure.

It would therefore appear that, to a large extent, the stereochemistry of the dihydrogen-iridium(III) adduct, and even the reactivity of the initial iridium(I) complex, is largely dependent upon the nature of the anionic ligand  $\text{X}$  in the starting  $d^8$  square planar complex. As discussed previously, when  $\text{X} = \text{H}$ , carborane,  $\text{CH}_2\text{CN}$ , and amide, the kinetically stable isomer is either mainly (in the former two cases) or exclusively (in the latter two cases) the one having cis dihydrides which

are trans to cis diphosphines. It is therefore arguable that Vaska's complex shows "typical" reactivity with dihydrogen but rather, may be the exception to the rule.

### Spectral Trends in the Stereochemical Assignment of Iridium(III)

#### Amidophosphine Hydrides

As mentioned earlier, stereochemical analysis of iridium(III) hydrides has been largely made by spectrochemical means. Where complex stability and crystallinity permit, x-ray crystal structure and neutron diffraction analysis have been invaluable; however, these methods are, as yet, very expensive and appropriate only for solid samples.

For the iridium(III) amido phosphine hydride systems, the bulk of stereochemical information has been obtained from the  $^1\text{H}$ NMR spectra. In particular, analysis of the upfield region (ie.  $\delta < 0$  ppm) in terms of chemical shifts and coupling patterns has usually precluded x-ray crystal structure analysis. Selective homodecoupling, phosphorus decoupling, and variable temperature experiments have also been very helpful diagnostically.

A number of trends has been noted in the  $^1\text{H}$ NMR hydride resonances of the iridium amido phosphine hydrides; their chemical shifts and coupling constants are given in Table V (page 154).

Hydrides trans to the tridentate ligand's amide (or amine) centre typically resonate at  $-20 \rightarrow -25$  ppm (upfield of TMS). For a hydride trans to a phosphine (either as part of the tridentate ligand or a unidentate tertiary

phosphine), the chemical shift range is  $-8.5 \rightarrow -11.5$  ppm. For the single example of a hydride trans to a carbonyl group, the signal appears at  $-7.86$  ppm. In the complex, mer trans- $[\text{Ir}(\text{H})_2(\text{CO})\text{N}(\text{SiMe}_2\text{CH}_2\text{PPh}_2)_2]$ , in which the two hydrides are mutually trans, the chemical shift is  $-6.00$  ppm. Not surprisingly, the order of chemical shift values parallels the trans influence order (of the group trans to the hydride), ie.  $\text{H} > \text{CO} > \text{P} > \text{N} \approx \text{NH}^{107}$ .

The coupling constants are quite typical of other Ir(III) hydrides with  $^2J_{\text{H,P}}$  (cis) in the range  $12.5 \rightarrow 21$  Hz while  $^2J_{\text{H,P}}$  (trans) are much larger ( $130-150$  Hz). Couplings between chemically or magnetically inequivalent hydrides are approximately  $2 \rightarrow 5.5$  Hz.

Although the  $^{31}\text{P}\{^1\text{H}\}$  NMR spectra of these complexes are not quite as informative, an interesting pattern is observed for the octahedral di- and trihydrides. For those derivatives in which the tridentate ligand is coordinated meridionally, the chemical shift of the  $\text{PPh}_2$  centre is normally  $\sim 11.00$  ppm. Such a shift is well within the normal  $10-35$  ppm range observed in all of the Ni(0), Ni(II), Pd(II), Pt(II), Rh(I) and Ir(I) amido phosphines prepared to date. However, for the complexes in which the ligand is bound facially, the  $^{31}\text{P}\{^1\text{H}\}$  signal (for the  $\text{PPh}_2$  groups) is observed much further upfield, ( $< 0$  ppm). Once again, this may reflect the fact that for the dihydrides  $\underline{67}$  and  $\underline{68}$ , the  $\text{PPh}_2$  centres are trans to hydrides (a strong trans influence ligand) whereas in the other complexes the  $\text{PPh}_2$  is trans to another  $\text{PPh}_2$  (moderate trans influence). A similar trend in  $^{31}\text{P}$  values has been noted by others for a wide variety of metals<sup>57,152</sup>.

The high  $^{31}\text{P}\{^1\text{H}\}$  chemical shift of fac cis- $[\text{Ir}(\text{H})_2\text{LN}(\text{SiMe}_2\text{CH}_2\text{-PPh}_2)_2]$  may also be a function of the relatively unusual stereochemistry of the tridentate ligand. Meek<sup>57</sup> and others<sup>94</sup> have noted that upon coordination to a transition metal, a phosphine ligand usually resonates downfield as compared to the free ligand. Such is the case for all of the Group VIII amidophosphines. Since the  $^{31}\text{P}$  for the free ligand,  $\text{HN}(\text{SiMe}_2\text{CH}_2\text{PPh}_2)_2$ , is a singlet at -23.2 ppm, the chemical shift difference  $\Delta$ , defined as  $\delta\text{P}(\text{coordinated}) - \delta\text{P}(\text{free ligand})$ <sup>57</sup>, is typically in the range of 30 → 60. However, it has also been observed that the  $^{31}\text{P}$  values of transition metal complexes incorporating chelating phosphines show a dependency upon the size of the metal chelate ring<sup>94</sup>; this contribution has been designated  $\Delta_R$  and reflects the ring strain involved upon coordination. Thus, it is quite probable that the unusually high chemical shift observed for the facial amido phosphines may indicate a more strained conformation of the two five-membered chelate rings, as compared to the mer stereochemistry.

Infra-red spectral correlations also follow the trans influence series. The iridium-hydride stretching frequency for hydride trans to an amino group (as in fac and mer- $[\text{Ir}(\text{H})_3\text{NH}(\text{SiMe}_2\text{CH}_2\text{PPh}_2)_2]$ ) is 2175-2180  $\text{cm}^{-1}$ , which is slightly higher than for the corresponding absorption when the hydride is trans to an amide (2075-2110). For hydride trans to a phosphine centre,  $\nu_{\text{Ir-H}}$  is in the range 2065-2115  $\text{cm}^{-1}$ ; when trans to CO, this band shifts down to 1925  $\text{cm}^{-1}$ . An even more drastic effect is noted for trans H-Ir-H groupings; in this case,  $\nu_{\text{Ir-H}}$  is in the region 1705-1725

$\text{cm}^{-1}$ . Although  $\nu_{\text{Ir-H}}$  values have been well correlated for iridium complexes having trans phosphine, carbonyl, and hydride ligands<sup>144</sup> (and the iridium amidophosphine hydrides absorb within these quoted ranges), no such assignment has previously been made for hydrides trans to amides. However, it would seem that, on the basis of the amide's weak trans influence character, the high energy absorptions observed (for H-Ir trans to N) are quite reasonable.

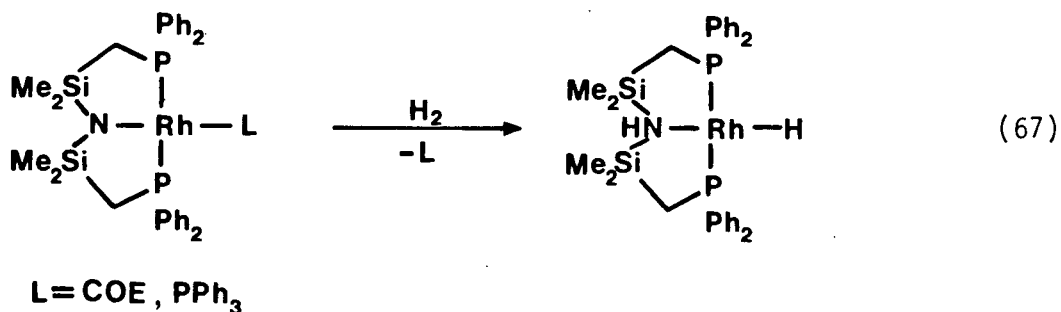
#### Hydrido Intermediates Involved in Catalytic Hydrogenations using Rhodium and Iridium Amido Phosphines

As discussed in Chapter 3, the mechanism of olefin hydrogenation and isomerization catalyzed by a number of rhodium and iridium amido-phosphines is, as yet, largely speculation. However, the results of the oxidative addition reactions of dihydrogen with iridium amidophosphines have been somewhat informative. It would appear reasonable that for the  $[\text{Ir}(\text{COE})\text{N}(\text{SiMe}_2\text{CH}_2\text{PPh}_2)_2]$  system, the active catalyst is probably  $[\text{Ir}(\text{H})_2\text{N}(\text{SiMe}_2\text{CH}_2\text{PPh}_2)_2]$ , <sup>59</sup>. Coordination of the substrate should then proceed to give mer cis- $[\text{Ir}(\text{H})_2(\text{ol})\text{N}(\text{SiMe}_2\text{CH}_2\text{PPh}_2)_2]$ , analogous to formation of mer cis- $[\text{Ir}(\text{H})_2\text{LN}(\text{SiMe}_2\text{CH}_2\text{PPh}_2)_2]$  (L = CO,  $\text{PMe}_3$ ). The following steps, migratory insertion and reductive elimination, should proceed in a straightforward manner to yield the saturated alkane. Involvement of either the fac or mer trihydrides <sup>60</sup>, <sup>61</sup> should be suppressed in the presence of excess substrate, since it is reasonable to assume that olefin coordination to the coordinatively unsaturated, 16-electron complex

59 should be more facile than a second oxidative addition to an Ir(III) centre (or a heterolytic cleavage of  $H_2$ ).

The fact that  $[IrLN(SiMe_2CH_2PPh_2)_2]$  ( $L = PPh_3, PMe_3$ ) do not hydrogenate olefins is undoubtedly a consequence of the inability of the dihydrogen adduct to dissociate a phosphine ligand (at least at room temperature); the required coordination site for olefin binding is therefore not generated. The inactivity of  $[Ir(CO)N(SiMe_2CH_2PPh_2)_2]$  towards olefin hydrogenation is also understandable in light of the fact that this complex does not even oxidatively add  $H_2$ .

As far as the isomerization activity of some of the amido phosphine complexes, it has been proposed that this may indicate the presence of an amine monohydride in the catalytic cycle. That such a species can form via reductive elimination of the metal-amide bond has been lent credence by the isolation of the iridium amine trihydrides 60 and 61. Note that formation of  $Rh(H)NH(SiMe_2CH_2PPh_2)_2$ , like 60 and 61, corresponds to an overall heterolytic splitting of  $H_2$  (equation 67).



Chapter V Experimental

General Information: All manipulations were performed under pre-purified nitrogen in a Vacuum Atmospheres HE-553-2 glove box equipped with a MO-40-2H purifier, or in standard Schlenk-type glassware.

Palladium dichloride was purchased from Ventron and used as received to prepare  $\text{PdCl}_2(\text{C}_6\text{H}_5\text{CN})_2$  by a literature method<sup>153</sup>. Potassium tetrachloroplatinate was also obtained from Ventron and recrystallized from hot ethanol prior to use in the preparation of  $\text{K}[\text{PtCl}_3(\text{C}_2\text{H}_4)]^{154}$ ,  $\text{Pt}(\text{COD})\text{Cl}_2^{155}$ ,  $\text{PtCl}_2(\text{C}_6\text{H}_5\text{CN})_2^{156}$ , trans- $\text{PtCl}_2(\text{PR}_3)_2$  ( $\text{R}=\text{Ph}^{157}$  or  $\text{Et}^{158}$ ), and trans- $\text{Pt}(\text{H})\text{Cl}(\text{PEt}_3)_2^{158}$ . Rhodium trichloride hydrate and iridium trichloride hydrate were obtained on loan from Johnson-Mathey and used directly in the synthesis of  $\{\text{Rh}(\text{C}_8\text{H}_{14})_2\text{Cl}\}_2^{159}$ ,  $\{\text{Rh}(\text{C}_2\text{H}_4)_2\text{Cl}\}_2^{160}$ ,  $\{\text{Rh}(\text{CO})_2\text{Cl}\}_2^{161}$ ,  $\text{Rh}(\text{PMe}_3)_4^+\text{Cl}^-^{162}$ ,  $\text{Rh}(\text{PPh}_3)_3\text{Cl}^{163}$ ,  $\{\text{Rh}(\text{COD})\text{Cl}\}_2^{164}$ ,  $\{\text{Ir}(\text{COD})\text{Cl}\}_2^{165}$ , and  $\{\text{Ir}(\text{C}_8\text{H}_{14})_2\text{Cl}\}_2^{166}$ .

$\text{LiPPh}_2^{167}$  was prepared by the dropwise addition of n-butyllithium in hexane (1.6 M, Aldrich) to a hexane solution of  $\text{HPPH}_2$ . After several washings with hexane, the resultant lemon-yellow powder was used directly in the preparation of  $(\text{Ph}_2\text{PCH}_2\text{SiMe}_2)_2\text{NH}$ .

Methylene chloride ( $\text{CH}_2\text{Cl}_2$ ), cyclohexane, triethylamine and benzylamine were purified by distillation from  $\text{CaH}_2$  under argon. Toluene, hexanes, and diethyl ether were dried and deoxygenated from sodium benzophenone ketyl under argon. Acetone was dried by refluxing over  $\text{K}_2\text{CO}_3$  for several days followed by distillation under argon. Tetrahydrofuran (THF) was predried by refluxing over  $\text{CaH}_2$  and then distilled from sodium benzophenone ketyl under argon.

$^{13}\text{CO}$  (90 atom %  $^{13}\text{C}$ ) was purchased from MSD and used without further purification.  $^{15}\text{NH}_4\text{Cl}$  (99 atom %  $^{15}\text{N}$ ) was obtained from MSD and dried at

120°C for 24 h prior to use.

The hydrogenation substrates (1-hexene and cis/trans-2-hexenes) were purchased from Aldrich (Gold Label) and dried over 4 Å molecular sieves, vacuum transferred, and freeze-pump-thawed several times. Any trace peroxides were removed by passing the dried olefins through a short column of activated alumina (Fisher 80-200 mesh).

Melting points were determined on a Mel-Temp apparatus in sealed capillaries under nitrogen and are uncorrected. Carbon, hydrogen, nitrogen analyses were performed by Mr. P. Borda of this department.

<sup>1</sup>H NMR were recorded on one of the following instruments, depending upon the complexity of the particular spectrum: Varian EM-360L, Bruker WP-80, Varian XL-100, Nicolet-Oxford H-270, and Bruker WH-400. (Spectral simulations were performed using the Bruker Aspect 2000 computer system with the UBCPANIC program (PANIC = Parameter Adjustment in NMR by Iteration and Calculation)). <sup>31</sup>P{<sup>1</sup>H} NMR spectra were run at 32.442 MHz on the Bruker WP-80 in 10 mm tubes fitted with inserts for the internal standard P(OMe)<sub>3</sub>. <sup>13</sup>C{<sup>1</sup>H} NMR spectra were run at 20.1 MHz and 100 MHz on the Bruker WP-80 and WH-400, respectively. Infrared spectra were recorded either on a Pye-Unicam SP-1100 or a Perkin-Elmer 598 as KBr discs or in solution.

Gas liquid chromatographic analyses were performed using a Varian Vista 6000 GC (with a 401 Computer Data System) equipped with a flame ionization detector (FID). The following column specifications apply to all sample analyses: 60/80 Chromosorb P(AW)/20% tri-o-cresyl phosphate; 20 ft x 1/8" ss; Col. temp.: 40°C; sample size: 0.5 µl.

C<sub>6</sub>D<sub>6</sub>, (CD<sub>3</sub>)<sub>2</sub>CO, C<sub>7</sub>D<sub>8</sub>, CD<sub>2</sub>Cl<sub>2</sub>, and CCl<sub>3</sub> were purchased from Aldrich; the C<sub>6</sub>D<sub>6</sub>, (CD<sub>3</sub>)<sub>2</sub>CO, CD<sub>2</sub>Cl<sub>2</sub>, and C<sub>7</sub>D<sub>8</sub> were dried over activated 4 Å

molecular sieves and vacuum transferred, while the  $\text{CDCl}_3$  was dried by refluxing over  $\text{CaH}_2$  followed by vacuum transferral.

The Grignard reagents methylmagnesium chloride (in THF) and vinylmagnesium chloride (in THF) were purchased from Ventron; phenylmagnesium bromide (in  $\text{Et}_2\text{O}$ ) was obtained from Aldrich. Allyl magnesium chloride was prepared from freshly distilled allyl chloride and excess magnesium turnings in THF, filtered through cotton wool, and standardized using a gas buret (with 0.1 N HCl).

Note: All recorded infra-red absorptions are given in  $\text{cm}^{-1}$ ; all chemical shifts ( $^1\text{H}$ ,  $^{13}\text{C}$ ,  $^{31}\text{P}$ ) are in ppm with the coupling constants expressed in Hz. All  $^1\text{H}$ NMR were recorded in  $\text{C}_6\text{D}_6$  at room temperature (referenced to  $\text{C}_6\text{D}_5\text{H}$  at 7.15 ppm) unless otherwise noted.

#### Preparation of the hybrid ligands.

##### $(\text{ClCH}_2\text{SiMe}_2)_2\text{NH}$ and $(\text{ClCH}_2\text{SiMe}_2)_2^{15}\text{NH}$

1,3-bis(chloromethyl)tetramethyldisilazane,  $(\text{ClCH}_2\text{SiMe}_2)_2\text{NH}$ , was prepared as described by Osthoff and Kantor<sup>168</sup>. However, for its  $^{15}\text{N}$ -labelled analogue, a modification of this method was employed. This preparation was carried out in a 250 ml heavy-walled flask fitted with a Kontes 9 mm needle-valve inlet.

To a suspension of finely-crushed  $^{15}\text{NH}_4\text{Cl}$  (1.09 g, 0.02 mol) in THF (100 ml) was added  $\text{ClCH}_2\text{SiMe}_2\text{Cl}$  (5.7 g, 0.04 mol). The mixture was cooled to  $0^\circ\text{C}$ . Triethylamine (6.1 g, 0.06 mol) was added, via syringe, and the suspension was then stirred vigorously at room temperature for 7 days.

The solvent was removed in vacuo and the product extracted with hexanes, filtered and pumped down. Distillation of the resultant yellowish oil (b.p. 103°/10 mm) gave the product in ~60% yield as a clear, colorless liquid. The synthesis of the  $^{15}\text{N}$ -labelled tridentate ligand was carried out in an identical manner as described below for its  $^{14}\text{N}$  analogue.

$(\text{Ph}_2\text{PCH}_2\text{SiMe}_2)_2\text{NH}$ . To a cooled solution (-4°C) of  $\text{LiPPh}_2$  (9.6 g, 0.05 mol) in THF (50 ml) was added  $(\text{ClCH}_2\text{SiMe}_2)_2\text{NH}$  (5.35 g, 0.025 mol) dropwise with stirring. The initially clear red solution gradually decolourized to a very pale yellow when all of the silyl chloride had been added. The solution was stirred at room temperature for 0.5 h; the THF was then removed in vacuo. The residue was extracted with pentane (50 ml) and filtered through a medium porosity frit. Removal of the pentane in vacuo yielded a pale yellow oil which was immediately taken up in hexane (10 ml), filtered and cooled to -30°C. Fine white needles of the product formed; these were filtered and washed with cold hexane. Yield: 10.2 g (77%). m.p. 45-46°C. Anal. Calcd. for  $\text{C}_{30}\text{H}_{37}\text{NP}_2\text{Si}_2$ : C, 68.05; H, 6.99; N, 2.65. Found: C, 68.33; H, 7.25; N, 2.55. IR (KBr):  $\nu_{\text{N-H}} = 3365$  (w).  $^{31}\text{P}\{^1\text{H}\}\text{NMR}$  ( $\text{C}_6\text{D}_6$ ): -22.45 (s).

$\text{LiN}(\text{SiMe}_2\text{CH}_2\text{PPh}_2)_2$ . To a vigorously stirred solution of freshly recrystallized  $(\text{Ph}_2\text{CH}_2\text{SiMe}_2)\text{NH}$  (5.3 g, 0.01 mol) in pentane (50 ml) at room temperature, was slowly added n-BuLi in hexane (1.6 M, 8 ml, 0.016 mol). A fine white precipitate immediately formed. After stirring at room temperature for 0.5 h, the white solid was filtered and washed with pentane. Yield: 3.8 g (71%). Although the product is sufficiently pure at this stage to be used in metathetical reactions with transition metal salts, it may be recrystallized from toluene/hexane to give colorless plates. m.p. 120°C

(decomp.). Anal. Calcd for  $C_{30}H_{36}LiNP_2Si_2$ : C, 67.29; H, 6.73; N, 2.61. Found: C, 67.00; H, 6.78; N, 2.48. Molecular weight (Signer): theoretical (monomer), 535; found, 1516.  $^{31}P\{^1H\}NMR$  ( $C_6D_6$ ): -23.20 (s).

$(ClCH_2SiMe_2)(C_6H_5CH_2)NH$ . The apparatus for this reaction consisted of a 1ℓ 3-necked round-bottom flask to which was attached a 250 ml addition funnel. To a solution of benzylamine (21.4 g, 0.20 mol) in hexane (200 ml) was slowly added  $ClCH_2SiMe_2Cl$  (14.3 g, 0.10 mol) in hexane (150 ml). Immediately, a white granular precipitate (benzylamine hydrochloride) formed. After addition of the silyl chloride was completed (~3 h), the mixture was stirred vigorously for several hours at room temperature and then filtered under argon. The precipitate was washed with copious quantities of hexane. The combined hexane fractions were then pumped down, yielding an almost colorless oil. Distillation gave the product as a colorless liquid (b.p. 76-80°C/1 mm). Yield: 16 g (76%).

$(Ph_2PCH_2SiMe_2)(C_6H_5CH_2)NH$ . Preparation of this bidentate ligand was carried out in a manner directly analogous to that described for  $(Ph_2PCH_2SiMe_2)_2NH$  (*vide supra*) from  $(ClCH_2SiMe_2)(C_6H_5CH_2)NH$  (2.1 g, 0.01 mol) and  $LiPPh_2$  (1.9 g, 0.01 mol) in THF (25 ml). Work-up (as previously outlined) resulted in a yellowish oil which was distilled (b.p. 140°C/1 mm) as a colorless liquid. Yield: 3.0 g (83%). IR(hexane):  $\nu_{N-H} = 3380$  (w).  $^{31}P\{^1H\}NMR$  ( $C_6D_6$ ): -22.31 (s).

$Li(C_6H_5CH_2)(SiMe_2CH_2PPh_2)$ . Formation of this lithium salt proceeded smoothly using n-BuLi and the ligand  $(Ph_2CH_2SiMe_2)(C_6H_5CH_2)NH$  in hexane at room temperature (see above preparation of  $Li(SiMe_2CH_2PPh_2)$ ). Recrystallization at -30°C from hexanes resulted in colorless crystals of the product. This

complex is very thermally sensitive and must be stored at  $-30^{\circ}\text{C}$  (storage at room temperature results in decomposition to a mauve oil). Yield: 92%. Anal. Calcd. for  $\text{C}_{22}\text{H}_{25}\text{LiNPSi}$ : C, 71.54; H, 6.78; N, 3.79. Found: C, 71.53; H, 6.80; N, 3.78. Molecular weight (Signer): theoretical (monomer), 369; found, 943.  $^{31}\text{P}\{^1\text{H}\}\text{NMR}(\text{C}_6\text{D}_6)$ :  $-23.54$  (br s).

#### Amido Phosphine Complexes of the Ni Triad

$[\text{NiClN}(\text{SiMe}_2\text{CH}_2\text{PPh}_2)_2]$ . Method 1. A solution of  $\text{LiN}(\text{SiMe}_2\text{CH}_2\text{PPh}_2)_2$  (1.34 g, 2.5 mmol) in  $\text{Et}_2\text{O}$  (25 ml) was added dropwise with stirring to a cooled ( $0^{\circ}\text{C}$ ) solution of  $[\text{Ni}(\text{PMe}_3)_2\text{Cl}_2]^{169}$  (0.7 g, 2.5 mmol) in THF (30 ml). The initially clear deep red solution immediately became dark brown in colour. After stirring at  $0^{\circ}\text{C}$  for 0.5 h, the solution was stirred at room temperature for 1 h. The solvent was removed in vacuo and the resultant brown oil extracted with cyclohexane. Upon filtration through a medium porosity frit, a clear deep brown solution was obtained; the cyclohexane was then removed in vacuo. Recrystallization from toluene/hexane yielded diamond-shaped brown prisms. m.p.  $153-155^{\circ}\text{C}$ . Anal. Calcd. for  $\text{C}_{30}\text{H}_{36}\text{ClNNiP}_2\text{Si}_2$ : C, 57.83; H, 5.78; N, 2.25. Found: C, 57.71; H, 5.87; N, 2.23. Yield: 1.01 g (65%).  $^{31}\text{P}\{^1\text{H}\}\text{NMR}(\text{C}_6\text{D}_6)$ :  $14.76$  (s).

Method 2. To a suspension of  $\text{NiCl}_2 \cdot \text{DME}^{170}$  (0.22 g, 1.0 mmol) in toluene (30 ml) was added a solution of  $(\text{Ph}_2\text{PCH}_2\text{SiMe}_2)_2\text{NH}$  (0.53 g, 1.0 mmol) in toluene (10 ml). Immediately, a clear deep-red solution formed and, upon stirring at room temperature for 0.5 h, green shiny needles began to precipitate. An excess of triethylamine (0.15 g, 1.5 mmol) was added dropwise, producing a deep brown solution. After stirring at room temperature for 1 h, the solution was filtered through Celite. Removal of the solvent in vacuo yielded large brown prisms of analytically pure  $[\text{NiClN}(\text{SiMe}_2\text{CH}_2\text{PPh}_2)_2]$ . Yield: 0.55 g (88%).

[PdClN(SiMe<sub>2</sub>CH<sub>2</sub>PPh<sub>2</sub>)<sub>2</sub>]. A solution of LiN(SiMe<sub>2</sub>CH<sub>2</sub>PPh<sub>2</sub>)<sub>2</sub> (0.54 g, 1.0 mmol) in Et<sub>2</sub>O (10 ml) was slowly added to a cooled (-78°C) solution of freshly prepared (C<sub>6</sub>H<sub>5</sub>CN)<sub>2</sub>PdCl<sub>2</sub> (0.39 g, 1.0 mmol) in THF (30 ml); the mixture was stirred at -78°C for 0.5 h. The clear orange-gold solution was then stirred at 0°C for 1 h and finally at room temperature for an additional hour. The solvent was removed in vacuo and the product extracted with cyclohexane. Recrystallization from toluene/hexane gave orange blocks of the palladium amide, which contains one mole of toluene as solvent of crystallization. Anal. Calcd. for C<sub>37</sub>H<sub>44</sub>ClNP<sub>2</sub>PdSi<sub>2</sub>: C, 58.26; H, 5.77; N, 1.83. Found: C, 58.27; H, 5.96; N, 1.81. m.p. 136-137°C. Yield: 0.40 g (60%). The complex may also be recrystallized from acetone/hexane, yielding orange rod-like crystals. m.p. 140°C. Anal. Calcd. for C<sub>30</sub>H<sub>36</sub>ClNP<sub>2</sub>PdSi<sub>2</sub>: C, 53.72; H, 5.37; N, 2.07. Found: C, 53.73; H, 5.54; N, 2.04. <sup>31</sup>P{<sup>1</sup>H}NMR((CD<sub>3</sub>)<sub>2</sub>CO): 18.71 (s).

[PtClN(SiMe<sub>2</sub>CH<sub>2</sub>PPh<sub>2</sub>)<sub>2</sub>]. To a cooled (0°C) solution of freshly prepared Zeise's salt, K[PtCl<sub>3</sub>(C<sub>2</sub>H<sub>4</sub>)], (0.37 g, 1.0 mmol) in THF (25 ml) was slowly added a solution of LiN(SiMe<sub>2</sub>CH<sub>2</sub>PPh<sub>2</sub>)<sub>2</sub> (0.54 g, 1.0 mmol) in Et<sub>2</sub>O (10 ml). The originally clear lemon-yellow solution did not undergo any noticeable colour changes during the addition. The solution was stirred at 0°C for 0.5 h and then at room temperature for 4 h. The solvent was removed in vacuo; the product was then extracted with cyclohexane, filtered, and pumped down to a fine yellow glass. Upon recrystallization from toluene/hexane, shiny yellow plates of the platinum amide were obtained. Yield: 0.48 g (63%). m.p. 147-149°C. Anal. Calcd. for C<sub>37</sub>H<sub>94</sub>ClNP<sub>2</sub>PtSi<sub>2</sub>: C, 52.23; H, 5.18; N, 1.65. Found: C, 52.10; H, 5.27; N, 1.61. <sup>31</sup>P{<sup>1</sup>H}NMR (C<sub>6</sub>D<sub>6</sub>): 34.27 (t, <sup>2</sup>J<sub>Pt,P</sub> = 2690.0).

[NiCl<sub>2</sub>NH(SiMe<sub>2</sub>CH<sub>2</sub>PPh<sub>2</sub>)<sub>2</sub>]. A solution of freshly recrystallized (Ph<sub>2</sub>PCH<sub>2</sub>SiMe<sub>2</sub>)<sub>2</sub>NH (0.53 g, 1.0 mmol) in THF (10 ml) was added to a suspension of NiCl<sub>2</sub>·DME (0.22 g, 1.0 mmol) in THF (25 ml). The solution immediately became clear deep red in colour and, upon stirring at room temperature for 0.5 h, green crystals began to form. After an additional 0.5 h, the solvent was removed in vacuo. Recrystallization of the green solid from CH<sub>2</sub>Cl<sub>2</sub>/hexane produced fluffy green crystals which, upon standing, gradually re-formed as shiny blue-black prisms. Yield: 0.58 g (88%). m.p. 185-187°C. Anal. Calcd. for C<sub>30</sub>H<sub>37</sub>Cl<sub>2</sub>NNiP<sub>2</sub>Si<sub>2</sub>: C, 54.65; H, 5.66; N, 2.12. Found: C, 54.43; H, 5.67; N, 2.00. IR(KBr): ν<sub>NH</sub> = 3365 (w).

[PdCl<sub>2</sub>NH(SiMe<sub>2</sub>CH<sub>2</sub>PPh<sub>2</sub>)<sub>2</sub>]. A solution of PdCl<sub>2</sub>(C<sub>6</sub>H<sub>5</sub>CN)<sub>2</sub> (0.38 g, 1.0 mmol) and (Ph<sub>2</sub>PCH<sub>2</sub>SiMe<sub>2</sub>)<sub>2</sub>NH (0.53 g, 1.0 mmol) in THF (35 ml) was stirred at room temperature for two days. Removal of the solvent in vacuo yielded a gold-coloured oil which was then recrystallized from CH<sub>2</sub>Cl<sub>2</sub>/cyclohexane to give yellow prisms of the product. This complex contains one mole of cyclohexane as solvent of crystallization. m.p. 140°C. Anal. Calcd. for C<sub>36</sub>H<sub>49</sub>Cl<sub>2</sub>NP<sub>2</sub>PdSi<sub>2</sub>: C, 54.68; H, 6.20; N, 1.77. Found: C, 55.06; H, 6.39; N, 1.75. <sup>31</sup>P{<sup>1</sup>H}NMR((CD<sub>3</sub>)<sub>2</sub>CO): 21.86 (s). IR(KBr): ν<sub>NH</sub> = 3305 (w).

[PtCl<sub>2</sub>NH(SiMe<sub>2</sub>CH<sub>2</sub>PPh<sub>2</sub>)<sub>2</sub>]. Pt(COD)Cl<sub>2</sub> (0.19 g, 0.5 mmol) and (Ph<sub>2</sub>PCH<sub>2</sub>SiMe<sub>2</sub>)<sub>2</sub>NH (0.27 g, 0.5 mmol) were dissolved in THF (20 ml). Upon refluxing, the milky solution gradually became clear lemon-yellow in colour; the solution was refluxed overnight. The solution was then cooled to room temperature and, upon addition of hexane (30 ml), a fine white solid precipitated. The solid was filtered under nitrogen and recrystallized from CH<sub>2</sub>Cl<sub>2</sub>/cyclohexane to give a colourless gel which, upon standing at room temperature overnight,

formed large colourless blocks. Yield: 0.31 g (78%). m.p. 220-222°C.

Anal. Calcd. for  $C_{30}H_{37}Cl_2NP_2PtSi_2$ : C, 45.28; H, 4.65; N, 1.76. Found: C, 45.31; H, 4.65; N, 1.69.  $^{31}P\{^1H\}NMR(CD_3)_2CO$ : 41.44 (t,  $J_{Pt,P} = 3599.6$ ). IR (KBr):  $\nu_{NH} = 3280$  (w).

Conversion of Ni(II), Pd(II), and Pt(II) - dichloro amino diphosphines to the corresponding chloro amido diphosphines. This reaction is exemplified with the palladium complex.  $[PdCl_2NH(SiMe_2CH_2PPh_2)_2 \cdot C_6H_{12}]$  (0.15 g, 0.2 mmol) was dissolved in toluene (15 ml) at room temperature, forming a clear gold solution. An excess of triethylamine (~0.5 ml) was added and the solution stirred for 24 h. The resultant deep orange solution was filtered through Celite in order to remove the colourless granular  $NEt_3 \cdot HCl$ . Removal of the solvent in vacuo yielded the product as well-formed crystals (no further recrystallization necessary). In contrast to the palladium and platinum derivatives, the analogous reaction to form the nickel complex is complete within one hour.

Alkyl Derivatives of the Ni(II) and Pd(II) Amido Phosphines.

$[Ni(CH_3)N(SiMe_2CH_2PPh_2)_2]$ . To a cooled solution (-30°C) of  $[NiCl_2N(SiMe_2CH_2PPh_2)_2]$  (62 mg, 0.1 mmol) in toluene (15 ml) was added  $CH_3MgCl$  in THF (2.9 M, 35  $\mu l$ , 0.1 mmol). The initially deep brown solution rapidly became deep orange in colour. After standing at -30°C for 0.5 h, the solvent was removed in vacuo. The product was extracted with cyclohexane, filtered through Celite and pumped down to yield fine yellow-orange crystals. Recrystallization from toluene/hexane at -30°C gave analytically pure product. m.p. 134-136°C. Yield: 44 mg (74%). Anal. Calcd. for  $C_{31}H_{39}NNiP_2Si_2$ : C, 61.80; H, 6.53; N, 2.33. Found: C, 61.60; H, 6.43; N, 2.20.

$^{31}P\{^1H\}NMR(C_6D_6)$ : 26.73 (s).

$[\text{Ni}(\text{CH}_2\text{CH}=\text{CH}_2)\text{N}(\text{SiMe}_2\text{CH}_2\text{PPh}_2)_2]$ . Allyl magnesium chloride in THF (0.55 M, 91  $\mu\text{l}$ , 0.05 mmol) was added to a cooled ( $-30^\circ\text{C}$ ) solution of  $[\text{NiClN}(\text{SiMe}_2\text{CH}_2\text{PPh}_2)_2]$  (31 mg, 0.05 mmol) in toluene (15 ml). The resultant deep red-brown solution was kept at  $-30^\circ\text{C}$  for 0.5 h. After warming to room temperature, the solvent was removed in vacuo. Extraction and recrystallization was carried out in the same manner as described for the methyl derivative, yielding deep red-brown crystals. Anal. Calcd. for  $\text{C}_{33}\text{H}_{41}\text{NNiP}_2\text{Si}_2$ : C, 63.06; H, 6.53; N, 2.23. Found: C, 62.82; H, 6.80; N, 2.13. m.p.  $130^\circ\text{C}$  (decomp.). Yield: 24 mg (78%).  $^{31}\text{P}\{^1\text{H}\}\text{NMR}(\text{C}_6\text{D}_6)$ : 17.81 (br s).

$[\text{Ni}(\text{CH}=\text{CH}_2)\text{N}(\text{SiMe}_2\text{CH}_2\text{PPh}_2)_2]$ . Addition of vinyl magnesium bromide in THF (1.4 M, 72  $\mu\text{l}$ , 0.1 mmol) to a cooled ( $-30^\circ\text{C}$ ) solution of  $[\text{NiClN}(\text{SiMe}_2\text{CH}_2\text{PPh}_2)_2]$  (62 mg, 0.1 mmol) in  $\text{Et}_2\text{O}$  (60 ml) produced a cloudy pale yellow solution. After 5 minutes at  $-30^\circ\text{C}$ , the solvent was rapidly removed in vacuo. Extraction with hexane, followed by filtration through Celite and solvent removal, yielded gold-yellow crystals of the vinyl derivative. Recrystallization from toluene/hexane at  $-30^\circ\text{C}$  produces analytically pure material. Yield: 40 mg (65%). Anal. Calcd. for  $\text{C}_{32}\text{H}_{35}\text{NNiP}_2\text{Si}_2$ : C, 62.54; H, 6.35; N, 2.28. Found: C, 62.48; H, 6.44; N, 2.11.  $^{31}\text{P}\{^1\text{H}\}\text{NMR}(\text{C}_6\text{D}_6)$ : 21.00 (s).

$[\text{Ni}(\text{C}_6\text{H}_5)\text{N}(\text{SiMe}_2\text{CH}_2\text{PPh}_2)_2]$ . To a cooled solution ( $-30^\circ\text{C}$ ) of  $[\text{NiClN}(\text{SiMe}_2\text{CH}_2\text{PPh}_2)_2]$  (62 mg, 0.1 mmol) in THF (60 ml) was added phenyl magnesium bromide in  $\text{Et}_2\text{O}$  (3.0 M, 34  $\mu\text{l}$ , 0.1 mmol). After 15 minutes at  $-30^\circ\text{C}$ , the solvent was removed in vacuo. Extraction with hexane gave gold coloured crystals of the phenyl derivative. m.p.  $160\text{--}162^\circ\text{C}$  (decomp.). Yield: 40 mg

(60%). Anal. Calcd. for  $C_{36}H_{41}NNiP_2Si_2$ : C, 65.06; H, 6.35; N, 2.28.

Found: C, 65.58; H, 6.35; N, 2.06.  $^{31}P\{^1H\}NMR(C_6D_6)$ : 20.32 (s).

$[Ni(CN)N(SiMe_2CH_2PPh_2)_2]$ . Freshly distilled  $Me_3SiCN^{171}$  (44 mg, 0.45 mmol) was added at room temperature to a solution of  $[NiClN(SiMe_2CH_2PPh_2)_2]$  (0.25 g, 0.4 mmol) in toluene (25 ml). After stirring at room temperature for 45 minutes, the reaction mixture rapidly changed from its initial deep brown colour to a clear orange. The solution was stirred at room temperature for an additional 2 h, after which time the solvent was removed in vacuo. Recrystallization of the resultant oil from toluene/hexane yielded small orange blocks of the cyanide complex. m.p. 142-143°C. Yield: 20 mg (83%).

Anal. Calcd. for  $C_{31}H_{36}N_2NiP_2Si_2$ : C, 60.68; H, 5.87; N, 4.56. Found: C, 61.00; H, 6.00; N, 4.40. IR(KBr):  $\nu_{CN} = 2122$  (s).

$[Pd(CH_3)N(SiMe_2CH_2PPh_2)_2]$ . The synthesis of this complex was performed in an identical fashion as outlined for its nickel analogue. Upon addition of the Grignard, the starting gold-coloured solution became completely colourless. Recrystallization of the product from minimum hexane at -30°C yielded colorless plates. Anal. Calcd. for  $C_{31}H_{39}NP_2PdSi_2$ : C, 57.28; H, 6.05; N, 2.15. Found: C, 57.17; H, 6.10; N, 1.82. Yield: 48 mg (74%).  $^{31}P\{^1H\}NMR(C_6D_6)$ : 24.92 (s).

$[Pd(CH_2CH=CH_2)N(SiMe_2CH_2PPh_2)_2]$ . Preparation of this complex followed that of the corresponding nickel derivative. The product was obtained as pale yellow crystals from hexane. m.p. 90°C (decomp.). Yield: 29 mg (86%).

Anal. Calcd. for  $C_{33}H_{41}NP_2PdSi_2$ : C, 58.67; H, 6.07; N, 2.07. Found: C, 59.23; H, 6.42; N, 2.13.

### Carbonylation Reactions

All reactions of the Ni(II) alkyls with CO and  $^{13}\text{C}$ O to produce the Ni(0) derivatives  $[\text{Ni}(\text{CO})_2\text{N}(\text{COR})(\text{SiMe}_2\text{CH}_2\text{PPh}_2)_2]$  were performed at one atmosphere pressure at room temperature in toluene. Typically, 0.02 M solutions of the Ni complexes,  $\text{Ni}(\text{R})\text{N}(\text{SiMe}_2\text{CH}_2\text{PPh}_2)_2$  (R = methyl, allyl, vinyl, phenyl), were rapidly stirred under carbon monoxide. A typical preparation is given below.

$[\text{Ni}(\text{CO})_2\text{N}(\text{COCH}_3)(\text{SiMe}_2\text{CH}_2\text{PPh}_2)_2]$ . A solution of  $[\text{Ni}(\text{CH}_3)\text{N}(\text{SiMe}_2\text{CH}_2\text{PPh}_2)_2]$  (0.12 g, 0.20 mmol) in toluene (10 ml) was stirred under 1 atm. carbon monoxide at room temperature. Within 5 minutes, the original gold-orange colour faded to a clear, colourless solution. The solvent was removed in vacuo and the resultant oil taken up in minimum hexanes. Colorless crystalline clusters were filtered and washed with cold hexanes.

Yield: 0.12 g (85%). m.p. 122°C. Anal. Calcd. for  $\text{C}_{34}\text{H}_{39}\text{NNiO}_3\text{P}_2\text{Si}_2$ : C, 59.48; H, 5.68; N, 2.04. Found: C, 59.30; H, 5.73; N, 1.80. Molecular weight (Signer): theoretical, 689; found, 698. IR( $\text{CH}_2\text{Cl}_2$ ):  $\nu_{\text{CO}} = 1995$  (vs),  $\nu_{\text{COCH}_3} = 1715$  (s).  $^{31}\text{P}\{^1\text{H}\}\text{NMR}(\text{C}_6\text{D}_6)$ : 15.10 (s).  $^{13}\text{C}\{^1\text{H}\}\text{NMR}(\text{C}_6\text{D}_6)$ :  $\text{COCH}_3$ , 161.9 (s); Ni-CO, 200.2 (t,  $^2J_{31\text{P}-13\text{C}} = 2.4$ ).

$[\text{Ni}(\text{CO})_2\text{N}(\text{COC}_3\text{H}_5)(\text{SiMe}_2\text{CH}_2\text{PPh}_2)_2]$ . The synthesis of this complex was carried out in an identical manner as outlined for its acetyl analogue. Yield: 80%. m.p. 138-140°C. Anal. Calcd. for  $\text{C}_{36}\text{H}_{41}\text{NNiO}_3\text{P}_2\text{Si}_2$ : C, 60.67; H, 5.76; N, 1.97. Found: C, 60.66; H, 5.89; N, 1.80. IR( $\text{CH}_2\text{Cl}_2$ ):  $\nu_{\text{CO}} = 1995$  (vs), 1935 (vs);  $\nu_{\text{COC}_3\text{H}_5} = 1715$  (s).

$[\text{Ni}(\text{CO})_2\text{N}(\text{COC}_2\text{H}_3)(\text{SiMe}_2\text{CH}_2\text{PPh}_2)_2]$ . Upon stirring a toluene solution of  $[\text{Ni}(\text{C}_2\text{H}_3)\text{N}(\text{SiMe}_2\text{CH}_2\text{PPh}_2)_2]$  under CO for 3 h, followed by rapid removal of

solvent under reduced pressure, a mixture of two identifiable products was obtained.  $[\text{Ni}(\text{CO})_2\text{N}(\text{COC}_2\text{H}_3)(\text{SiMe}_2\text{CH}_2\text{PPh}_2)_2]$  was the major product ( $\sim 90\%$ ) but has not yet been obtained analytically pure due to contamination by  $[\text{Ni}(\text{CO})\text{N}(\text{COC}_2\text{H}_3)(\text{SiMe}_2\text{CH}_2\text{PPh}_2)_2]$  (*vide infra*). IR( $\text{CH}_2\text{Cl}_2$ ):  $\nu_{\text{CO}} = 1996$  (vs), 1935 (vs);  $\nu_{\text{COC}_2\text{H}_3} = 1700$  (s).  $^{31}\text{P}\{^1\text{H}\}\text{NMR}(\text{C}_6\text{D}_6)$ : 15.01 (s).  $^{13}\text{C}\{^1\text{H}\}\text{NMR}(\text{C}_6\text{D}_6)$ :  $\text{COC}_2\text{H}_3$ , 157.4 (s); Ni-CO, 199.9 (s).

$[\text{Ni}(\text{CO})\text{N}(\text{COC}_2\text{H}_3)(\text{SiMe}_2\text{CH}_2\text{PPh}_2)_2]$ . The yield of this derivative can be increased from  $\sim 10\%$  (*vide supra*) to greater than 90% by the following modification. After the above reaction mixture had become colorless ( $\sim 3$  h), the excess CO was removed *in vacuo* and the solution stirred under partial vacuum for an additional 24 h, gradually becoming yellow-orange in colour. The solvent was then removed and the product recrystallized from hexane. m.p. 131 - 133°C. Anal. Calcd. for  $\text{C}_{34}\text{H}_{39}\text{NNiO}_2\text{P}_2\text{Si}_2$ : C, 60.89; H, 5.82; N, 2.09. Found: C, 60.86; H, 6.00; N, 1.82. IR( $\text{CH}_2\text{Cl}_2$ ):  $\nu_{\text{CO}} = 1950$  (vs);  $\nu_{\text{COC}_2\text{H}_3} = 1625$  (s).  $^{31}\text{P}\{^1\text{H}\}\text{NMR}(\text{C}_6\text{D}_6)$ : 16.38 (d,  $J_{\text{P}_1, \text{P}_2} = 57.4$ ); -1.38 (d).  $^{13}\text{C}\{^1\text{H}\}\text{NMR}(\text{C}_6\text{D}_6)$ :  $\text{COC}_2\text{H}_3$ , 166.0 (s); Ni-CO, 205.2 (dd,  $J_{^{13}\text{C}, \text{P}_1} = 10.9$ ,  $J_{^{13}\text{C}, \text{P}_2} = 6.3$ ).

$[\text{Ni}(\text{CO})_2\text{N}(\text{COC}_6\text{H}_5)(\text{SiMe}_2\text{CH}_2\text{PPh}_2)_2]$ . Although the preparation of this derivative was as described for the acetyl analogue, it is a much slower reaction, going to completion in  $\sim 2$  days. Yield: 72%. m.p. 158°C. Anal. Calcd. for  $\text{C}_{39}\text{H}_{41}\text{NNiO}_3\text{P}_2\text{Si}_2$ : C, 62.57; H, 5.48; N, 1.87. Found: C, 63.00; H, 5.73; N, 1.65. IR(KBr):  $\nu_{\text{CO}} = 1990$  (vs), 1930 (vs);  $\nu_{\text{COPh}} = 1680$  (s).  $^{31}\text{P}\{^1\text{H}\}\text{NMR}(\text{C}_6\text{D}_6)$ : 15.09 (s).  $^{13}\text{C}\{^1\text{H}\}\text{NMR}(\text{C}_6\text{D}_6)$ :  $\text{COPh}$ , 158.1 (s); Ni-CO, 200.2 (s).

$[\text{Ni}(\text{COCH}_3)\text{N}(\text{SiMe}_2\text{CH}_2\text{PPh}_2)_2]$ . Exactly one equivalent of carbon monoxide was added to a toluene (20 ml) solution of  $[\text{Ni}(\text{CH}_3)\text{N}(\text{SiMe}_2\text{CH}_2\text{PPh}_2)_2]$  (0.12 g, 0.20 mmol) through the use of a calibrated gas bulb (25 ml, 0.18 atm). The solution was stirred under CO for ~5 h; no apparent color change took place during this time period. The solvent was removed in vacuo and the product recrystallized from toluene/hexane. Yield: 0.10 g (78%). Anal. Calcd. for  $\text{C}_{32}\text{H}_{39}\text{NNiOP}_2\text{Si}_2$ : C, 60.95; H, 6.19; N, 2.22. Found: C, 61.06; H, 6.20; N, 2.14. IR(KBr):  $\nu_{\text{COCH}_3} = 1615$  (s).  $^{31}\text{P}\{^1\text{H}\}\text{NMR}(\text{C}_7\text{D}_8)$ : 15.60 (s).

$[\text{Ni}(\text{COC}_6\text{H}_5)\text{N}(\text{SiMe}_2\text{CH}_2\text{PPh}_2)_2]$ . A solution of  $[\text{Ni}(\text{C}_6\text{H}_5)\text{N}(\text{SiMe}_2\text{CH}_2\text{PPh}_2)_2]$  (0.06 g, 0.10 mmol) in toluene (10 ml) was stirred under 1 atm. CO for 20 minutes. During this time period, the original gold-colored solution became clear deep orange. The solvent was pumped off and the product recrystallized as large orange blocks from toluene/hexane. Yield: 48 mg (70%). m.p. 163-165°C. Anal. Calcd. for  $\text{C}_{37}\text{H}_{41}\text{NNiOP}_2\text{Si}_2$ : C, 64.16; H, 5.92; N, 2.02. Found: C, 64.31; H, 5.98; N, 2.16. IR(KBr):  $\nu_{\text{COPh}} = 1602$  (m).  $^{31}\text{P}\{^1\text{H}\}\text{NMR}(\text{C}_6\text{D}_6)$ : 15.89 (s).

$[\text{Pd}(\text{COCH}_3)\text{N}(\text{SiMe}_2\text{CH}_2\text{PPh}_2)_2]$ . In a Parr Mini-Reactor (300 ml) was added a toluene (30 ml) solution of  $[\text{Pd}(\text{CH}_3)\text{N}(\text{SiMe}_2\text{CH}_2\text{PPh}_2)_2]$  (0.13 g, 0.20 mmol). The reactor was sealed under  $\text{N}_2$ , taken out to the vacuum line, evacuated and then filled with 20 atm CO. The solution was stirred magnetically for 5 h at room temperature. The excess CO was then vented and the reactor flushed with  $\text{N}_2$ . The resultant orange-red solution was pumped down and the product recrystallized from toluene/hexane. Yield: 81 mg (60%). Anal. Calcd. for  $\text{C}_{32}\text{H}_{39}\text{NOP}_2\text{PdSi}_2$ : C, 56.72; H, 5.76; N, 2.07. Found: C, 57.03; H, 5.64; N, 2.41. IR( $\text{C}_6\text{D}_6$ ):  $\nu_{\text{COCH}_3} = 1640$  (m). m.p. 153°C.

Amido Phosphine Complexes of Rhodium and Iridium

$[\text{Rh}(\text{C}_8\text{H}_{14})\text{N}(\text{SiMe}_2\text{CH}_2\text{PPh}_2)_2]$ . A solution of  $\text{LiN}(\text{SiMe}_2\text{CH}_2\text{PPh}_2)_2$  (1.07 g, 2.0 mmol) in  $\text{Et}_2\text{O}$  (10 ml) was added dropwise to a stirred, cold ( $-78^\circ\text{C}$ ) solution of  $\{\text{Rh}(\text{C}_2\text{H}_4)_2\text{Cl}\}$  (0.72 g, 1.0 mmol) in  $\text{Et}_2\text{O}$  (80 ml). The original clear orange solution darkened slightly during the addition. After 1 h at  $-78^\circ\text{C}$ , the solution was stirred at  $0^\circ\text{C}$  for an additional hour and then at room temperature for 2 h. Removal of the solvent yielded an oily residue which was extracted with hexanes, filtered through Celite, and pumped down. Recrystallization from minimum hexanes gave gold-brown crystals which were washed with ~10 ml cold ( $-30^\circ\text{C}$ ) hexanes. Yield: 0.48 g (65%). m.p.  $188-191^\circ\text{C}$ . Anal. Calcd. for  $\text{C}_{38}\text{H}_{50}\text{NP}_2\text{RhSi}_2$ : C, 61.54; H, 6.75; N, 1.89. Found: C, 61.33; H, 6.66; N, 1.87.  $^{31}\text{P}\{^1\text{H}\}\text{NMR}(\text{C}_6\text{D}_6, 50^\circ\text{C})$ : 31.93 (br d,  $J_{\text{Rh,P}} = 140.4$ ).

$[\text{Rh}(\text{CO})\text{N}(\text{SiMe}_2\text{CH}_2\text{PPh}_2)_2]$ . Method 1. To a cold ( $-78^\circ\text{C}$ ) solution of  $\{\text{Rh}(\text{CO})_2\text{Cl}\}_2$  (0.20 g, 0.50 mmol) in  $\text{Et}_2\text{O}$  (60 ml) was added, dropwise with stirring, a solution of  $\text{LiN}(\text{SiMe}_2\text{CH}_2\text{PPh}_2)_2$  (0.53 g, 1.0 mmol) in  $\text{Et}_2\text{O}$  (10 ml). The mixture was stirred at  $-78^\circ\text{C}$  for 30 minutes, warmed to  $0^\circ\text{C}$  for an hour, and finally stirred at room temperature for 2 h. The originally clear yellow solution deepened to a murky orange during the course of this reaction. The solvent was then removed in vacuo and the residue extracted with hexanes, filtered and pumped down. The product was recrystallized as yellow-orange needles from hexanes. Yield: 0.47 g (71%). m.p.  $128-130^\circ\text{C}$ . Anal. Calcd. for  $\text{C}_{31}\text{H}_{36}\text{NOP}_2\text{RhSi}_2$ : C, 56.45; H, 5.46; N, 2.12. Found: C, 56.70; H, 5.50; N, 2.01.  $\text{IR}(\text{CH}_2\text{Cl}_2)$ :  $\nu_{\text{CO}} = 1950$  (vs).  $^{31}\text{P}\{^1\text{H}\}\text{NMR}(\text{C}_6\text{D}_6)$ : 30.92 (d,  $J_{\text{Rh,P}} = 129.4$ ).

Method 2. A solution of  $[\text{Rh}(\text{C}_8\text{H}_{14})\text{N}(\text{SiMe}_2\text{CH}_2\text{PPh}_2)_2]$  (0.12 g, 0.20 mmol) in toluene (20 ml) was stirred under 1 atm. CO at room temperature for 30 minutes. During this time period, the original gold-coloured solution lightened rapidly to a clear yellow. The solvent was removed and the oily residue recrystallized from hexanes. Yield: 90%.

$[\text{Rh}(\text{C}_2\text{H}_4)\text{N}(\text{SiMe}_2\text{CH}_2\text{PPh}_2)_2]$ . This complex was prepared by either Method 1, using  $\{\text{Rh}(\text{C}_2\text{H}_4)_2\text{Cl}\}_2$  in  $\text{Et}_2\text{O}$ , or Method 2, from  $[\text{Rh}(\text{C}_8\text{H}_{14})\text{N}(\text{SiMe}_2\text{CH}_2\text{PPh}_2)_2]$  in toluene under 1 atm  $\text{C}_2\text{H}_4$ . The reaction conditions and work-up procedures for both methods were as described for the carbonyl derivative. Yield: method 1, 70%; method 2, 83%. m.p. 156-158°C. Anal. Calcd. for

$\text{C}_{32}\text{H}_{40}\text{NP}_2\text{RhSi}_2$ : C, 58.27; H, 6.07; N, 2.12. Found: C, 58.55; H, 5.95; N, 2.09.  $^{31}\text{P}\{^1\text{H}\}\text{NMR}(\text{C}_6\text{D}_6)$ : 32.48 (d,  $J_{\text{Rh,P}} = 131.8$ ).

$[\text{Rh}(\text{PMe}_3)\text{N}(\text{SiMe}_2\text{CH}_2\text{PPh}_2)_2]$ . Synthesis of this derivative was carried out using  $\text{Rh}(\text{PMe}_3)_4^+\text{Cl}^-$  in  $\text{Et}_2\text{O}$  (Method 1); alternatively, this complex was more easily prepared via Method 2, using a slight excess of  $\text{PMe}_3$ , added to a toluene solution of  $[\text{Rh}(\text{C}_8\text{H}_{14})\text{N}(\text{SiMe}_2\text{CH}_2\text{PPh}_2)_2]$ . Yield: method 1, 68%; method 2, 92%. m.p. 225-227°C. Anal. Calcd. for  $\text{C}_{33}\text{H}_{45}\text{NP}_3\text{RhSi}_2$ : C, 56.01; H, 6.36; N, 1.98. Found: C, 56.35; H, 6.40; N, 1.91.  $^{31}\text{P}\{^1\text{H}\}\text{NMR}(\text{C}_6\text{D}_6)$ :  $\text{PPh}_2$ , 33.42 (dd,  $J_{\text{Rh,PPh}_2} = 144.3$ ,  $J_{\text{PPh}_2, \text{PMe}_3} = 44.4$ );  $\text{PMe}_3$ , -10.26 (dt,  $J_{\text{Rh, PMe}_3} = 148.0$ ).

$[\text{Rh}(\text{PPh}_3)\text{N}(\text{SiMe}_2\text{CH}_2\text{PPh}_2)_2]$ . This complex was prepared via Method 1, from Wilkinson's catalyst,  $[\text{Rh}(\text{PPh}_3)_3\text{Cl}]$ , in THF, or by means of Method 2, from  $[\text{Rh}(\text{C}_8\text{H}_{14})\text{N}(\text{SiMe}_2\text{CH}_2\text{PPh}_2)_2]$  and one equivalent recrystallized  $\text{PPh}_3$  in toluene. Yield: method 1, 63%; method 2, 86%. m.p. 172-174°C. Anal. Calcd. for  $\text{C}_{48}\text{H}_{51}\text{NP}_3\text{RhSi}_2$ : C, 64.50; H, 5.71; N, 1.57. Found: C, 64.83;

H, 5.60; N, 1.49.  $^{31}\text{P}\{^1\text{H}\}\text{NMR}(\text{C}_6\text{D}_6)$ :  $\text{PPh}_3$ , 50.00 (dt,  $J_{\text{Rh},\text{PPh}_3} = 163.6$ ,  $J_{\text{PPh}_2,\text{PPh}_3} = 40.3$ );  $\text{PPh}_2$ , 31.94 (dd,  $J_{\text{Rh},\text{PPh}_2} = 142.8$ ).

$[\text{Rh}(\text{C}_8\text{H}_{12})\text{N}(\text{C}_6\text{H}_5\text{CH}_2)(\text{SiMe}_2\text{CH}_2\text{PPh}_2)_2]$ . To a solution of  $\{\text{Rh}(\text{C}_8\text{H}_{12})\text{Cl}\}_2$  (0.10 g, 0.2 mmol) in toluene (40 ml) was added a solution  $\text{LiN}(\text{C}_6\text{H}_5\text{CH}_2)(\text{SiMe}_2\text{CH}_2\text{PPh}_2)$  (0.15 g, 0.4 mmol) in toluene (20 ml) at room temperature. The mixture was stirred at R.T. for 1 h; the solvent was then removed in vacuo, the product extracted with hexanes, filtered and pumped down.

Recrystallization gave large gold blocks. Yield: 0.20 g (88%). Molecular weight (Signer): theoretical, 573; found, 522. Anal. Calcd. for  $\text{C}_{30}\text{H}_{37}\text{NPRhSi}$ : C, 62.83; H, 6.46; N, 2.44. Found: C, 62.99; H, 6.40; N, 2.54.  $^{31}\text{P}\{^1\text{H}\}\text{NMR}(\text{C}_6\text{D}_6)$ : 32.36 (d,  $J_{\text{Rh},\text{P}} = 166.2$ ).

$[\text{Ir}(\text{C}_8\text{H}_{14})\text{N}(\text{SiMe}_2\text{CH}_2\text{PPh}_2)_2]$ . A solution of  $\{\text{Ir}(\text{C}_8\text{H}_{14})_2\text{Cl}\}_2$  (0.45 g, 1.0 mmol) in toluene (100 ml) was cooled to  $0^\circ\text{C}$ . Addition of  $\text{LiN}(\text{SiMe}_2\text{CH}_2\text{PPh}_2)_2$  (1.07 g, 2.0 mmol) in toluene (30 ml) was carried out in a drop-wise manner, via syringe. The solution was stirred at  $0^\circ\text{C}$  for 3 h and then gradually warmed to room temperature. The solvent was then removed and the resultant deep orange oily residue extracted with hexanes, filtered through Celite, and pumped down. Recrystallization from minimum hexanes gave large orange blocks. Yield: 0.50 g (60%). m.p.  $204\text{--}205^\circ\text{C}$ . Anal. Calcd. for  $\text{C}_{38}\text{H}_{50}\text{IrNP}_2\text{Si}_2$ : C, 54.94; H, 6.02; N, 1.69. Found: C, 54.78; H, 6.13; N, 1.59.  $^{31}\text{P}\{^1\text{H}\}\text{NMR}(\text{C}_6\text{D}_6)$ : 18.95 (s, br).

$[\text{Ir}(\text{CO})\text{N}(\text{SiMe}_2\text{CH}_2\text{PPh}_2)_2]$ . This complex was prepared in an identical fashion to that described for its rhodium analogue (Method 2 only) from  $[\text{Ir}(\text{C}_8\text{H}_4)\text{N}(\text{SiMe}_2\text{CH}_2\text{PPh}_2)_2]$  in toluene under 1 atm CO. Yield: 95%. m.p.  $138\text{--}139^\circ\text{C}$ . Anal. Calcd. for  $\text{C}_{31}\text{H}_{36}\text{IrNOP}_2\text{Si}_2$ : C, 49.73; H, 4.81; N, 1.87.

Found: C, 49.96; H, 5.00; N, 1.76. IR(CH<sub>2</sub>Cl<sub>2</sub>):  $\nu_{\text{CO}}$  = 1930 (vs).

<sup>31</sup>P{<sup>1</sup>H}NMR(C<sub>6</sub>D<sub>6</sub>): 23.94 (s).

[Ir(C<sub>2</sub>H<sub>4</sub>)N(SiMe<sub>2</sub>CH<sub>2</sub>PPh<sub>2</sub>)<sub>2</sub>]. Preparation of this derivative was as outlined for its rhodium analogue (Method 2 only). Yield: 74%. Anal. Calcd. for C<sub>32</sub>H<sub>40</sub>IrNP<sub>2</sub>Si<sub>2</sub>: C, 51.34; H, 5.35; N, 1.87. Found: C, 51.43; H, 5.45; N, 1.93. <sup>31</sup>P{<sup>1</sup>H}NMR(C<sub>6</sub>D<sub>6</sub>): 21.95 (s).

[Ir(PMe<sub>3</sub>)N(SiMe<sub>2</sub>CH<sub>2</sub>PPh<sub>2</sub>)<sub>2</sub>]. The synthesis of this complex was carried out as described for its rhodium analogue (Method 2). Yield: 82%. Anal. Calcd. for C<sub>33</sub>H<sub>45</sub>IrNP<sub>3</sub>Si<sub>2</sub>: C, 49.75; H, 5.65; N, 1.76. Found: C, 49.77; H, 5.78; N, 1.68. <sup>31</sup>P{<sup>1</sup>H}NMR(C<sub>6</sub>D<sub>6</sub>): PPh<sub>2</sub>, 24.10 (d, J<sub>PPh<sub>2</sub>,PMe<sub>3</sub></sub> = 28.4); PMe<sub>3</sub>, -51.17 (t).

[Ir(PPh<sub>3</sub>)N(SiMe<sub>2</sub>CH<sub>2</sub>PPh<sub>2</sub>)<sub>2</sub>]. A solution of [Ir(C<sub>8</sub>H<sub>14</sub>)N(SiMe<sub>2</sub>CH<sub>2</sub>PPh<sub>2</sub>)<sub>2</sub>] (0.17 g, 0.2 mmole) and freshly recrystallized triphenylphosphine (52 mg, 0.2 mmole) in toluene (30 ml) was refluxed for 24 h under nitrogen. The deep orange solution was then allowed to cool to room temperature and the solvent removed in vacuo. Recrystallization from neat hexane yielded analytically pure orange needles. Yield: 0.15 g (78%). Anal. Calcd. for C<sub>48</sub>H<sub>51</sub>IrNP<sub>3</sub>Si<sub>2</sub>: C, 58.66; H, 5.19; N, 1.42. Found: C, 58.74; H, 5.20; N, 1.34.

[Ir(C<sub>8</sub>H<sub>12</sub>)N(C<sub>6</sub>H<sub>5</sub>CH<sub>2</sub>)(SiMe<sub>2</sub>CH<sub>2</sub>PPh<sub>2</sub>)]. Preparation of the complex was carried out in an identical manner to that outlined for its rhodium analogue. Yield: 91%. Anal. Calcd. for C<sub>30</sub>H<sub>37</sub>IrNPSi: C, 54.38; H, 5.59; N, 2.11. Found: C, 54.10; H, 5.36; N, 1.91. <sup>31</sup>P{<sup>1</sup>H}NMR(C<sub>6</sub>D<sub>6</sub>): 21.28 (s).

$[\text{Ir}(\text{PMe}_3)\text{N}(\text{SiMe}_2\text{CH}_2\text{PPh}_2)_2]$ . The synthesis of this complex was carried out as described for its rhodium analogue (Method 2). Yield: 82%. Anal. Calcd. for  $\text{C}_{33}\text{H}_{45}\text{IrNP}_3\text{Si}_2$ : C, 49.75; H, 5.65; N, 1.76. Found: C, 49.77, H, 5.78; N, 1.68.  $^{31}\text{P}\{^1\text{H}\}\text{NMR}(\text{C}_6\text{D}_6)$ :  $\text{PPh}_2$ , 24.10 (d,  $J_{\text{PPh}_2, \text{PMe}_3} = 28.4$ );  $\text{PMe}_3$ , -51.17(t).

### Hydrogenation Procedure

A typical run was carried out in a 250 ml heavy-walled flask fitted with a Kontes 9 mm needle-valve inlet, attached directly to a vacuum line which had access to vacuum and purified hydrogen (passed through MnO on vermiculite and activated molecular sieves<sup>172</sup>). Reaction temperature was maintained at 22°C through the use of a glass water-jacket attached to a Haake temperature controlling unit. Samples were withdrawn via syringe and separated from the catalyst (via vacuum transfer) prior to GLC analysis.

### Iridium(III) Amido Phosphine Dihydrides and Amine Trihydrides

$[\text{Ir}(\text{H})_2\text{N}(\text{SiMe}_2\text{CH}_2\text{PPh}_2)_2]$ . A solution of  $[\text{Ir}(\text{C}_8\text{H}_{14})\text{N}(\text{SiMe}_2\text{CH}_2\text{PPh}_2)_2]$  (0.17 g, 0.20 mmol) in toluene (20 ml) was stirred under 1 atm. dihydrogen for 1 h. During this time period, the solution's original deep orange color faded to a clear yellow. Upon removal of excess  $\text{H}_2$  in vacuo, the solution immediately deepened to a clear orange color. The solvent was pumped off and the oily residue recrystallized from toluene/hexane. Yield: 0.12 g (87%). Anal. Calcd. for  $\text{C}_{30}\text{H}_{38}\text{IrNP}_2\text{Si}_2$ : C, 49.86; H, 5.26; N, 1.94. Found: C, 50.20; H, 5.56; N, 2.00. IR(KBr):  $\nu_{\text{Ir-H}} = 2200$  (m).  $^{31}\text{P}\{^1\text{H}\}\text{NMR}(\text{C}_6\text{D}_6)$ : 23.9 (s).

mer- $[\text{Ir}(\text{H})_3\text{NH}(\text{SiMe}_2\text{CH}_2\text{PPh}_2)_2]$ . Since this trihydride derivative is stable only under dihydrogen,  $^1\text{H}$  and  $^{31}\text{P}$  NMR measurements were made by sealing  $\text{C}_6\text{D}_6$  solutions of  $[\text{Ir}(\text{C}_8\text{H}_{14})\text{N}(\text{SiMe}_2\text{CH}_2\text{PPh}_2)_2]$  or  $[\text{Ir}(\text{H})_2\text{N}(\text{SiMe}_2\text{CH}_2\text{PPh}_2)_2]$  (~10 mg) under 1 atm  $\text{H}_2$  in NMR tubes. Infra-red spectra were recorded by transferring, under  $\text{H}_2$ , a sample (formed after stirring

$[\text{Ir}(\text{C}_8\text{H}_{14})\text{N}(\text{SiMe}_2\text{CH}_2\text{PPh}_2)_2]$  in  $\text{C}_6\text{D}_6$  under 1 atm  $\text{H}_2$  for 1 h) to a solution IR cell (NaCl, 0.1 mm). IR( $\text{C}_6\text{D}_6$ ):  $\nu_{\text{N-H}} = 3210$  (w);  $\nu_{\text{Ir-H}} = 2175$  (m), 1705 (s).  $^{31}\text{P}$   $^1\text{H}$  NMR( $\text{C}_6\text{D}_6$ ): 11.44 (s).

fac- $[\text{Ir}(\text{H})_3\text{NH}(\text{SiMe}_2\text{CH}_2\text{PPh}_2)_2]$ . The apparatus for this reaction consisted of a Schlenck-type frit assembly to which was attached two 100 ml round bottomed flasks. All manipulations were carried out on a high vacuum line. A clear orange solution of  $[\text{Ir}(\text{C}_8\text{H}_{14})\text{N}(\text{SiMe}_2\text{CH}_2\text{PPh}_2)_2]$  (0.17 g, 0.20 mmol) in pentane (60 ml) (vacuum-transferred from sodium benzophenone ketyl directly into the reaction flask) was vigorously stirred for 3 h under 1 atm.  $\text{H}_2$ . After ~1 h, the solution lightened in color to a pale yellow and, after 2 h, a fine yellow precipitate formed. The precipitate was filtered and washed several times with pentane. Yield: 0.10 g (70%). Anal. Calcd. for  $\text{C}_{30}\text{H}_{40}\text{IrNO}_2\text{Si}_2$ : C, 49.72; H, 5.52; N, 1.93. Found: C, 49.86; H, 5.66; N, 1.97. IR(KBr):  $\nu_{\text{N-H}} = 3200$  (w);  $\nu_{\text{Ir-H}} = 2115$  (m), 2180 (w).

mer-cis- $[\text{Ir}(\text{H})_2(\text{CO})\text{N}(\text{SiMe}_2\text{CH}_2\text{PPh}_2)_2]$ . A solution of  $[\text{Ir}(\text{H})_2\text{N}(\text{SiMe}_2\text{CH}_2\text{PPh}_2)_2]$  (0.07 g, 0.1 mmol) in toluene (10 ml) was stirred under 1 atm. CO for 15 minutes. The solution became almost colorless within seconds of exposure to CO. The solvent was removed in vacuo and the product recrystallized from hexanes. Yield: 64 mg (86%). Anal. Calcd. for  $\text{C}_{31}\text{H}_{38}\text{IrNOP}_2\text{Si}_2$ : C, 49.60; H, 5.07; N, 1.87. Found: C, 49.90; H, 5.13; N, 1.90. IR(KBr):  $\nu_{\text{Ir-H}} = 2075$  (s), 1925 (s);  $\nu_{\text{CO}} = 1965$  (s).  $^{31}\text{P}\{^1\text{H}\}$  NMR( $\text{C}_6\text{D}_6$ ): 24.29 (s).

mer-trans- $[\text{Ir}(\text{H})_2(\text{CO})\text{N}(\text{SiMe}_2\text{CH}_2\text{PPh}_2)_2]$ . To a solution of  $[\text{Ir}(\text{C}_8\text{H}_{14})\text{N}(\text{SiMe}_2\text{CH}_2\text{PPh}_2)_2]$  (0.08 g, 0.1 mmol) in toluene (25 ml) was added solid  $(\text{HCHO})_n$  (10 mg, 0.3 mmol). The suspension was stirred at room temperature

for 24 h, during which time the original orange color faded to a pale yellow. The solvent was removed in vacuo. The product was extracted with hexanes, filtered through Celite, and pumped down. Recrystallization from hexanes produced small yellow crystalline clusters. Yield: 53 mg (71%). Anal. Calcd. for  $C_{31}H_{38}IrNOP_2Si_2$ : C, 49.60; H, 5.07; N, 1.87. Found: C, 50.00; H, 5.15; N, 1.88. IR(KBr):  $\nu_{CO} = 1990$  (vs),  $\nu_{Ir-H} = 1725$  (s).  $^{31}P\{^1H\}NMR(C_6D_6)$ : 9.68 (s).

mer-[Ir(H)<sub>2</sub>(PMe<sub>3</sub>)N(SiMe<sub>2</sub>CH<sub>2</sub>PPh<sub>2</sub>)<sub>2</sub>]. To a solution of [Ir(H)<sub>2</sub>N(SiMe<sub>2</sub>CH<sub>2</sub>-PPh<sub>2</sub>)<sub>2</sub>] (0.07 g, 0.1 mmol) in toluene (10 ml) was added an excess of PMe<sub>3</sub> (10  $\mu$ l, 0.15 mmol) via syringe. The initial orange color faded slightly upon addition of the phosphine. After standing at room temperature for 15 minutes, the solvent was removed in vacuo and the product recrystallized from hexanes. Yield: 0.07 g (88%). Anal. Calcd. for  $C_{33}H_{47}IrNP_3Si_2$ : C, 49.62; H, 5.89; N, 1.75. Found: C, 50.00; H, 6.00; N, 1.74. IR(KBr):  $\nu_{Ir-H} = 2110$  (s, br).  $^{31}P\{^1H\}NMR(C_6D_6)$ :  $\underline{PPh_2}$ , 11.00 (d,  $^2J_{PMe_3, PPh_2} = 19.0$ );  $\underline{PMe_3}$ , -56.83 (t, br).

fac-[Ir(H)<sub>2</sub>(PMe<sub>3</sub>)N(SiMe<sub>2</sub>CH<sub>2</sub>PPh<sub>2</sub>)<sub>2</sub>]. A solution of [Ir(PMe<sub>3</sub>)N(SiMe<sub>2</sub>CH<sub>2</sub>-PPh<sub>2</sub>)<sub>2</sub>] (0.08 g, 0.1 mmol) in toluene (10 ml) was stirred under 1 atm. H<sub>2</sub> for 0.5 h at room temperature. Within minutes, the solution had become virtually colorless. The solvent was pumped off, yielding a beige solid. Recrystallization from hexane resulted in off-white blocks. Yield: 64 mg (90%). Anal. Calcd. for  $C_{33}H_{47}IrNP_3Si_2$ : C, 49.62; H, 5.89; N, 1.75. Found: C, 49.91; H, 5.87; N, 1.84. IR(KBr):  $\nu_{Ir-H} = 2065$  (s), 2020 (s).  $^{31}P\{^1H\}NMR(C_6D_6)$ :  $\underline{PPh_2}$ , -1.67 (br d,  $^2J_{PMe_3, PPh_2} = 9.0$ );  $\underline{PMe_3}$ , -51.62 (t).

fac-[Ir(H)<sub>2</sub>(PPh<sub>3</sub>)N(SiMe<sub>2</sub>CH<sub>2</sub>PPh<sub>2</sub>)<sub>2</sub>]. This complex was prepared as outlined (vide supra) for its PPh<sub>3</sub> analogue. Recrystallization from hexane produced colorless needles; the recrystallized yield was rather low (65%) owing to loss of H<sub>2</sub> in solution with re-formation of the starting material. Anal. Calcd. for C<sub>48</sub>H<sub>53</sub>IrNP<sub>3</sub>Si<sub>2</sub>: C, 58.54; H, 5.39; N, 1.42. Found: C, 58.20; H, 5.39; N, 1.22. <sup>31</sup>P{<sup>1</sup>H}NMR(C<sub>6</sub>D<sub>6</sub>): PPh<sub>3</sub>, 10.50 (m); PPh<sub>2</sub>, -8.19 (m).

Table II. <sup>1</sup>H NMR Data

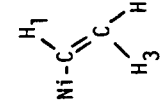
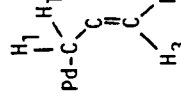
	Si-CH <sub>3</sub>	P-CH <sub>2</sub>	-P(C <sub>6</sub> H <sub>5</sub> ) <sub>2</sub>	Other
(Ph <sub>2</sub> PCH <sub>2</sub> SiMe <sub>2</sub> ) <sub>2</sub> NH	0.1 (d, <sup>4</sup> J <sub>P,H</sub> =1.0)	1.36 (d, <sup>2</sup> J <sub>P,H</sub> <1.0)	7.18(m,para/meta), 7.58(m,ortho)	Ni-CH <sub>3</sub> : -0.55 (t, <sup>3</sup> J <sub>H,P</sub> =10.0)
LiN(SiMe <sub>2</sub> CH <sub>2</sub> PPh <sub>2</sub> ) <sub>2</sub>	-0.05 (br s)	1.58 (br s)	7.08(m,para/meta), 7.75(m,ortho)	 H <sub>1</sub> : 6.32 (m, <sup>3</sup> J <sub>1,2</sub> =10.8) H <sub>2</sub> : 5.18 (m, <sup>2</sup> J <sub>2,3</sub> =1.5, <sup>4</sup> J <sub>P,2</sub> =3.5) H <sub>3</sub> : 4.60 (m, <sup>4</sup> J <sub>P,3</sub> =2.1)
[NiClN(SiMe <sub>2</sub> CH <sub>2</sub> PPh <sub>2</sub> ) <sub>2</sub> ]	0.25 (s)	1.42 (t, <sup>3</sup> J <sub>app</sub> =5.4)	7.08(m,para/meta), 8.05(m,ortho)	
[Ni(CH <sub>3</sub> )N(SiMe <sub>2</sub> CH <sub>2</sub> PPh <sub>2</sub> ) <sub>2</sub> ]	0.25 (s)	1.65 (t, <sup>3</sup> J <sub>app</sub> =6.0)	7.05(m,para/meta), 7.78(m,ortho)	
[Ni(CH=CH <sub>2</sub> )N(SiMe <sub>2</sub> CH <sub>2</sub> PPh <sub>2</sub> ) <sub>2</sub> ]	0.25 (s)	1.62 (t, <sup>3</sup> J <sub>app</sub> =6.0)	7.10(m,para/meta), 7.80(m,ortho)	
[Ni( <sup>3</sup> -C <sub>3</sub> H <sub>5</sub> )N(SiMe <sub>2</sub> CH <sub>2</sub> PPh <sub>2</sub> ) <sub>2</sub> ]	0.25 (br s)	1.65 (br t)	7.00(m,para/meta), 7.55(m,ortho)	CH(CH <sub>2</sub> ) <sub>2</sub> : 5.32 (quint, J=10.0) CH(CH <sub>2</sub> ) <sub>2</sub> : 2.32 (br d)
[Ni(C <sub>6</sub> H <sub>5</sub> )N(SiMe <sub>2</sub> CH <sub>2</sub> PPh <sub>2</sub> ) <sub>2</sub> ]	0.25 (s)	1.62 (t, <sup>3</sup> J <sub>app</sub> =6.0)	7.00(m,para/meta), 7.50(m,ortho)	Ni-C <sub>6</sub> H <sub>5</sub> : 7.07 (m,2,ortho) 6.40 (m,3,para/meta)
[Ni(CN)N(SiMe <sub>2</sub> CH <sub>2</sub> PPh <sub>2</sub> ) <sub>2</sub> ]	0.18 (s)	1.45 (t, <sup>3</sup> J <sub>app</sub> =6.0)	7.08(m,para/meta), 7.98(m,ortho)	
[PdClN(SiMe <sub>2</sub> CH <sub>2</sub> PPh <sub>2</sub> ) <sub>2</sub> ]	0.25 (s)	1.52 (t, <sup>3</sup> J <sub>app</sub> =5.0)	7.02(m,para/meta), 7.96(m,ortho)	
[Pd(CH <sub>3</sub> )N(SiMe <sub>2</sub> CH <sub>2</sub> PPh <sub>2</sub> ) <sub>2</sub> ]	0.23 (s)	1.78 (t, <sup>3</sup> J <sub>app</sub> =5.4)	7.02(m,para/meta), 7.61(m,ortho)	Pd-CH <sub>3</sub> : 0.38 (t, <sup>3</sup> J <sub>H,P</sub> =6.0)
[Pd( <sup>1</sup> -C <sub>3</sub> H <sub>5</sub> )N(SiMe <sub>2</sub> CH <sub>2</sub> PPh <sub>2</sub> ) <sub>2</sub> ]	0.15 (s)	1.78 (t, <sup>3</sup> J <sub>app</sub> =6.0)	7.05(m,para/meta), 7.69(m,ortho)	 H <sub>1</sub> : 2.24 (m, <sup>3</sup> J <sub>1,2</sub> =7.7) H <sub>2</sub> : 5.59 (m, <sup>3</sup> J <sub>2,3</sub> =18.0, <sup>3</sup> J <sub>2,4</sub> =9.5) H <sub>3</sub> : 3.96 (br d) H <sub>4</sub> : 4.31 (br d)
[PtClN(SiMe <sub>2</sub> CH <sub>2</sub> PPh <sub>2</sub> ) <sub>2</sub> ]	0.22 (s)	1.52 (tt, <sup>3</sup> J <sub>app</sub> =6.0, <sup>3</sup> J <sub>H,Pt</sub> =31.0)	7.05(m,para/meta), 7.95(m,ortho)	

Table III. <sup>1</sup>H NMR Data

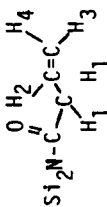
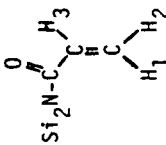
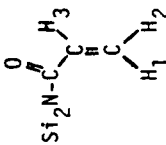
	Si-CH <sub>3</sub>	CH <sub>2</sub> -P	(C <sub>6</sub> H <sub>5</sub> ) <sub>2</sub> P	Other
Ni(CO) <sub>2</sub> N(COCH <sub>3</sub> )(SiMe <sub>2</sub> CH <sub>2</sub> PPh <sub>2</sub> ) <sub>2</sub>	-0.11(s)	1.89(br d)	6.95 (m,para/meta) 7.53 (m,ortho)	COCH <sub>3</sub> , 1.91(s)
Ni(CO) <sub>2</sub> N(COC <sub>3</sub> H <sub>5</sub> )(SiMe <sub>2</sub> CH <sub>2</sub> PPh <sub>2</sub> ) <sub>2</sub>	-0.10(s)	1.89(br d)	6.95 (m,para/meta) 7.52 (m,ortho)	 H <sub>1</sub> , 3.08(dt, 2, J <sub>1,2</sub> =6.59; J <sub>1,3</sub> =J <sub>1,4</sub> =1.46) H <sub>2</sub> , 5.85(m, 1, J <sub>2,4</sub> =10.01; J <sub>2,3</sub> =17.09) H <sub>3</sub> , 5.02(m, 1, J <sub>3,4</sub> =1.71) H <sub>4</sub> , 4.85(m, 1)
Ni(CO) <sub>2</sub> N(COC <sub>2</sub> H <sub>3</sub> )(SiMe <sub>2</sub> CH <sub>2</sub> PPh <sub>2</sub> ) <sub>2</sub>	-0.08(s)	1.85(br m)	6.95 (m,para/meta) 7.15 (m,ortho)	 H <sub>1</sub> , 6.17(dd, J <sub>1,3</sub> =17.0; J <sub>1,2</sub> =2.0) H <sub>2</sub> , 5.38(dd, J <sub>2,3</sub> =10.2) H <sub>3</sub> , 5.99(dd)
Ni(CO)N(COC <sub>2</sub> H <sub>3</sub> )(SiMe <sub>2</sub> CH <sub>2</sub> PPh <sub>2</sub> ) <sub>2</sub>	-0.65(s) -0.35(s) 0.35(d, 4J <sub>H,P</sub> =0.98) 0.65(d, 4J <sub>H,P</sub> =0.98)	0.82(dd, J <sub>H,P</sub> =7.0; J <sub>gem</sub> =10.5) 1.08(dd, J <sub>H,P</sub> =13.0; J <sub>gem</sub> =12.0) 1.46(dd, J <sub>H,P</sub> =15.0; J <sub>gem</sub> =12.0) 1.69(dd, J <sub>H,P</sub> =6.0; J <sub>gem</sub> =10.5)	6.70, 6.98 (m,para/meta) 7.48, 7.92 (m,ortho)	 H <sub>1</sub> , 4.34(m, J <sub>1,3</sub> =11.72; J <sub>1,P</sub> =6.59; J <sub>1,P2</sub> =1.46) H <sub>2</sub> , 3.89(m, J <sub>2,3</sub> =7.57; J <sub>2,P</sub> =5.62; J <sub>2,P2</sub> =4.15) H <sub>3</sub> , 4.14(m, J <sub>3,P</sub> =13.92; J <sub>3,P2</sub> =3.17)
Ni(CO) <sub>2</sub> N(COPh)(SiMe <sub>2</sub> CH <sub>2</sub> PPh <sub>2</sub> ) <sub>2</sub>	-0.03	1.93(br m)	6.92 (m,para/meta) 7.52 (m,ortho)	COCH <sub>3</sub> , 6.92(m)
Ni(COCH <sub>3</sub> )N(SiMe <sub>2</sub> CH <sub>2</sub> PPh <sub>2</sub> ) <sub>2</sub>	0.30 (s, br)	1.82(br t)	7.25 (m,para/meta) 8.00 (m,ortho)	COCH <sub>3</sub> , 1.71(t, J <sub>H,P</sub> =1.2)
Ni(COPh)N(SiMe <sub>2</sub> CH <sub>2</sub> PPh <sub>2</sub> ) <sub>2</sub>	-0.01(s) 0.45(s)	1.54(dt, J <sub>gem</sub> =13.7; J <sub>app</sub> =6.5) 1.80(dt, J <sub>app</sub> =5.0)	6.75, 7.12 (m,para/meta) 7.90, 8.21 (m,ortho)	COCH <sub>3</sub> , 7.28(m)
Pd(COCH <sub>3</sub> )N(SiMe <sub>2</sub> CH <sub>2</sub> PPh <sub>2</sub> ) <sub>2</sub>	0.24(s)	1.75(t, J <sub>app</sub> =6.2)	7.02 (m,para/meta) 7.74 (m,ortho)	COCH <sub>3</sub> , 1.64(t, J <sub>H,P</sub> =2.2)

Table IV. <sup>1</sup>H NMR Data ((a) recorded at 45°C)

	Si-CH <sub>3</sub>	CH <sub>2</sub> P	P(C <sub>6</sub> H <sub>5</sub> ) <sub>2</sub>	Other
[Ir(C <sub>8</sub> H <sub>14</sub> )N(SiMe <sub>2</sub> CH <sub>2</sub> PPh <sub>2</sub> ) <sub>2</sub> ] <sup>(a)</sup>	0.10 (s)	1.80 (t, J <sub>app</sub> = 4.2)	7.08 (m, para/meta) 7.82 (m, ortho)	C <sub>6</sub> H <sub>14</sub> : 1.25 (br m) 2.15 (br m)
[Ir(CO)N(SiMe <sub>2</sub> CH <sub>2</sub> PPh <sub>2</sub> ) <sub>2</sub> ]	0.20 (s)	1.78 (t, J <sub>app</sub> = 5.9)	7.00 (m, para/meta) 7.95 (m, ortho)	
[Ir(PMe <sub>3</sub> )N(SiMe <sub>2</sub> CH <sub>2</sub> PPh <sub>2</sub> ) <sub>2</sub> ]	0.15 (s)	1.82 (t, J <sub>app</sub> = 5.0)	7.07 (m, para/meta) 8.07 (m, ortho)	P(CH <sub>3</sub> ) <sub>3</sub> : 0.80 (d, J <sub>P,CH<sub>3</sub></sub> = 8.6)
[Ir(PPh <sub>3</sub> )N(SiMe <sub>2</sub> CH <sub>2</sub> PPh <sub>2</sub> ) <sub>2</sub> ]	0.20 (s)	1.82 (t, J <sub>app</sub> = 4.5)	6.93 (m, para/meta) 7.65 (m, ortho)	P(C <sub>6</sub> H <sub>5</sub> ) <sub>3</sub> : 6.76 (m)
[Rh(C <sub>8</sub> H <sub>12</sub> )N(C <sub>6</sub> H <sub>5</sub> CH <sub>2</sub> )(SiMe <sub>2</sub> CH <sub>2</sub> PPh <sub>2</sub> )]	0.04 (s)	1.57 (dd, J <sub>Rh,CH<sub>2</sub></sub> = 0.98, J <sub>P,CH<sub>2</sub></sub> = 12.7)	7.05 (m, para/meta) 7.60 (m, ortho)	C <sub>8</sub> H <sub>12</sub> (endo/exo CH <sub>2</sub> ): 2.02 (br m), 2.17 (m), 2.28 (m). C <sub>8</sub> H <sub>12</sub> (=CH): 2.97 (br s), 5.19 (br s). CH <sub>2</sub> C <sub>6</sub> H <sub>5</sub> : 4.60 (s) CH <sub>2</sub> C <sub>6</sub> H <sub>5</sub> : 7.09 (m), 7.25 (m).
[Ir(C <sub>8</sub> H <sub>12</sub> )N(C <sub>6</sub> H <sub>5</sub> CH <sub>2</sub> )(SiMe <sub>2</sub> CH <sub>2</sub> PPh <sub>2</sub> )]	-0.04 (s)	1.55 (d, J <sub>P,CH<sub>2</sub></sub> = 12.7)	7.20 (m, para/meta)	C <sub>8</sub> H <sub>12</sub> (endo/exo CH <sub>2</sub> ): 1.74 (br m), 2.15 (m), 1.16 (m). C <sub>8</sub> H <sub>12</sub> (=CH): 2.55 (m), 4.83 (m). CH <sub>2</sub> C <sub>6</sub> H <sub>5</sub> : 4.95 (s). CH <sub>2</sub> C <sub>6</sub> H <sub>5</sub> : 7.37 (m).
[Rh(CO)N(SiMe <sub>2</sub> CH <sub>2</sub> PPh <sub>2</sub> ) <sub>2</sub> ]	0.22 (s)	1.73 (t, J <sub>app</sub> = 5.0)	7.02 (m, para/meta) 7.82 (m, ortho)	
[Rh(C <sub>8</sub> H <sub>14</sub> )N(SiMe <sub>2</sub> CH <sub>2</sub> PPh <sub>2</sub> ) <sub>2</sub> ]	0.10 (s)	1.77 (dt, J <sub>app</sub> = 4.2, J <sub>Rh,CH<sub>2</sub></sub> = 0.9)	7.09 (m, para/meta) 7.81 (m, ortho)	C <sub>8</sub> H <sub>14</sub> : 1.22 (br m) 2.21 (br m) 2.79 (br m)
[Rh(C <sub>2</sub> H <sub>4</sub> )N(SiMe <sub>2</sub> CH <sub>2</sub> PPh <sub>2</sub> ) <sub>2</sub> ]	0.26 (s)	1.78 (t, J <sub>app</sub> = 4.5)	7.11 (m, para/meta) 7.78 (m, ortho)	C <sub>2</sub> H <sub>4</sub> : 2.24 (dt, J <sub>Rh,C<sub>2</sub>H<sub>4</sub></sub> = 1.75, J <sub>P,C<sub>2</sub>H<sub>4</sub></sub> = 4.0)
[Rh(PMe <sub>3</sub> )N(SiMe <sub>2</sub> CH <sub>2</sub> PPh <sub>2</sub> ) <sub>2</sub> ]	0.11 (s)	1.82 (t, J <sub>app</sub> = 4.8)	7.10 (m, para/meta) 7.99 (m, ortho)	P(CH <sub>3</sub> ) <sub>3</sub> : 0.62 (dd, J <sub>P,CH<sub>3</sub></sub> = 8.1, J <sub>Rh,CH<sub>3</sub></sub> = 1.0)
[Rh(PPh <sub>3</sub> )N(SiMe <sub>2</sub> CH <sub>2</sub> PPh <sub>2</sub> ) <sub>2</sub> ]	0.24 (s)	1.92 (t, J <sub>app</sub> = 4.1)	7.00 (m, para/meta) 7.66 (m, ortho)	P(C <sub>6</sub> H <sub>5</sub> ) <sub>3</sub> : 6.86 (m)

Table V.  $^1\text{H}$ NMR Data

	Si-CH <sub>3</sub>	CH <sub>2</sub> P	(C <sub>6</sub> H <sub>5</sub> ) <sub>2</sub> P	Other
Ir(H) <sub>2</sub> N(SiMe <sub>2</sub> CH <sub>2</sub> PPh <sub>2</sub> ) <sub>2</sub>	0.24 (s)	1.89 (t, J <sub>app</sub> =5.2)	7.02(m, para/meta) 7.92(m, ortho)	Ir-H, -24.86 (t, $^2J_{H,P}$ =13.2)
mer-Ir(H) <sub>3</sub> NH(SiMe <sub>2</sub> CH <sub>2</sub> PPh <sub>2</sub> ) <sub>2</sub>	-0.02 (s) 0.05 (s)	1.70 (dt, J <sub>app</sub> = 4.9, J <sub>gem</sub> =14.1) 2.36 (dt, J <sub>app</sub> = 4.1)	6.99, 7.12(m, para/meta) 8.20, 8.35(m, ortho)	Ir-H, -8.99 (td, $^2J_{P,H}$ =19.5, $^2J_{H,H}$ =5.0) -9.69 (td, $^2J_{P,H}$ =18.0) -24.6 (tt, $^2J_{P,H}$ =15.5)
fac-Ir(H) <sub>3</sub> NH(SiMe <sub>2</sub> CH <sub>2</sub> PPh <sub>2</sub> ) <sub>2</sub>	0.23 (s) 0.25 (s)	1.91 (dd, $^2J_{H,P}$ =9.0, J <sub>gem</sub> =14.1) 2.09 (dd, $^2J_{H,P}$ =11.0)	6.98(m, para/meta) 8.28(m, ortho)	Ir-H <sub>A</sub> (trans to PPh <sub>2</sub> ), -8.5 (m, from spectral simulation of AA'MXX' pattern: $^2J_{A,A'}=2.2$ ; $^2J_{A,M}=^2J_{A',M}=5.5$ ; $^2J_{A,X}=^2J_{A',X'}=-19.0$ ; $^2J_{M,X}=^2J_{M,X'}=14.0$ ; $^2J_{A,X'}=^2J_{A',X}=130.0$ ; $^2J_{X,X'}=1.0$ ) Ir-H <sub>M</sub> (trans to NH), -24.3 (tt)
mer-cis-Ir(H) <sub>2</sub> (CO)N(SiMe <sub>2</sub> CH <sub>2</sub> PPh <sub>2</sub> ) <sub>2</sub>	0.31 (s) 0.34 (s)	1.80 (dt, J <sub>app</sub> = 5.4, J <sub>gem</sub> =13.8) 2.09 (dt, J <sub>app</sub> = 6.5)	6.96, 7.04(m, para/meta) 7.70, 7.95(m, ortho)	Ir-H (trans to CO), -7.86 (dt, $^2J_{H,P}$ =17.6, $^2J_{H,H}$ =4.4) Ir-H (trans to N), -16.09 (dt, $^2J_{H,P}$ =12.5)
mer-trans-Ir(H) <sub>2</sub> (CO)N(SiMe <sub>2</sub> CH <sub>2</sub> PPh <sub>2</sub> ) <sub>2</sub>	0.18 (s)	2.04 (t, J <sub>app</sub> =5.7)	6.98(m, para/meta) 7.87(m, ortho)	Ir-H, -6.00 (t, $^2J_{H,P}$ =14.7)
fac-cis-Ir(H) <sub>2</sub> (PMe <sub>3</sub> )N(SiMe <sub>2</sub> CH <sub>2</sub> PPh <sub>2</sub> ) <sub>2</sub>	0.18 (s) 0.53 (s)	1.79 (dt, J <sub>app</sub> = 5.2, J <sub>gem</sub> =13.0) 2.22 (dt, J <sub>app</sub> = 5.2)	6.95, 7.05(m, para/meta) 7.83, 8.14(m, ortho)	P(CH <sub>3</sub> ) <sub>3</sub> , 0.76 (d, $^2J_{H,P}$ =8.0) Ir-H (trans to PPh <sub>2</sub> ), -10.21 (ddt, $^2J_{H,P}(\text{cis})$ =17.6; $^2J_{H,P}(\text{trans})$ =135.0; $^2J_{H,H}$ =5.1) Ir-H (trans to N), -19.96 (d quart, $^2J_{H,P}$ =19.5)
mer-cis-Ir(H) <sub>2</sub> (PMe <sub>3</sub> )N(SiMe <sub>2</sub> CH <sub>2</sub> PPh <sub>2</sub> ) <sub>2</sub>	0.32 (s) 0.72 (s)	1.95 (m) 2.05 (m)	6.89(m, para/meta) 7.08(m, ortho)	Ir-H, -11.01 (m; from spectral simulation of AA'XX'Y pattern: $^2J_{A,X}=^2J_{A',X'}=-21.0$ ; $^2J_{A,Y}=^2J_{A',Y}=21.0$ ; $^2J_{A,X'}=^2J_{A',X}=147.0$ ; $^2J_{A,A'}=4.0$ ; $^2J_{X,Y}=9.0$ ; $^2J_{X,X'}=4.0$ ).

## References

1. Pearson, R.G. J. Chem. Ed. 1968, 45, 581, 643.
2. Datta, S.; Wreford, S.S. Inorg. Chem. 1977, 16, 1134.
3. Datta, S.; Fischer, M.B.; Wreford, S.S. J. Organomet. Chem. 1980, 188, 353.
4. Fellman, J.D.; Rupprecht, G.A.; Schrock, R.R. J. Am. Chem. Soc. 1981, 103, 5752.
5. Parshall, G.W.; Schrock, R.R. Chem. Rev. 1976, 76, 243.
6. Tolman, C.A. Chem. Rev. 1977, 77, 313.
7. Levason, W.; MacAuliffe, C.A. Acc. Chem. Res. 1978, 11, 363.
8. Levason, W.; MacAuliffe, C.A. "Phosphine, Arsine, and Stibine Complexes of Transition Elements", Elsevier, Amsterdam, 1979.
9. Lappert, M.F.; Power, P.P.; Sanger, A.R.; Srivastava, R.C. "Metal and Metalloid Amides", Horwood-Wiley, Chichester - New York, 1980.
10. Bertini, I.; Dapporta, P.; Fallani, G.; Sacconi, L. Inorg. Chem. 1971, 10, 1703.
11. Rigo, P. Inorg. Chim. Acta. 1980, 44, L223.
12. Reference 8, p. 18.
13. Cotton, F.A.; Wilkinson, G. "Advanced Inorganic Chemistry", 4th ed., Wiley, New York, 1980, p. 71.
14. Fryzuk, M.D.; Williams, H.D. Organometallics 1983, 2, 162.
15. Fryzuk, M.D.; Williams, H.D. Inorg. Chem. 1983, in press.
16. Collman, J.P.; Hegedus, L.S. "Principles and Applications of Organotransition Metal Chemistry", University Science, Mill Valley, California, 1980, Chapter 11.
17. Dermer, D.C.; Fernelius, W.C. Z. Anorg. Chem. 1935, 221, 83.
18. Burger, H.; Wannagat, U. Monatsch. Chem. 1965, 94, 1007.
19. Bradley, D.C.; Hursthouse, M.B.; Smallwood, R.J.; Welch, A.J. J. Chem. Soc. Chem. Commun. 1972, 872.

20. Bradley, D.C.; Thomas, I.M. Can. J. Chem. 1962, 40, 1355.
21. Angelici, R.J. J. Chem. Soc. Chem. Commun. 1965, 486.
22. Bradley, D.C.; Thomas, I.M. J. Chem. Soc. 1960, 3857.
23. Aylett, B.J.; Beagley, B.; Cruikshank, D.W.J.; Ellis, I.A.; Monaghan, J.J.; Robiette, A.G.; Sheldrick, G.M.; Sheldrick, W.S. J. Chem. Soc. Chem. Commun. 1968, 909.
24. Diamond, S.E.; Mares, F. J. Organomet. Chem. 1977, 142, C55.
25. Cetinkaya, B.; Lappert, M.F.; Torroni, S. J. Chem. Soc. Chem. Commun. 1979, 843.
26. Bradley, D.C. Adv. Inorg. Chem. Radiochem. 1972, 15, 259.
27. Alyea, E.C.; Bradley, D.C.; Lappert, M.F.; Sanger, A.R. J. Chem. Soc. Chem. Commun. 1969, 1064.
28. Lappert, M.F.; Sanger, A.R. J. Chem. Soc. A. 1971, 874.
29. Basi, J.S.; Bradley, D.C. Proc. Chem. Soc., London 1963, 305.
30. Heath, C.E.; Hursthouse, M.B. J. Chem. Soc. Chem. Commun. 1971, 143.
31. Bradley, D.C.; Chisholm, M.H.; Heath, C.E.; Hursthouse, M.B. J. Chem. Soc. Chem. Commun. 1969, 1261.
32. Alyea, E.C.; Basi, J.S.; Bradley, D.C.; Chisholm, M.H. J. Chem. Soc. Chem. Commun. 1968, 495.
33. Bradley, D.C.; Ghotra, J.S.; Hart, F.A. J. Chem. Soc. Chem. Commun. 1972, 349.
34. Bradley, D.C.; Eller, P.G.; Hursthouse, M.B.; Meek, D.W. Coord. Chem. Rev. 1977, 24, 1.
35. Bradley, D.C.; Hursthouse, M.B.; Malik, K.M.A.; Mösseler, R. Transition Met. Chem. 1978, 3, 253.
36. Bradley, D.C.; Hursthouse, M.B.; Rodesiler, P.F. J. Chem. Soc. Chem. Commun. 1969, 14.
37. Bradley, D.C.; Chisholm, M.H. Acc. Chem. Res. 1976, 9, 273.
38. Bürger, H.; Smsekar, O.; Wannagat, U. Monatsh. 1964, 95, 292.
39. Bürger, H.; Smsekar, O.; Wannagat, U. Monatsh. 1964, 95, 1099.

40. Shiotani, A.; Schmidbauer, H. J. Am. Chem. Soc. 1970, 92, 7003.
41. Schore, N.E. J. Am. Chem. Soc. 1979, 101, 7410.
42. Grobe, J.; Heyer, G.J. J. Organomet. Chem. 1973, 61, 133.
43. Clark, E.P. Indust. Eng. Chem. Anal. Ed. 1941, 13, 820.
44. a) Böttcher, B.; Mootz, D.; Zinnius, A. Angew. Chem. Int. Ed. Engl. 1969, 8, 378. b) Atwood, J.L.; Grüning, R.; Rogers, R.D. J. Organomet. Chem. 1978, 157, 229.
45. Brookes, P.R.; Shaw, B.L. J. Chem. Soc. A. 1967, 1079.
46. Moore, D.S.; Robinson, S.D. Inorg. Chim. Acta. 1981, 53, L171.
47. Cotton, F.A., Wilkinson, G. "Advanced Inorganic Chemistry", 3rd. ed., Wiley, New York, 1972, p. 899.
48. Evans, D.F. J. Chem. Soc. 1959, 2003.
49. Bauder, M.; Beck, W. Chem. Ber. 1970, 103, 583.
50. Eadie, D.T.; Pidcock, A.; Stobart, S.R. Inorg. Chim. Acta. 1982, 65, L111.
51. Holm, R.H. "Dynamic Nuclear Magnetic Resonance Spectroscopy"; Jackman, L.M.; Cotton, F.A., Eds.; Academic Press, New York, 1975; chapter 9, p. 328.
52. Orioli, P.L.; Sacconi, L. J. Chem. Soc. Chem. Commun. 1968, 1310.
53. Al-Salem, N.A.; Empsall, H.D.; Markham, R.; Shaw, B.L.; Weeks, B. J. Chem. Soc., Dalton Trans. 1980, 59.
54. Bruce, M.I. Angew. Chem. Int. Ed. 1977, 16, 73.
55. Parshall, G. Acc. Chem. Res. 1975, 8, 113.
56. Dehand, J.; Pfeiffer, M. Coord. Chem. Rev. 1976, 18, 327.
57. Mazanec, T.J.; Meek, D.W. Acc. Chem. Res. 1981, 14, 266.
58. Kermode, N.J.; Lappert, M.F.; Samways, B.J., presented in part at the International Conference on the Chemistry of the Platinum Group Metals, Bristol, England, July 1981.
59. Reference 16, Chapter 8.
60. Reference 16, Chapter 9.
61. Wojcicki, A. Adv. Organomet. Chem. 1973, 11, 87.

62. Calderazzo, F. Angew. Chem. Int. Ed. Engl. 1977, 16, 299.
63. Closson, R.D.; Coffield, T.H.; Kozikowski, J. J. Org. Chem. 1957, 22, 598.
64. Calderazzo, F.; Cotton, F.A. Inorg. Chem. 1962, 1, 30.
65. Calderazzo, F.; Noack, K. Coord. Chem. Rev. 1966, 1, 118.
66. Basolo, F.; Mawby, R.; Pearson, R.G. J. Am. Chem. Soc. 1964, 86, 3994.
67. Halpern, J.; James, B.R.; Kemp, A.L.W. J. Am. Chem. Soc. 1961, 83, 4097.
68. Glyde, R.W.; Mawby, R.J. Inorg. Chem. 1971, 10, 854.
69. Basolo, F.; Butler, I.S.; Pearson, R.G. Inorg. Chem. 1967, 6, 2074.
70. Craig, P.G.; Green, M. J. Chem. Soc. A. 1968, 1978.
71. Boschetto, D.J.; Whitesides, G.M. J. Am. Chem. Soc. 1969, 91, 4313.
72. Bock, P.L.; Boschetto, D.J.; Demers, J.P.; Whitesides, G.M. J. Am. Chem. Soc. 1974, 96, 2814.
73. Calderazzo, F.; Cotton, F.A. Abstr. Int. Conf. Coord. Chem., Stockholm, 1962, paper 6H7.
74. Craig, P.J.; Green, M. J. Chem. Soc. A. 1969, 157.
75. Heck, R.F. J. Am. Chem. Soc. 1964, 86, 2796.
76. Deeming, A.J.; Shaw, B.L. J. Chem. Soc. A. 1969, 597.
77. Collman, J.P.; Sears, C.T. Inorg. Chem. 1968, 7, 27.
78. Blake, D.M.; Kubota, M. J. Am. Chem. Soc. 1971, 93, 1368.
79. Chiusoli, G.P. Acc. Chem. Res. 1973, 6, 422.
80. Jolly, P.W.; Wilke, G. "The Organic Chemistry of Nickel", Academic Press, New York. 1974, Vol. 1, p. 166.
81. Barnett, K.W. J. Organomet. Chem. 1970, 21, 477.
82. Klein, H.F. Angew. Chem. Int. Ed. Engl. 1973, 12, 402.
83. Karsch, H.H.; Klein, H.F. Chem. Ber. 1976, 109, 2524.
84. Atwood, J.L.; Carmona, E.; González, F.; Proveda, M.L.; Rogers, R.D. J. Chem. Soc. Dalton Trans. 1980, 2108.

85. Dapporto, P.; Sacconi, L.; Stopponi, P. Inorg. Chem. 1978, 17, 718.
86. Fahey, D.R.; Mahan, J.E. J. Am. Chem. Soc. 1977, 99, 2501.
87. Klein, H.F. Angew. Chem. Int. Ed. Engl. 1980, 19, 362.
88. Fahey, D.R. Organomet. Chem. Rev. A. 1972, 7, 245.
89. Reference 80, p. 169-171.
90. Reference 16, p. 539.
91. "CRC Handbook of Chemistry and Physics"; Weast, R.C., Ed.; CRC Press, Cleveland, Ohio 1976, Vol. 56, F237.
92. Jolly, P.W.; Mynott, R. Adv. Organomet. Chem. 1981, 19, 257.
93. Ford, R.A.; Gordon, A.J. "The Chemist's Companion", Wiley, New York, 1972, p. 281.
94. Garrou, P.E. Chem. Rev. 1981, 81, 229.
95. Klebe, J.F. J. Am. Chem. Soc. 1964, 86, 3399, 4400.
96. Bentz, F.; Birkofer, L.; Ritter, A. Chem. Ber. 1964, 97, 2196.
97. Birkofer, L.; Ritter, A. Angew. Chem. Int. Ed. Engl. 1965, 4, 417.
98. Kruger, C.; Rochow, E.G., Wannagat, U. Chem. Ber. 1963, 96, 2138.
99. Pump, J.; Rochow, E.G. Chem. Ber. 1964, 97, 627.
100. Bonelli, D.; Yoder, C.H. Inorg. Nucl. Chem. Lett. 1972, 8, 1027.
101. Komoriya, Y.; Yoder, C.H. J. Am. Chem. Soc. 1972, 94, 5285.
102. Drens, W.; Engelhardt, G.; Hertzog, G.; Janke, H.; Rühlmann, K.; Thieme, E.; Wagner, S. J. Organomet. Chem. 1977, 134, 21.
103. Day, C.S.; Day, V.W.; Fagan, P.J.; Manriquez, J.M.; Marks, T.J.; Vollmer, S.H. J. Am. Chem. Soc. 1981, 103, 2206.
104. Booth, G.; Chatt, J. Proc. Chem. Soc. 1961, 67.
105. Booth, G.; Chatt, J. J. Chem. Soc. A. 1966, 634.
106. Clark, H.C.; Puddephatt, R.J. Inorg. Chem. 1970, 9, 2670.
107. Appleton, T.G.; Clark, H.C.; Manzer, L.E. Coord. Chem. Rev. 1973, 10, 335.
108. Cooper, M.K.; Downes, J.M. J. Chem. Soc. Chem. Commun. 1981, 381.

109. Jardine, F.H.; Osborn, J.A.; Wilkinson, G.; Young, J.F., J. Chem. Soc. Chem. Commun. 1965, 131.
110. Coffey, R.S. Imperial Chemical Industries, Brit. Pat. 1,121,642 (1966): Chem. Abs. 1967, 66, 10556.
111. Pearson, R.G. Coll. Acc. Trans. Met. Chem. 1973, 1, 124.
112. Halpern, J. J. Organomet. Chem. 1980, 200, 133.
113. Crabtree, R.H.; Felkin, H.; Fillebeen-Khan, T.; Morris, G.E. J. Organomet. Chem. 1979, 168, 183.
114. Martin, B.; McWhinnie, W.R.; Waind, G.M. J. Inorg. Nucl. Chem. 1961, 23, 207.
115. Augustine, R.L.; Van Peppen, J. Ann. N.Y. Acad. Sci. 1969, 158, 482.
116. Bond, G.C.; Hillyard, R.A. Disc. Faraday Soc. 1968, 46, 20.
117. Abley, P.; McQuillin, F.J. Disc. Faraday Soc. 1968, 46, 31.
118. Reference 16, Chapter 6.
119. Halpern, J. Trans. Am. Crystallogr. Assoc. 1978, 14, 59.
120. Halpern, J.; Okamoto, T.; Zakhariev, A. J. Mol. Cat. 1976, 2, 65.
121. Chan, A.S.C.; Halpern, J.; Pluth, J.J.; Riley, D.P. J. Am. Chem. Soc. 1977, 99, 8055.
122. Osborn, J.A.; Schrock, R.R. J. Am. Chem. Soc. 1976, 98, 2134.
123. Brown, J.M.; Chaloner, P.A. J. Chem. Soc. Chem. Commun. 1978, 321, 646.
124. Vaska, L. Acc. Chem. Res. 1968, 1, 335.
125. Jesson, J.P. in "Transition Metal Hydrides", Muetterties, E.L., Ed.; Marcel Dekker, 1971, p. 75.
126. Jardine, F.H.; Osborn, J.A.; Wilkinson, G.; Young, J.F. J. Chem. Soc. (A) 1966, 1711.
127. Birch, A.J.; Williamson, D.H. Organic Reactions 1976, 24, 1.
128. Crabtree, R. Acc. Chem. Res. 1979, 12, 331.
129. James, B.R. in "Comprehensive Organometallic Chemistry", Wilkinson, G., Ed.; Pergamon Press: New York, 1982; Vol. 5, Chapter 51.

130. Blaser, H.U.; Byrne, J.W.; Osborn, J.A. J. Am. Chem. Soc. 1975, 97, 3871.
131. Orchin, M. Adv. Catal. 1966, 16, 1.
132. James, B.R. "Homogeneous Hydrogenation", Wiley: New York, 1974, p.250.
133. Turnover numbers given are those values averaged over a number (>5) of experimental runs and were calculated using the expression:  
Turnover number = mol substrate converted/mol catalyst/unit time.
134. Chan, A.S.C.; Halpern, J. J. Am. Chem. Soc. 1980, 102, 838.
135. Osborn, J.A.; Schrock, R.R. J. Am. Chem. Soc. 1976, 98, 2134.
136. Reference 16, Chapter 4.
137. Vaska, L. Inorg. Chim. Acta 1971, 5, 295.
138. Deeming, A.J.; Shaw, B.L. J. Chem. Soc. A 1969, 1128.
139. Hamer, G.; Harrod, J.F.; Yorke, W. J. Am. Chem. Soc. 1979, 101, 3987.
140. Halpern, J. Coll. Acc. Trans. Met. Chem. 1973, 1, 133.
141. Bresadola, S.; Longato, B.; Morandini, F. Inorg. Chem. 1976, 15, 650.
142. Pilloni, G.; Zecchin, S.; Zotti, G. J. Organomet. Chem. 1982, 235, 353.
143. Reference 9, p. 490.
144. Adams, D.M. "Metal-Ligand and Related Vibrations", Edward Arnold (Publishers) Ltd., London, 1967, p. 6.
145. Brothers, J.P. Prog. Inorg. Chem. 1981, 28, 1.
146. Chatt, J.; Coffey, R.S.; Shaw, B.L. J. Chem. Soc. 1965, 7391.
147. Mann, B.E.; Masters, C.; Shaw, B.L. J.C.S. Chem. Commun. 1970, 703.
148. Errington, R.J.; Shaw, B.L. J. Organomet. Chem. 1982, 238, 319.
149. Norton, J.R. Acc. Chem. Res. 1979, 12, 139.
150. Gladysz, J.A.; Johnson, D.L.; Tam, W.; Williams, G.M. J. Organomet. Chem. 1977, 140, C1.
151. Thorn, D.L. Organometallics 1982, 1, 927.

152. Balimann, G.; Pregosin, P.S. J. Magn. Reson. 1976, 22, 235.
153. Kharasch, M.S.; Mayo, F.R.; Seyler, R.C. J. Am. Chem. Soc. 1938, 60, 882.
154. Chock, P.B.; Halpern, J.; Paulik, F.E. Inorg. Synth. 1973, 14, 90.
155. McDermott, J.X.; White, J.F.; Whitesides, G.M. J. Am. Chem. Soc. 1976, 98, 6521.
156. Hartley, F.R. Organomet. Chem. Rev. A. 1970, 6, 119.
157. Hsu, C.Y.; Leshner, B.T.; Orchin, M. Inorg. Synth. 1979, 19, 114.
158. Parshall, G.W. Inorg. Synth. 1970, 12, 26.
159. Van der Ent, A.; Onderlinden, A.L. Inorg. Synth. 1973, 14, 93.
160. Cramer R. Inorg. Chem. 1962, 1, 722.
161. McCleverty, J.A.; Wilkinson, G. Inorg. Synth. 1966, 8, 211.
162. Wilkinson, G. J. Chem. Soc. Chem. Commun. 1979, 489.
163. Jardine, F.H.; Osborn, J.A.; Wilkinson, G.; Young, J.F. J. Chem. Soc. (A), 1966, 1711.
164. Crabtree, R.H.; Giordano, G. Inorg. Synth. 1979, 19, 218.
165. Herde, J.L.; Lambert, J.C.; Senoff, C.V. Inorg. Synth. 1977, 17, 18.
166. Van der Ent, A.; Onderlinden, A.L. Inorg. Synth. 1973, 14, 94.
167. Sollott, G.P.; Snead, J.L.; Strecker, R.A. J. Am. Chem. Soc. 1973, 95, 210.
168. Kantor, S.W.; Osthoff, R.C. Inorg. Synth. 1957, 5, 55,
169. Dahl, O. Acta. Chem. Scand. 1969, 23, 2342.
170. Ward, L.G.L. Inorg. Synth. 1972, 13, 154.
171. Andersen, R.A. Inorg. Nucl. Chem. Lett. 1980, 16, 31.
172. Bafus, D.A.; Brown, T.L.; Dickerhoff, D.W.; Morgan, G.L. Rev. Sci. Instrum. 1962, 33, 491.

Appendix

Crystallographic Data

Single crystal x-ray analyses of  $[\text{NiClN}(\text{SiMe}_2\text{CH}_2\text{PPh}_2)_2]$ ,  $[\text{PdClN}(\text{SiMe}_2\text{CH}_2\text{PPh}_2)_2]$ ,  $[\text{NiCl}_2\text{NH}(\text{SiMe}_2\text{CH}_2\text{PPh}_2)_2]$ ,  $[\text{Ni}(\text{CO})\text{N}(\text{COC}_2\text{H}_5)(\text{SiMe}_2\text{CH}_2\text{PPh}_2)_2]$ , and fac- $[\text{Ir}(\text{H})_2(\text{PMe}_3)\text{N}(\text{SiMe}_2\text{CH}_2\text{PPh}_2)_2]$  were processed by S.J. Rettig and A.S. Secco of the UBC Department of Chemistry. Crystals were mounted on an Enraf-Nonius CAD4-F diffractometer in non-specific orientations. Final unit-cell parameters were obtained by least-squares on  $2 \sin \theta / \lambda$  values for 25 reflections measured with  $\text{MoK}\alpha_1$  radiation ( $\lambda = 0.70930 \text{ \AA}$ ). All structures were solved by conventional heavy-atom techniques. The computer programs used include locally written programs for data processing and locally modified versions of the following: AGNOST, absorption correction from Northwestern University, ORFLS, full-matrix least squares, and ORFFE, function and errors, by W.R. Busing, K.O. Martin, and H.A. Levy; FORDAP, Patterson and Fourier synthesis, by A. Zalkin; ORTEP II, illustrations, by C.K. Johnson. Corrected bond lengths appear along with the uncorrected values in Tables VI to X, and corrected bond angles are essentially equal to the uncorrected values listed in Tables XI to XV. Stereoscopic views of these structures are given on pages 174 and 175.

Table VI  
Bond lengths (Å) with estimated  
standard deviations in parentheses  
[NiClN(SiMe<sub>2</sub>CH<sub>2</sub>PPh<sub>2</sub>)<sub>2</sub>]

Bond	uncorr.	corr.	Bond	uncorr.	corr.
Ni -Cl	2.1703(6)	2.172	C(9) -C(10)	1.368(4)	1.374
Ni -P(1)	2.2086(6)	2.212	C(10) -C(11)	1.363(4)	1.371
Ni -P(2)	2.1975(5)	2.201	C(11) -C(12)	1.387(3)	1.391
Ni -N	1.924(2)	1.929	C(13) -C(14)	1.371(3)	1.384
P(1) -C(1)	1.816(2)	1.819	C(13) -C(18)	1.384(3)	1.395
P(1) -C(7)	1.825(2)	1.830	C(14) -C(15)	1.381(4)	1.384
P(1) -C(13)	1.817(2)	1.822	C(15) -C(16)	1.357(4)	1.367
P(2) -C(2)	1.807(2)	1.810	C(16) -C(17)	1.357(4)	1.371
P(2) -C(19)	1.824(2)	1.828	C(17) -C(18)	1.384(4)	1.387
P(2) -C(25)	1.813(2)	1.818	C(19) -C(20)	1.389(3)	1.394
Si(1) -N	1.710(2)	1.716	C(19) -C(24)	1.381(3)	1.390
Si(1) -C(1)	1.887(2)	1.895	C(20) -C(21)	1.381(4)	1.383
Si(1) -C(3)	1.859(3)	1.868	C(21) -C(22)	1.374(4)	1.383
Si(1) -C(4)	1.867(3)	1.876	C(22) -C(23)	1.368(4)	1.373
Si(2) -N	1.713(2)	1.721	C(23) -C(24)	1.390(4)	1.392
Si(2) -C(2)	1.893(3)	1.904	C(25) -C(26)	1.371(3)	1.381
Si(2) -C(5)	1.857(4)	1.867	C(25) -C(30)	1.381(3)	1.395
Si(2) -C(6)	1.860(4)	1.872	C(26) -C(27)	1.381(4)	1.384
C(7) -C(8)	1.381(3)	1.389	C(27) -C(28)	1.364(4)	1.379
C(7) -C(12)	1.387(3)	1.394	C(28) -C(29)	1.349(4)	1.356
C(8) -C(9)	1.386(4)	1.390	C(29) -C(30)	1.385(4)	1.389

## Unit-cell parameters:

a = 10.091(3)

 $\alpha$  = 81.06(2)

Z = 2

b = 10.224(3)

 $\beta$  = 78.51(2)

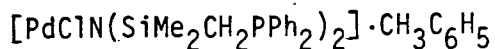
R = 0.029

c = 17.237(4)

 $\gamma$  = 65.93(3)space group =  $P\bar{1}$

Table VII

Bond lengths (Å) with estimated  
standard deviations in parentheses



Bond			uncorr.	corr.	Bond			uncorr.	corr.
Pd	-P(1)	2.3078(5)	2.311		C(13)-C(18)	1.372(3)	1.388		
Pd	-P(2)	2.3112(5)	2.314		C(14)-C(15)	1.384(4)	1.389		
Pd	-Cl	2.3143(6)	2.317		C(15)-C(16)	1.355(6)	1.372		
Pd	-N	2.063(2)	2.069		C(16)-C(17)	1.359(5)	1.370		
P(1)	-C(1)	1.805(2)	1.809		C(17)-C(18)	1.380(4)	1.384		
P(1)	-C(7)	1.821(2)	1.827		C(19)-C(20)	1.392(3)	1.402		
P(1)	-C(13)	1.819(2)	1.823		C(19)-C(24)	1.376(4)	1.388		
P(2)	-C(2)	1.807(2)	1.811		C(20)-C(21)	1.390(4)	1.395		
P(2)	-C(19)	1.816(2)	1.821		C(21)-C(22)	1.354(5)	1.366		
P(2)	-C(25)	1.820(2)	1.825		C(22)-C(23)	1.373(5)	1.382		
Si(1)	-N	1.713(2)	1.719		C(23)-C(24)	1.383(4)	1.388		
Si(1)	-C(1)	1.885(3)	1.891		C(25)-C(26)	1.380(3)	1.394		
Si(1P	-C(3)	1.873(3)	1.881		C(25)-C(30)	1.379(4)	1.391		
Si(1)	-C(4)	1.871(4)	1.879		C(26)-C(27)	1.385(4)	1.388		
Si(2)	-N	1.711(2)	1.717		C(27)-C(28)	1.361(5)	1.372		
Si(2)	-C(2)	1.885(3)	1.892		C(28)-C(29)	1.361(5)	1.376		
Si(2)	-C(5)	1.872(3)	1.881		C(29)-C(30)	1.385(4)	1.389		
Si(2)	-C(6)	1.855(3)	1.863		C(31)-C(32)	1.396(6)	1.413		
C(7)	-C(8)	1.374(4)	1.390		C(31)-C(36)	1.367(5)	1.386		
C(7)	-C(12)	1.370(4)	1.383		C(31)-C(37)	1.492(7)	1.503		
C(8)	-C(9)	1.388(4)	1.394		C(32)-C(33)	1.359(8)	1.374		
C(9)	-C(10)	1.345(6)	1.357		C(33)-C(34)	1.383(8)	1.400		
C(10)	-C(11)	1.360(6)	1.376		C(34)-C(35)	1.352(7)	1.367		
C(11)-C(12)	1.386(4)	1.391			C(35)-C(36)	1.365(6)	1.379		
C(13)-C(14)	1.388(4)	1.399							

Unit-cell parameters:

$$a = 11.538(2)$$

$$\alpha = 92.91(1)$$

$$Z = 2$$

$$b = 15.366(2)$$

$$\beta = 104.10(1)$$

$$R = 0.022$$

$$c = 10.951(1)$$

$$\gamma = 84.75(1)$$

$$\text{space group} = \overline{P1}$$

Table VIII  
Bond lengths (Å) with estimated  
standard deviations in parentheses  
[NiCl<sub>2</sub>NH(SiMe<sub>2</sub>CH<sub>2</sub>PPh<sub>2</sub>)<sub>2</sub>]

Bond	uncorr.	corr.	Bond	uncorr.	corr.
Ni -Cl(1)	2.2216(8)	2.2251	C(9) -C(10)	1.373(5)	1.379
Ni -Cl(2)	2.2058(8)	2.2081	C(10)-C(11)	1.377(5)	1.383
Ni -P(1)	2.3180(7)	2.3202	C(11)-C(12)	1.390(4)	1.392
Ni -P(2)	2.3469(7)	2.3502	C(13)-C(14)	1.394(5)	1.403
P(1) -C(1)	1.815(3)	1.817	C(13)-C(18)	1.373(5)	1.382
P(1) -C(7)	1.814(3)	1.817	C(14)-C(15)	1.397(5)	1.402
P(1) -C(13)	1.826(3)	1.832	C(15)-C(16)	1.360(7)	1.370
P(2) -C(2)	1.817(3)	1.820	C(16)-C(17)	1.363(7)	1.371
P(2) -C(19)	1.826(3)	1.831	C(17)-C(18)	1.389(4)	1.393
P(2) -C(25)	1.824(3)	1.829	C(19)-C(20)	1.392(4)	1.400
Si(1) -N	1.718(2)	1.724	C(19)-C(24)	1.389(4)	1.396
Si(1) -C(1)	1.885(3)	1.891	C(20)-C(21)	1.389(5)	1.393
Si(1) -C(3)	1.859(4)	1.866	C(21)-C(22)	1.376(6)	1.382
Si(1) -C(4)	1.848(3)	1.854	C(22)-C(23)	1.357(5)	1.365
Si(2) -N	1.718(2)	1.723	C(23)-C(24)	1.390(4)	1.394
Si(2) -C(2)	1.886(3)	1.892	C(25)-C(26)	1.390(4)	1.398
Si(2) -C(5)	1.861(3)	1.868	C(25)-C(30)	1.384(4)	1.395
Si(2) -C(6)	1.845(3)	1.851	C(26)-C(27)	1.367(4)	1.370
C(7) -C(8)	1.390(4)	1.397	C(27)-C(28)	1.367(5)	1.379
C(7) -C(12)	1.382(4)	1.388	C(28)-C(29)	1.366(5)	1.373
C(8) -C(9)	1.373(4)	1.376	C(29)-C(30)	1.384(4)	1.387

## Unit-cell parameters:

a = 10.224(7)

$\alpha$  = 72.978(6)

Z = 1.356

b = 10.5769(8)

$\beta$  = 78.424(6)

R = 0.031

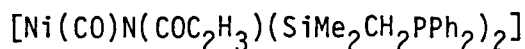
c = 17.770(2)

$\gamma$  = 61.864(8)

space group =  $P\bar{1}$

Table IX

Bond Lengths (Å) with estimated  
standard deviations in parentheses



Bond	Length(Å)	Bond	Length(Å)
Ni -P(1)	2.214(3)	C(11)-C(12)	1.346(15)
Ni -P(2)	2.244(3)	C(11)-C(16)	1.37(2)
Ni -C(3)	1.731(15)	C(12)-C(13)	1.39(2)
Ni -C(9)	2.08(2)	C(13)-C(14)	1.32(2)
Ni -C(10)	2.083(13)	C(14)-C(15)	1.38(2)
P(1)-C(1)	1.838(11)	C(15)-C(16)	1.39(2)
P(1)-C(11)	1.842(13)	C(17)-C(18)	1.423(13)
P(1)-C(17)	1.848(11)	C(17)-C(22)	1.362(13)
P(2)-C(2)	1.798(11)	C(18)-C(19)	1.41(2)
P(2)-C(23)	1.869(13)	C(19)-C(20)	1.40(2)
P(2)-C(29)	1.848(11)	C(20)-C(21)	1.369(15)
Si(1)-N	1.729(14)	C(21)-C(22)	1.414(14)
Si(1)-C(1)	1.859(13)	C(23)-C(24)	1.385(15)
Si(1)-C(4)	1.862(15)	C(23)-C(28)	1.343(15)
Si(1)-C(5)	1.847(15)	C(24)-C(25)	1.37(2)
Si(2)-O(1)	1.687(11)	C(25)-C(26)	1.35(2)
Si(2)-C(2)	1.911(13)	C(26)-C(27)	1.34(2)
Si(2)-C(6)	1.846(14)	C(27)-C(28)	1.38(2)
Si(2)-C(7)	1.806(15)	C(29)-C(30)	1.424(15)
O(1)-C(8)	1.393(15)	C(29)-C(34)	1.366(14)
O(2)-C(3)	1.164(14)	C(30)-C(31)	1.40(2)
N -C(8)	1.31(2)	C(31)-C(32)	1.31(2)
C(8)-C(9)	1.46(2)	C(32)-C(33)	1.41(2)
C(9)-C(10)	1.35(2)	C(33)-C(34)	1.409(15)

Unit-cell parameters:

a = 16.2396

$\beta$  = 105.392

space group =  $P2_1/n$

b = 11.5336

Z = 4

c = 19.0764

R = 0.050

Bond lengths (Å) with estimated  
standard deviations in parentheses  
fac-[Ir(H)<sub>2</sub>(PMe<sub>3</sub>)N(SiMe<sub>2</sub>CH<sub>2</sub>PPh<sub>2</sub>)<sub>2</sub>]

Bond		Uncorr.	Bond		Uncorr.
Ir	-P(1)	2.366(2)	C(8)	-C(9)	1.36(2)
Ir	-P(2)	2.343(3)	C(9)	-C(10)	1.36(2)
Ir	-P(3)	2.235(3)	C(10)	-C(11)	1.34(2)
Ir	-N	2.211(8)	C(11)	-C(12)	1.392(15)
P(1)	-C(1)	1.806(9)	C(13)	-C(14)	1.377(15)
P(1)	-C(7)	1.826(9)	C(13)	-C(18)	1.346(14)
P(1)	-C(13)	1.846(9)	C(14)	-C(15)	1.39(2)
P(2)	-C(2)	1.847(10)	C(15)	-C(16)	1.38(2)
P(2)	-C(19)	1.839(12)	C(16)	-C(17)	1.38(2)
P(2)	-C(25)	1.843(10)	C(17)	-C(18)	1.37(2)
P(3)	-C(31)	1.802(12)	C(19)	-C(20)	1.40(2)
P(3)	-C(32)	1.82(-)	C(19)	-C(24)	1.37(2)
P(3)	-C(33)	1.813(15)	C(20)	-C(21)	1.37(2)
Si(1)	-N	1.705(9)	C(21)	-C(22)	1.42(2)
Si(1)	-C(1)	1.913(9)	C(22)	-C(23)	1.33(2)
Si(1)	-C(3)	1.864(11)	C(23)	-C(24)	1.43(2)
Si(1)	-C(4)	1.883(11)	C(25)	-C(26)	1.41(2)
Si(2)	-N	1.671(8)	C(25)	-C(30)	1.358(14)
Si(2)	-C(2)	1.892(10)	C(26)	-C(27)	1.37(2)
Si(2)	-C(5)	1.900(11)	C(27)	-C(28)	1.39(2)
Si(2)	-C(6)	1.873(12)	C(28)	-C(29)	1.36(2)
C(7)	-C(8)	1.400(14)	C(29)	-C(30)	1.37(2)
C(7)	-C(12)	1.391(13)			

Unit-cell parameters:

a = 19.858(2)

β = 112.330(4)

Z = 4

b = 10.5744(5)

R = 0.030

c = 18.564(2)

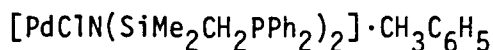
space group = C<sub>c</sub>

Table XI  
Bond angles (deg) with estimated  
standard deviations in parentheses  
[NiClN(SiMe<sub>2</sub>CH<sub>2</sub>PPh<sub>2</sub>)<sub>2</sub>]

Bonds			Angle(deg)	Bonds			Angle(deg)
Cl	-Ni	-P(1)	95.40(2)	P(2)	-C(2)	-Si(2)	104.36(12)
Cl	-Ni	-P(2)	93.74(2)	P(1)	-C(7)	-C(8)	124.1(2)
Cl	-Ni	-N	178.16(6)	P(1)	-C(7)	-C(12)	116.8(2)
P(1)	-Ni	-P(2)	167.72(2)	C(8)	-C(7)	-C(12)	119.1(2)
P(1)	-Ni	-N	85.96(6)	C(7)	-C(8)	-C(9)	120.1(3)
P(2)	-Ni	-N	85.10(5)	C(8)	-C(9)	-C(10)	120.2(3)
Ni	-P(1)	-C(1)	102.96(9)	C(9)	-C(10)	-C(11)	120.3(3)
Ni	-P(1)	-C(7)	120.11(7)	C(10)	-C(11)	-C(12)	120.2(3)
Ni	-P(1)	-C(13)	115.14(7)	C(7)	-C(12)	-C(11)	120.1(2)
C(1)	-P(1)	-C(7)	105.73(10)	P(1)	-C(13)	-C(14)	118.8(2)
C(1)	-P(1)	-C(13)	107.27(11)	P(1)	-C(13)	-C(18)	123.0(2)
C(7)	-P(1)	-C(13)	104.67(10)	C(14)	-C(13)	-C(18)	118.2(2)
Ni	-P(2)	-C(2)	106.98(8)	C(13)	-C(14)	-C(15)	120.3(2)
Ni	-P(2)	-C(19)	121.29(7)	C(14)	-C(15)	-C(16)	121.0(3)
Ni	-P(2)	-C(25)	106.46(7)	C(15)	-C(16)	-C(17)	119.7(3)
C(2)	-P(2)	-C(19)	108.49(11)	C(16)	-C(17)	-C(18)	120.0(3)
C(2)	-P(2)	-C(25)	108.56(11)	C(13)	-C(18)	-C(17)	120.9(3)
C(19)	-P(2)	-C(25)	104.54(9)	P(2)	-C(19)	-C(20)	119.3(2)
N	-Si(1)	-C(1)	104.15(9)	P(2)	-C(19)	-C(24)	122.1(2)
N	-Si(1)	-C(3)	114.6(2)	C(20)	-C(19)	-C(24)	118.5(2)
N	-Si(1)	-C(4)	114.87(15)	C(19)	-C(20)	-C(21)	121.0(2)
Ci(1)	-Si(1)	-C(3)	107.4(2)	C(20)	-C(21)	-C(22)	119.9(2)
C(1)	-Si(1)	-C(4)	108.3(2)	C(21)	-C(22)	-C(23)	119.9(3)
C(3)	-Si(1)	-C(4)	107.2(2)	C(22)	-C(23)	-C(24)	120.5(3)
N	-Si(2)	-C(2)	105.15(9)	C(19)	-C(24)	-C(23)	120.2(2)
N	-Si(2)	-C(5)	113.8(2)	P(2)	-C(25)	-C(26)	118.1(2)
N	-Si(2)	-C(6)	112.7(2)	P(2)	-C(25)	-C(30)	123.5(2)
C(2)	-Si(2)	-C(5)	108.6(2)	C(26)	-C(25)	-C(30)	118.4(2)
C(2)	-Si(2)	-C(6)	107.4(2)	C(25)	-C(26)	-C(27)	121.2(3)
C(5)	-Si(2)	-C(6)	108.8(3)	C(26)	-C(27)	-C(28)	119.6(3)
Ni	-N	-Si(1)	118.02(9)	C(27)	-C(28)	-C(29)	120.0(3)
Ni	-N	-Si(2)	113.83(10)	C(28)	-C(29)	-C(30)	121.0(3)
Si(1)	-N	-Si(2)	128.13(10)	C(25)	-C(30)	-C(29)	119.7(3)
P(1)	-C(1)	-Si(1)	105.70(12)				

Table XII

Bond angles (deg) with estimated  
standard deviations in parentheses



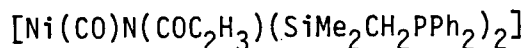
Bonds			Angle(deg)	Bonds			Angle(deg)
P(2)	-Pd	-P(2)	177.11(2)	C(7)	-C(8)	-C(9)	119.9(3)
P(1)	-Pd	-Cl	90.56(2)	C(8)	-C(9)	-C(10)	121.0(4)
P(1)	-Pd	-N	88.66(5)	C(9)	-C(10)	-C(11)	120.1(3)
P(2)	-Pd	-Cl	91.29(2)	C(10)	-C(11)	-C(12)	119.4(4)
P(2)	-Pd	-N	89.47(5)	C(7)	-C(12)	-C(11)	121.3(3)
Cl	-Pd	-N	179.04(5)	P(1)	-C(13)	-C(14)	120.6(2)
Pd	-P(1)	-C(1)	106.77(8)	P(1)	-C(13)	-C(18)	121.0(2)
Pd	-P(1)	-C(7)	120.39(7)	C(14)	-C(13)	-C(18)	118.4(2)
Pd	-P(1)	-C(13)	111.94(7)	C(13)	-C(14)	-C(15)	120.3(3)
C(1)	-P(1)	-C(7)	108.28(11)	C(14)	-C(15)	-C(16)	120.4(3)
C(1)	-P(1)	-C(13)	104.93(11)	C(15)	-C(16)	-C(17)	119.7(3)
C(7)	-P(1)	-C(13)	103.52(11)	C(16)	-C(17)	-C(18)	120.9(3)
Pd	-P(2)	-C(2)	105.88(8)	C(13)	-C(18)	-C(17)	120.3(3)
Pd	-P(2)	-C(19)	115.27(8)	P(2)	-C(19)	-C(20)	121.5(2)
Pd	-P(2)	-C(25)	116.38(7)	P(2)	-C(19)	-C(24)	119.0(2)
C(2)	-P(2)	-C(19)	107.97(12)	C(20)	-C(19)	-C(24)	119.4(2)
C(2)	-P(2)	-C(25)	107.03(11)	C(19)	-C(20)	-C(21)	119.4(3)
C(19)	-P(2)	-C(25)	103.85(10)	C(20)	-C(21)	-C(22)	120.7(3)
N	-Si(1)	-C(1)	105.61(10)	C(21)	-C(22)	-C(23)	120.1(3)
N	-Si(1)	-C(3)	113.59(15)	C(22)	-C(23)	-C(24)	120.2(4)
N	-Si(1)	-C(4)	113.7(2)	C(19)	-C(24)	-C(23)	120.1(3)
C(1)	-Si(1)	-C(3)	109.2(2)	P(2)	-C(25)	-C(26)	123.2(2)
C(1)	-Si(1)	-C(4)	106.1(2)	P(2)	-C(25)	-C(30)	118.6(2)
C(3)	-Si(1)	-C(4)	108.3(2)	C(26)	-C(25)	-C(30)	118.2(2)
N	-Si(2)	-C(2)	105.66(10)	C(25)	-C(26)	-C(27)	120.1(3)
N	-Si(2)	-C(5)	112.90(15)	C(26)	-C(27)	-C(28)	121.1(3)
N	-Si(2)	-C(6)	113.36(14)	C(27)	-C(28)	-C(29)	119.4(3)
C(2)	-Si(2)	-C(5)	105.9(2)	C(28)	-C(29)	-C(30)	120.2(3)
C(2)	-Si(2)	-C(6)	109.8(2)	C(25)	-C(30)	-C(29)	121.0(3)
C(5)	-Si(2)	-C(6)	108.9(2)	C(32)	-C(31)	-C(36)	117.3(4)
Pd	-N	-Si(1)	119.34(10)	C(32)	-C(31)	-C(37)	120.7(4)
Pd	-N	-Si(2)	118.39(9)	C(36)	-C(31)	-C(37)	122.0(4)
Si(1)	-N	-Si(2)	122.27(11)	C(31)	-C(32)	-C(33)	120.2(5)
P(1)	-C(1)	-Si(1)	106.90(12)	C(32)	-C(33)	-C(34)	121.1(5)
P(2)	-C(2)	-Si(2)	107.22(12)	C(33)	-C(34)	-C(35)	119.0(6)
P(1)	-C(7)	-C(8)	121.1(2)	C(34)	-C(35)	-C(36)	120.1(6)
P(1)	-C(7)	-C(12)	120.6(2)	C(31)	-C(36)	-C(35)	122.4(4)
C(8)	-C(7)	-C(12)	118.2(3)				

Table XIII  
Bond angles (deg) with estimated  
standard deviations in parentheses  
[NiCl<sub>2</sub>NH(SiMe<sub>2</sub>CH<sub>2</sub>PPh<sub>2</sub>)<sub>2</sub>]

Bonds	Angle(deg)	Bonds	Angle(deg)
Cl(1)-Ni -Cl(2)	130.36(3)	P(1) -C(7) -C(8)	120.5(2)
Cl(1)-Ni -P(1)	98.89(3)	P(1) -C(7) -C(12)	120.5(2)
Cl(1)-Ni -P(2)	103.33(3)	C(8) -C(7) -C(12)	118.9(3)
Cl(2)-Ni -P(1)	102.40(3)	C(7) -C(8) -C(9)	120.5(3)
Cl(2)-Ni -P(2)	105.81(3)	C(8) -C(9) -C(10)	120.6(3)
P(1) -Ni -P(2)	116.99(2)	C(9) -C(10) -C(11)	119.6(3)
Ni -P(1) -C(1)	118.46(10)	C(10) -C(11) -C(12)	120.3(3)
Ni -P(1) -C(7)	119.59(9)	C(7) -C(12) -C(11)	120.2(3)
Ni -P(1) -C(13)	103.94(8)	P(1) -C(13) -C(14)	119.4(2)
C(1) -P(1) -C(7)	104.85(12)	P(1) -C(13) -C(18)	121.4(2)
C(1) -P(1) -C(13)	105.05(13)	C(14) -C(13) -C(18)	119.1(3)
C(7) -P(1) -C(13)	102.92(12)	C(13) -C(14) -C(15)	119.4(4)
Ni -P(2) -C(2)	116.15(10)	C(14) -C(15) -C(16)	120.4(4)
Ni -P(2) -C(19)	118.86(8)	C(15) -C(16) -C(17)	120.4(4)
Ni -P(2) -C(25)	109.17(8)	C(16) -C(17) -C(18)	120.1(4)
C(2) -P(2) -C(19)	106.59(13)	C(13) -C(18) -C(17)	120.5(4)
C(2) -P(2) -C(25)	102.34(12)	P(2) -C(19) -C(20)	123.5(2)
C(19) -P(2) -C(25)	101.53(11)	P(2) -C(19) -C(24)	118.0(2)
N -Si(1) -C(1)	109.87(12)	C(20) -C(19) -C(24)	118.6(3)
N -Si(1) -C(3)	111.8(2)	C(19) -C(20) -C(21)	120.5(3)
N -Si(1) -C(4)	108.8(2)	C(20) -C(21) -C(22)	119.9(3)
C(1) -Si(1) -C(3)	105.5(2)	C(21) -C(22) -C(23)	120.1(3)
C(1) -Si(1) -C(4)	112.42(14)	C(22) -C(23) -C(24)	120.9(4)
C(3) -Si(1) -C(4)	108.5(2)	C(19) -C(24) -C(23)	120.0(3)
N -Si(2) -C(2)	111.12(12)	P(2) -C(25) -C(26)	120.9(2)
N -Si(2) -C(5)	111.5(2)	P(2) -C(25) -C(30)	121.2(2)
N -Si(2) -C(6)	110.24(15)	C(26) -C(25) -C(30)	117.9(2)
C(2) -Si(2) -C(5)	106.01(15)	C(25) -C(26) -C(27)	121.2(3)
C(2) -Si(2) -C(6)	108.7(2)	C(26) -C(27) -C(28)	120.7(3)
C(5) -Si(2) -C(6)	109.2(2)	C(27) -C(28) -C(29)	119.0(3)
Si(1) -N (Si(2)	134.1(2)	C(28) -C(29) -C(30)	121.2(3)
P(1) -C(1) -Si(1)	118.85(14)	C(25) -C(30) -C(29)	120.1(3)
P(2) -C(2) -Si(2)	120.94(15)		

Table XIV

Bond angles (deg) with estimated  
standard deviations in parentheses

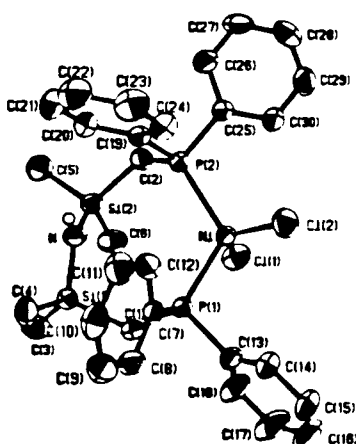
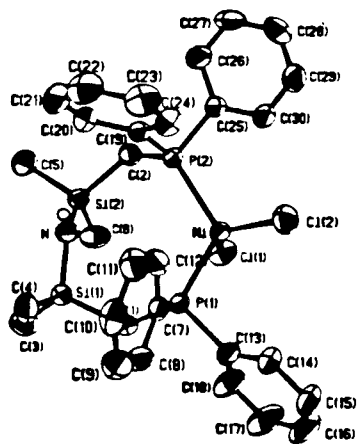
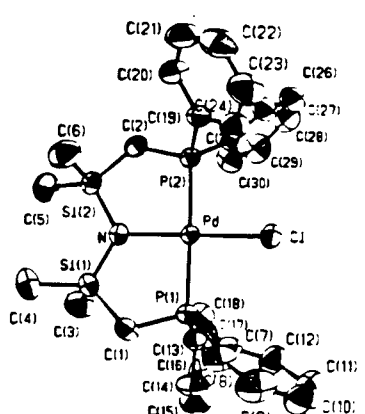
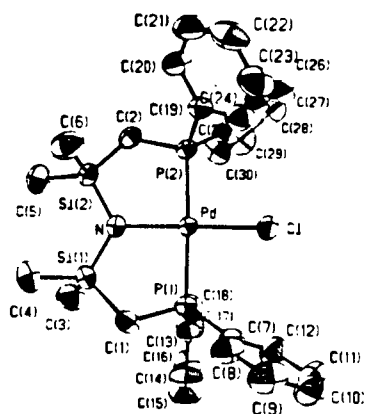
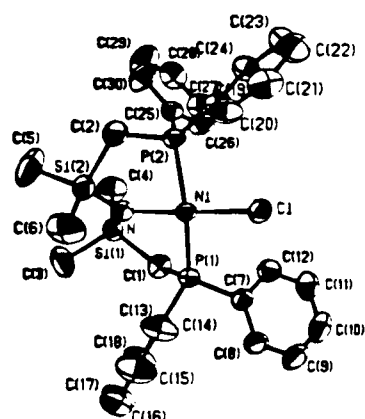
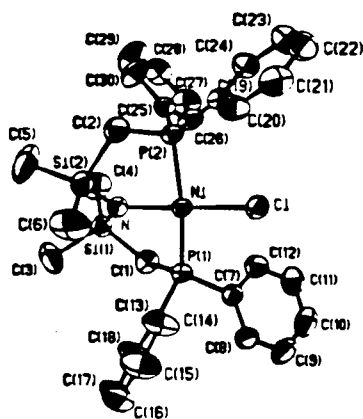


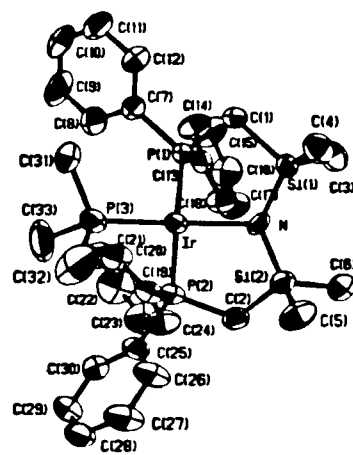
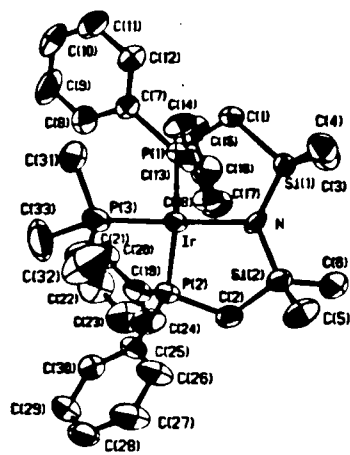
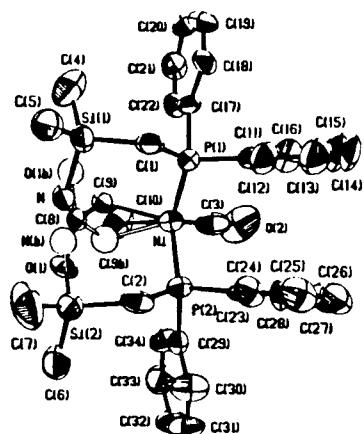
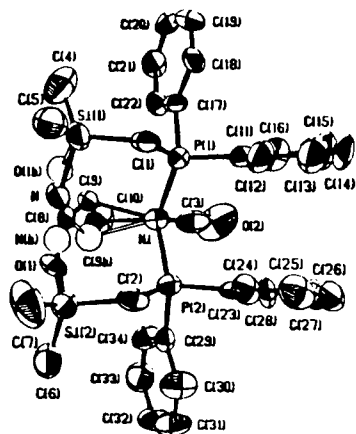
Bonds		Angle(deg)	Bonds		Angle(deg)
P(1)-Ni	-P(2)	106.50(12)	O(1) -C(8) -N		117.2(14)
P(1)-Ni	-C(3)	105.9(4)	O(1) -C(8) -C(9)		112.9(14)
P(1)-Ni	-C(9)	94.0(5)	N -C(8) -C(9)		129.9(15)
P(1)-Ni	-C(10)	124.8(5)	Ni -C(9) -C(8)		105.0(10)
P(2)-Ni	-C(3)	106.2(4)	Ni -C(9) -C(10)		71.4(10)
P(2)-Ni	-C(9)	112.2(5)	C(8) -C(9) -C(10)		132(2)
P(2)-Ni	-C(10)	115.0(5)	Ni -C(10)-C(9)		70.9(9)
C(3)-Ni	-C(9)	129.1(7)	P(1) -C(11)-C(12)		125.6(11)
C(3)-Ni	-C(10)	95.9(6)	P(1) -C(11)-C(16)		118.7(12)
C(9)-Ni	-C(10)	37.7(6)	C(12)-C(11)-C(16)		115.6(13)
Ni -P(1) -C(1)		118.9(4)	C(11)-C(12)-C(13)		121.9(15)
Ni -P(1) -C(11)		116.8(4)	C(12)-C(13)-C(14)		121(2)
Ni -P(1) -C(17)		114.1(4)	C(13)-C(14)-C(15)		120(2)
C(1)-P(1) -C(11)		102.1(6)	C(14)-C(15)-C(16)		117(2)
C(1)-P(1) -C(17)		101.6(5)	C(11)-C(16)-C(15)		124.2(15)
C(11)-P(1)-C(17)		100.7(5)	P(1) -C(17)-C(18)		118.1(10)
Ni -P(2) -C(2)		120.6(4)	P(1) -C(17)-C(22)		121.7(9)
Ni -P(2) -C(23)		112.4(4)	C(18)-C(17)-C(22)		120.2(11)
Nu -P(2) -C(29)		116.3(4)	C(17)-C(18)-C(19)		117.4(11)
C(2)-P(2) -C(23)		104.3(6)	C(18)-C(19)-C(20)		121.8(11)
C(2)-P(2) -C(29)		100.7(5)	C(19)-C(20)-C(21)		118.6(11)
C(23)-P(2)-C(29)		99.9(5)	C(20)-C(21)-C(22)		120.5(11)
N -Si(1)-C(1)		104.2(6)	C(17)-C(22)-C(21)		120.9(11)
N -Si(1)-C(4)		122.9(7)	P(2) -C(23)-C(24)		119.7(12)
N -Si(1)-C(5)		100.0(7)	P(2) -C(23)-C(28)		120.3(11)
C(1)-Si(1)-C(4)		112.6(6)	C(24)-C(23)-C(28)		120.0(13)
C(1)-Si(1)-C(5)		107.6(6)	C(23)-C(24)-C(25)		120.4(14)
C(4)-Si(1)-C(5)		108.1(6)	C(24)-C(25)-C(26)		118.2(15)
O(1)-Si(2)-C(2)		106.2(5)	C(25)-C(26)-C(27)		121(2)
O(1)-Si(2)-C(6)		98.4(6)	C(26)-C(27)-C(28)		121.0(15)
O(1)-Si(2)-C(7)		120.4(7)	C(23)-C(28)-C(27)		118.8(13)
C(2)-Si(2)-C(6)		114.0(6)	P(2) -C(29)-C(30)		120.8(10)
C(2)-Si(2)-C(7)		110.1(7)	P(2) -C(29)-C(34)		119.9(9)
C(6)-Si(2)-C(7)		107.5(7)	C(30)-C(29)-C(34)		119.3(11)
Si(2)-O(1)-C(8)		119.4(9)	C(29)-C(30)-C(31)		118.4(11)
Si(1)-N -C(8)		123.4(13)	C(30)-C(31)-C(32)		121.9(14)
P(1)-C(1)-Si(1)		118.8(6)	C(31)-C(32)-C(33)		121.8(13)
P(2)-C(2)-Si(2)		117.4(6)	C(32)-C(34)-C(34)		118.0(13)
Ni -C(3) -O(2)		178.1(13)	C(29)-C(34)-C(33)		120.7(12)

Table XV

Bond angles (deg) with estimated  
standard deviations in parentheses  
fac-[Ir(H)<sub>2</sub>(PMe<sub>3</sub>)N(SiMe<sub>2</sub>CH<sub>2</sub>PPh<sub>2</sub>)<sub>2</sub>]

Bonds	Angle(deg)	Bonds	Angle(deg)
P(1) -Ir -P(2)	109.58(9)	Ir -N -Si(2)	111.7(4)
P(1) -Ir -P(3)	104.75(9)	Si(1)-N -Si(2)	131.4(5)
P(1) -Ir -N	78.9(2)	P(1) -C(1) -Si(1)	106.1(4)
P(2) -Ir -P(3)	100.24(10)	P(2) -C(2) -Si(2)	110.0(5)
P(2) -Ir -N	85.6(2)	P(1) -C(7) -C(8)	119.5(8)
P(3) -Ir -N	171.4(2)	P(1) -C(7) -C(12)	122.4(7)
Ir -P(1)-C(1)	102.7(3)	C(8) -C(7) -C(12)	118.0(9)
Ir -P(1)-C(7)	122.9(3)	C(7) -C(8) -C(9)	120.0(11)
Ir -P(1)-C(13)	121.3(3)	C(8) -C(9) -C(10)	121.0(11)
C(1) -P(1)-C(7)	104.5(4)	C(9) -C(10)-C(11)	120.6(10)
C(1) -P(1)-C(13)	102.0(4)	C(10)-C(11)-C(12)	120.3(11)
C(7) -P(1)-C(13)	100.5(4)	C(7) -C(12)-C(11)	119.9(10)
Ir -P(2)-C(2)	107.4(3)	P(1) -C(13)-C(14)	119.9(7)
Ir -P(2)-C(19)	124.0(4)	p(1) -C(13)-C(18)	121.0(8)
Ir -P(2)-C(25)	114.9(3)	C(14)-C(13)-C(18)	119.1(9)
C(2) -P(2)-C(19)	104.5(5)	C(13)-C(14)-C(15)	120.3(10)
C(2) -P(2)-C(25)	104.3(5)	C(14)-C(15)-C(16)	120.0(12)
C(19)-P(2)-C(25)	99.8(5)	C(15)-C(16)-C(17)	118.4(12)
Ir -P(3)-C(31)	116.9(4)	C(16)-C(17)-C(18)	120.4(11)
Ir -P(3)-C(32)	115.0(6)	C(13)-C(18)-C(17)	121.5(11)
Ir -P(3)-C(33)	121.0(5)	P(2) -C(19)-C(20)	117.9(9)
C(31)-P(3)-C(32)	100.7(8)	P(2) -C(19)-C(24)	122.8(9)
C(31)-P(3)-C(33)	101.1(7)	C(20)-C(19)-C(24)	119.3(11)
C(32)-P(3)-C(33)	98.8(11)	C(19)-C(20)-C(21)	121.0(12)
N -Si(1)-C(1)	106.2(4)	C(20)-C(21)-C(22)	118.5(13)
N -Si(1)-C(3)	112.7(5)	C(21)-C(22)-C(23)	121.1(12)
N -Si(1)-C(4)	115.2(5)	C(22)-C(23)-C(24)	119.9(13)
C(1)-Si(1)-C(3)	105.5(5)	C(19)-C(24)-C(23)	120.1(12)
C(1)-Si(1)-C(4)	107.4(5)	P(2) -C(25)-C(26)	118.2(7)
C(3)-Si(1)-C(4)	109.1(5)	P(2) -C(25)-C(30)	124.8(8)
N -Si(2)-C(2)	104.8(4)	C(26)-C(25)-C(30)	117.0(10)
N -Si(2)-C(5)	115.3(5)	C(25)-C(26)-C(27)	121.7(11)
N -Si(2)-C(6)	114.5(5)	C(26)-C(27)-C(28)	119.2(12)
C(2)-Si(2)-C(5)	111.9(5)	C(27)-C(28)-C(29)	119.4(10)
C(2)-Si(2)-C(6)	104.5(5)	C(28)-C(29)-C(30)	120.9(11)
C(5)-Si(2)-C(6)	105.5(6)	C(25)-C(30)-C(29)	121.8(11)
Ir -N -Si(1)	113.0(4)		





## Publications:

1. Fryzuk, M.D.; MacNeil, P.A. Organometallics, in press.  
"Stereoselective Formation of Iridium(III) Amides and Ligand-Assisted Heterolytic Splitting of Dihydrogen."
2. Fryzuk, M.D.; MacNeil, P.A. Organometallics, 1983, 2, 355.  
"Amides of Rhodium and Iridium Stabilized as Hybrid Multidentate Ligands."
3. Fryzuk, M.D.; MacNeil, P.A. Organometallics, 1982, 1, 1540.  
"Ancillary Ligand Rearrangements Promoted by the Migratory Insertion of Carbon Monoxide into Nickel(II) Carbon Bonds."
4. Fryzuk, M.D.; MacNeil, P.A.; Rettig, S.J.; Secco, A.S.; Trotter, J. Organometallics, 1982, 1, 918.  
"Tridentate Amidophosphine Derivatives of the Nickel Triad: Synthesis, Characterization, and Reactivity of Nickel(II), Palladium(II), and Platinum(II) amide Complexes."
5. Fryzuk, M.D.; MacNeil, P.A. J. Am. Chem. Soc., 1981, 103, 3592.  
"Hybrid Multidentate Ligands. Tridentate Amidophosphine Complexes of Nickel(II) and Palladium(II)."
6. Bosnich, B.; MacNeil, P.A.; Roberts, N.K. J. Am. Chem. Soc., 1981, 103, 2273.  
"Asymmetric Synthesis. Asymmetric Catalytic Hydrogenation Using Chiral Chelating Six-Membered Ring Diphosphines."